UNIVERSITY OF SOUTHAMPTON

FACULTY OF NATURAL & ENVIRONMENTAL SCIENCES

School of Ocean and Earth Sciences

Biogeochemistry of Hydrothermal Systems in the Scotia Sea

by

Catherine Sarah Cole

Thesis for the degree of Doctor of Philosophy

October 2013

UNIVERSITY OF SOUTHAMPTON

ABSTRACT

FACULTY OF NATURAL & ENVIRONMENTAL SCIENCES

Ocean and Earth Sciences

Doctor of Philosophy

BIOGEOCHEMISTRY OF HYDROTHERMAL SYSTEMS IN THE SCOTIA SEA

by Catherine Sarah Cole

Submarine hot springs play an important role in global heat transfer; element cycling; economic ore deposition; and as an energy source for chemosynthetic ecosystems. Almost four decades of deep-sea exploration have revealed hydrothermal venting to be a ubiquitous phenomenon across the global ocean floor, yet these systems have only recently been discovered in Antarctica. Between 1998 and 2012, high-temperature vents were detected and sampled along the East Scotia Ridge (ESR) and within the Kemp Caldera, which forms part of the South Sandwich island arc, during four research cruises to the Scotia Sea. These vent sites are the first discovered south of the polar front, and they have a distinct faunal assemblage that has characterised them as a new biogeographic province. In this thesis, I investigate the controls on hydrothermal fluid chemistry at the ESR and the Kemp Caldera, using the rare earth elements (REEs) as geochemical tracers. I demonstrate that REE distributions in hydrothermal fluids and associated sulphate deposits are variably influenced by reaction with the host rock; temperature and phase separation; fluid composition and magmatic gas injection; and anhydrite precipitation/dissolution. Secondly, I assess tissue bioaccumulation of metals in *Kiwa tyleri* sp. nov., the dominant macrofaunal species at the ESR vent sites, in response to their environmental exposure. Significant variation in metal burden between tissues reflects both abiotic and biotic controls on metal uptake, including external concentration; trophic position; ecological niche and behavioural traits; in addition to cellular mechanisms of regulation. Finally, I investigate proteomic pathways of metal regulation in the shallow water mussel, *Mytilus edulis*, and the vent-living mussel, *Bathymodiolus* sp. I show that both species have strong defence mechanisms against metal toxicity and oxidative stress, which may be important for successful colonisation of hydrothermal systems. This work highlights the diversity in chemical compositions of fluids venting in back-arc and island-arc settings, and provides an insight into metal regulatory mechanisms that may have facilitated faunal colonisation of these extreme habitats.

Contents

List of Figures

List of Tables

Academic Thesis: Declaration Of Authorship

I, Catherine Sarah Cole, declare that this thesis entitled **Biogeochemistry of Hydrothermal Systems in the Scotia Sea** and the work presented in it are my own and has been generated by me as the result of my own original research.

I confirm that:

1. This work was done wholly or mainly while in candidature for a research degree at this University;
2. Where any part of this thesis has previously been submitted for a degree or any other qualification at this University or any other institution, this has been clearly stated;
3. Where I have consulted the published work of others, this is always clearly attributed;
4. Where I have quoted from the work of others, the source is always given. With the exception of such quotations, this thesis is entirely my own work;
5. I have acknowledged all main sources of help;
6. Where the thesis is based on work done by myself jointly with others, I have made clear exactly what was done by others and what I have contributed myself;
7. Parts of this work have been published as: **Cole, C.**, Coelho, A., James, R. H., Connelly, D., Sheehan, D., Proteomic responses to metal-induced oxidative stress in hydrothermal vent-living mussels, *Bathymodiolus* sp., on the Southwest Indian Ridge, Marine Environmental Research (2013), doi: 10.1016/j.marenvres.2013.09.003.

Signed:……

Date: ……

Acknowledgements

In completing this thesis I am indebted to a great number of people, not only for scientific advice and laboratory assistance, but also for making the past three years such an enjoyable and varied experience.

Firstly, I would like to thank my supervisors, Rachael James and Doug Connelly, for the opportunity to be involved in such an exciting and dynamic research project, and for the extraordinary experience of participating in both Arctic and Antarctic research cruises. Their support and encouragement throughout, particularly in the changing direction of my work, has been exceptional. I'd also like to thank Steve Roberts for his guidance and direction as the chair of my advisory panel.

I have been lucky enough to take part in three cruises, for which I would like to thank Paul Tyler and the ChEsSO consortium, and Ian Wright. I have come to understand the astonishing challenge of remote deep-sea sampling, particularly in isolated areas of the ocean, and I am grateful to the Captain and crew of the *RRS James Cook*, and to the technical team of the ROV *ISIS*, for their expert facilitation of sample collection during JC42, JC55, and JC80. Both at sea and onshore, I have benefited hugely from the advice and technical support of Matt Cooper, Andy Milton, Agnes Michalik, Darryl Green, Belinda Alker, and Ross Williams, and I would like to thank Rachel Mills, Jeff Hawkes, Aly Lough, Laura Hepburn and Alfred Aquilina for stimulating this thesis through scientific discussion. Veerle Huvenne provided the bathymetric maps of the hydrothermal vent fields of the Scotia Sea featured in this thesis, and was (is) a constant source of inspiration. Thanks also to Chris Sweeting, Will Reid and Leigh Marsh for helping a clueless geochemist with dissection at sea; and to Jon Copley and Leigh Marsh for kindly adding to my sample suite with hydrothermal mussels collected from the Southwest Indian Ridge during JC67.

During my exchange visit to University College Cork, Ireland, I was kindly hosted by David Sheehan, who was an incredible source of knowledge and encouragement during my introduction to the field of redox proteomics. I am particularly indebted to David's research students, Louis Charles-Rainville and Tahirah Ja'afar, for their help and patience in the laboratory, and for introducing me to yoga and Malay cooking. My summer in Ireland was hugely enriched by their company. I would also like to

thank Martin Frank and Ed Hathorne for hosting my visit to GEOMAR in Kiel, Germany, and for their expertise and assistance in using the SeaFast pre-concentration system and ICP-MS for REE analyses. Thanks to Chris Sturdy, for his invaluable advice and assistance throughout my experiments with mussels in the NOC; to Chris Hauton for his guidance with my experimental design and statistical treatment; and to Ana Coelho at ITQB, Portugal, for the protein identifications featured in this thesis.

I would like to say a special thank you to my office mates; Carolyn Graves, Jessy Klar, Sarah Wright and Morelia Urlaub. I feel very lucky to have shared an office with you, and the inevitable rollercoaster of emotions that comes with a PhD. Thanks for all the office-cake sessions, for listening, and for regularly putting things into perspective. Thanks so much to Becky, for providing tea or rum (depending on the situation) and an escape from the world of science when I needed it, and to Kate and Gennie for lifting my spirits and always being there. Most importantly, thank you to my family for opening the world up for me, and for supporting me always, through everything. My cousin Judy made the wonderful hydrothermal vent cake pictured below, and has always been an inspiration to me, both in science and in life. Finally, thank you to Drew; for his love, friendship and patience, and for keeping me well-fed and happy, particularly over the last few months.

This work was funded by the Natural Environment Research Council (NERC) National Capability Programme, supplemented by a grant from the Graduate School of the National Oceanography Centre (GSNOCS), NERC and University of Southampton, and by an InterRidge Student Fellowship.

Definitions and Common Abbreviations

AMC	Axial magma chamber
ANH	Anhydrite
B&W	Black & White Smoker vent, E9 North on the East Scotia Ridge
$CaSO_4$	Calcium sulphate (anhydrite)
CH_4	Methane
CO_2	Carbon dioxide
DG	Digestive Gland
E2; E9	Hydrothermal vent fields of the ESR
EPR	East Pacific Rise
ESR	East Scotia Ridge
FTSC	Fluorescein-5-thiosemicarbide
GSH	Reduced Glutathione
GST	Glutathione-S-Transferase
H_2S	Hydrogen Sulphide
HCl	Hydrochloric acid
HDPE	High-density polyethylene
HNO_3	Nitric acid
HREE	Heavy-REE
IAF	Iodoacetamidofluorescein
ICP-MS	Inductively coupled plasma - mass spectrometry
ISIS	Remotely operated vehicle belonging to National Marine Facilities Sea Systems, NERC
KW	Kruskal-Wallis
LDPE	Low-density polyethylene
LREE	Light-REE
MAR	Mid-Atlantic Ridge
MARK	Hydrothermal site at 23 °N on the MAR
MOR	Mid-ocean ridge
MORB	Mid-ocean ridge basalt
MREE	Mid-REE
MT	Metallothionein
MW	Mann-Whitney U
Mw	Molecular weight

PACMANUS	Papua New Guinea-Australia-Canada-Manus hydrothermal vent field
PAGE	Polyacrylamide gel electrophoresis
pI	Isoelectric point
REE	Rare earth element
REE_{CN}	Chondrite-normalised REE
ROS	Reactive oxygen species
ROV	Remotely operated vehicle
-SH	Thiol group
SD	Standard Deviation
SO_2	Sulphur dioxide
SO_4^{2-}	Sulphate
SWIR	Southwest Indian Ridge
TAG	Trans-Atlantic Geotraverse hydrothermal field, 26 °N MAR
TD	Thermally distilled

Chapter 1

1 Introduction

The discovery of geothermally-heated fluids, enriched in ore-forming metals and sulphide, venting from the seafloor at Galapagos in 1977 (Corliss *et al.*, 1979), sparked an era of extensive exploration of the 65,000 km global mid-ocean ridge. Almost 300 vent fields are now known and are distributed within every ocean basin; in geologic settings ranging from mid-ocean ridges to back-arc basins and intraoceanic submarine volcanoes; in sediment-starved and highly sedimented basins; basalt- to peridotite- hosted crustal rock types; and at both high and low latitudes. Hydrothermal vent sites, and the astounding chemosynthetic ecosystems that they host, are believed to exist wherever there is a heat source and sufficient permeability to drive fluid convection through the crust (Van Dover, 2000). The chemical composition of the vent fluids encompasses a remarkable range and highlights the diversity in venting regimes, yet our understanding of hydrothermal fluids and their role in ocean chemistry and global biogeochemical cycles is far from complete.

1.1 Hydrothermal Vents

1.1.1 What are hydrothermal vents?

Hydrothermal vents are seafloor emissions of geothermally-altered seawater. They are generated by the thermal and chemical alteration of seawater through subsurface circulation in regions of tectonic or magmatic activity. In volcanic areas such as spreading ridges and convergent plate boundaries, shallow bodies of magma pool in the ocean crust (Sleep and Rosendahl, 1979). Seawater permeates into the crust through porous sediments and faults and is conductively heated as it approaches the magma chamber, generating a buoyant plume of fluid, which rises and is expelled from the seafloor through focused chimneys or diffuse cracks (Figure 1.1). This

magmatically-fuelled convection of seawater is critically involved in transferring heat away from newly emplaced oceanic crust, and facilitates high-temperature chemical reactions between seawater and the host rock (Von Damm, 1990). In particular, magnesium and oxygen are quantitatively removed from the circulating seawater, whilst transition metals and gases such as H_2S, H_2 and CH_4 are enriched. Temperatures of up to 407 °C have been measured in venting hydrothermal fluids (Haase *et al.*, 2007).

The physical expression of hydrothermal vents on the seafloor varies depending on the extent of seawater mixing, the temperature of venting and the composition of the fluid. As high-temperature (> 300 °C) fluids, enriched in sulphide and metals such as iron, copper and zinc, mix with cold seawater, the precipitation of metal sulphides and oxides give rise to 'black smoker' plumes, which are particle-rich and detectable in the water column by light scattering sensors. At temperatures above 150 °C, where seawater is conductively heated or mixes with fluids, precipitation of the calcium sulphate mineral, anhydrite, initiates chimney growth (Haymon, 1983). Metal sulphides subsequently precipitate within the anhydrite shell, insulating the inner cavity and generating a temperature gradient within the chimney which gives rise to strong mineral zonation (Von Damm, 1990). Chimneys have been observed to grow very quickly (up to 30 cm per day; Tivey, 1995) and can reach up to 60 m in height, though 10-20 m is more common (Kelley *et al.*, 2001). Where fluids vent at intermediate temperatures (100 – 300 °C), concentrations of metals and sulphide are insufficient to precipitate metal sulphides. These vents are known as 'White Smokers' owing to their plumes of silica, anhydrite and barite. Where significant subsurface seawater mixing has taken place, venting is diffuse and temperature is much reduced (< 100 °C). Diffuse venting accounts for the majority of the hydrothermal heat flux (> 90% in oceanic crust younger than 1 Ma) (Schultz and Elderfield, 1997) and sustains thermophilic microorganisms which support a high faunal biomass (Van Dover, 2000).

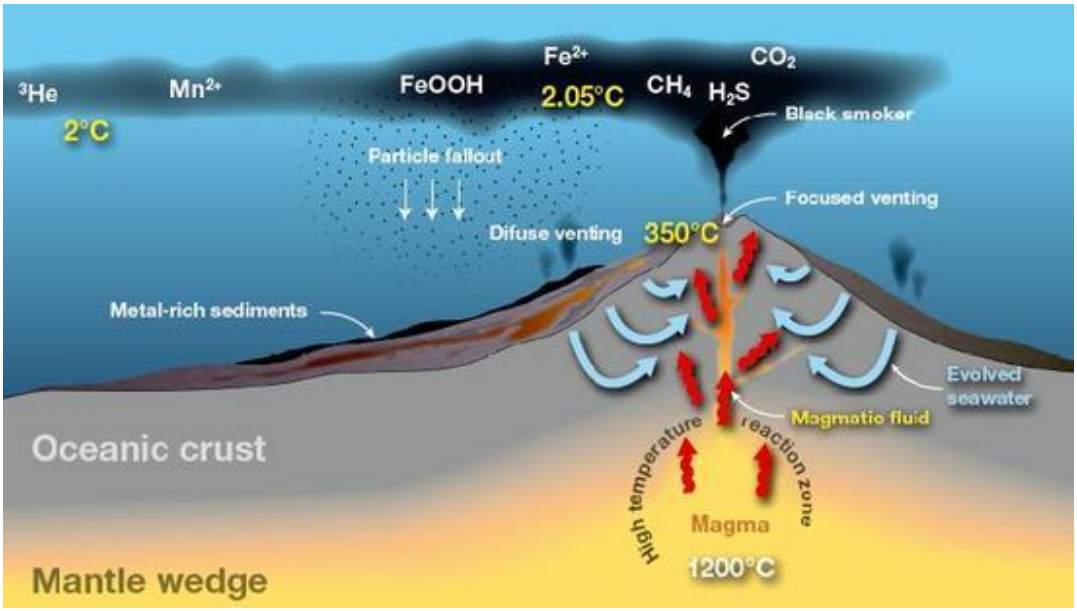

Figure 1.1 Conceptual diagram of a hydrothermal vent system (www.gns.cri.nz)

Hydrothermal convection in the oceanic lithosphere was first predicted to explain the deficiency of conduction as a mechanism for transferring heat away from the apex of a spreading centre (Anderson *et al.*, 1977; Stein and Stein, 1994; Elderfield and Schultz, 1996). The first direct observations of hydrothermal activity were made in 1977 on the Galápagos Rift with the aid of the deep submersible *Alvin* (Corliss *et al.*, 1979). Hydrothermal circulation is now known to play a very important role in the evolution of the Earth's crust, the geochemical cycling of major and trace elements, and in the formation of economically valuable metal sulphide deposits. Hydrothermal vents also represent a source of energy for life in the deep-sea, hosting ecosystems supported by communities of extremophile bacteria, capable of synthesising organic carbon through the oxidation of reduced vent-sourced compounds.

1.1.2 Global distribution

Almost four decades of exploration have revealed over 150 different hydrothermal fields (Figure 1.2) in a diverse range of geological settings in every ocean basin (Baker and German, 2004). Hydrothermal activity is a widespread phenomenon, cooling the oceanic lithosphere along both the fast-spreading ridges of the Pacific and the Southern Oceans, and the slow- and ultraslow-spreading ridges that dominate the Arctic, Atlantic and Southwest Indian Oceans. Back-arc basins, island arcs and seamounts, sediment-rich and sediment-starved, mafic and ultramafic

systems have all been found to host hydrothermal vents. At present, a further 80% of the global ocean ridge remains unexplored. German *et al*. (2011) predict that as many as 1000 high-temperature vent fields exist along the global ridge, with a further 300 – 600 low-temperature systems.

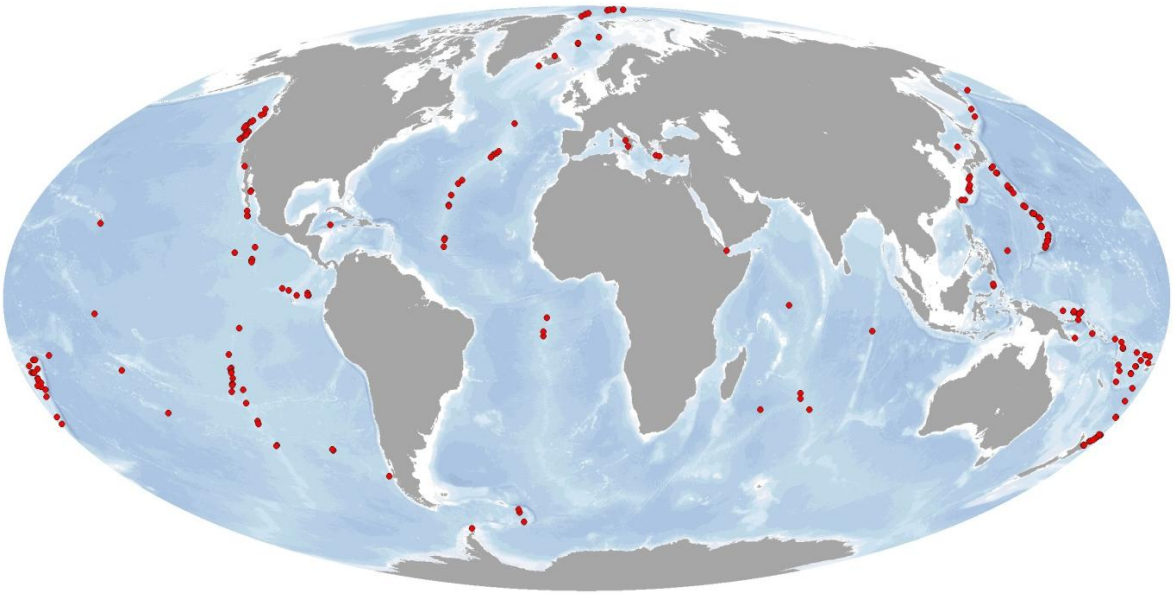

Figure 1.2 Global distribution of hydrothermally active sites known to date, indicated by red dots (Baker *et al.*, 2010).

1.1.2.1 Mid-ocean ridges

Mid-ocean ridges are the surface expressions of seafloor spreading between tectonic plates where new oceanic crust is emplaced (Van Dover, 2000), stretching for ~67,000 km around the globe (Bird, 2003). The morphology of the ridge is largely controlled by spreading rate, and varies both between ridge systems and segments of the same ridge (Purdy *et al.*, 1992). Intermediate (55 – 80 mm/yr; full-spreading rate) and fast (> 80 mm/yr) spreading ridge axes are defined by a shallow (10 – 50 m), narrow (50 – 1000 m) summit caldera or eruptive fissure, and are typically underlain by a shallow axial melt lens (Van Dover, 2000; Alt, 2013). In contrast, slow-spreading ridges (10 – 50 mm/yr) are driven by deeper magma sources that exist as spatially and temporally discontinuous bodies, and ridge axes are characterised by a deep (1 – 3 km) and wide (5 – 15 km) rift valley (Macdonald, 1982). Hydrothermal activity has long been known along the fast-spreading East Pacific Rise (EPR) (Edmond, 1980; Speiss *et al.*, 1980; Hekinian *et al.*, 1983; Von Damm *et al.*, 1985)

and later the northern section of the slow-spreading Mid-Atlantic Ridge (MAR) (Rona *et al.*, 1986; James *et al.*, 1995; Murton *et al.*, 1995; Langmuir *et al.*, 1997), but has only recently been discovered along the southern section of the MAR (Haase *et al.*, 2007; German *et al.*, 2008) and ultraslow-spreading ridges (< 20 mm/yr) such as the Mid-Cayman Rise (German *et al.*, 2010; Connelly *et al.*, 2012), the Gakkel Ridge (Edmonds *et al.*, 2003; Pedersen *et al.*, 2010), the Knipovich Ridge (Connelly *et al.*, 2007), and the Southwest Indian Ridge (German *et al.*, 1998; Bach *et al.*, 2002). The incidence of hydrothermal venting is related to the depth of the axial magma chamber (AMC), as heat from the AMC is the primary driver of hydrothermal circulation (Baker, 2009). Consequently, fast-spreading ridges generally host greater hydrothermal activity (Von Damm *et al.*, 1985; Haymon *et al.*, 1991). However, slow spreading ridges, which occupy 50% of the global ocean ridge, host a greater diversity of venting regimes and may significantly influence ocean biogeochemistry despite their less frequent occurrence (German *et al.*, 2010).

1.1.2.2 Ultra-mafic systems

In addition to the high-temperature reaction between seawater and fresh basalts, slow-spreading ridges also support hydrothermal activity driven by the serpentinisation of ultramafic mantle rock (Gràcia *et al.*, 2000). The exothermic oxidation of Fe^{2+} ions in mantle peridotite by protons in seawater produces H_2 and reduces CO_2 to CH_4, generating relatively low-temperature vent fluids (< 90 °C), which are strongly alkaline (pH 9 – 11) (Charlou *et al.*, 1998). 'Lost City' is an example of this, located at 30 °N near the MAR, 15 km from the spreading axis on 1.5 Myr-old crust, where high pH triggers the precipitation of carbonate chimneys that can be up to 60 m tall (Kelley *et al.*, 2001; Kelley *et al.*, 2005). Further north on the MAR at 36 °N, both volcanic- and serpentinisation-driven hydrothermal activity affect fluids at 'Rainbow' where mantle peridotites intrude into the basaltic crust, giving rise to high-temperature (365 °C), acidic (pH 2.8) effluent, highly enriched in H_2, CH_4 and CO (Charlou *et al.*, 2002; Douville *et al.*, 2002). These types of vent system are likely to be widespread as they are not restricted to axial spreading centres, and they can persist over long timescales (~30,000 years at Lost City) (Früh-Green *et al.*, 2003). Ultramafic-hosted vent systems have sparked particular interest owing to their potential for abiotic organic synthesis, with implications for the origins of life (German *et al.*, 2010).

1.1.2.3 Back-arc spreading centres

Hydrothermal venting is also a common feature of back-arc spreading centres, such as the East Scotia Ridge (Rogers *et al.*, 2012), the Valu Fa Ridge in the Lau Basin (Fouquet *et al.*, 1991), and the Manus basin (Both *et al.*, 1986; Gamo *et al.*, 1997). Back-arc spreading ridges form behind island arcs along convergent plate margins as the pull of the sinking slab initiates extension and rifting in the overriding plate (Figure 1.3). Full-spreading rates are similar to those of mid-ocean ridges, varying from the fast-spreading northern Lau Basin (160 mm/yr) to the slow spreading Mariana Trough (30 mm/yr) (Bibee *et al.*, 1990; Bevis *et al.*, 1995). Fast-spreading back-arc basins tend to have inflated ridge axes underlain by an axial magma chamber (Turner *et al.*, 1999), whilst slow-spreading ridges have an axial rift valley, and exposed mantle peridotites are not uncommon (Ohara *et al.*, 2002). In comparison to mid-ocean ridge settings, hydrothermal venting at back-arc spreading centres can be periodic and fluids tend to have a more variable composition owing to subsurface entrainment of volatile chemical species released from the subducting slab and sediments (Van Dover, 2000; Stern, 2002).

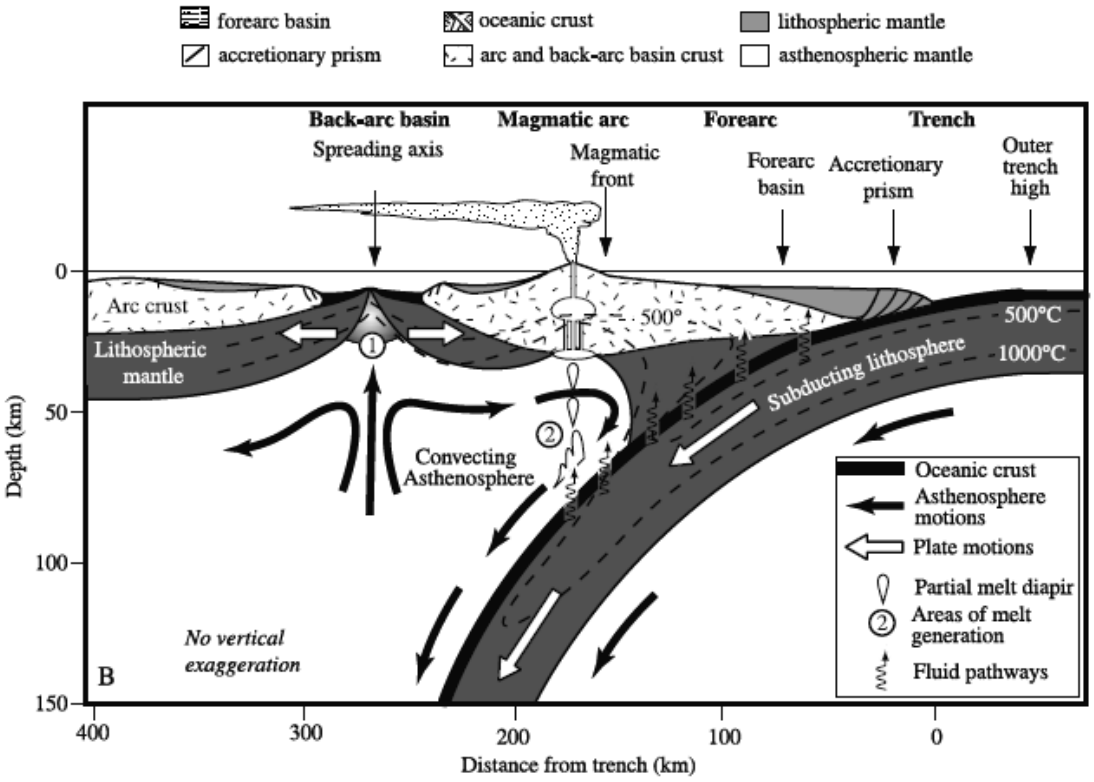

Figure 1.3 Cross section of a convergent margin illustrating the formation of a back-arc spreading centre by rifting as an old oceanic plate is subducted (Stern, 2002).

1.1.2.4 Seamounts

Submerged island arc and ridge-crest volcanoes are also common sites of hydrothermal activity associated with convergent and divergent margins, respectively. Venting associated with arc volcanism is very different from that at mid-ocean ridges as volatiles released during subduction generate lavas that are more siliceous and gas-rich than mid-ocean ridge basalt (MORB). Along the Mariana and Tonga-Kermadec arcs, hydrothermal fluid compositions are strongly influenced by magmatic de-gassing, evident in the extreme-enrichment of CO_2 and the presence of elemental sulphur (McMurty *et al.*, 1993; Embley *et al.*, 2006; Lupton *et al.*, 2006; 2008). Seamounts are also characteristically shallow, and fluid chemistry can vary as a result of sub-critical phase separation and segregation of vapour and brine (Butterfield *et al.*, 1990). Hydrothermal venting at shallow seamounts may influence the chemistry of the upper ocean, with important implications for surface biota and ocean-atmosphere equilibria.

Whilst hydrothermal vents are a common feature of plate boundaries, they are not restricted to these margins. Active intra-plate submarine volcanoes (seamounts) have also been found to host hydrothermal activity, driven by shallow bodies of magma. Hydrothermal systems at mid-plate 'hot spots' are fundamentally different from those of oceanic spreading ridges; most notably the vent fluids have highly elevated volatile concentrations (Gamo *et al.*, 1987). The Loihi Seamount in Hawaii was the first discovered to be hydrothermally active, venting low temperature fluids (< 31 °C), substantially enriched in magmatically-injected CO_2 compared to MOR vent fluids (Karl *et al.*, 1988; Sedwick *et al.*, 1992). Gas enrichment may be partly controlled by the depth of the magma reservoir and eruptive activity. The MacDonald Seamount on the Austral hotspot is underlain by a shallower melt lens compared to that of Loihi, and concentrations of CH_4, H_2S and CO_2 in fluids are far higher (Chemineé *et al.*, 1991).

1.1.2.5 Sedimented systems

Seafloor spreading axes are usually characterised by relatively bare rock as sediment has not had time to accumulate on the young crust. However, in localised areas where sedimentation rates are exceptionally high, the neovolcanic zone of divergent margins may be overlain by thick sedimentary deposits, which can have a

profound effect on the chemistry of hydrothermal fluids (Von Damm, 1988). In the Guaymas Basin, Gulf of California, the intrusion of basaltic magmas into sediments generates hot sills, leading to low-grade metamorphism and large-scale expulsion of thermally-altered pore fluids (Einsele *et al.*, 1980). This process, also a feature of the Escanaba Trough on the slow-spreading Gorda Ridge, initiates a hydrothermal system that does not involve typical seawater recharge (Ishibashi *et al.*, 2002). Sedimented hydrothermal systems are of particular economic interest owing both to their massive sulphide ore deposits, and as a source of petroleum generated through the thermal alteration of sedimentary organic carbon within the hydrothermal convection cell (Simoneit and Lonsdale, 1982; Gieskes *et al.*, 2002).

1.1.3 Controls on fluid chemistry

Hydrothermal fluids are generated by high-temperature reaction of seawater with oceanic crust, and their chemical composition can be highly variable. Sampling pure hydrothermal fluids is challenging and seawater can be easily entrained. To enable comparison between different vent sites, the chemical composition of the vent fluid is usually reported as the zero-Mg end-member concentration as Mg is near-quantitatively removed from seawater at temperatures > 150 °C by precipitation of chlorite and montmorillonite (Bischoff and Dickson, 1975). The zero-Mg end-member is calculated by extrapolating from the composition of bottom seawater through the Mg concentration of the vent fluids.

In order to preserve electrical neutrality in fluids as Mg^{2+} ions are incorporated into hydrothermal minerals, protons are released from the host rock, and pH decreases. As fluids become more acidic, anions such as HCO_3^- are titrated by H^+ ions and alkalinity declines. The only major anion present in vent fluids is chloride, and seawater Cl^- concentrations are generally conserved during hydrothermal circulation (~540 mM), unless the temperature and pressure of the reaction zone favour phase separation (Von Damm, 1988). Sodium concentrations are closely tied to those of chloride, whilst the alkali metals (Li, K, Rb, Cs), transition metals (Fe, Mn, Zn, Cu, Cd, Co, Ag, Pb) and Al are leached from minerals in the host rock (typically basalt), and are variably enriched in fluids compared to seawater. Silica is also enriched, primarily controlled by the solubility of quartz in the reaction zone (Von

Damm *et al.*, 1985). With the exception of Mg, the alkaline earths (Be, Ca, Sr, Ba, Ra) are generally mobilised in fluids, though concentrations of Sr can be enriched or depleted relative to seawater (Von Damm, 1990). Sulphate is near-quantitatively removed by precipitation of anhydrite ($CaSO_4$) from heated seawater in the down-flow zone of the hydrothermal convection cell (Von Damm, 1990). Fluids are typically enriched in gases such as H_2S, CO_2, CH_4, He, and H_2. Sulphide is primarily derived from basalt, but is also generated from seawater sulphate that has not been removed as anhydrite (Von Damm, 1990). CO_2, He and H_2 are degassed from the mantle and can be entrained in circulating fluids, whilst CH_4 can have both biogenic or abiogenic (out-gassing from the mantle, or synthesis by high temperature reaction of CO_2 and H_2) sources (Welhan, 1988). Fluoride concentrations are typically low relative to seawater as mineral phases such as magnesite and magnesium hydroxide sulphate hydrate have a high affinity for F^- (Edmond *et al.*, 1979; Seyfried Jr and Ding, 1995). Bromide and iodide retain similar concentrations to those of seawater, except in sedimented systems where these elements can be enriched as a result of organic matter degradation (Yao *et al.*, 2009).

Many factors influence the composition of endmember solutions, including temperature, pressure, host-rock composition, path length, phase separation, magmatic input, subsurface seawater mixing, mineral alteration and the influence of sediments (Von Damm and Bischoff, 1987; Von Damm, 1990). Endmember fluid compositions from a range of geological settings are reported in Table 1.1, and the main controls are summarised below.

1.1.3.1 Phase separation

In the hydrothermal reaction zone, temperature and pressure determine whether phase separation will take place, according to the two-phase curve shown in Figure 1.4. If a fluid transects the curve at a pressure lower than the critical point of seawater (407 °C; 298 bars), boiling will produce a low salinity vapour and a high salinity brine (sub-critical phase separation). In contrast, at pressure-temperature conditions above the critical point, a small volume of dense and highly saline brine will condense from the vapour phase in supercritical phase separation (Bischoff and Rosenbauer, 1984).

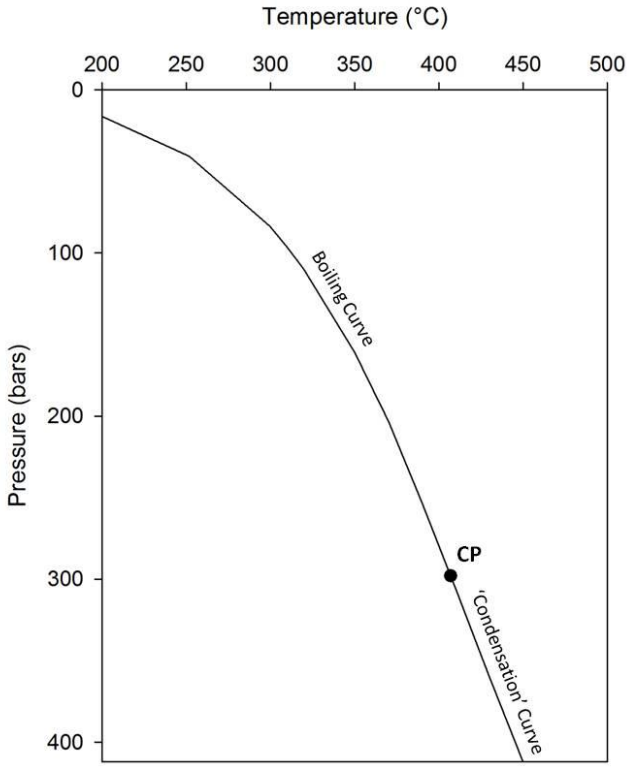

Figure 1.4 Two-phase boundary curve for 3.2 wt % NaCl in H_2O showing the critical point (CP), at 407 °C and 298 bars, where liquid and vapour phases coexist. Data from Bischoff and Rosenbauer (1988).

Chemically different fluids, sometimes venting at distances of a few metres apart, have been attributed to phase separation and segregation followed by variable mixing of vapour and brine phases and cold seawater (Von Damm *et al.*, 2003). At Axial Seamount on the Juan de Fuca Ridge, phase separation followed by partial phase segregation results in a spectrum of vent fluid compositions from low chlorinity (176 mM), gas-rich vapours to high chlorinity (624 mM), gas-depleted brines (Butterfield *et al.*, 1990). Vapour-dominated fluids, depleted in chloride and trace metals, and highly enriched in volatile components, have been sampled at numerous vent sites on the MAR (James *et al.*, 1995) and the Juan de Fuca Ridge (Massoth *et al.*, 1989; Butterfield *et al.*, 1997). High-chlorinity fluids have been sampled at Kairei and Edmond vent fields on the Central Indian Ridge; these fluids are exceptionally metal-rich and gas-depleted (Gallant and Von Damm, 2006). Brines are generally sequestered at depth in the hydrothermal system, and their incorporation in venting effluents may indicate waning of magmatic heat, as single-phase fluids are required to mine these dense pools (Coumou *et al.*, 2009). At basalt-hosted mid-ocean ridge

spreading centres in particular, phase separation and segregation is the dominant control on fluid composition (Von Damm *et al.*, 2003).

1.1.3.2 Rock type

Host-rock composition is also important in determining hydrothermal fluid chemistry. Whilst the oceanic crust is predominantly basaltic in composition, hydrothermal circulation in regions of uplifted ultramafic mantle rocks at slow and ultra-slow spreading centres has been found to generate diverse fluid compositions. Serpentinisation reactions drive fundamentally different styles of hydrothermal venting, through the highly exothermic oxidation of Fe^{2+} in peridotite by protons in seawater, generating hydrogen and methane gas. Fluids venting at ultra-mafic hosted systems such as 'Lost City' and 'Rainbow' vent fields on the MAR are enriched in H_2, CH_4 and Fe, and strongly alkaline compared to typical basalt-hosted systems (Douville *et al.*, 2002; Kelley *et al.*, 2005). In contrast, the lithology of back-arc spreading centres is dominantly felsic owing to the subduction influence and eruption of silicic- and water-rich magmas. The Valu Fa Ridge in the Lau Basin, and Pual Ridge in the Manus Basin, are examples of back-arc, felsic-hosted hydrothermal systems. Compared to basalt-hosted mid-ocean ridge vents, fluids venting at these sites are very acidic (pH < 2) owing to the entrainment of magmatically-degassed acid volatiles (H_2O, CO_2, SO_2, HCl, HF). Concentrations of economically valuable metals (including Zn, Cu, Pb, Cd, As, Ba) are extremely high, reflecting enhanced mobilisation from host minerals at low pH in addition to a significant magmatic source (Fouquet *et al.*, 1991; Yang and Scott, 1996; Reeves *et al.*, 2011).

1.1.3.3 Magmatic input

Magmatic degassing strongly influences the composition of hydrothermal fluids. At the shallow depths of many seamounts and island arc volcanoes, the solubility of CO_2 in volatile-rich magma is low. Juvenile CO_2, entrained in the hydrothermal circulation cell, dissolves to form carbonic acid, leaching H^+, metal cations and HCO_3^- from basalt and generating fluids with remarkably low pH, high metal concentrations and high alkalinity (Sedwick *et al.*, 1992). SO_2 is also degassed from hotspot magmas, and contributes to fluid acidity through disproportionation to form H_2S and H_2SO_4 (Iwasaki and Ozawa, 1960). Concentrations of H_2S are low in emerging fluids, however, owing to subsurface titration by iron. At Pele's Vents on

the Loihi hotspot, measured fluid temperatures are low (~ 30 °C), but low chloride concentrations, indicative of phase separation, suggest fluids contain a high-temperature component (Sedwick *et al.*, 1992). Seawater mixing can significantly alter fluid chemistry, particularly for chemical species that do not behave conservatively and are precipitated as sulphate or sulphide minerals prior to venting.

1.1.3.4 Sediment input

The Southern Trough of the Guaymas Basin in the Gulf of California, and the Escanaba Trough on the southernmost segment of the Gorda Ridge in the Northeast Pacific, are rare examples of active spreading centres overlain by thick sedimentary deposits (500 m or more). In the Guaymas Basin, hydrothermal circulation is driven by intrusions of warm igneous sills in addition to heat from an axial magma chamber, resulting in both low-temperature (< 100 °C) and high-temperature (270 – 314 °C) discharge at the seafloor (Lonsdale and Becker, 1985). Sediment buffering during fluid ascent raises the pH of vent effluents, and $CaCO_3$ dissolution results in high alkalinity. 'Black smoker' chimneys are minor features of these vent systems and the metal content of fluids is depleted relative to high-temperature effluents of the nearby EPR owing to extensive sulphide precipitation in the sediment column (Edmond and Von Damm, 1982). Sedimented hydrothermal systems consequently host economic massive sulphide ore deposits (Morton *et al.*, 1987).

Table 1.1 Summary of hydrothermal vent fluid compositions from a number of well-studied mid-ocean ridge, back-arc and seamount settings.

Site	Rock Type	Full Spreading Rate (cm/yr)	Depth (m)	Sediments	Tmax (°C)	pH	Mg (mM)	Alkalinity (mEq/L)	Cl (mM)	Br (µM)	F (µM)	Na (mM)
Mid-Ocean Ridges												
East Pacific Rise												
13 °N	Basalt	10.4	2600	No	380	3.3	0	-0.40	760	nd	0.2	596
11 °N	Basalt	10.4	2600	No	347	3.1	0	-1.02	563	nd	nd	472
21 °N	Basalt	6.2	2500	No	350	3.4	0	-0.4	489	nd	nd	432
Juan de Fuca Ridge												
North Cleft	Basalt	4	2270	No	327	3.0	0	-0.82	875	nd	nd	682
Guaymas Basin												
South Field	Basalt	6	2000	500m thick	315	5.9	0	9.6	580	nd	nd	472
Mid-Atlantic Ridge												
TAG	Basalt	2.6	3650	No	360	3.1	0	nd	659	880	5.2	584
MARK	Basalt	2.6	3500	No	350	3.9	0	nd	559	847	nd	510
Lucky Strike	Basalt	2.6	1650	No	324	3.65	0	nd	465	840	21.9	390
Broken Spur	Basalt	2.6	3100	No	364		0	nd	469	749	nd	419
Rainbow	Peridotite	2.6	2300	No	365	2.8	0	nd	750	1,178	nd	nd
Lost City	Peridotite/Gabbro		750	No	< 90	9.8	9-19	nd	546-549	nd	nd	479-485
Back-Arc Spreading Centres												
Lau Basin												
Vai Lilli	Basalt/Andesite	16	1700	No	334	2.4	0	nd	667	nd	49.4	nd
Manus Basin												
Vienna Woods	Basalt	13.7	2780	No	285	4.2	0	nd	690	1,060	19	504
Fenway	Dacite/Rhyolite	13.7	1705	No	358	4.5	0	nd	562	882	172	397
Snowcap	Dacite/Rhyolite	13.7	1645	Thick hydrothermal	180	3.4	0	nd	526	831	259	408
DESMOS	Basalt/Andesite	13.7	1925	No	117	1.0	46	nd	492	750	137	391
Seamounts												
Axial Volcano												
Inferno	Basalt		1540	No	328	3.5	0	-0.48	624	956	nd	499
Virgin Mound	Basalt		1540	No	299	4.4	0	0.66	176	250	nd	148
Loihi Seamount												
Pele's Vents	Basalt		980	No	30	5.3	50.3	> 8	524	nd	nd	464
Seawater					3	7.9	52.4	2.35	540	808	64	471

Table 1.1 Continued.

Site	Ca (mM)	Sr (µM)	Li (µM)	K (mM)	Si (mM)	Fe (µM)	Mn (µM)	Zn (µM)	Cu (µM)	H_2S (mM)	CO_2 (mM)	CH_4 (mM)	H_2 (µM)	Refs
Mid-Ocean Ridges														
East Pacific Rise														
13 °N	54.8	168	591	28.8	17.9	10,760	2,035	2	nd	4.5	nd	nd	nd	1,2
11 °N	22.5	80	884	32.0	18.8	6,470	766	105	nd	8.0	nd	nd	nd	1
21 °N	15.6	81	891	23.2	17.6	1664	960	106	35	7.3	nd	nd	nd	3
Juan de Fuca Ridge														
North Cleft	72.9	224	1,434	40.4	19.9	2960	1190	160-340	2.5-9	3.65	nd	nd	nd	4
Guaymas Basin														
South Field	27.7	158	993	44.1	13	8-24	217	nd	nd	6.0	nd	nd	nd	5
Mid-Atlantic Ridge														
TAG	26.0	99	411	17.0	22.0	1,640	1,000	46	150	3.5	3	0.1	200	2,6
MARK	9.9	50	843	23.6	18.2	2,180	491	50	17	5.9	6	0.02	200	6
Lucky Strike	35.6	88	307	23.4	14.4	308	249	29	10.6	2.7	24.2	0.52	207	2,7
Broken Spur	12.8	42.9	1035	18.8		2,156	260	88	68.6	11.0	6.5	0.1	400	8
Rainbow		199	338	20.3	6.9	24,100	2,280	160	140	1.0	16	2.5	16,000	9
Lost City	21.0-23.3	nd	nd	nd	nd	nd	nd	nd	nd	0.06	nd	0.13-0.28	250-430	10
Back-Arc Spreading Centres														
Lau Basin														
Vai Lilli	28-41	105-135	580-745	55-80	14	1200-2900	5800-7100	1200-3100	15-35	nd	nd	nd	nd	11
PacManus														
Vienna Woods	70.7	247	1,070	20.1	14.6	120	211	10	<2	1.6	4.43	71	56	12,13
Fenway	22.3	84.2	917	76.1	12.2	11,800	3,800	nd	nd	18.8	56.1	42	306	12
Snowcap	3.38	24.9	893	55.9	17.5	270	3,020	nd	nd	1.9	187	66	32	12
DESMOS	9.4			8.3	8.1	12,400	40	12	<2	0	23.1	nd	4.0	13,14
Seamounts														
Axial Volcano														
Inferno	46.8	192	192	26.8	15.1	1,065	1,150	111	9.9	7.1	50	nd	nd	15
Virgin Mound	10.2	46	184	6.98	13.5	12	142	2.2	0.4	18	285	nd	nd	15
Loihi Seamount														
Pele's Vents	11.2	88.5	36.5	12.3	1.29	1,010	21.1	nd	nd	2100	300	0.007	nd	16,17
Seawater	10.5	91	28	9.87	0.13	0.0	0.0	0.0	0.0	0.0	2.3	0.0	0.0	12

Refs: 1(Bowers *et al.*, 1988); 2(Douville *et al.*, 1999); 3(Von Damm *et al.*, 1985); 4(Butterfield and Massoth, 1994); 5(Campbell *et al.*, 1988a); 6(Campbell *et al.*, 1988b); 7(Charlou *et al.*, 2000); 8(James *et al.*, 1995); 9(Douville *et al.*, 2002); 10(Kelley *et al.*, 2001); 11(Fouquet *et al.*, 1991); 12(Reeves *et al.*, 2011); 13(Bach *et al.*, 2003); 14(Craddock *et al.*, 2010); 15(Butterfield *et al.*, 1990); 16(Karl *et al.*, 1988); 17(Sedwick *et al.*, 1992). Not determined: nd.

1.1.4 Life at hydrothermal vents

Hydrothermal alteration of seawater generates highly reducing fluids, which are variably enriched in sulphide and other reduced compounds (e.g. CH_4 and H_2), providing a source of chemical energy to the deep sea that can support life through chemosynthesis. Chemosynthesis is the microbial production of organic carbon from inorganic carbon, driven by the oxidation of reduced compounds such as sulphide (Equation 1.1). This process was first observed over 100 years ago, but was not considered to be a significant component of the carbon cycle until the discovery of deep-sea vent systems in the late 1970s (Van Dover, 2000).

$$S^{2-} + CO_2 + O_2 + H_2O \longrightarrow SO_4^{2-} + [CH_2O] \qquad (1.1)$$

Hydrogen sulphide is the primary electron donor used by chemoautotrophic bacteria in vent environments but other substrates can be used, including different forms of sulphur, methane, iron, manganese and ammonia (Van Dover, 2000). By their ability to synthesise organic carbon, the bacterial community supports a high faunal biomass, providing nutrition for macroinvertebrates through symbiotic association. In return, the host provides the symbionts with a regulated supply of sulphide, CO_2 and O_2 (Cavanaugh, 1994). Tube worms such as *Riftia pachyptila*, which are a dominant vent species along the East Pacific Rise, do not have a functional gut and rely entirely on their endosymbionts for nutrition (Cavanaugh *et al.*, 1981). Other species, such as the MAR vent mussel, *Bathymodiolus thermophilus*, host endosymbiotic bacteria in their gill but can also actively filter-feed (Le Pennec *et al.*, 1990). In contrast, dense populations of chemoautotrophic episymbionts occur on the exoskeletons of the MAR vent shrimp, *Rimicaris exoculata*, which may be grazed as the primary energy source in this species (Wirsen *et al.*, 1993). The hugely successful symbiotic relationships between chemoautotrophic bacterial populations and macroinvertebrates distinguish hydrothermal vent ecosystems from all others (Van Dover, 2000).

The macrofaunal assemblages inhabiting hydrothermal vent fields are often characterised by exceptionally high biomass but limited species diversity (Ramirez-Llodra *et al.*, 2010). Continued exploration throughout the past 3 - 4 decades has revealed that vent communities vary hugely between different ridge systems and ocean basins (Tyler *et al.*, 2003; Bachraty *et al.*, 2009). Differences in both the

dominant taxa and the structure of the assemblages define a number of distinct biogeographical provinces (Figure 1.5).

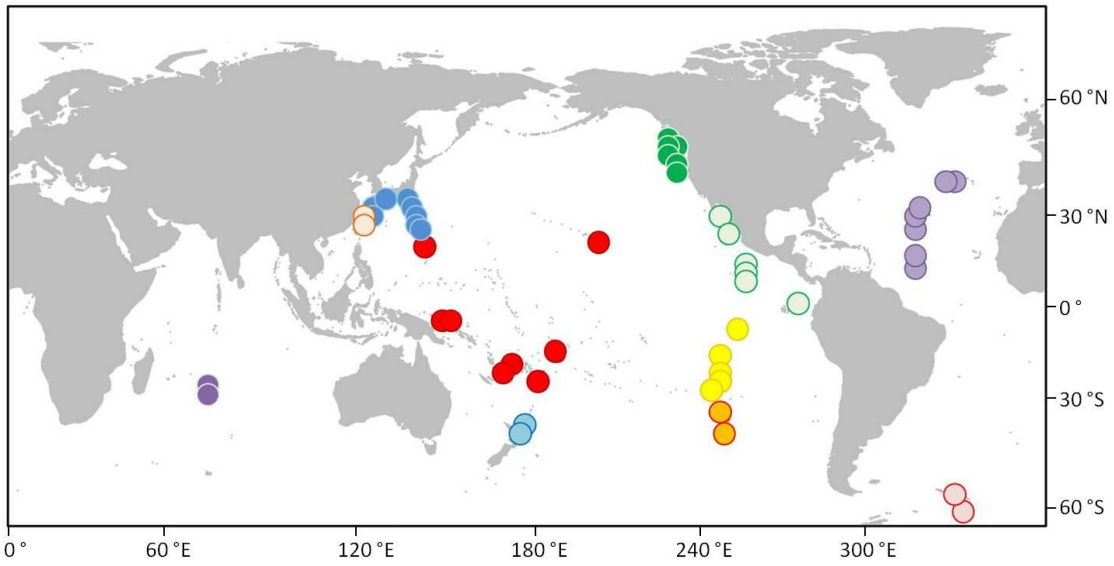

Figure 1.5 Map of 11 deep-sea hydrothermal vent biogeographical provinces showing distinct faunal assemblages along the Mid-Atlantic Ridge; the East Scotia Ridge; the northern, central and southern East Pacific Rise; south of the Easter microplate; four back-arc provinces in the Western Pacific; and the Indian Ocean. Adapted from Rogers *et al*. (2012).

The most studied of these are the vent fields of the EPR and the MAR. At 13 °N and 21 °N on the EPR, the dominant fauna are tube worms (*Riftia pachyptila*), clams (*Calyptogena magnifica*), mussels (*Bathymodiolus thermophilus*) and alvinellid polychaetes (Frustec *et al.*, 1987), whilst further north on the Juan de Fuca Ridge *Ridgeia piscesae* tube worms occupy the niche of *R. pachyptila* (Tunnicliffe *et al.*, 1986). Faunal assemblages of the MAR are very different, hosting dense populations of shrimp (*Rimicaris exoculata*) and mussels (*Bathymodiolus azoricus* and *Bathymodiolus puteosepentis*) (Desbruyères *et al.*, 2000). A new species of alvinocaridid shrimp has been found in dense swarms around deep vents (4960m) of the Cayman Trough in the Caribbean, showing genetic similarities with the MAR shrimp despite the 4000 km isolation of the Mid Cayman Spreading Centre from the global ridge system (Connelly *et al.*, 2012). In the Western Pacific, four distinct provinces have been documented associated with back-arc basins: the Lau Basin, the Manus Basin, the Marianas Trough, the Fiji Basin and the Okinawa Trough (Hessler and Lonsdale, 1991; Desbruyères *et al.*, 1994; Tyler *et al.*, 2003). These vent communities are heterogeneous but generally dominated by gastropods, with variable

populations of mussels and tube worms. More recently, distinct biogeographic provinces have been identified along the Central Indian Ridge, with dense populations of shrimp (*Rimicaris* aff. *exoculata*), anemones (*Marianactis* sp.), mussels (*Bathymodiolus* aff. *brevior*), gastropods (*Alviniconcha* sp. and a scaly-foot species), brachyuran crabs (*Austinograea* sp.) and turbellarian flatworms (Van Dover, 2001). Along the East Scotia Ridge a new species of anomuran crab, *Kiwa tyleri* nov. sp., is dominant amoungst anemones, lepetodrilid limpets, provannid gastropods, stalked barnacles, and pycnogonids (Rogers *et al.*, 2012). In the Arctic, a distinct faunal assemblage dominated by siboglinid tube worms (*Sclerolinum contortum*) in addition to endosymbionts-hosting amphipods, small grazing gastropods and tube-dwelling polychaetes have recently been discovered at Loki's Castle between the Mohns and the Knipovich Ridge (Pedersen *et al.*, 2010). These vent sites are isolated by oceanographic barriers such as low ambient water temperature and strong southerly deep-water currents, and by Iceland, which prevents along-axis dispersion, and are therefore likely to represent a further distinct biogeographic province.

As new hydrothermal vent fields and their associated faunal communities are discovered, our understanding of larval dispersion and the emergence of discrete biogeographical provinces is advancing. Known provinces appear to correspond well with ocean basins and degrees of isolation from the global mid-ocean ridge (Tunnicliffe and Fowler, 1996), but the influence of vent geochemistry, sedimentation and photosynthetic detrital inputs is poorly understood. The dispersal potential of a species is defined by life-history modes, particularly larval development stages, in addition to ocean circulation pattern and topography (Van Dover *et al.*, 2002; Ramirez-Llodra *et al.*, 2007), and continued exploration of deep-sea vent systems is likely to help unravel some of the complex mechanisms controlling colonisation.

1.2 Tracing Hydrothermal Processes: The Rare Earth Elements

"The rare earth elements perplex us in our researches, baffle us in our speculations, and haunt us in our very dreams. They stretch like an unknown sea before us, mocking, mystifying and murmuring strange revelations and possibilities."

These are the words of a 19th Century chemist, Sir William Crookes, reflecting on the difficulties encountered in separating and refining the rare earth elements (REEs) at the time (Crooks, 1887). Despite their name, the REEs (lathanum to lutetium) are lithophilic elements and some members of the group have crustal abundances that exceed those of many economic metals, including copper, lead, tin, molybdenum and silver (Taylor and McClennan, 1985). Similarities in their ionic radii and oxidation state enable liberal inter-group substitution within the lattice of various minerals, and facilitate their wide dispersion throughout the earth's crust. The chemical similarity of the REEs also renders them highly sensitive tracers of biogeochemical processes in the earth and oceans.

1.2.1 Chemical properties of the rare earths

The electronic structure of the REEs is responsible for their coherent chemical behaviour. As the atomic number increases across the group from lanthanum (La) to lutetium (Lu), electrons are progressively added to the inner 4f orbital, which is efficiently shielded by outermost orbitals, limiting changes in chemical reactivity (Elderfield, 1988). Where these elements differ is in their atomic radius, which contracts systematically across the group. In natural fluids, the concentration of the REEs is often a function of solubility, influenced by temperature, pH and complexation with ligands such as CO_3^{2-}, SO_4^{2-}, OH^-, Cl^- and F^-. The strength of these complexes varies with ionic radius, resulting in distinct fractionation of the light REE (LREE; La - Nd) from the heavy REE (HREE; Sm - Lu) (Wood, 1990a).

Changes in oxidation state can also fractionate the REEs. Whilst all members of the group exist in their trivalent state, cerium (Ce) and europium (Eu) also exist as Ce^{4+} and Eu^{2+} under certain redox conditions (Equations 1.2 and 1.3). In seawater, Ce is oxidised to insoluble CeO_2, so its concentration is far lower than the trivalent REEs. Eu is stable as a trivalent ion in seawater, exhibiting similar behaviour to its

neighbouring REEs, but is reduced to Eu^{2+} in high-temperature, reducing environments (Sverjensky, 1984; Bau, 1991). Divalent Eu has a larger ionic radius than its oxidised form, and is therefore more strongly complexed in solution and less compatible in a crystal lattice. Under these conditions, fluids are typically enriched in Eu relative to the trivalent REEs.

$$Ce^{3+} + 2H_2O \leftrightarrow CeO_2 + 4H^+ + e^- \quad (1.2)$$

$$Eu^{3+} + e^- \leftrightarrow Eu^{2+} \quad (1.3)$$

Abundances of the REEs in natural systems have a saw-tooth pattern as a result of variations in nuclear binding energy between elements with odd and those with even atomic numbers (Elderfield, 1988). Concentrations are conventionally normalised to chondrite or shale to resolve changes in the relative abundance of the REE that indicate geochemical fractionation (Piepgras, 1984; Douville *et al.*, 1999).

1.2.2 Hydrothermal fluids

REEs are highly enriched in hydrothermal fluids relative to seawater, owing to the high-temperature alteration of oceanic crust within the hydrothermal circulation cell (Michard *et al.*, 1983). When normalised to chondrite, endmember fluids exhibit remarkably similar REE fractionation patterns across a wide range of geological settings, whereby the LREE are enriched relative to the HREE, and the concentration of Eu is anomalously high relative to its neighbouring REEs (Figure 1.6). This pattern is characteristic of fluids venting from basalt-hosted mid-ocean ridge vent fields such as TAG (Mitra *et al.*, 1994; James and Elderfield, 1996), Broken Spur (James *et al.*, 1995), MARK (Campbell *et al.*, 1988b) and Lucky Strike (Douville *et al.*, 1999) on the MAR, and 13 °N and 21 °N on the EPR (Michard *et al.*, 1983; Michard and Albarède, 1986), in addition to ultramafic-hosted systems such as Rainbow on the MAR (Douville *et al.*, 2002); felsic-hosted back-arc systems such as the Lau Basin (Douville *et al.*, 1999); and the heavily sedimented Guaymas Basin and Escanaba Trough (Klinkhammer *et al.*, 1994).

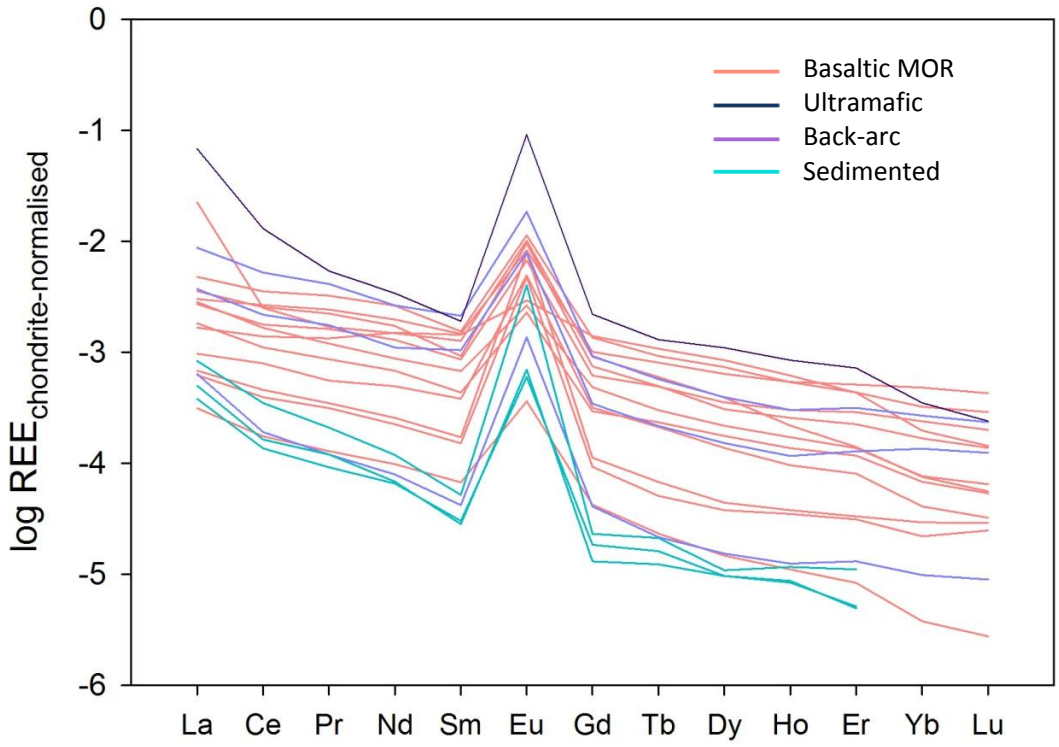

Figure 1.6 Chondrite-normalised REE concentrations in endmember fluids from the MAR, EPR, Lau Basin, Manus Basin (Vienna Woods) and Guaymas Basin, illustrating the similarity in distribution patterns across a broad range of geological settings (references in text). Fluids from basalt-hosted MOR systems are shown in pink; ultramafic-hosted systems in dark blue; felsic-hosted back-arc systems in purple; sediment-hosted systems in turquoise.

This apparent consistency in REE behaviour across a broad range of geological settings has been interpreted to reflect exchange reactions between circulating hydrothermal fluid and plagioclase phenocrysts in the host rock (Onuma *et al.*, 1968; Klinkhammer *et al.*, 1994). REE partition coefficients between hydrothermal fluids and basalt exhibit a relatively linear relationship when plotted against their ionic radius in octahedral coordination (Figure 1.7). This trend is remarkably similar to that of plagioclase, and distinctly different from other common crustal minerals, suggesting that REEs in fluids may be primarily controlled by crystochemical exchange with plagioclase.

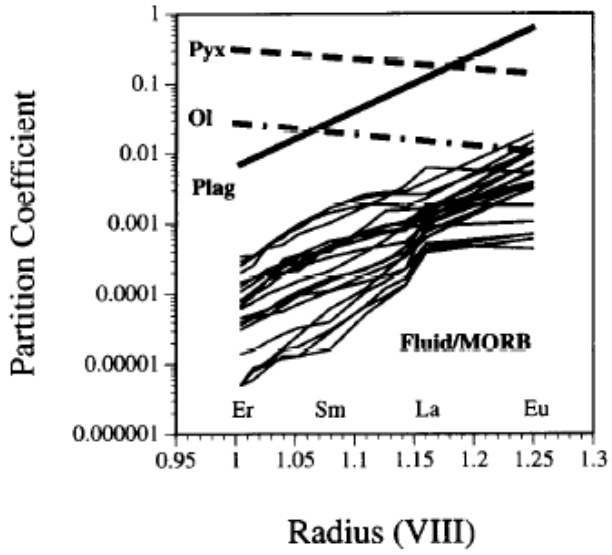

Figure 1.7 Partition coefficients of the rare earth elements between endmember hydrothermal fluids and MORB, and in common basaltic mineral phases; pyroxene (Pyx), olivine (Ol) and plagioclase (Plag), plotted against ionic radius in eight-fold coordination (Klinkhammer *et al.*, 1994).

However, in ultramafic-hosted hydrothermal environments such as Rainbow on the MAR, fluids are enriched in the LREE and Eu despite the absence of plagioclase (Allen and Seyfried Jr, 2005). Olivine and pyroxene dominate the mineralogy of peridotites, and possess very different REE distributions compared to plagioclase (Figure 1.7). Whilst the substitution of trace ions through mineral dissolution during hydrothermal circulation may be largely responsible for the REE fractionation patterns commonly observed in vent effluents, fluid composition and speciation can also influence, and in some cases dominate, REE mobilisation (Wood, 1990b; Haas *et al.*, 1995; Gammons *et al.*, 1996; Douville *et al.*, 1999). In hydrothermal fluids, chloride is typically the dominant ligand available for REE complexation, and speciation calculations indicate that 97-100% of all aqueous REEs are complexed by chloride at temperatures of 300 °C (Haas *et al.*, 1995). Whilst OH^-, SO_4^{2-}, CO_3^{2-} and F^- are also able to form complexes with the REE, these species usually have far lower concentrations than Cl^- in high temperature hydrothermal fluids (Douville *et al.*, 1999). However, in certain geological settings, these species can be enriched in fluids, and their specific REE-binding capacities may influence the distribution patterns of the REEs.

In the Manus back-arc basin in the Bismarck Sea, Papua New Guinea, the chemical composition of hydrothermal fluids is highly variable owing to the interaction of fluids with both mafic and felsic rock types, and the injection of volatiles released from the subducting slab and degassed from water-rich magmas (Embley *et al.*, 2007; Craddock and Bach, 2010; Reeves *et al.*, 2011). The magmatic degassing of acid-volatile species such as HCl, HF, and SO_2, in addition to CO_2 and H_2O, strongly influences REE mobility in solution. Craddock *et al*. (2010) report different REE distribution patterns in fluids between the basalt-hosted arc-distal site 'Vienna Woods' on the Manus Spreading Centre (e.g. Figure 1.6), and the felsic-hosted vent fields of Pual Ridge, close to the active New Britain Arc in the Eastern Manus Basin (EMB). Fluid REE distributions range from LREE-enriched with a positive Eu anomaly at Vienna Woods, to variable LREE- or HREE-enrichment in the EMB. A further site, 'Desmos', has exceptionally high concentrations of the REEs in fluids and very little fractionation is observed across the group. The REE distributions in vent effluents are interpreted to reflect complexation effects on solubility, determined by pH, temperature, and a diverse and variable ligand pool.

1.2.3 Hydrothermal minerals

Although hydrothermal fluids are strongly enriched in the REEs relative to seawater, vent systems are a highly efficient sink for these elements (Mills and Elderfield, 1995). In particular, widespread precipitation of anhydrite, extending to depths of > 300 m below the seafloor, represents a major depository for the REEs (Roberts *et al.*, 2003; Craddock and Bach, 2010). The rare earths are readily assimilated into the $CaSO_4$ lattice by substitution with Ca^{2+}, and crystallographic constraints dictate that ion exchange will favour those REE cations most closely resembling calcium in their ionic radius (Guichard *et al.*, 1979; Morgan and Wandless, 1980). Accordingly, fluid-mineral partition coefficients (K_D) for the REEs, determined from experiments between saturated solutions and anhydrite, are highest for Ce^{3+}, Nd^{3+}, and Sm^{3+}, indicating preferential uptake of the middle-REEs (MREEs) into anhydrite (Kagi *et al.*, 1993). However, anhydrites recovered from the TAG hydrothermal field (26 °N, MAR) possess variable REE distribution patterns when normalised to the vent fluids (Humphris, 1998), and K_D values for La, Ce and Nd are anomalously low (Mills and Elderfield, 1995). Anhydrites from the PACMANUS

hydrothermal site in the Manus Basin, Papua New Guinea, also show variable distribution of the REE, indicating that uptake into $CaSO_4$ may be dominantly controlled by fluid speciation. Fluid composition is strongly influenced by the entrainment of seawater and/or magmatic volatiles, and variations in these inputs can affect REE complexation and consequently the availability of free ions for incorporation into anhydrite (Humphris and Bach, 2005).

Anhydrite will precipitate at temperatures > 150 °C, either from conductively heated seawater or from mixtures of high-temperature hydrothermal fluid and seawater (Bischoff and Seyfried, 1978). Whilst anhydrite is an important structural mineral enabling initial chimney growth, it also forms massive sub-seafloor deposits, which can provide a valuable record of hydrothermal fluid evolution in the subsurface. Such concretions have been sampled extensively at TAG, and at PACMANUS in the Manus Basin, Papua New Guinea, revealing a wide range of REE distributions. When normalised to end-member vent fluids, the REE composition of anhydrites sampled at TAG show two distinct patterns (Humphris, 1998). Flat REE distributions, where the Eu anomaly is absent or reduced, indicate non-selective REE uptake during mineral precipitation from a low temperature, relatively oxidising fluid formed by extensive seawater mixing with circulating high-temperature fluids. Alternatively, anhydrites depleted in the LREEs with exclusion of Eu, indicate deposition from a high-temperature fluid formed by mixing between endmember fluids and conductively heated seawater. Under these conditions, strong complexes of the LREEs with chloride, and the ionic radii mismatch of divalent Eu with Ca^{2+}, inhibit their substitution into anhydrite (Humphris, 1998). These variations have been observed on the scale of individual anhydrite grains at TAG, demonstrating the propensity for rapid fluctuations in hydrothermal regime (Humphris and Bach, 2005).

In the Manus Basin, REE distributions within anhydrites are more variable, ranging from light-, mid- and heavy-REE enriched, to flat, and with variable Eu anomalies, Eu/Eu*, where Eu* = ½([Sm]+[Gd]) (Figure 1.8). Anhydrites precipitated at the Fenway and Roman Ruins vent sites show similar REE distribution to those observed at TAG (described above), whilst those at Snowcap and North Su appear to have deposited from 'acid sulphate' fluids, which form by the injection of volatile magmatic species (CO_2, SO_2, HCl, HF) into circulating seawater. Heterogeneity in

REE distribution patterns indicates highly variable episodes of magmatic degassing in the Manus Basin, both spatially and temporally, with fluctuating fluxes of acid sulphate-type and black smoker-type fluids (Craddock and Bach, 2010).

These examples demonstrate that the partitioning of REEs into precipitating anhydrite is strongly affected by temperature and redox conditions, modified by fluid-seawater mixing ratios and conductive heat exchange, in addition to magmatic gas injection.

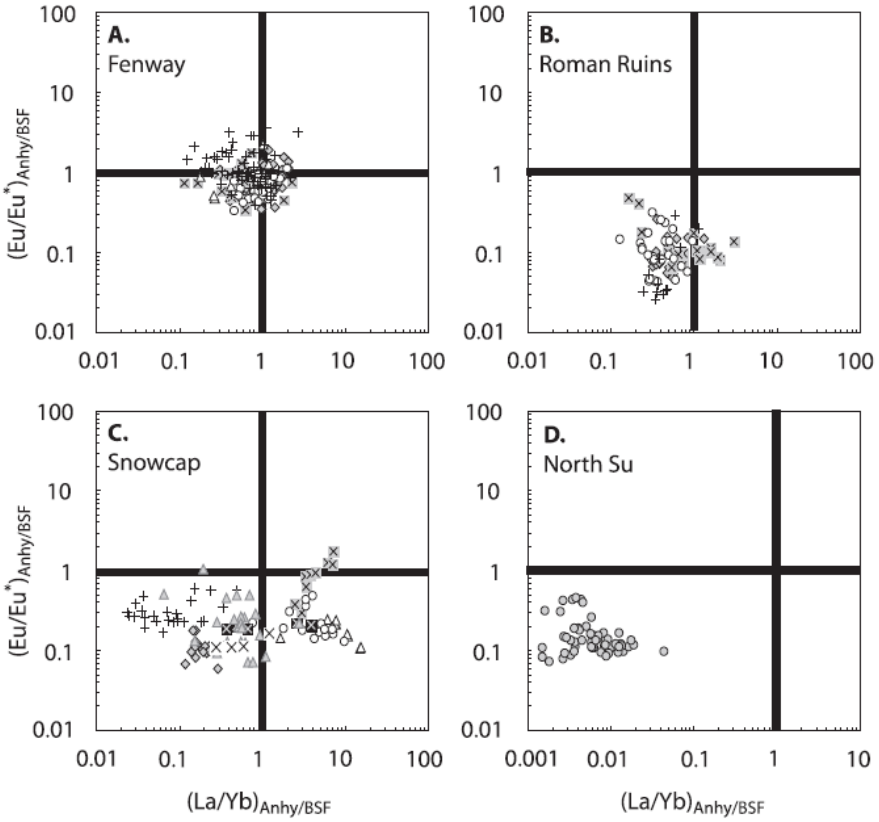

Figure 1.8 LREE/HREE (La/Yb) and Eu anomaly (Eu/Eu*) in anhydrite (Anhy) grains, normalised to contemporary black smoker fluids (BSF), from four active vent fields in the Manus Basin; Fenway (A), Roman Ruins (B), Snowcap (C), and North Su (D). Deviations from the bold lines indicate REE fractionation during anhydrite precipitation (Craddock and Bach, 2010).

In contrast to anhydrite, sulphides precipitated from hydrothermal fluids contain low concentrations of the REEs due to size discrimination against the large REE cations (Gillis *et al.*, 1990). At TAG, white smoker chimney sulphides are enriched in the HREE relative to fluids, indicating crystallographic control whereby substitution of smaller ions is favoured. Similarly, Eu is anomalously depleted in

sulphides and the size of the Eu anomaly has been suggested as a proxy for fluid evolution, correlating with the extent of fluid circulation (Mills and Elderfield, 1995). In contrast, REEs in black smoker chimney sulphides do not show a clear relationship with ionic radius, indicating that fluid composition may be important in controlling REE assimilation in both sulphate and sulphide phases (Mills and Elderfield, 1995). These minerals may therefore provide a valuable record of hydrothermal regime changes across a vent field, serving as an indication of fluid temperature, redox state, and chemical composition at the time of deposition.

1.3 Metal Regulation in Vent-Living Fauna

Sub-marine hydrothermal vents host highly productive ecosystems, supported by microbial chemoautotrophy in the mixing zone between high-temperature fluids and seawater. These two endmembers provide the necessary ingredients for organic carbon synthesis: electron donors (such as sulphide or other reduced substrates) and inorganic carbon (such as CO_2) from the hydrothermal effluent, and electron acceptors (principally oxygen) from seawater (Van Dover, 2000). Hydrothermal fluids are also highly enriched in heavy metals, posing a serious toxicity threat to vent-living fauna (Sarradin *et al.*, 1999). The concepts of cellular metal uptake and regulation, and new proteomic techniques that have improved our understanding of the impact of metal stress and the mechanisms of detoxification at a fine molecular scale are introduced below.

1.3.1 Mechanisms of metal uptake

For aquatic biota, metal bioavailability is determined both by external physico-chemical factors, which affect all organisms in a similar way, and by internal physiological factors, which differ between different organisms. Metal absorption involves traversing the epithelial cell membrane, either at external surfaces such as gill or internal surfaces within the alimentary tract (Luoma and Rainbow, 2008). The cell membrane consists primarily of a phospholipid bilayer, in which the hydrophilic phosphate groups face out towards the aqueous cellular environment, enclosing the hydrophobic fatty acid chains (Singer and Nicolson, 1972). The amphiphilic nature of

the phospholipids enables the cell membrane to regulate entry/exit to and from the cell. Whilst uncharged molecules with limited polar groups can traverse the lipid bilayer freely, hydrated species carrying a charge are restricted to embedded protein channels. Particles can also be taken up into the cytoplasm via endocytosis. The mechanism by which a metal can be absorbed into the cell is determined by its speciation and charge (Figure 1.9).

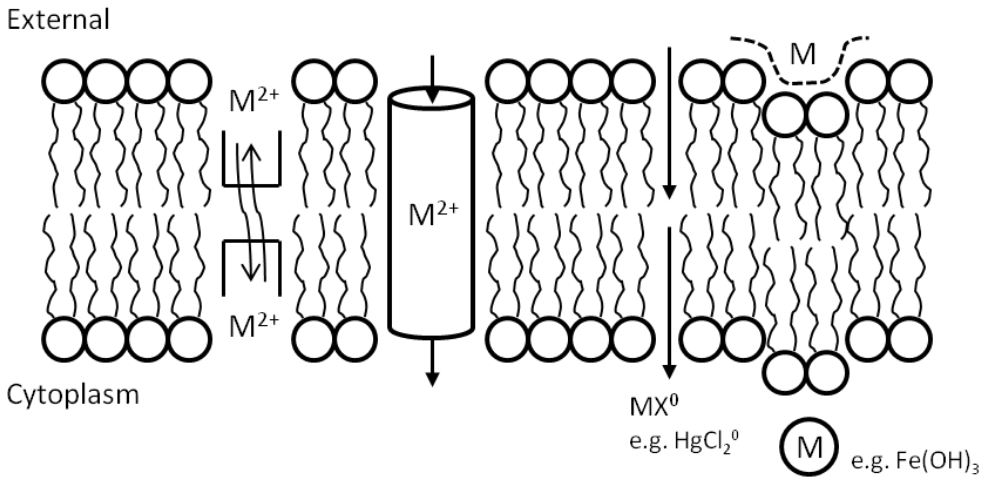

Figure 1.9 Schematic diagram of a cell membrane, showing possible pathways for metal uptake into the cell across the phospholipid bilayer. From left to right: carrier proteins, major ion channels, hydrophobic diffusion and endocytosis. Adapted from Luoma and Rainbow (2008).

In an aqueous environment, dissolved metal ions are highly hydrophilic and can only enter the cell by passing down concentration gradients though carrier or channel proteins (Quinnell *et al.*, 2004). In natural waters, metals are often complexed by a variety of ligands, and whilst these complexes can be uncharged, they are typically heavily hydrated and unable to cross the lipid bilayer. In rare cases where metal complexes are unhydrated, such as $HgCl_2^0$, or where metals are bound as organometallic compounds, these lipophilic molecules gain exceptional membrane permeability and are able to freely diffuse into the cell. Insoluble particles can also be taken up by endocytosis, a mechanism which enables aquatic organisms to satisfy their requirements for insoluble essential elements (Simkiss, 1998).

1.3.2 Metal stress and mechanisms of detoxification

Regulating cellular metal uptake is a critical metabolic process in all organisms. Metals can generally be classified in two groups: those that play an essential biochemical role within an organism whereby deficiency inhibits performance, and those which are toxic to an organism even at trace levels (Luoma and Rainbow, 2008). Essential elements include Fe, Mn, Cu, Zn, and Co, many of which are integral to key metalloproteins and enzymes. Whilst Hg, As and Pb are considered to be amongst the 'toxic' metals, all essential metals will become toxic at elevated concentrations. Metals have a high affinity for ligands such as sulphur and nitrogen, and can readily bind to proteins. The toxic effects of metal overexposure can therefore result from reduced catalytic activity of an enzyme due to metal substitution in the active site, or structural distortion of a protein caused by metal binding (Luoma and Rainbow, 2008). Metals also catalyse the production of reactive oxygen species, which can disrupt the redox balance of a cell and lead to serious protein damage due to oxidative stress.

Mechanisms of detoxification include immobilisation of metals within membrane-bound lysosomes, or sequestration within insoluble granules, which can store metals in an inert form prior to excretion (Viarengo *et al.*, 1981). Metal complexes can also be secreted in extracellular mineral or organic form such as exoskeletons or byssal threads, and in crustaceans the moulting process is a well-known strategy for detoxifying metals (Ahearn *et al.*, 2004; Bergey and Weis, 2007). Metal-binding proteins, such as metallothioneins (MT), are critical components of the antioxidant defence system and are normal constituents of most cells throughout the animal kingdom. MTs are low molecular weight cytosolic proteins with exceptionally high cysteine content, and can be produced by raised environmental exposure to a number of metals (Langston *et al.*, 1998). These proteins are important in controlling the availability of essential metal ions in addition to toxic metals, and enable tissues to accumulate high metal concentrations (Bebianno and Langston, 1991, 1993; Bebianno and Serafim, 2003; Wang and Rainbow, 2010). Other peptides, such as glutathione, are also important in buffering toxicity, and can be particularly important during the initial stages of acute exposure prior to MT induction (Masella *et al.*, 2005).

In hydrothermal vent habitats, concentrations of dissolved metals can be highly enriched relative to 'normal' seawater, and concentrations within faunal tissues

tend to be high in comparison with related non-vent species (Cosson and Vivier, 1997; Gonzalez-Rey *et al.*, 2008). Whilst numerous authors have reported a positive correlation between metal exposure and MT levels (Roesijadi, 1994; Langston *et al.*, 1998; Lecoeur *et al.*, 2004; Amiard *et al.*, 2006; Hardivillier *et al.*, 2006; Martins *et al.*, 2011b), the impact of elevated metal burden on individual proteins is poorly understood. In vent-living organisms, knowledge of metal tolerance limits is particularly sparse. The recent emergence of a new field of analytical molecular biochemistry, redox proteomics, has made it possible to investigate changes in the expression and oxidation of individual proteins, and to rapidly evaluate metal-induced stress across the whole proteome (Sheehan *et al.*, 2010).

1.3.3 Redox proteomics

Since the onset of aerobic metabolism, cells have evolved a battery of defences to protect against the highly toxic derivatives of molecular oxygen. Reactive oxygen species (ROS) are produced during normal metabolic pathways, but can also be generated by exposure to radiation, metal ions and many other external agents (Davies, 2005). These oxidant species possess extreme chemical reactivity, and can cause serious damage to all biological molecules, including DNA, RNA, lipids and proteins. Cells maintain redox homeostasis by regulating the activity of a number of antioxidant enzymes and proteins. Cysteine-rich proteins are particularly important buffers against oxidant damage owing to the redox sensitivity of the thiol (-SH) group, which readily reacts to form a number of sulphoxidation products under oxidising conditions, including disulphides (-S-S-), nitrosothiols (-SNO), and sulphenic (-SOH), sulphinic ($-SO_2H$) and sulphonic ($-SO_3H$) acids (Sheehan *et al.*, 2010). Whilst the first three of these redox transformations are important in redox regulation and cell signalling, the latter two are indicative of more severe, irreversible oxidation. Cellular redox status is typically determined by the ratio of reduced glutathione (GSH) to its oxidised disulphide forms (GSSG or GSSP) (Hansen *et al.*, 2009). If ROS levels exceed cellular defences, oxidative stress can occur. Thiol oxidation and carbonylation (Figure 1.10) yield stable products, which can be used as biomarkers of oxidative stress.

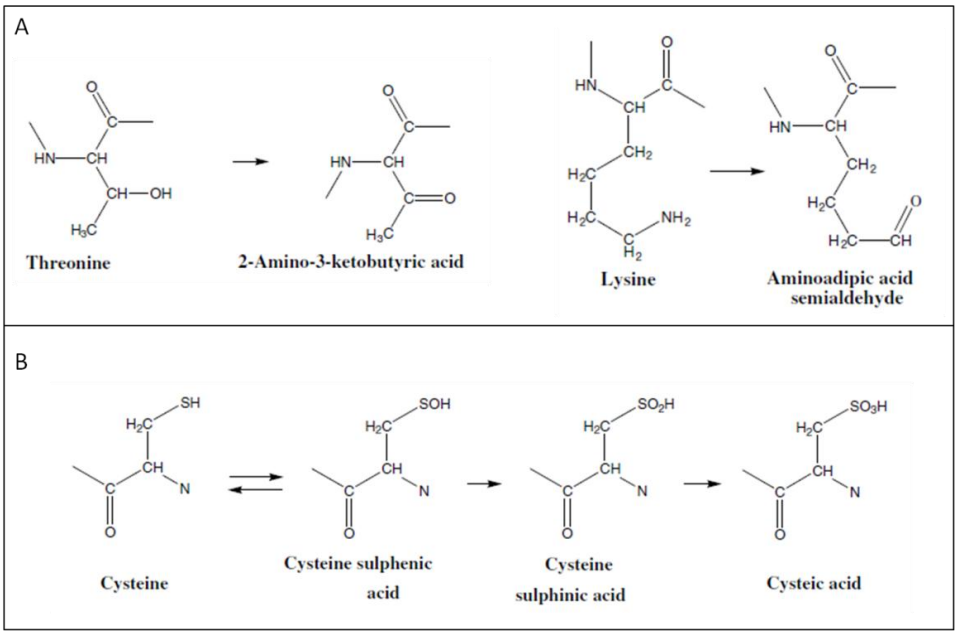

Figure 1.10 Redox modifications of selected amino acid residues in proteins resulting from oxidative stress: (A) carbonylation and (B) thiol oxidation (Sheehan, 2006).

Changes in the expression of individual proteins and the covalent structure of key amino acid side groups, resulting from oxidative stress, can be determined using redox proteomics. Protein extracts are separated according to their isoelectric point and molecular mass using two-dimensional polyacrylamide gel electrophoresis (2D PAGE), which is a widely used, highly-reproducible and semi-quantitative technique (Sheehan, 2006). Proteins are resolved by dye staining (e.g. Dyballa and Metzger (2009)) and image analysis tools facilitate statistical determination of differences in protein spot intensities resulting from varied stressors. The proteome is remarkably resilient to oxidative stress, and changes in just a small number of proteins are typical (Sheehan *et al.*, 2010). The strength of this technique is primarily derived from the potential to label targeted functional groups, such as thiol or carbonyl groups, and to map oxidative modifications that may indicate reduced protein function (e.g. McDonagh *et al*., (2005), McDonagh and Sheehan, (2007; 2008), Chora *et al*. (2008), Company *et al*., (2012)).

1.4 Rationale and Project Objectives

The exchange of elements and isotopes between the oceans and the ocean crust, via hydrothermal activity associated with seafloor rifting, is a key component of the Earth's geochemical cycle. Submarine hydrothermal vents have been observed at numerous locations throughout the world's oceans but, until recently, none had been discovered to the south of the Polar Front. However, as part of an expedition in January-February 2010 to study chemosynthetic environments in high southern latitudes, a series of hydrothermal vents were observed and sampled on the East Scotia Ridge back-arc spreading centre, and at a submarine volcano located to the south of the South Sandwich Islands. These vent systems are remarkably diverse, with highly variable fluid compositions reflecting differing influences of phase separation, magmatic inputs, and seawater entrainment, in addition to different reaction zone conditions, across the back-arc ridge and volcanic seamount settings. Further, these Antarctic vent sites represent a new and distinct biogeographical province. This project aims to evaluate the controls on back-arc and island arc hydrothermal fluid chemistry using rare earth elements (REEs) as geochemical tracers, and to investigate the relationships between seawater chemistry and organism function within the hydrothermal habitat. The specific objectives are:

1. To understand the controls on REE solubility in hydrothermal systems where fluid chemistry is highly variable.
2. To evaluate the conditions of hydrothermal sulphate deposition, and to assess the nature of past venting regimes based on REE distribution patterns within chimney anhydrite grains.
3. To investigate tissue compartmentalisation, bioaccumulation and regulation of metals in vent fauna in relation to their environmental exposure.
4. To assess the potential for pre-adaptation to a metal-enriched environment in related non-vent species.
5. To quantify metal-induced oxidative damage in faunal tissues and to identify molecular pathways of metal detoxification in both vent-living and related non-vent organisms.

1.5 Thesis Structure

This thesis combines geochemical and biochemical analyses to enrich current understanding of the relationships between subsurface hydrothermal processes, fluid composition, vent colonisation, and metal tolerance in vent-living fauna. The newly-discovered vent systems of the East Scotia Sea in the Southern Ocean are the primary focus of this research, and in Chapter 2 the geological settings and fluid chemistry of these vent fields are described. Rare earth elements are thought to be powerful indicators of hydrothermal-magmatic regimes, and their diverse distribution patterns in the back-arc spreading Manus Basin are thought to reflect differences in the relative abundance and stability of REE-chloride, -sulphate and -fluoride complexes as a function of temperature, pH and ligand availability. Chapter 3 discusses whether variable REE distribution patterns are characteristic of back-arc and island-arc environments, and evaluates the dominant influences on fluid composition based on the distribution patterns of the REEs in both fluids and associated chimney sulphates sampled from the East Scotia Sea vent fields.

Hydrothermal fluids are highly enriched in many metals relative to seawater, and Chapter 4 investigates the relationship between environmental metal exposure and tissue uptake in a new species of anomuran decapod, *Kiwa tyleri* nov. sp., which dominates the vent communities along the East Scotia Ridge. The Decapoda are typically impoverished in deep waters south of the polar front, and the discovery of dense aggregations of *K. tyleri* clustering around black smoker chimneys and diffuse vents is extraordinary.

Chapters 5 and 6 take us away from the Southern Ocean and concentrate on the molecular mechanisms of metal detoxification employed by related vent-living and non-vent species. In Chapter 5 the potential for a shallow water mussel, *Mytilus edulis*, to tolerate a metal environment representative of a hydrothermal vent habitat is evaluated. *M. edulis* are a close shallow water relative of the vent-living mussel family, the Bathymodiolinae, and pre-adaptation to elevated metal exposure is assessed based on a redox proteomics study following experimental treatment. Chapter 6 evaluates the impact of metal burden on the proteome in tissues of *Bathymodiolus* sp. sampled from two hydrothermal vent sites on the Southwest Indian Ridge. Bathymodiolin mussels are dominant vent-living organisms found in the Atlantic, Pacific and Indian Oceans, and their success may be partly related to their

ability to cope with metal stress. Mechanisms of metal regulation and antioxidant defence in *M. edulis* and *Bathymodiolus* sp. are evaluated with a discussion on maintenance of redox homeostasis in a chemically fluctuating environment. Finally, Chapter 7 presents a synopsis of this research and highlights the key findings, with suggestions for future work.

Chapter 2

2 Study Area: The East Scotia Sea

2.1 Geological Setting

The Scotia Sea (Figure 2.1) is a marginal basin in the Atlantic region of the Southern Ocean, underlain by the Scotia plate and the much smaller Sandwich plate (Livermore *et al.*, 1994). The most westerly boundary of the Scotia Sea is defined by the Shackleton Fracture Zone, whilst the South Sandwich Trench represents its eastern border. To the north and south respectively, amagmatic transform boundaries separate the Scotia and Sandwich plates from the major South American and Antarctic plates via the North Scotia Ridge and the South Scotia Ridge (Pelayo and Wiens, 1989).

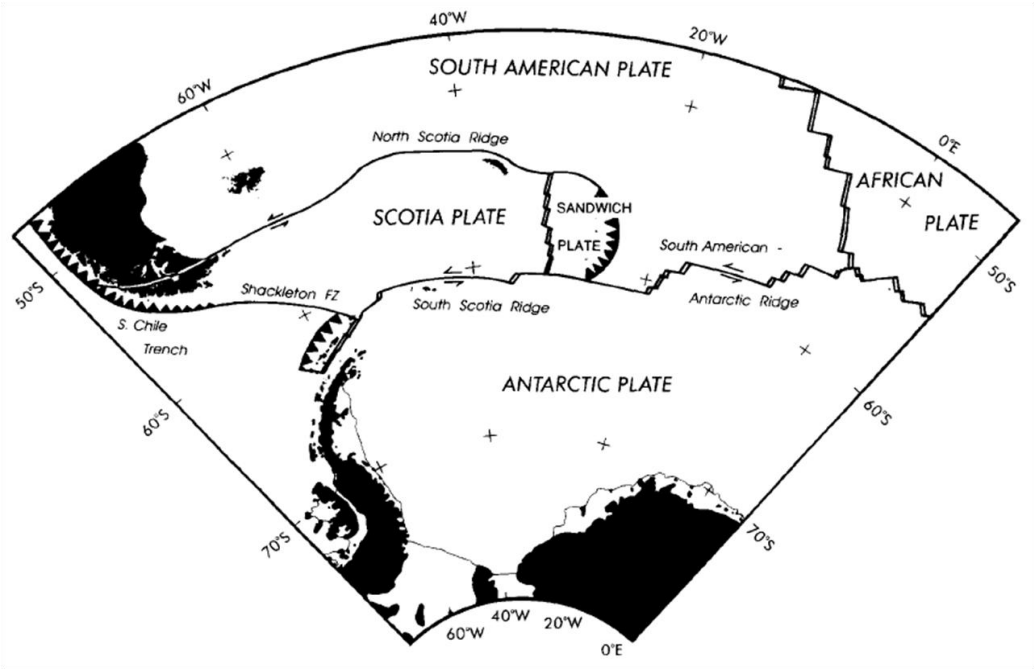

Figure 2.1 Map illustrating the tectonic setting of the Scotia Sea in the Southern Ocean, bordered by active margins to the east and west, and amagmatic transform margins to the north and south (Livermore *et al.*, 1994).

In the eastern Scotia Sea, the South American plate is subducting beneath the Sandwich plate at a rate of 70 – 85 mm/yr, giving rise to the deep Sandwich Trench

(Pelayo and Wiens, 1989). Volcanism associated with this converging plate boundary is responsible for the formation of the South Sandwich Island Arc, and for the back-arc spreading centre approximately 200 km to the west of the arc, the East Scotia Ridge (ESR).

2.1.1 The East Scotia Ridge

The ESR is an isolated inter-oceanic back-arc spreading centre associated with the subduction of the South American plate beneath the overriding Sandwich plate, at 55 – 60 °S in the eastern Scotia Sea (Barker, 1970). Spreading was initiated between the Scotia and Sandwich plates > 15 Ma ago (Larter *et al.*, 2003), and current spreading rates vary between 60 – 70 mm/yr along the ridge (Thomas *et al.*, 2003). Despite its intermediate spreading rate, much of the ESR has an axial morphology more typical of a slow spreading ridge (Leat *et al.*, 2000). Deep median valleys associated with most of the ridge segments, are attributed to reduced mantle temperature and melt production by subduction-related conduction and convection (Livermore *et al.*, 1994; 1997).

The ESR is ~ 500 km in length, consisting of nine ridge segments (E1 – E9), separated by non-transform faults (Figure 2.2), and is an example of a very simple back-arc spreading centre. Strike-slip, subduction and back-arc spreading characterise the tectonic environment, replacing a much more complex extensional regime that formed the Drake Passage and central Scotia Sea (Livermore *et al.*, 1994).

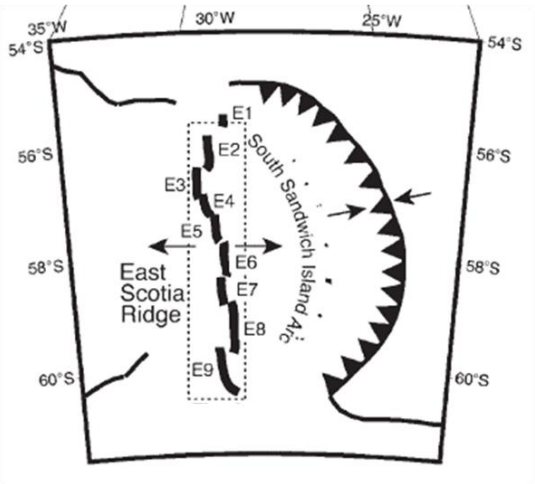

Figure 2.2 Map illustrating the back-arc spreading East Scotia Ridge (ESR) in relation to the subduction zone. The nine ridge segments are labelled E1 – E9 (Fretzdorff *et al.*, 2002).

Segments E2 and E9 are distinct in that they possess magmatically inflated axial highs, more characteristic of fast-spreading ridges (Leat *et al.*, 2000; Bruguier and Livermore, 2001). Locally enhanced melting and magma production is evident from the seismically imaged melt lens beneath E2 and that postulated to exist beneath E9 (Leat *et al.*, 2000). Eastward tearing of the South American plate, as suggested from intense seismic activity at 50 - 130 km depth beneath the northern ESR (Brett, 1977), may facilitate mantle flow from the South Atlantic around the edges of the subducting slab, feeding these axial magma chambers (Figure 2.3). Mantle flow by displacement may also be important as a result of the rapid eastward rollback of the South Sandwich Trench (Pelayo and Wiens, 1989; Bruguier and Livermore, 2001).

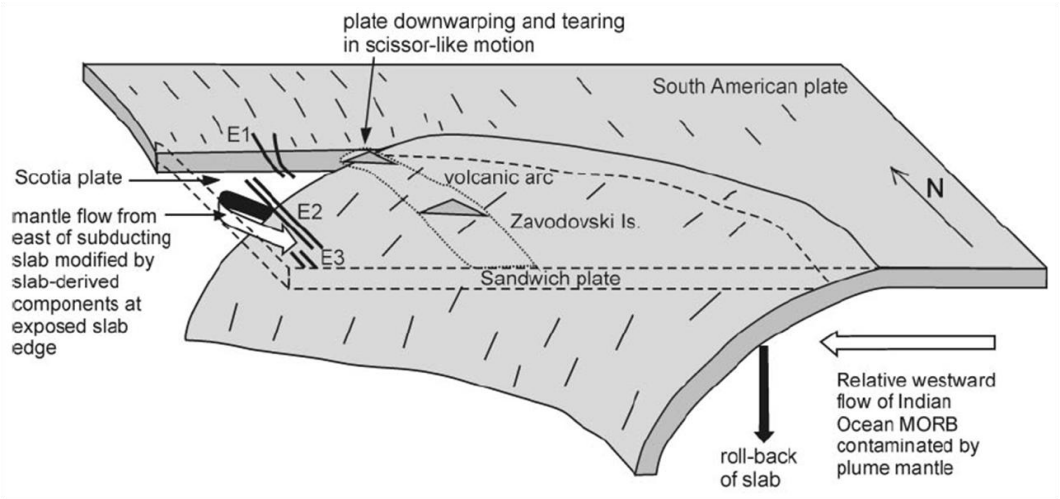

Figure 2.3 Schematic diagram illustrating a likely mechanism for producing the melt anomaly beneath segment E2, showing tearing of the South American plate during subduction (Leat *et al.*, 2000). A similar mechanism is suggested beneath segment E9.

Slab dehydration may also cause melt anomalies at segments close to the convergent margin (Livermore *et al.*, 1997), however dredged rocks indicate limited subduction influence. The dominant crustal lithology of the ESR is mid-ocean ridge basalt (Leat *et al.*, 2000).

2.1.1.1 Segment E2

Segment E2 is 70 km in length with a narrow axial high, which rises to 2,600 m water depth in the centre at a topographic feature known as 'Mermaids Purse' (Livermore *et al.*, 1997). Approximately 3 km below the seafloor, a discreet and narrow melt lens (< 1 km wide) has been seismically imaged, differentiating E2 from

the most northerly segment, E1, where water depths of more than 5,500 m reflect depression by mantle cooling (Livermore *et al.*, 1997). Geochemical analyses of E2 summit basalts compared with the segment ends indicate the presence of an enriched mantle source. Whilst the segment ends and neighbouring ESR segments are likely to be underlain by a normal mid-ocean ridge basaltic source, the E2 summit is influenced by westward asthenospheric flow of a mantle plume from the Bouvet Triple Junction (Kurz *et al.*, 1998; Leat *et al.*, 2000; Fretzdorff *et al.*, 2002). Further, basalts sampled from E2 are not depleted in high field strength elements as observed in the South Sandwich arc lavas, indicating that magmatism is fed from different mantle sources at the arc compared to the back-arc ridge (Leat *et al.*, 2000).

2.1.1.2 Segment E9

The most southerly segment of the ESR, E9, is 105 km in length and possesses a prominent axial volcanic ridge, elevated to 500 m above a median valley and extending for 40 km along the segment (Bruguier and Livermore, 2001). A large axial summit caldera, the 'Devil's Punchbowl', 300 m in depth and 1 km in diameter, is postulated to have formed in the last 10 kyr and indicates collapse associated with magma withdrawal. The E9 ridge axis is likely to be periodically underlain by a shallow magma chamber, and the circular shape of the caldera suggests a locally pooled melt body beneath the central ridge summit in the past, with restricted along-axis flow (Bruguier and Livermore, 2001). Similar to E2, enhanced melt production at E9 is thought to reflect mantle flow around the southern edge of the subducting South American plate. Dredged basalts indicate an enriched mantle source, characteristic of a mantle plume, influenced by volatiles released during subduction (Fretzdorff *et al.*, 2002).

2.1.2 South Sandwich Island Arc

The South Sandwich Island Arc is an intra-oceanic, volcanic arc associated with the subduction of the southernmost South American plate beneath the Sandwich plate (Larter *et al.*, 2003). Basement crust here is young (8 – 10 Ma), generated by back-arc spreading at the ESR and has a thickness of 16 - 20 km (Leat *et al.*, 2004). The arc consists of seven main islands (up to 3 km in height above the seafloor) and several smaller islands and seamounts varying in composition from basaltic to

rhyolitic (Leat *et al.*, 2004). The South Sandwich trench is overlain by ~ 750 m of sediment, but a small accretionary prism suggests that a significant proportion of the accumulated sediment is subducted (Vanneste and Larter, 2002). Correspondingly, lavas erupted along the volcanic arc show a strong sediment influence from the subducting wedge compared to mid-ocean ridge basalts (Fretzdorff *et al.*, 2002).

Kemp Seamount is an active submarine volcano located at the southern end of the arc, ~50 km west-south-west of Thule Island and ~70 km north of the southern subducting edge. The dominant crustal lithology of Kemp is tholeiitic basalt and basaltic andesite, but high concentrations of Nd, and high $^{87}Sr/^{86}Sr$, Nd/Hf and Ba/Th ratios indicate a strong subduction component (Leat *et al.*, 2004).

2.2 Oceanographic Setting

The Southern Ocean is isolated from the rest of the global ocean by the Polar Front (PF), which extends from the sea surface to the seabed (Figure 2.4). The Polar Front is one of three isopycnal features of the eastward-flowing Antarctic Circumpolar Current (ACC), driven by exceptionally strong westerly winds at 45 – 55 °S, and is globally continuous (Orsi *et al.*, 1995). These currents form a major barrier to faunal dispersion, and are likely to explain the highly endemic nature of Antarctic marine communities. Many taxa which are commonly found throughout the world's oceans are absent from the Antarctic, largely due to physiological barriers and life history limitations (Clarke and Johnston, 2003). The chemosynthetic ecosystems of the East Scotia Ridge hydrothermal vent fields, first discovered in 2010 (Rogers *et al.*, 2012), have been classified as a new and distinct biogeographical province, and their unique oceanographic environment may have played an important role in their colonisation history.

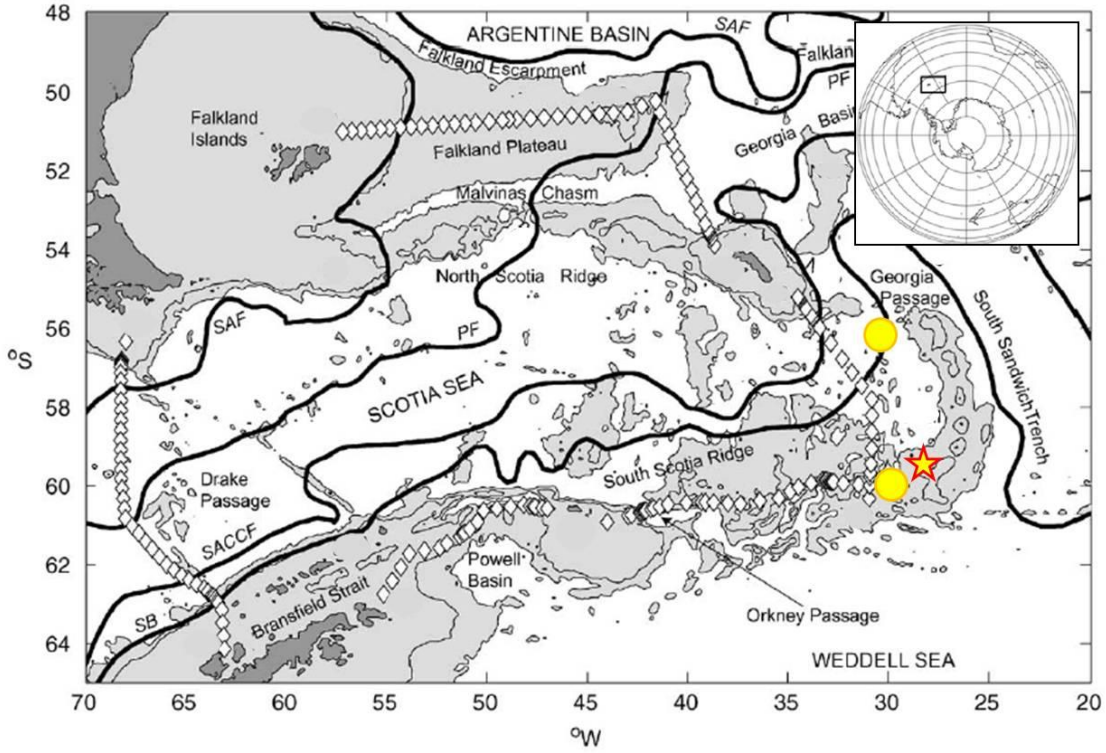

Figure 2.4 Major oceanographic features within the Scotia Sea (Naveira-Garabato *et al.*, 2002), showing the climatological trajectories of the Antarctic Circumpolar Current (ACC) fronts in black lines: the Subantarctic Front (SAF), the Polar Front (PF), the Southern ACC Front (SACCF) and the Southern Boundary of the ACC (SB). Shaded areas define depths < 1500 m. ESR segments E2 and E9 are indicated by yellow spots and Kemp Caldera by the red star.

In the region of the ESR, local deep water is principally Weddell Sea Deep Water (-0.7 – 0.2 °C), whilst partial mixing with Lower Circumpolar Deep Water (0.2 – 0.7 °C) is evident at the most northerly active segment, E2 (Naveira-Garabato *et al.*, 2002). Depth profiles of temperature and salinity in background seawater, recorded by CTD in the region of the ESR and the Kemp Caldera during the *RRS James Cook* cruise JC55 in 2011, indicate that these sites are enveloped by the same water masses (Figure 2.5); however Kemp Caldera is situated in considerably shallower water (1400 – 1550 m) relative to the hydrothermally active segments of the ESR (2400 - 2600 m).

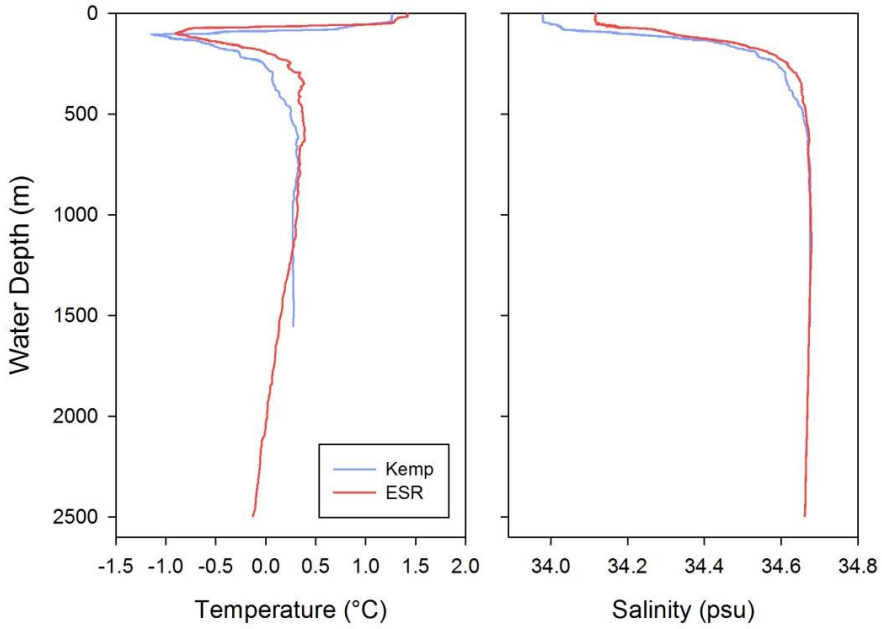

Figure 2.5 Depth profiles showing the temperature and salinity of background seawater in the region of the ESR (JC55 CTD 422; 59°40' S; 33°06' W) and the Kemp Caldera (JC55 CTD 437; 59°42' S, 28°19' W).

2.3 Hydrothermal Venting

Hydrothermal plumes were first detected above segments E2 and E9 of the ESR in 1998 from geochemical surveys of the water column (German *et al.*, 2000). In 2009, active, high-temperature 'black smoker' vents were observed for the first time using a deep-towed camera system, and a further 'white smoker' vent site was discovered within a submarine volcanic crater to the west of Kemp Seamount. These were subsequently sampled by the remotely operated vehicle (ROV) ISIS during RRS *James Cook* cruises, JC42 in early 2010 (Rogers *et al.*, 2012) and JC80 in December 2012. Hydrothermal end-member fluid compositions are remarkably diverse (Table 2.1), indicating large differences in vent regimes (Connelly *et al.*, in prep; James *et al.*, in review). The major seafloor features, and key differences in fluid chemistry, are described for each site below.

2.3.1 The E2 vent field

The E2 hydrothermal site is located just south of the axial volcanic ridge (AVR), between 56° 5.2′ and 56° 5.4′ S and between 30° 19.0' and 30° 19.35′ W at ~2600 m water depth (Figure 2.6). 'Dog's Head' consists of a series of four

chimneys, up to ~10 m high, that actively vent black smoker fluids at temperatures of up to 351 °C. The 'Sepia' vent site lies 75 m to the south east of Dog's Head, and chimneys up to ~10 m high vent fluids at temperatures of up to 353 °C. A further site 'Crab City' emits diffuse fluids at temperatures of ~13 °C, and is host to a large population of the anomuran decapod, *Kiwa tyleri* nov. sp. The chloride concentration of the endmember fluids (532 - 536 mM) is close to local bottom seawater (540 mM) and the lowest recorded fluid pH is 3.02 (James *et al.*, in review). Sulphate behaves conservatively during seawater mixing and extrapolates to a near-zero concentration in endmember fluids (0.97 - 1.31 mM). Concentrations of H_2S and fluoride in the endmember fluids (6.7 – 7.1 mM and ~39 μM, respectively) are typical of basalt-hosted mid-ocean ridge systems (e.g. Von Damm, 1990; Kelley *et al*., 2002), suggesting that input of magmatic volatiles (which produce fluids with low pH and high [F^-]; e.g. Gamo *et al*., 2006) is negligible (James *et al.*, in review).

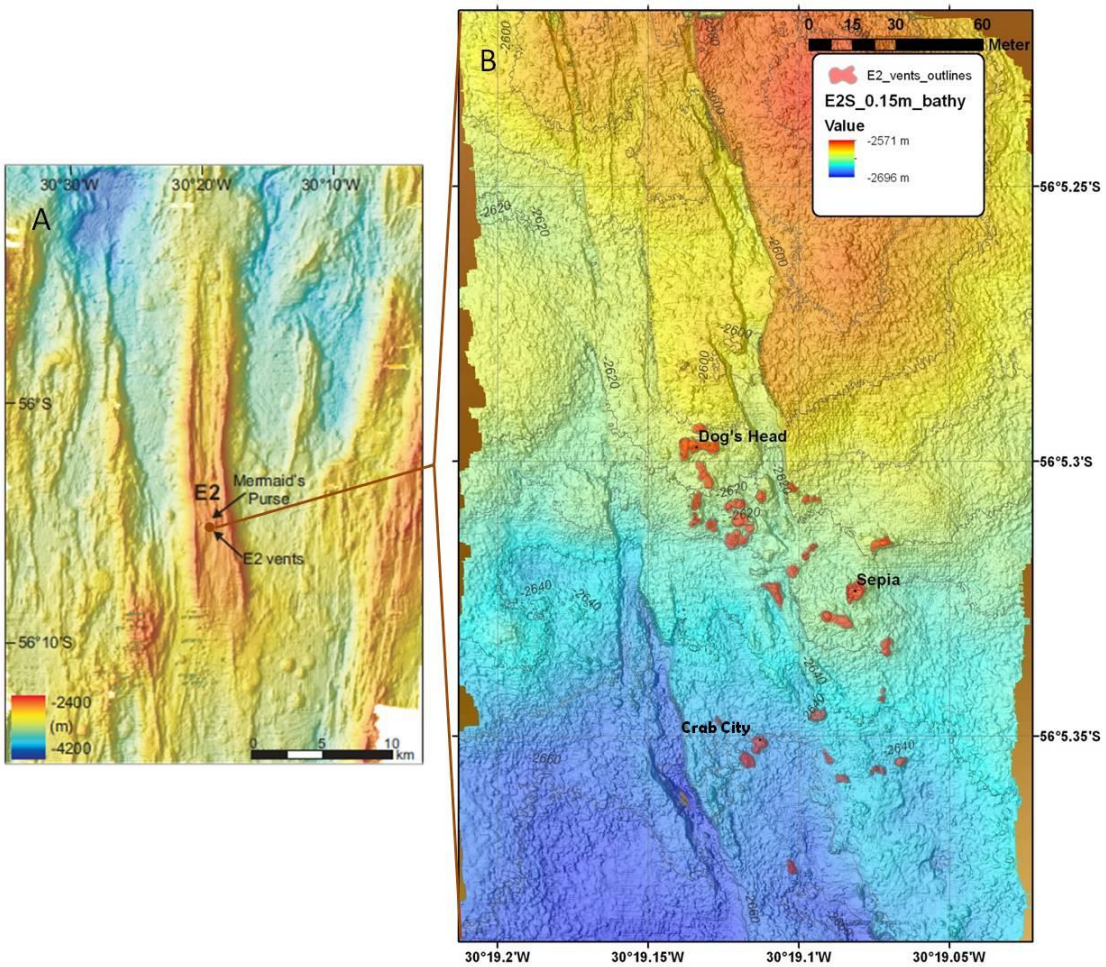

Figure 2.6 Ship and ROV-based swath bathymetry of ESR segment E2, showing (A) the 'Mermaid's Purse' topographic feature and the location of the E2 vents, and (B) an expanded view of the E2 vent field indicating the locations of Dog's Head, Sepia and Crab City sites.

2.3.2 The E9 vent field

There are two sites of high temperature hydrothermal activity at E9, located between 60° 02.5' and 60° 03.0' S and between 29° 59.0' and 29° 58.6' W at ~2400 m water depth (Figure 2.7). At the northern site, fluids issue from the ~10 m high 'Black & White' chimney at temperatures of up to 383 °C. At the southern site, high temperature fluids (348 – 351 °C) are expelled from three chimney structures. 'Ivory Towers' is located to the north of the site, and emits high temperature fluids through a number of exits, including clusters of 'beehive' diffusers. Approximately 50 m to the south of Ivory Towers two further structures, 'Pagoda' and 'Launch Pad', occur in close proximity.

In contrast to E2, the chloride concentration of the E9 fluids is distinctly lower than local bottom seawater, ranging from 98.2 mM at Black & White, to 179 mM at Launch Pad and 218 - 221 mM at Ivory Towers and Pagoda. This is attributed to phase separation of the fluids (James *et al.*, in review); note that the temperature of the Black & White fluids lies on the two-phase boundary for seawater at this depth (Bischoff and Rosenbauer, 1984). Consequently, concentrations of H_2S in the endmember fluids are higher (9.5 – 14 mM) than they are in the higher-Cl fluids from E2. The pH (3.08 – 3.42) and fluoride (34.6 – 54.4 μM) concentrations of the endmember fluids are similar to E2, indicating that input of magmatic volatiles is negligible (James *et al.*, in review). Sulphate concentrations of endmember fluids from the southern sites (Launch Pad, Ivory Tower and Pagoda) are close to zero (0.25 ± 0.71 mM), but considerably higher at Black & White (3.57 mM). This suggests that Black & White fluids are affected by input of anhydrite, either because of entrainment of chimney material during sampling, or dissolution of material precipitated at lower temperatures in the subsurface and incorporation into the fluids (James *et al.*, in review).

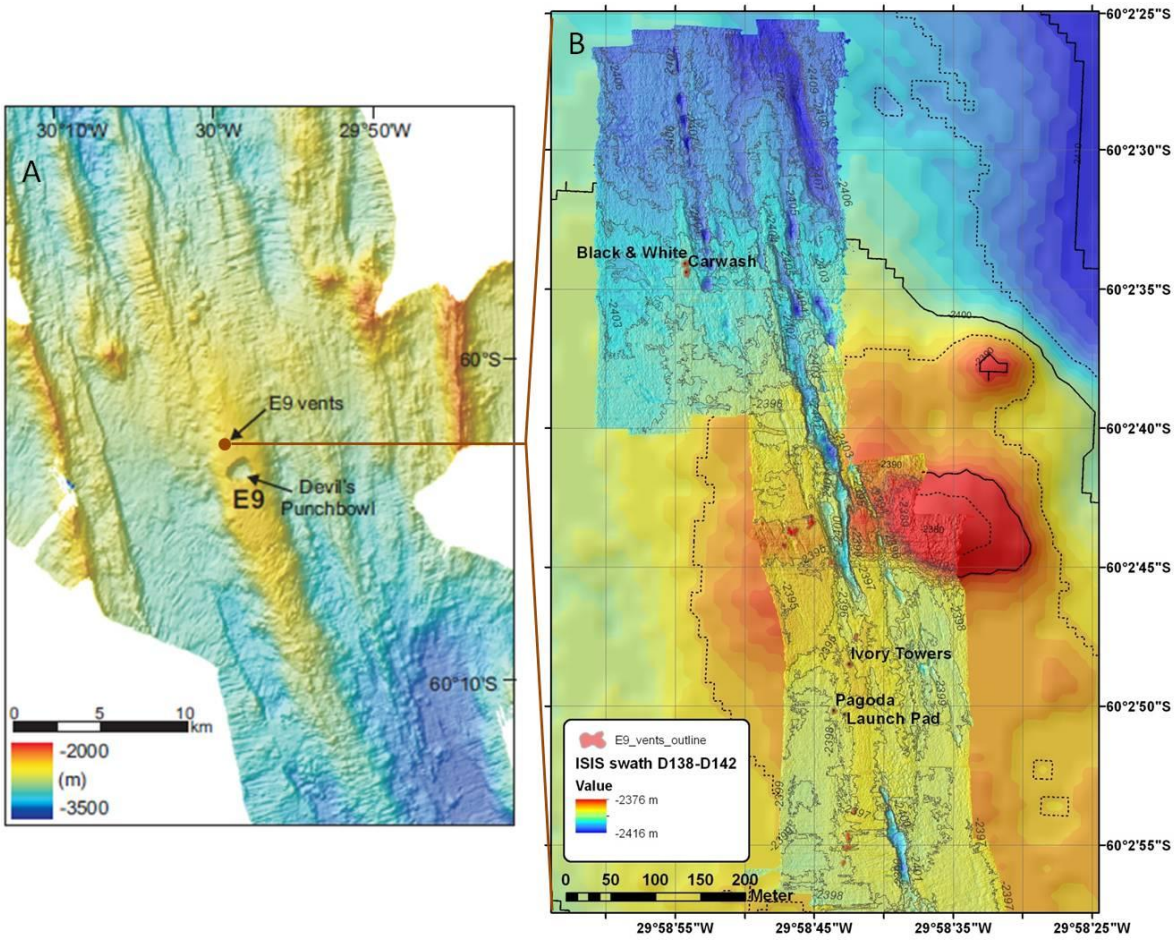

Figure 2.7 Ship and ROV-based swath bathymetry of ESR segment E9, showing (A) the Devil's Punchbowl collapse feature and the location of the E9 vents, and (B) an expanded view indicating the locations of Black & White, Ivory Towers, Pagoda and Launch Pad sites.

2.3.3 Kemp Caldera

Hydrothermal activity in the vicinity of Kemp Seamount occurs within a submarine volcanic crater located to its west, at 59° 42'S and 28° 18.59'W, in a water depth of ~ 1420m (Figure 2.8). White smoker-type fluids issue from friable chimney structures at temperatures of up to 212 °C to the west of the centre of the caldera, at a site named 'Winter Palace'. Low temperature (< 28 °C) diffuse fluids issue through a seafloor fissure at another site, called 'Great Wall', ~ 100 m to the northwest of Winter Palace. Sulphur-rich minerals precipitate from the Great Wall fluids, forming a ~50 cm high 'wall' along the fissure. The floor of the caldera is currently covered with sulphur and ash deposits, suggesting that there has been a recent volcanic blow-out event (Connelly *et al.*, in prep).

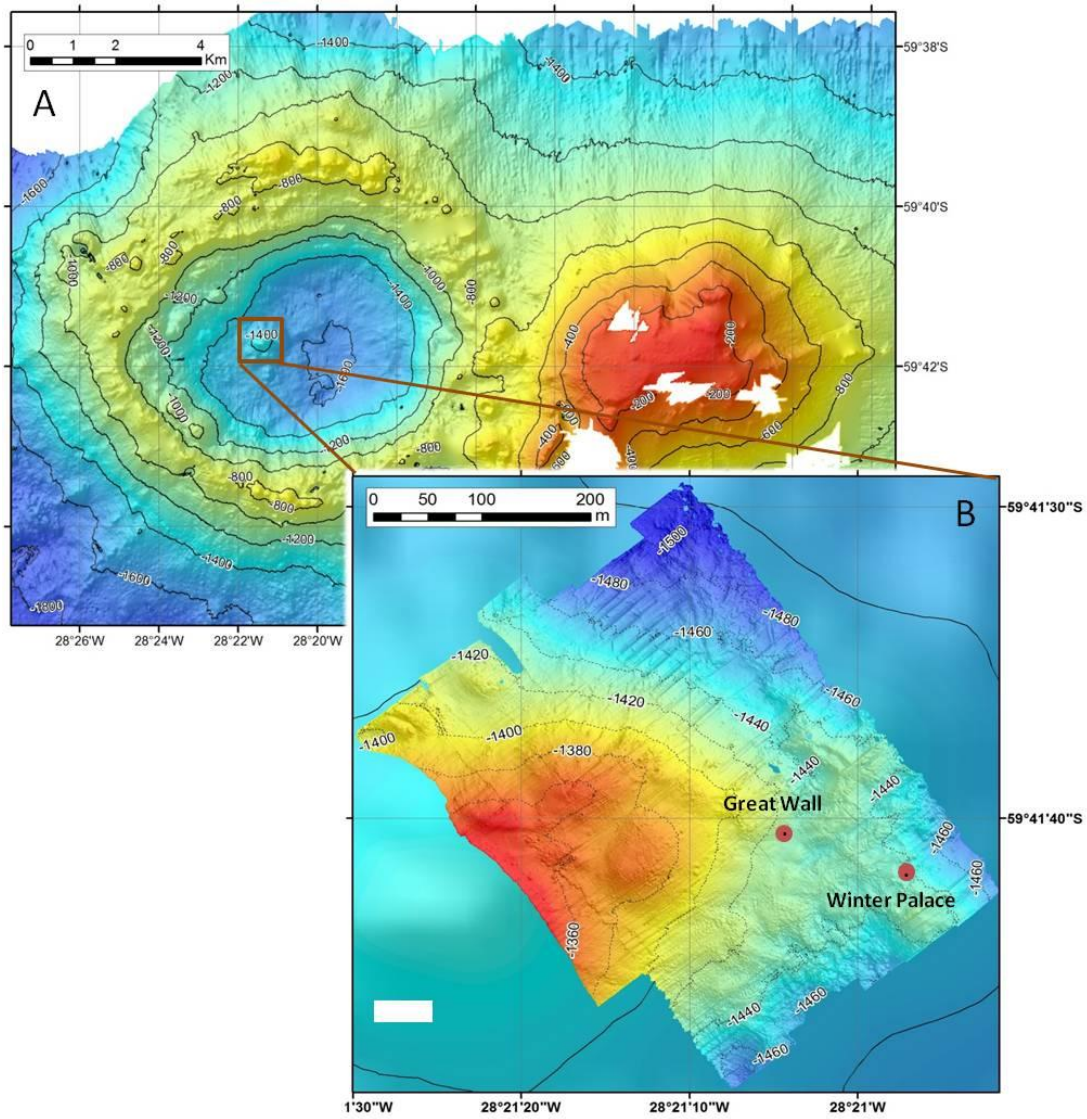

Figure 2.8 Ship and ROV-based swath bathymetry of the Kemp Caldera situated to the west of Kemp Seamount (A). An expanded view of the vent field (B) indicates the locations of Great Wall and Winter Palace hydrothermal fields.

Fluids recovered from Kemp have much higher concentrations of Mg (> 43 mmol/kg), relative to the high-temperature fluids sampled at the ESR (Table 2.1). This may be explained either by (i) dissolution of Mg-rich minerals, in which case the assumption that the endmember fluid has zero Mg is inappropriate, or (ii) the entrainment of a large volume of seawater (> 80%) during sampling. With regards to (i), widespread deposition of elemental sulphur, and the presence of liquid sulphur throughout the matrix of white smoker chimney walls, in addition to the elevated concentrations of H_2S and F^- in sampled fluids (Table 2.1), suggests that the vent fluids are affected by input of magmatic volatiles. Disproportionation of magmatic

SO_2 (Equation 2.1) produces sulphuric acid, which is thought to be the source of sulphate in 'acid sulphate' fluids venting in the eastern Manus Basin (Gamo *et al.*, 1997; Craddock *et al.*, 2010; Reeves *et al.*, 2011). These highly acidic fluids can leach Mg from minerals in the host rock during hydrothermal circulation, giving rise to a vent fluid that has Mg > 0 mmol/kg (Gamo *et al.*, 1997).

$$2H_2O + 3SO_2 \longrightarrow S + 2H_2SO_4 \quad (2.1)$$

Interestingly, none of the fluids sampled at Kemp are enriched in sulphate above seawater values, and pH (> 4.53) is relatively high (Table 2.1). Magmatic activity is likely to have been higher at this site in the recent past, and may now be waning. Despite continued input of magmatic volatiles, the composition of the hydrothermal fluids at Kemp is very different from the 'acid-sulphate' fluids from the Manus Basin. The high levels of H_2S (and F^-) in the Kemp fluids likely reflects subsurface mixing between a H_2S-enriched, low-chloride hydrothermal fluid, and SO_2 degassed from the mantle. The SO_2 is reduced to H_2S as it interacts with redox active mineral phases (Equation 2.2) over a long flow pathway (Giggenbach, 1987).

$$SO_2 + 6FeO + H_2O \longrightarrow H_2S + 6FeO_{1.5} \quad (2.2)$$

In the absence of very low pH or [Mg] higher than seawater in sampled fluids, it seems most likely that the high Mg values measured in Kemp fluids primarily reflect extensive seawater entrainment during sampling, as chimneys were exceptionally friable. Fluid temperatures up to 212 °C were recorded prior to sampling, confirming a high-temperature component, but this reduced to < 28 °C after insertion of the Ti syringe for fluid collection. Further, all of the major elements, and any element unaffected by precipitation, fall on a straight line when plotted against Mg. The only elements that produce a negative endmember value at Mg = 0 are SO_4, Sr and Ca (Table 2.1), which can be explained by precipitation of anhydrite in the subsurface. Consequently, whilst there is considerable uncertainty associated with such a large extrapolation, a zero-Mg endmember is suggested to exist at Kemp. Endmember fluids are likely to be strongly phase-separated as chloride is estimated to be very low (90 ± 37 mM), with substantial input of magmatic volatiles indicated by highly elevated concentrations of H_2S (200 ± 15 mM) and fluoride (1000 ± 108 μM), with very low pH (1 ± 1) (Table 2.1; Connelly *et al.*, in prep).

Table 2.1 Composition of sampled (lowest [Mg]) and end-member hydrothermal fluids recovered from the ESR and Kemp Caldera

Vent		Temp (°C)	Mg (m)	pH*	Na (m)	K (m)	Li (µ)	Cs (n)	Fe (µ)	Cu (µ)	Ca (m)	Sr (µ)	SO_4 (m)	Cl (m)	F (µ)	H_2S (m)
E2																
Dog's Head	*s.*	351	1.02	3.05	427	38.8	598	594	1350	1.56	30.0	103	3.7	528	42.8	6.9
	EM	**-**	**0**	**3.02**	**428**	**39.3**	**602**	**603**	**1280**	**19**	**30.7**	**102**	**1.3**	**536**	**39.1**	**6.7**
Sepia	*s.*	353	1.60	3.05	418	37.0	591	586	971	13.8	31.1	101	1.9	535	43.1	7.0
	EM	**-**	**0**	**3.05**	**419**	**38.1**	**606**	**598**	**1010**	**19**	**31.7**	**102**	**1.3**	**532**	**38.4**	**7.1**
E9																
Black & White	*s.*	383	0.58	3.52	99.1	5.53	114	63.6	803	26.1	5.53	16.4	2.2	106	40.3	8.2
	EM	**-**	**0**	**3.42**	**96**	**6.53**	**122**	**64.5**	**800**	**160**	**6.68**	**22.7**	**3.6**	**98.2**	**34.6**	**9.5**
Ivory Tower	*s.*	348	1.96	3.08	201	14.7	210	160	1070	13.9	5.79	26.7	0.8	227	42.3	10.8
	EM	**-**	**0**	**3.08**	**191**	**14.8**	**217**	**164**	**1210**	**85**	**6.01**	**25.4**	**0.3**	**220**	**40.1**	**11**
Pagoda	*s.*	351	0.84	3.44	196	14.8	215	158	831	32.4	6.42	27.6	1.3	227	54.7	10.5
	EM	**-**	**0**	**3.40**	**291**	**14.8**	**217**	**164**	**830**	**32**	**6.01**	**25.4**	**0.9**	**220**	**54.4**	**11**
Launch Pad	*s.*	351	4.45	3.21	188	12.2	156	112	1110	557	6.08	26.6	2.1	211	56.3	12.0
	EM	**-**	**0**	**3.21**	**163**	**12.4**	**170**	**123**	**2520**	**1530**	**5.68**	**20.8**	**-0.5**	**179**	**53.7**	**14**
Kemp Caldera																
Winter Palace	*s.*	28	43.0	4.53	392	9.11	27.7	8.59	2.36	1.96	8.53	70.9	21.6	462	250	30.5
Great Wall	*s.*	21	49.9	5.88	449	9.70	28.0	1.43	1.32	0.11	9.95	83.3	25.6	511	51.1	8.5
	EM	**-**	**0**	**[1 ± 1]**	**60 ± 12**	**5 ± 1**	**id**	**40 ± 8**	**id**	**id**	**-0.1 ± 1**	**-10 ± 12**	**-8 ± 3**	**90 ± 37**	**1000 ± 108**	**200 ± 15**
Seawater																
Bottom Seawater		-1 to 0	53.5	n.d	465	9.97	25.0	0.23	bdl	bdl	10.0	88.4	~28	540	nd	bdl

s: sampled fluids; **EM**: endmember fluids; **m**: mmol/kg; **µ**: µmol/kg; **n**: nmol/kg; *lowest measured value (except for Kemp Caldera endmember where the extrapolated pH is indicated in square brackets); **nd**: not determined; **bdl**: below detection limit; **id**: insufficient data to calculate endmember. Data from James *et al*., in review and Connelly *et al*., in prep. Kemp Caldera end-member values are reported with the standard error of each extrapolation to zero-Mg.

2.4 Hydrothermal Fauna

Antarctic chemosynthetic ecosystems define a new biogeographical province, distinct from known hydrothermal communities occupying the remainder of the global ocean (Rogers *et al.*, 2012). At E2 and E9, a new species of anomuran yeti crab, *Kiwa tyleri* nov. sp., which is closely related to *K. hirsuta* from the Pacific-Antarctic Ridge, dominates the macrofaunal assemblage (Figure 2.9) (Marsh *et al.*, 2012). *K. tyleri* are found in regions bathed by warm fluids close to chimney structures venting high-temperature fluids, in addition to areas of diffuse flow, and gain nutrition primarily by harvesting filamentous thiotrophic bacteria on their dense ventral setae (Reid *et al.*, 2013). The biomass of *K. tyleri* at the ESR vents is exceptionally high, especially as the decapoda are typically scarce in deep Southern Ocean waters (Hall and Thatje, 2010), and their niche as primary consumers is also unusual compared to the peripheral scavenging behaviour more commonly observed in vent-living crabs (Colaço *et al.*, 2002).

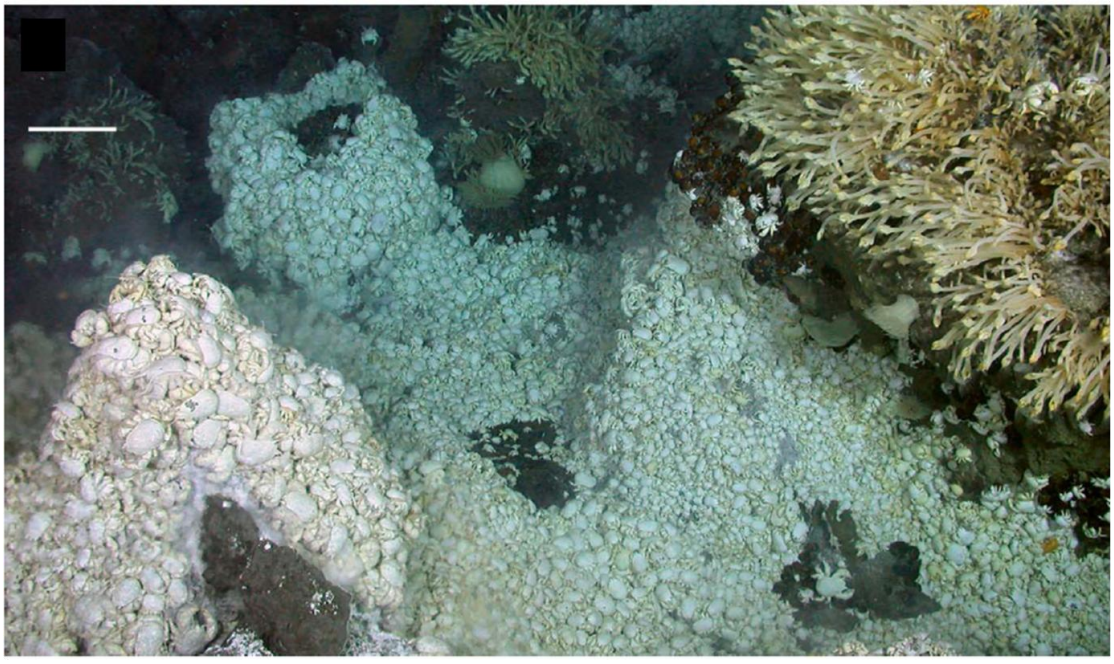

Figure 2.9 Photograph taken by the ROV ISIS of a dense population of *Kiwa tyleri* nov. sp. bathed in diffuse fluids (shimmering water) in the E9 vent field, East Scotia Ridge. Stalked barnacles can also be seen in the top right corner. The scale bar defines 10 cm (foreground). From Rogers *et al*. (2012).

A distinct distribution of *K. tyleri* based on sex and size is observed, with the largest males found closest to the vent orifices and non-berried females in slightly cooler waters, whilst berried females and juveniles are associated with low-temperature, often peripheral, diffuse fluids (Rogers *et al.*, 2012). The density of microbial episymbionts declines with increasing distance from the vent source, indicating optimal bacterial growth in the near-vent regions (Rogers *et al.*, 2012).

Other abundant fauna inhabiting the ESR vents include five morphospecies of sea anemone (Actinostolidae and Hormathiidae); peltospiroid gastropods; stalked barnacles (*Vulcanolepas* n. sp.); limpets (*Lepetodrilus* n. sp.); and predatory sea stars. It is interesting to note that the dominant taxa associated with vent ecosystems in the Atlantic, Pacific and Indian Oceans (e.g. polychaete worms, bathymodiolid mussels and alvinocaridid shrimp) are absent from these vent sites (Rogers *et al.*, 2012).

2.5 Summary

This chapter describes the key geological, oceanographic, hydrothermal and biological characteristics of the main study sites of this thesis. The East Scotia Ridge and Kemp Caldera host geochemically diverse hydrothermal vent fields, reflecting their differing geological settings (both back-arc and island-arc); the effects of phase separation; the influence of magmatic volatiles; and subsurface mixing with seawater. In addition, these vents host a unique faunal assemblage, defining a new Antarctic biogeographic province. Whilst hydrothermal vents are now known to be common features of seafloor volcanism, the discovery of new vent fields at high Southern latitudes, with distinct biogeochemical characteristics, opens new avenues for our understanding of hydrothermal systems and their global impact.

Chapter 3

3 Rare earth elements as indicators of hydrothermal processes within the East Scotia subduction zone system

The East Scotia subduction zone, located in the Atlantic sector of the Southern Ocean, hosts a number of hydrothermal sites in both back-arc and island-arc settings. High temperature (> 353 °C) 'black smoker' vents have been sampled at three locations along segments E2 and E9 of the East Scotia back-arc spreading ridge, as well as 'white smoker' (< 212 °C) and diffuse (< 40 °C) hydrothermal fluids from within the caldera of the Kemp submarine volcano. The composition of the endmember fluids (Mg = 0 mmol/kg) is markedly different, with pH ranging from 0.8 to 3.4, [Cl^-] from 88 to 536 mM, [H_2S] from 6.7 – 200 mM and [F^-] from 35 to 1000 μM. All of the vent sites are basalt-hosted, providing an ideal opportunity for investigating the geochemical controls on rare earth element (REE) behaviour. Hydrothermal fluids from E2 and E9 have total REE concentrations ranging from 7 – 127 nmol/kg, and chondrite-normalised distribution patterns are either light REE-enriched (La_{CN}/Yb_{CN} = 12.9 – 30.0) with a positive europium anomaly (Eu_{CN}/Eu^*_{CN} = 3.51 – 59.4), or mid REE-enriched (La_{CN}/Nd_{CN} = 0.61) with a negative Eu anomaly (Eu_{CN}/Eu^*_{CN} = 0.59). By contrast, fluids from the Kemp Caldera have almost flat REE patterns (La_{CN}/Yb_{CN} = 0.8 – 2.2; Eu_{CN}/Eu^*_{CN} = 1.0 – 2.2).

This work demonstrates that the REE geochemistry of fluids from the East Scotia back-arc spreading ridge is variably influenced by ion exchange with host minerals, phase separation, competitive complexation with ligands, and anhydrite deposition, whereas fluids from the Kemp submarine volcano are also affected by the injection of magmatic volatiles which enhances the solubility of all the REEs. It is also apparent that the REE patterns of anhydrite deposits from Kemp differ from those of the present-day fluids, potentially providing critical information about the nature of hydrothermal activity in the past, where access to hydrothermal fluids is precluded.

3.1 Introduction

The chemical properties of the rare earth elements (REEs) are fundamentally similar, and differences in their behaviour in natural materials and fluids can usually be attributed to atomic radii controls on their speciation and mobility (Elderfield, 1988). In hydrothermal environments, the distribution of the REEs provides important information about fluid evolution during subsurface circulation (Elderfield, 1988; Haas *et al.*, 1995), sources of fluid constituents and the extent of seawater mixing (Van Dover, 2000; Embley *et al.*, 2007; Craddock *et al.*, 2010), conditions of mineral deposition and venting history (Craddock and Bach, 2010) and the transport and fate of plume particulate material (German *et al.*, 1990; Bau and Dulski, 1999; Sherrell *et al.*, 1999).

Most hydrothermal fluids have remarkably uniform chondrite-normalised REE (REE_{CN}) distribution patterns, with enrichment in the light-REEs relative to the heavy-REEs and a positive europium anomaly (Michard and Albarède, 1986). This pattern has been observed in fluids from basalt-hosted hydrothermal systems on the Mid-Atlantic Ridge (Mitra *et al.*, 1994; James and Elderfield, 1996) and the East Pacific Rise (Michard *et al.*, 1983; Michard and Albarède, 1986), but also in fluids from the Lau Basin, where andesite and basaltic andesite dominates (Douville *et al.*, 1999), heavily-sedimented ridges such as the Guaymas Basin and Escanaba Trough (Klinkhammer *et al.*, 1994), and ultramafic-hosted vent systems including Rainbow (Douville *et al.*, 2002). Vent fluid REE_{CN} patterns are usually attributed to exchange of REEs during plagioclase recrystallisation (Campbell *et al.*, 1988b; Klinkhammer *et al.*, 1994; Douville *et al.*, 1999), but some studies indicate that REE speciation may also be an important control (Bau, 1991; Bach *et al.*, 2003; Allen and Seyfried Jr, 2005; Craddock *et al.*, 2010).

A recent study of hydrothermal fluids from the Manus back-arc basin has revealed a wide range of REE_{CN} distribution patterns, from fluids that are enriched in the heavy REE elements, to fluids with relatively flat REE_{CN} patterns (Craddock *et al.*, 2010). These different distribution patterns are attributed to differences in REE solubility due to variations in the relative abundance and stability of REE-chloride, fluoride and sulphate complexes as a function of fluid temperature, pH and ligand concentration. To this end, these authors suggest that the REEs can be used as tracers

for input of fluoride- and sulphur-rich magmatic volatiles in seafloor hydrothermal fluids.

To test whether variable REE_{CN} patterns are characteristic of arc and back-arc environments, REE concentrations were determined in hydrothermal fluids and chimney sulphates recovered from newly-discovered vent sites in the East Scotia subduction zone system (Rogers *et al.*, 2012). Two sites (E2 and E9) are located on the East Scotia Ridge (ESR) basalt-hosted back-arc spreading ridge; the other is a recently erupted submarine volcano (Kemp Caldera) that forms part of the South Sandwich Island volcanic arc (Chapter 2; 2.1). The chemical composition and temperature of the hydrothermal fluids (Chapter 2; 2.3) differs significantly between the sites (German *et al.*, 2000; Rogers *et al.*, 2012; Connelly *et al.*, in prep; James *et al.*, in review), allowing the controls on REE abundances and REE_{CN} distribution patterns to be examined. This study shows that the REEs can provide key information as to subsurface hydrothermal processes in back-arc and island-arc systems such as fluid-rock interaction, phase separation, secondary-mineral dissolution, and magmatic gas injection. Further, this work shows that deposits of anhydrite can preserve past fluid compositions and consequently record changes in hydrothermal and magmatic regimes.

3.2 Materials and methods

3.2.1 Sample collection and preparation

3.2.1.1 Focused and diffuse fluids

Focused and diffuse vent fluids were collected by ROV *ISIS* from E2, E9 and Kemp Caldera in 2010 during RRS *James Cook* cruise JC42. Titanium syringe samplers, equipped with an inductively coupled link (ICL) temperature sensor at the nozzle tip, were inserted into the chimney orifice to collect focused vent fluids. Diffuse fluids were collected using a specially-constructed Ti diffuse sampler to minimise seawater entrainment during sampling. The sampler was placed over the target area and allowed to equilibrate to a constant temperature reading before a fluid sample was taken. Back onboard, the fluids were transferred to acid-cleaned 1L HDPE bottles, and any solid material ('dregs') that had presumably precipitated as the sample cooled was rinsed from the Ti samplers into a 30ml acid-cleaned HDPE bottle. All samples were acidified to pH 2 using thermally distilled (TD) HNO_3.

Onshore, fluid samples were filtered through a polycarbonate membrane filter (0.2 μm; Whatman) and the filtrate was diluted with 2% HNO_3 for analysis of major elements. Particulate material retained on the filters was dissolved in 50% TD HNO_3 at 60 °C for several days, and then transferred to microwave digestion vessels for further dissolution as described in James *et al*., (in review). The solution was then dried down and re-dissolved in ~100 ml of 2% TD HNO_3 for metal analysis. The 'dregs' were filtered, dissolved, dried-down and re-dissolved in the same way. The concentration of the REEs was determined for each fraction, and the overall composition of the vent fluids was mathematically reconstituted.

3.2.1.2 Chimney samples

Samples of the uppermost section of the vent chimneys from Dog's Head (E2), Black & White, Ivory Towers and Launch Pad (E9) and Winter Palace (Kemp Caldera) were taken using the ROV manipulator arm and transferred to the ROV basket. Back on board the ship, the samples were photographed and their dimensions noted. Onshore, individual grains of anhydrite were handpicked from cut cross sections through the chimney wall using a binocular microscope. Mineral

identification was confirmed by X-ray diffraction (Philips X'Pert pro XRD) at the National Oceanography Centre, Southampton.

3.2.2 Analytical methods

3.2.2.1 REE concentration of fluids

Rare earth element concentrations in filtered fluid samples were determined by inductively coupled plasma mass spectrometry (ICP-MS; Agilent 7500) at GEOMAR, Kiel, using a SeaFast system for online matrix-removal and pre-concentration of the REEs following the method of Hathorne *et al.,* (2012). Indium (100 ppt) was used as an internal standard to monitor, and adjust for, signal drift. Based on replicate analyses (n = 8) of a well-characterised seawater sample from 2000 m water depth in the Southern Ocean (Circumpolar Deep Water, CDW, GEOTRACES sample ts PS71 131-1 (Hathorne *et al.*, 2012; Stichel *et al.*, 2012)), the external reproducibility of this method at the 95% confidence level (2σ) is < 10% for La – Pr, Eu, Dy – Lu; 11 – 17% for Nd, Sm, Yb, Tb and < 22% for Gd. The accuracy of this technique has been demonstrated in an inter-laboratory comparison study (van de Flierdt *et al.*, 2012).

The REE content of the particulate and dregs fractions was determined by ICP-MS (Thermo Fisher Scientific ELEMENT $_2$XR) at the National Oceanography Centre in Southampton. Single-element standards of Ba, Ce, Pr and Sm (Inorganic Ventures) were analysed alongside the samples to enable interference corrections to be made on Eu and the heavy REEs. Samples were calibrated against a set of five rock standards; BIR-1 and BHVO-2 (US Geological Survey), and JB-3, JA-2, JGb-1 (Geological Survey of Japan). Instrument drift was assessed by addition of internal standards (In and Re). Based on duplicate analyses of the rock standards, the external reproducibility (2σ) of the analyses is < 5% for La – Sm and Dy - Lu; < 8% for Eu and Tb and < 16% for Gd.

3.2.2.2 REE concentration of anhydrite

A minimum of 10 mg of anhydrite was dissolved in ~5 ml of Milli-Q water and a drop of 50 % TD HNO_3 by heating on a hotplate at 60 °C for several days. Once dissolved, the anhydrite sample was transferred into a 20 ml acid-cleaned LDPE bottle. A volume of fluid equivalent to 6 mg of anhydrite was sub-sampled, dried down and re-dissolved in 4 ml of 3 % TD HNO_3 spiked with 10 ppb In, Re, and 20

ppb Be as internal standards. Concentrations of the REEs, Y, and major cations (Ba, Ca, Sr) were determined by ICP-MS (Thermo Scientific X-Series) at the National Oceanography Centre, Southampton, calibrated against various rock standards and matrix-matched synthetic standards. The external reproducibility (2σ) of these analyses was < 4% for all of the REEs, based on duplicate analyses of the rock standards. The concentration of REEs in anhydrite was calculated by normalising to the mass of anhydrite, determined by the measured calcium concentration. Anhydrite is assumed to be the only source of REEs in each sample.

3.2.2.3 Sr Isotope composition of fluids and anhydrite

$^{87}Sr/^{86}Sr$ ratios in both the vent fluids and anhydrite were determined by thermal ionisation mass spectrometry (TIMS; VG Sector 54) at the National Oceanography Centre, Southampton. Sr was separated from a sub-sample of fluid or dissolved anhydrite containing ~1 μg of Sr by cation-exchange chromatography using Sr-spec resin (Eichrom). Matrix elements were eluted with 3M TD HNO_3, and the Sr fraction was collected in Milli-Q water, then dried down, re-dissolved in 1.5 μl of 1M TD HCl, and loaded with a Ta activator solution onto single Ta filaments. Analyses of the NIST987 Sr isotope standard, measured over the course of this work, give $^{87}Sr/^{86}Sr$ ratios of 0.710245 ± 0.000020 (2σ, n = 3), within error of the certified value (0.710250; National Institute of Standards and Technology).

3.3 Results

3.3.1 REE composition of hydrothermal fluids

Results of REE analyses of the fluids with lowest Mg recovered from each vent site are reported in Table 3.1. Of the samples collected from E2 and E9, all but 2 contain <5 mmol/kg Mg and thus consist of <10% bottom seawater. The zero-Mg end-member concentrations for these vents are calculated, as is the usual practise, by extrapolating from the composition of bottom seawater collected at each vent field, through the Mg concentration measured in the samples from a given vent. End-member concentrations are also given in Table 3.1.

Fluids recovered from Kemp Caldera have much higher levels of Mg (> 43 mM). As discussed in detail in Connelly *et al*. (in prep.), this is thought to be due to mixing with seawater in the subsurface prior to venting, and/or during the sampling procedure. Because the REEs do not behave conservatively during mixing with seawater, due to coprecipitation with iron and manganese (oxy)hydroxides and anhydrite (German *et al.*, 1990; Bau and Dulski, 1999; Sherrell *et al.*, 1999), it is not possible to accurately estimate the REE composition of the vent fluid endmember. For this reason, all subsequent discussion of the Kemp Caldera fluids will focus on REE_{CN} distribution patterns rather than absolute concentrations.

The total REE concentration (∑REE) of ESR endmember fluids varies from 30 - 40 nmol/kg at E2, to 127 nmol/kg at E9 North, and 7.3 - 8.2 nmol/kg at E9 South. This compares to a ∑REE value of 0.1 nmol/kg for background seawater (2000 m CDW) (Hathorne *et al.*, 2012).

REE distribution patterns, normalised to chondrite using values given in Taylor and McClennan (1985), are presented in Figure 3.1 together with representative patterns for fluids from basalt-hosted mid-ocean ridge systems (TAG, EPR, Two Boats) and the Manus back-arc basin (DESMOS, Snowcap), as well as Southern Ocean seawater from 2000 m depth (see Hathorne *et al*., 2012). Three distinct REE_{CN} patterns can be identified. Endmember fluids from E2 and E9 South are enriched in the light REEs (La_{CN}/Yb_{CN} = 25.4 and 30.0 for Dog's Head and Sepia, and 17.2, 17.1 and 21.9 for Ivory Towers, Pagoda and Launch Pad, respectively; Table 3.2) and have a positive europium anomaly (Eu_{CN}/Eu_{CN}* = 3.51 and 3.84 for Dog's Head and Sepia, and 14.3, 51.4 and 59.4 for Ivory Towers, Pagoda and Launch Pad, respectively). By

contrast, endmember fluids from E9 North are enriched in the middle REEs (La_{CN}/Nd_{CN} = 0.61; Nd_{CN}/Yb_{CN} = 21.1), and have a negative Eu anomaly (Eu_{CN}/Eu_{CN}* = 0.59). They also have extremely high REE concentrations (∑REE = 127 nmol/kg). Finally, white smoker and diffuse fluids sampled from the Kemp Caldera have almost flat REE patterns, with La_{CN}/Yb_{CN} = 0.8 – 2.2 and Eu_{CN}/Eu_{CN}* = 1.0 – 2.2.

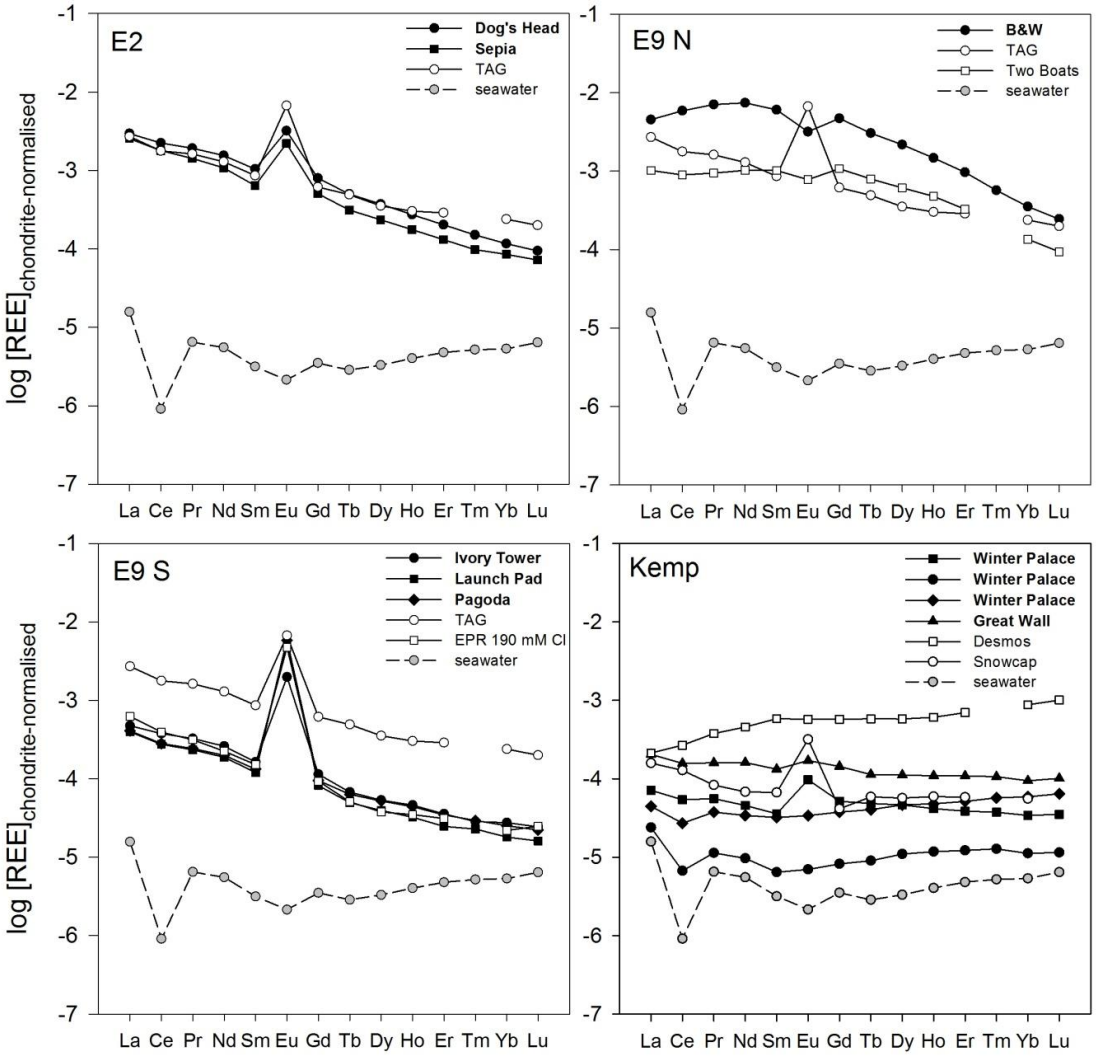

Figure 3.1 Chondrite-normalised REE patterns in endmember vent fluids from E2 (Dog's Head and Sepia), E9 North (Black & White) and E9 South (Ivory Tower, Launch Pad, Pagoda) on the East Scotia Ridge, and in sampled fluids from Kemp Caldera (Winter Palace and Great Wall). Data for other vent sites are from: Douville *et al*. (1999) (TAG, 17-19 °S East Pacific Rise, Desmos); Schmidt *et al*. (2010) (Two Boats); Craddock *et al*., (2010) (Snowcap). Data for Southern Ocean seawater were determined in this study; see also Hathorne et al. (2012).

Table 3.1 REE concentration of sampled (*s.*) and end-member (EM) hydrothermal fluids from the East Scotia Ridge and Kemp Caldera.

			T_{max} °C	Mg mmol/kg	La	Ce	Pr	Nd	Sm	Eu	Gd	Tb	Dy	Ho	Er	Tm	Yb	Lu	∑REE *nmol/kg*
E2																			
Dog's Head	130-B2-08	***s.***	323	2.28	8060	17,400	2200	9140	2060	1880	1900	233	1100	175	370	37	190	23	45
	130-B2-05	***s.***	323	2.11	8670	16,000	2000	8120	1800	2290	1800	201	955	155	321	34	175	21	42
	132-Y1-07	***s.***	351	1.02	6280	11,600	1360	5260	1060	1270	1000	117	566	94	215	23	130	16	29
		EM		**0**	**7950**	**15,600**	**1900**	**7790**	**1700**	**188**	**1620**	**191**	**908**	**146**	**313**	**32**	**171**	**21**	**40**
Sepia	135-B2-08	***s.***	347	1.61	6580	11,900	1340	5100	976	1210	960	111	533	88	191	20	119	15	29
		EM		**0**	**6790**	**12,200**	**1380**	**5260**	**1010**	**1250**	**986**	**114**	**549**	**91**	**197**	**21**	**123**	**16**	**30**
E9 North																			
Black & White	140-Y2-04	***s.***	380	0.58	9660	32,900	5740	30,100	7980	1450	7300	934	4320	643	1250	101	452	46	103
	142-Y2-01	***s.***	383	8.35	12,600	41,200	6880	36,500	9480	1890	9700	1120	5010	749	1420	120	483	53	127
		EM		**0**	**12,300**	**41,000**	**6990**	**36,900**	**9660**	**1860**	**9420**	**1130**	**5160**	**769**	**1470**	**122**	**514**	**54**	**127**
E9 South																			
Ivory Tower	142-B2-05	***s.***	348	1.96	1220	2480	306	1220	248	1090	220	24	121	23	52	5.8	39	5.2	7
		EM		**0**	**1260**	**2580**	**317**	**1270**	**257**	**1130**	**223**	**25**	**125**	**24**	**54**	**6.0**	**40**	**5.3**	**7.3**
Launch Pad	144-B1-02	***s.***	351	4.45	1010	1800	217	873	178	3250	150	18	89	18	37	5.2	26	4.2	7.7
	144-B1-03	***s.***	351	12.9	770	1360	167	671	140	2480	120	13	69	12	28	3.4	20	2.4	5.9
		EM		**0**	**1050**	**1880**	**228**	**915**	**189**	**3410**	**160**	**18**	**92**	**17**	**37**	**4.9**	**26**	**3.6**	**8.0**
Pagoda	144-Y1-06	***s.***	351	0.84	1129	2050	253	1050	223	3280	200	27	147	27	77	8.7	53	7.1	8.5
	144-Y1-07	***s.***	351	2.34	981	1700	207	844	184	3160	1200	19	95	18	33	4.2	24	3.2	7.4
		EM		**0**	**1090**	**1930**	**237**	**975**	**209**	**3320**	**186**	**23**	**124**	**23**	**56**	**6.7**	**39**	**5.2**	**8.2**
Kemp Caldera																			
Great Wall	147-Y2-04	***s.***	21	50.1	543	1070	155	783	208	97	280	41	260	56	163	22	136	22	3.8
Winter Palace	149-B1-02	***s.***	n/a	43.0	189	368	54	222	56	55	100	18	109	21	58	7.9	49	7.6	1.3
	152-Y2-01	***s.***	23	51.7	64	46	11	47	10	4.0	16	3.3	26	6.1	18	2.7	16	2.5	0.3
	152-Y1-06	***s.***	28	48.4	118	185	36	166	50	19	73	15	109	25	77	12	85	14	1.0
Seawater			0	53	42	6.2	6.3	27	5.0	1.2	6.8	1.0	7.7	2.1	7.2	1.1	7.7	1.4	0.1

s. = sampled fluids; EM = endmember fluids; n/a = not available; concentrations in pmol/kg unless otherwise stated.

Table 3.2 Temperature, [Cl], [Mg], [SO_4] and chondrite-normalised REE ratios of endmember fluids from the East Scotia Ridge and sampled fluids from Kemp Caldera, as well as other representative hydrothermal vent sites. The ratios La_{CN}/Yb_{CN}, La_{CN}/Nd_{CN}, and Nd_{CN}/Yb_{CN} allow comparison of, respectively, light to heavy (LREE/HREE), light to mid (LREE/MREE) and mid to heavy (MREE/HREE) REE abundance. The europium anomaly, (Eu_{CN}/Eu_{CN}*), where Eu* represents the averaged concentration of neighbouring REEs, Sm and Gd, is also given.

	T_{max} °C	$[Cl^-]$ mM	[Mg] mM	∑REE nM	La_{CN}/Yb_{CN}	La_{CN}/Nd_{CN}	Nd_{CN}/Yb_{CN}	Eu_{CN}/Eu_{CN}*	$[SO_4^{2-}]$ mM
East Scotia Ridge									
E2									
Dog's Head	351	536	0	40.2	25.4	1.92	13.3	3.51	1.31
Sepia	353	532	0	30.0	30.0	2.37	12.7	3.84	0.97
E9 North									
Black & White	383	98.2	0	127	12.9	0.61	21.1	0.59	3.57
E9 South									
Ivory Towers	348	220	0	7.3	17.2	1.82	9.47	14.3	0.26
Launch Pad	351	179	0	8.0	21.9	2.11	10.4	59.4	-0.47
Pagoda	351	220	0	8.2	17.1	2.05	8.24	51.4	0.96
Kemp Caldera									
Great Wall	21	511	50	3.8	2.16	1.27	1.70	1.23	25.6
Winter Palace	n/a	462	43	1.32	2.09	1.56	1.34	2.22	21.6
Mid-Atlantic Ridge									
TAG[Ŧ]	363	638	0	23.8	11.4	2.06	5.52	9.25	<0.2
Lucky Strike[Ŧ]	324	413	0	19.3	37.1	3.16	11.7	4.65	<0.2
Two Boats[λ]	412	298	0	104	5.79	0.80	7.23	0.53	-
East Pacific Rise									
Elsa, 13 °N[Ŧ]	340	723	0	45.3	14.8	1.78	8.30	7.94	<0.2
Nadir, 17-19 °S[Ŧ]	340	190	0	6.08	28.4	2.73	10.4	39.8	<0.2
Lau Basin									
Vai Lilli[Ŧ]	334	667	0	62.6	32.6	3.25	10.0	12.3	<0.2
Manus Basin									
Desmos[Ŧ]	87	490	51.5	7.84	0.24	0.46	0.53	1.01	32.2
Desmos[φ]	117	492	46.0	147	2.53	1.03	2.46	1.19	147
Snowcap[φ]	180	-	24.2	1.96	4.77	2.27	2.10	8.03	-

[Ŧ]Douville *et al.* (1999); [φ]Craddock *et al.* (2010); [λ]Schmidt *et al.* (2010). Only the samples with lowest [Mg] are shown for the Kemp Caldera and Manus Basin sites.

3.3.2 $^{87}Sr/^{86}Sr$ composition of vent fluids

The Sr isotopic composition of the endmember hydrothermal fluids is calculated by extrapolating measured values to (Mg/Sr) = 0. Lowest $^{87}Sr/^{86}Sr$ values were obtained for fluids from Sepia (E2; 0.704035), with more radiogenic ratios observed in phase separated fluids from Black & White at E9 North (0.705762), Ivory Tower (0.704610), Launch Pad (0.705014), and Pagoda (0.704890) at E9 South. These values are similar to those measured in fluids from other back-arc spreading systems, such as Lau Basin (0.7044 – 0.7056) and Manus Basin (0.70425 – 0.70435) (Fouquet *et al.*, 1991; Mottl *et al.*, 2011; Reeves *et al.*, 2011), and are higher than typical mid-ocean ridge fluids, such as TAG and 21°N EPR (0.7029 – 0.7034) (Palmer, 1992; Gamo *et al.*, 1996).

3.3.3 REE composition of chimney anhydrites

The REE-Y compositions of chimney anhydrites sampled from each vent site on the ESR and within the Kemp Caldera are presented in Table 3.3. Total REE abundance (∑REE) in anhydrite is much higher in chimney samples recovered from E9 North (24.3 ppm) than at any of the other vent sites (4.75 – 7.34 ppm at E2, 0.33 – 5.44 ppm at E9 South, and 0.61 – 5.19 ppm at Winter Palace, Kemp Caldera) (Table 3.4). At all sites, ∑REE is far higher for anhydrite than for the endmember hydrothermal fluids, by a factor of up to 1100 at E2, 1600 at E9 North and 5000 at E9 South. Differences in ∑REE between sites are mainly related to differences in the extent of seawater mixing in fluids from which the anhydrite precipitates (Table 3.4). The extent of seawater mixing is calculated from $^{87}Sr/^{86}Sr$ ratios by mass balance (Bach *et al.*, 2005):

$$\% \text{ seawater} = \frac{[(R_{HF} \times [Sr]_{HF}) - (R_{anh.} \times [Sr]_{HF})] \times 100}{[((R_{HF} \times [Sr]_{HF}) - (R_{sw} \times [Sr]_{sw}) - R_{anh.}) \times ([Sr]_{HF} - [Sr]_{sw})],}$$

where R is the $^{87}Sr/^{86}Sr$ ratio of endmember hydrothermal fluid (HF), anhydrite (anh.) and seawater (sw), and [Sr] is the concentration of Sr. Most anhydrite precipitates from a fluid consisting of >50% seawater (Table 3.4), but anhydrite from E9 North precipitates from a fluid that has undergone very little mixing with seawater, consisting of ~98% vent fluid.

Table 3.3 REE-Y concentrations (ppm) in hydrothermal chimney anhydrite from the East Scotia Ridge and Kemp Caldera

Sample ID	Sample Location	La	Ce	Pr	Nd	Sm	Eu	Gd	Tb	Dy	Ho	Er	Tm	Yb	Lu	Y
East Scotia Ridge																
130-9-S1	Dog's Head, E2	1.30	2.73	0.39	1.67	0.38	0.10	0.35	0.04	0.24	0.03	0.07	0.01	0.04	0.005	0.87
132-S11	Dog's Head, E2	0.80	1.65	0.24	1.12	0.29	0.03	0.27	0.04	0.18	0.03	0.06	0.007	0.04	0.005	0.71
140-S4-top	Black & White, E9N	2.53	7.65	1.36	7.04	1.82	0.36	1.79	0.21	0.99	0.15	0.28	0.02	0.10	0.01	4.18
142-S5	Ivory Towers, E9S	0.06	0.11	0.02	0.06	0.01	0.05	0.01	0.001	0.007	0.001	0.003	0.000	0.002	0.000	0.04
144-S7	Launch Pad, E9S	0.89	1.78	0.24	0.96	0.19	1.05	0.15	0.02	0.09	0.01	0.04	0.004	0.02	0.003	0.34
Kemp Caldera																
149-S11	Winter Palace	0.02	0.04	0.006	0.04	0.15	0.55	0.83	0.20	1.62	0.33	0.80	0.09	0.48	0.06	7.47
152-S13	Winter Palace	0.01	0.02	0.003	0.02	0.01	0.01	0.04	0.02	0.19	0.05	0.13	0.02	0.09	0.01	1.20
Mid-Atlantic Ridge																
957C-6W-1[a]	TAG	0.53	1.05	0.14	0.61	0.15	0.40	0.10	0.02	0.09	0.02	0.03	0.005	0.031	0.005	-
957H-5N-2[a]	TAG 2	0.64	1.32	0.20	0.95	0.33	0.88	0.26	0.04	0.20	0.03	0.06	0.006	0.032	0.003	-
123 ROV-4[b]	Two Boats, 5°S	1.39	2.78	0.40	2.05	0.59	0.13	0.70	0.10	0.53	0.09	0.19	0.02	0.09	0.01	2.81
139-415c[b]	Two Boats, 5°S	0.53	1.26	0.21	1.17	0.35	0.11	0.41	0.05	0.26	0.04	0.07	0.007	0.03	0.003	0.17
Manus Basin																
1188A-7R-1[c]	Desmos	1.37	3.77	0.60	2.98	0.91	0.31	1.36	0.23	1.59	0.37	1.15	-	1.37	0.24	9.89
1188A-7R-1[c]	Desmos	0.81	1.87	0.34	1.96	0.67	0.24	1.02	0.20	1.42	0.34	1.14	0.20	1.55	0.26	14.2
1188A_7R_1[d]	Snowcap	1.29	3.91	-	3.53	1.11	0.47	1.64	-	1.49	0.34	1	-	1.13	-	-
1188A_7R_1[d]	Snowcap	0.29	1	-	0.8	0.31	0.07	0.46	-	0.35	0.08	0.26	-	0.34	-	-

[a]Humphris, (1998); [b]Schmidt *et al*. (2010); [c]Bach *et al*. (2005); [d]Craddock and Bach (2010).

Table 3.4 Total REE concentration, REE ratios, and Sr isotope data for anhydrite samples from the East Scotia Ridge and Kemp Caldera. Data for anhydrites sampled from Mid-Atlantic Ridge and Manus Basin hydrothermal sites are also provided for comparison.

	∑REE ppm	La_{CN}/Yb_{CN}	La_{CN}/Nd_{CN}	Nd_{CN}/Yb_{CN}	Eu /Eu*	$^{87}Sr/^{86}Sr$	[Sr] ppm	% seawater
East Scotia Ridge								
E2 (Dog's Head 130)	7.34	21.6	1.50	14.4	0.85	0.70678	1520	55
E2 (Dog's Head 132)	4.75	14.3	1.37	10.4	0.35	0.70816	1050	82
E9 North (B&W)	24.3	17.1	0.69	24.7	0.61	0.70607	1310	2
E9 South (Ivory Tower)	0.33	16.6	1.78	9.31	13.9	0.70876	3330	73
E9 South (Launch Pad)	5.44	26.1	1.79	14.6	18.8	0.70669	2170	14
Kemp Caldera								
Winter Palace (149)	5.19	0.03	1.05	0.03	3.84	0.70658	2170	-
Winter Palace (152)	0.61	0.09	1.43	0.07	1.87	0.70886	3070	53
Mid-Atlantic Ridge								
TAG[a]	3.18	11.4	1.66	6.86	9.50	-	-	-
TAG[a]	3.56	12.2	1.21	10.1	8.55	0.70716	1490	68
TAG[a]	4.95	13.4	1.30	10.3	8.93	-	-	-
Two Boats[b]	9.04	10.1	1.30	7.78	0.62	-	-	-
Two Boats[b]	4.52	12.4	0.88	14.1	0.85	-	-	-
Manus Basin								
Pacmanus[c]	16.3	0.67	0.88	0.76	0.87	0.70835	3430	84
Pacmanus[d]	7.8	0.70	0.74	0.95	1.48	0.70856	2690	-

[a]Humphris, (1998); [b]Schmidt *et al*. (2010); [c]Bach *et al*. (2003); [d]Craddock and Bach (2010)

Chondrite-normalised REE distribution patterns for anhydrite samples from E9 (Figure 3.2) are similar to those measured in the hydrothermal fluids. Thus, samples from E9 South are enriched in the light REEs (La_{CN}/Yb_{CN} = 16.6 – 26.1; Table 3.4) and have a positive Eu anomaly (Eu/Eu* = 13.9 – 18.8), and samples from E9 North are enriched in the middle REEs (La_{CN}/Nd_{CN} = 0.7; Nd_{CN}/Yb_{CN} = 24.7) and have a small negative Eu anomaly (Eu/Eu* = 0.61). Normalisation of REE abundance to the vent fluids generates almost flat REE patterns, confirming that there is negligible fractionation of the REEs between anhydrite and the vent fluids (Figure 3.3).

By contrast, the REE_{CN} patterns of anhydrite recovered from E2 (Dog's Head) and Kemp Caldera (Winter Palace) are different from the vent fluid pattern. Like the

vent fluids, anhydrite from E2 is enriched in the light REEs (La_{CN}/Yb_{CN} = 14.3 – 21.6), but anhydrite has a negative, rather than a positive, Eu anomaly (Eu/Eu* = 0.3 – 0.9). At Kemp Caldera, anhydrite is strongly enriched in the heavy REEs relative to the light REEs (La_{CN}/Yb_{CN} = 0.03 – 0.09), whereas the vent fluids have relatively flat REE_{CN} patterns (Fig. 3.1). As a consequence, the vent fluid-normalised REE pattern for anhydrite from Kemp Caldera shows strong enrichment in the heavy REEs (Figure 3.3).

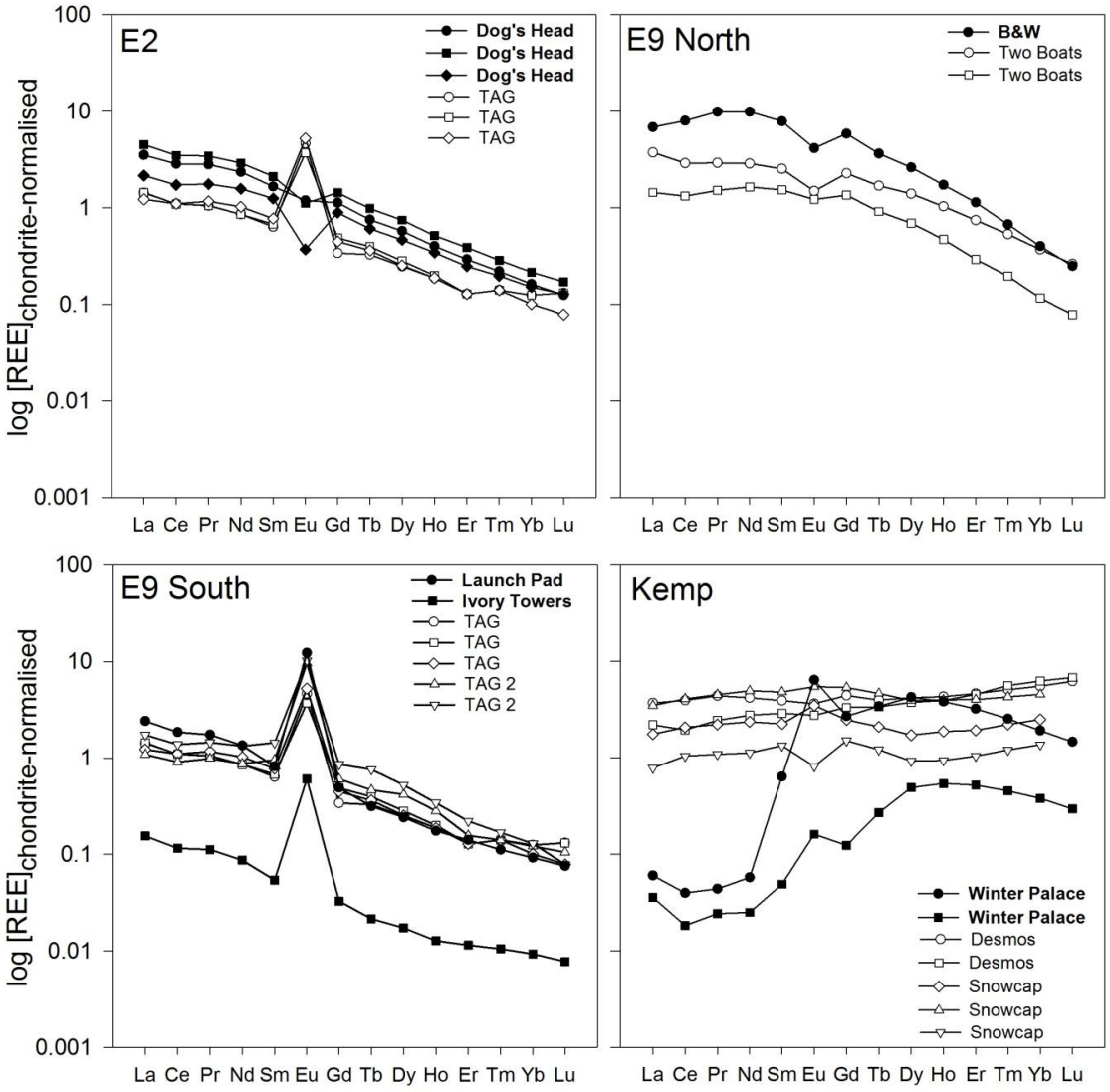

Figure 3.2 Chondrite-normalised REE distribution patterns for chimney anhydrite from E2 (Dog's Head), E9 North (Black & White), E9 South (Launch Pad and Ivory Towers), and Kemp Caldera (Winter Palace). Data for other vent sites are from: Humphris (1998) (TAG), Schmidt *et al*. (2010) (Two Boats), Bach *et al*. (2005) (DESMOS) and Craddock and Bach (2010) (Snowcap).

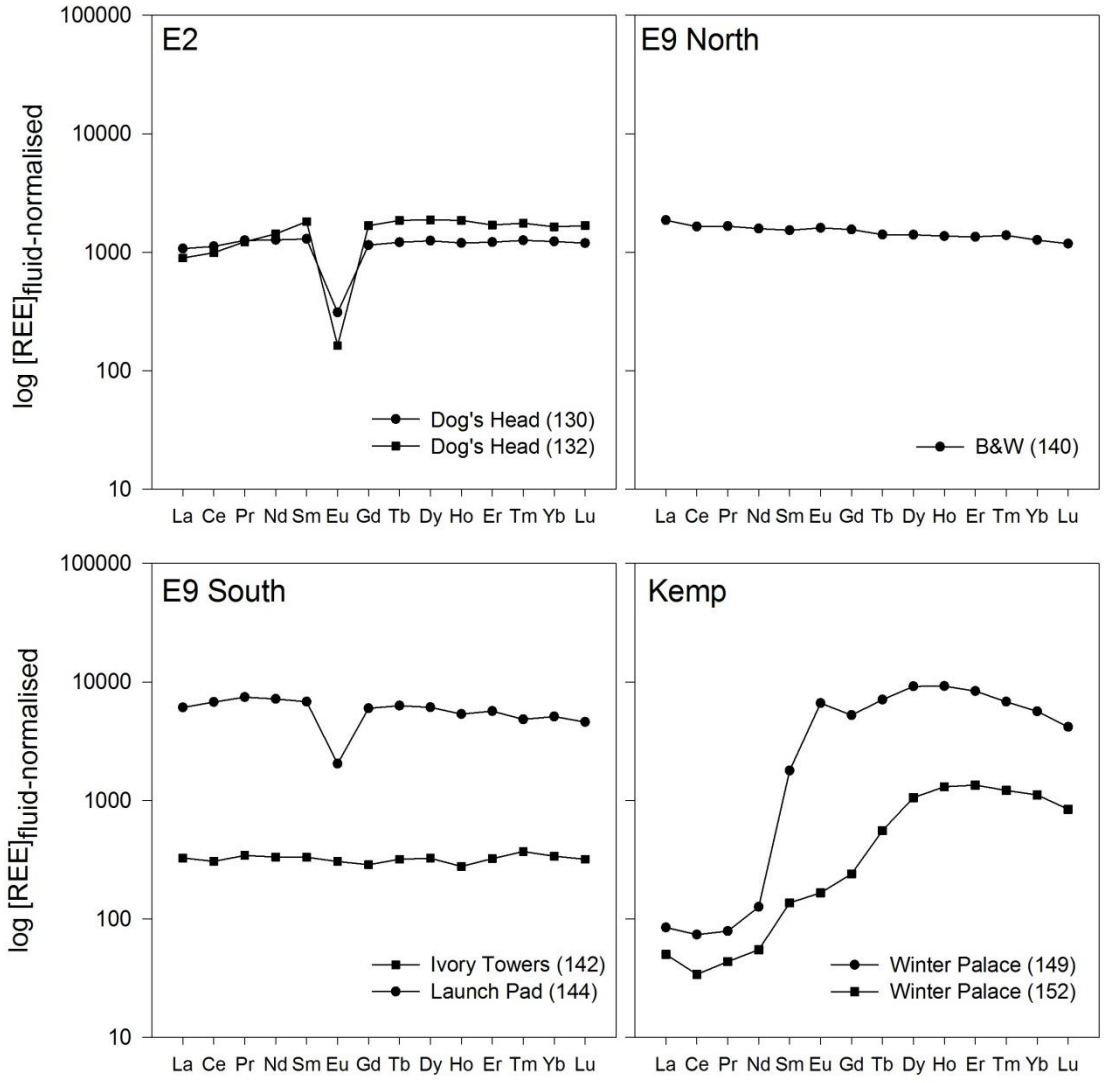

Figure 3.3 Vent fluid-normalised REE fractionation patterns for chimney anhydrite from E2 (Dog's Head), E9 North (Black and White Smoker), E9 South (Ivory Tower and Launch Pad), and Kemp Caldera (Winter Palace). Samples from the ESR are normalised to the endmember vent fluid composition; samples from Kemp Caldera are normalised to the composition of the vent fluid with lowest [Mg].

3.4 Discussion

Despite their close proximity, and similar host rock compositions, the REE_{CN} patterns of hydrothermal fluids and chimney anhydrite from the different vent sites are variable. The fluids are also different in terms of their pH, temperature, Cl, H_2S, F and SO_4 concentrations. Accordingly, these vent fluids can be used to identify the key controls on REE solubility in submarine hydrothermal fluids in subduction zone settings.

3.4.1 Host-rock influence

Hydrothermal fluids primarily derive their REE load through high-temperature reaction with basalts in the oceanic crust during subsurface circulation and are consequently highly enriched in all REEs compared with seawater (Michard *et al.*, 1983; Klinkhammer *et al.*, 1994). Comprehensive REE data for ESR and Kemp Caldera basalts, from dredge and wax core samples, are reported by Leat *et al*., (2000; 2004) and Fretzdorff *et al*., (2002). Basalts from the axial volcanic ridge of segments E2 and E9 have similar total REE concentrations (respectively, 65 - 78 and 60 - 75 ppm), and they are slightly enriched in the light REEs compared with the heavy REEs (La_{CN}/Yb_{CN} = 1.98 and 1.71). Basalts from Kemp Caldera have lower ∑REE (21 – 25 ppm) and relatively flat REE_{CN} patterns (La_{CN}/Yb_{CN} = 1.00). The main control on the REE composition of hydrothermal fluids is thought to be crystal-chemical exchange between plagioclase phenocrysts and seawater circulating in the reaction zone (Klinkhammer *et al.*, 1994). During hydrothermal alteration of plagioclase, the REEs are partitioned into the fluid phase in accordance to their ionic radius, with preferential dissolution of the larger ions. However, as europium is only stable as Eu^{2+} (which has a large ionic radius) under high temperature, reducing conditions, (Sverjensky, 1984), it is strongly enriched in hydrothermal fluids relative to its neighbours, Sm and Gd (Bau, 1991). Figure 3.4 demonstrates that partitioning of the REEs between the host rock and the vent fluids is similar to that of plagioclase during magma segregation at E2 and E9 South, suggesting that REE_{CN} patterns at these sites principally reflect discriminate leaching of REEs from plagioclase (Campbell *et al.*, 1988b; Klinkhammer *et al.*, 1994). By contrast, the middle REE enriched patterns of E9 North vent fluids, and the relatively flat REE patterns of Kemp Caldera vent fluids,

cannot be explained by plagioclase leaching and, if exchange reactions are involved, their original REE signatures must be overprinted by other processes.

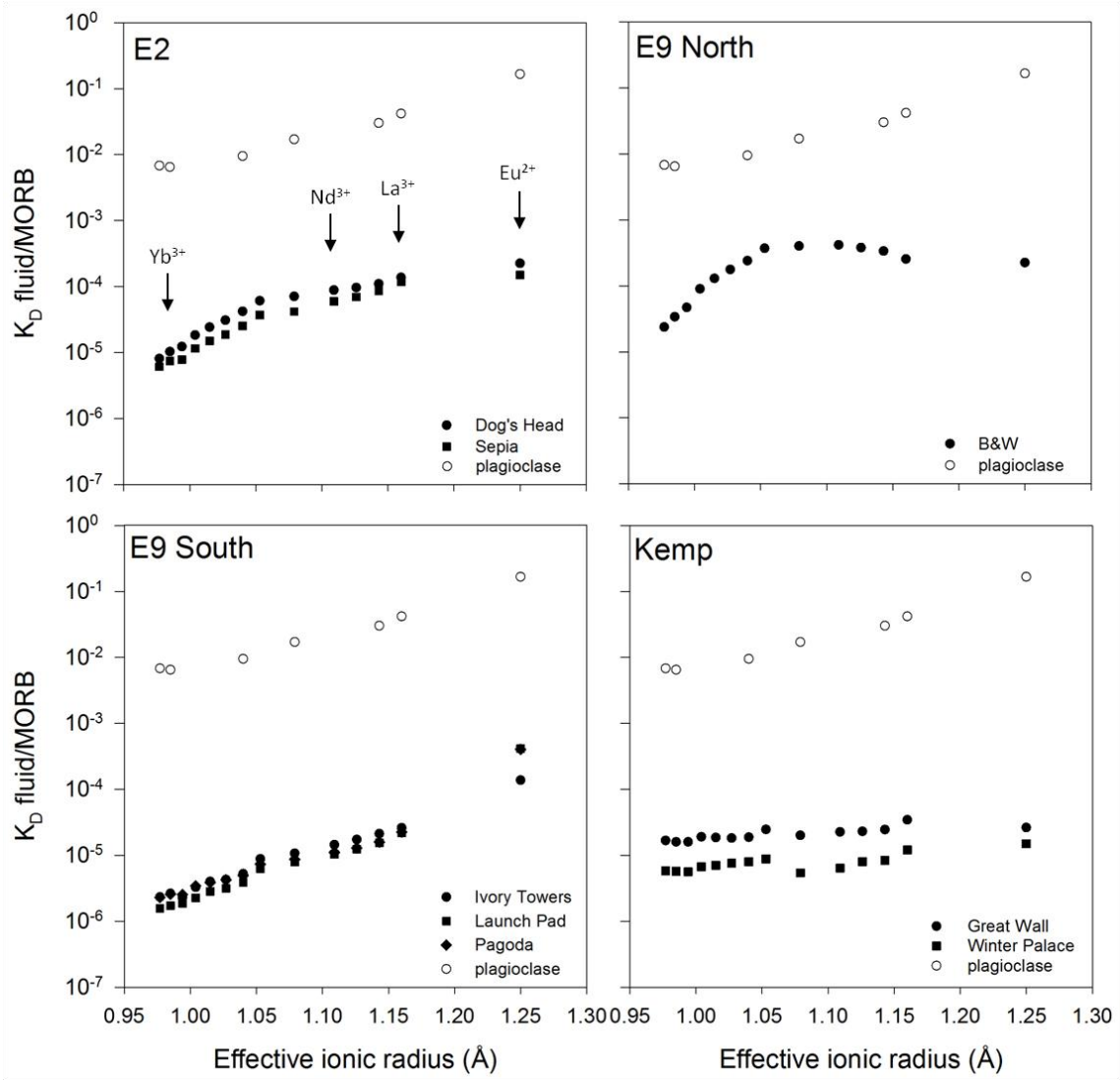

Figure 3.4 Distribution of the REEs between basalt and hydrothermal fluids, presented in terms of the partition coefficient, K_D, versus effective ionic radius (Å) in octahedral coordination (Shannon, 1976). Endmember and sampled (lowest Mg) fluids are used for ESR and Kemp, respectively. Data for basalts are from Leat *et al*. (2000; 2004); Fretzdorff *et al*. (2002). Also shown are K_D values for the REEs in plagioclase during magma segregation (Phinney and Morrison, 1990).

3.4.2 Influence of chlorinity and phase separation

The solubility of the REEs is strongly influenced by the availability of anionic ligands, which stabilise these elements in fluids through complexation (Wood, 1990b; Gammons *et al.*, 1996; Douville *et al.*, 1999). Chloride is typically a major constituent of hydrothermal fluids and speciation calculations indicate that, at

temperatures above 300 °C, 97 - 100 % of all REEs are stabilised as chloride complexes (Gammons *et al.*, 1996; Douville *et al.*, 1999). Chloride forms stronger complexes with the LREEs compared to the HREEs and is likely to be an important driver behind the light REE-enrichment observed in vent fluids from E2 and E9 South on the ESR, and for most mid-ocean ridge hydrothermal systems (Haas *et al.*, 1995; Migdisov *et al.*, 2009).

Endmember vent fluids at E9 South have typical mid-ocean ridge-type REE_{CN} patterns, i.e. they are enriched in the light REEs and have a positive Eu anomaly, but they have very low total REE concentrations, ~5 times lower than those measured at E2, and the Eu anomaly is more than an order of magnitude higher. Because of phase separation, the E9 South vent fluids have extremely low [Cl^-] (179 - 220 mM); thus low ∑REE values likely reflect the reduced availability of chloride ligands for complexation. Note that low [Cl^-] vent fluids from the East Pacific Rise also have low ∑REE (Table 3.2).

Although the effects of phase separation on the major-element chemistry of vent fluids have been well studied (Bischoff and Rosenbauer, 1984; Von Damm and Bischoff, 1987; Butterfield *et al.*, 1990; Auzende *et al.*, 1996; Charlou *et al.*, 1996; Coumou *et al.*, 2009), the effects on REE behaviour are less well known and, to our knowledge, there are no REE data in the literature for very low Cl fluids from subduction zone settings. REE concentrations tend to be higher in chloride-rich brines and lower in low-chloride fluids (Douville *et al.*, 1999; 2002), and low-Cl fluids tend to have larger Eu/Eu* anomalies (Douville *et al.*, 1999). Thermodynamic calculations suggest that Eu is more strongly complexed by ligands including chloride, fluoride and sulphate at 350 °C compared to Gd and Sm (Wood, 1990b), and experimental studies have indicated that Eu^{2+} has a stronger affinity for chloride relative to the trivalent REEs (Allen and Seyfried Jr, 2005). The fact that the low-Cl fluids at E9 South have a high Eu/Eu* anomaly suggests that Eu^{2+} has the strongest affinity for chloride, even when chloride concentrations are low.

3.4.3 Influence of magmatic volatiles

The chemical composition of hydrothermal fluids sampled at Kemp Caldera is markedly different from E2 and E9 fluids. Based on the assumption of a zero-Mg endmember (Connelly *et al.*, in prep), Kemp Caldera fluids have very high fluoride

(1000 ± 108 μM) and hydrogen sulphide (200 ± 15 mM) concentrations, and very low pH (1 ± 1). In comparison to the ESR, Kemp Caldera is located in close proximity to the subducting arc, where the entrainment of volatile gases (H_2O, CO_2, SO_2, HCl, HF) into circulating hydrothermal fluids (Reeves *et al.*, 2011) is likely to influence pH and the type and availability of anionic ligands (Bai and Koster van Groos, 1999). The distinctive composition of Kemp Caldera hydrothermal fluids, together with the widespread deposition of native sulphur (derived from disproportionation of SO_2 (Iwasaki and Ozawa, 1960; Gamo *et al.*, 1997; Reeves *et al.*, 2011)), is indicative of input of magmatically sourced acid volatiles (Connelly *et al.*, in prep).

These acid volatiles provide an additional source of anionic ligands capable of complexing with the REEs. The stability constants of REE-F complexes are significantly higher than those of REE-Cl, and fluoride complexes will dominate REE speciation in hydrothermal fluids where [F^-] is high (Wood, 1990b). Hydrothermal fluids from mid-ocean ridge settings typically have low [F^-] relative to seawater (Edmond *et al.*, 1979; Von Damm *et al.*, 1985), because mineral phases such as magnesite and magnesium hydroxide sulphate hydrate have a strong affinity for fluoride ions (Seyfried Jr and Ding, 1995). In arc settings, however, the release of HF by magmatic degassing (Aiuppa *et al.*, 2009) can generate fluids with high [F^-] and low pH, resulting in enhanced REE mobility in fluids as observed in the Eastern Manus Basin (Bach *et al.*, 2003; Craddock *et al.*, 2010; Reeves *et al.*, 2011).

This study supports this. Extrapolation of the Kemp Caldera fluid sample with lowest [Mg] to zero [Mg], which provides a minimum value for the REE content of the vent fluid endmember (because of precipitation; see Section 3.3.1), indicates that the endmember ∑REE value of Great Wall fluids is ~ 70 nmol/kg. This value is an order of magnitude higher than it is for fluids from E9 South (~ 8 nmol/kg), which have similarly low [Cl^-], suggesting that input of acid volatiles has significantly enhanced the solubility of the REEs.

Input of acid volatiles may also affect REE_{CN} distribution patterns. Fractionation between the LREEs and HREEs (La_{CN}/Yb_{CN}) and the size of the Eu anomaly (Eu_{CN}/Eu_{CN}*) in most vent fluids (including those from E2 and E9) decreases as the abundance of fluoride relative to chloride ([F^-]/[Cl^-]) increases (Figure 3.5). This is because stability constants for complexation of the REEs with chloride are

higher for the LREE than the HREEs (Wood, 1990b; Migdisov *et al.*, 2009), but this effect is reduced if fluoride concentrations are high as fluoride complexes of the heavy REEs are predicted to be more stable than those of the light REEs and Eu^{2+} (Wood, 1990b). However, experimentally determined formation constants for REE-F complexes in synthetic seawater solutions suggest that the stability of the HREE-F complexes at elevated temperatures (> 150 °C) have been significantly overestimated by theoretical calculations (Migdisov *et al.*, 2009). Further, Williams-Jones *et al.* (2012) indicate that fractionation of the LREEs from the HREEs in hydrothermal fluids is primarily controlled by temperature rather than fluid speciation, based on the observation that REE complexes with both chloride and fluoride are stronger for the LREEs than the HREEs at temperatures > 150 °C, and that this gradient in REE solubility across the group increases with temperature. Whilst these experimental observations support the importance of chloride complexation in REE fractionation in typical MOR-style hydrothermal fluids, they cannot explain the diversity in REE_{CN} patterns measured in high-temperature effluents at the Manus Basin. The REE data for Kemp Caldera does not support temperature control, as the fluids have flat REE distribution patterns even though measured in-situ temperatures are higher than 150 °C. In natural vent systems, pH and ligand concentration can be highly variable, and these parameters are likely to exert a strong influence on the relative solubility of the REEs. Indeed vent fluids from Kemp Caldera, and 'acid-sulphate' fluids from the Manus Basin (Craddock *et al.*, 2010), have low La_{CN}/Yb_{CN} and Eu_{CN}/Eu_{CN}* values for a wide range of F^-/Cl^-. These relatively flat REE_{CN} distribution patterns may be characteristic of very low pH fluids, as suggested by (Craddock *et al.*, 2010).

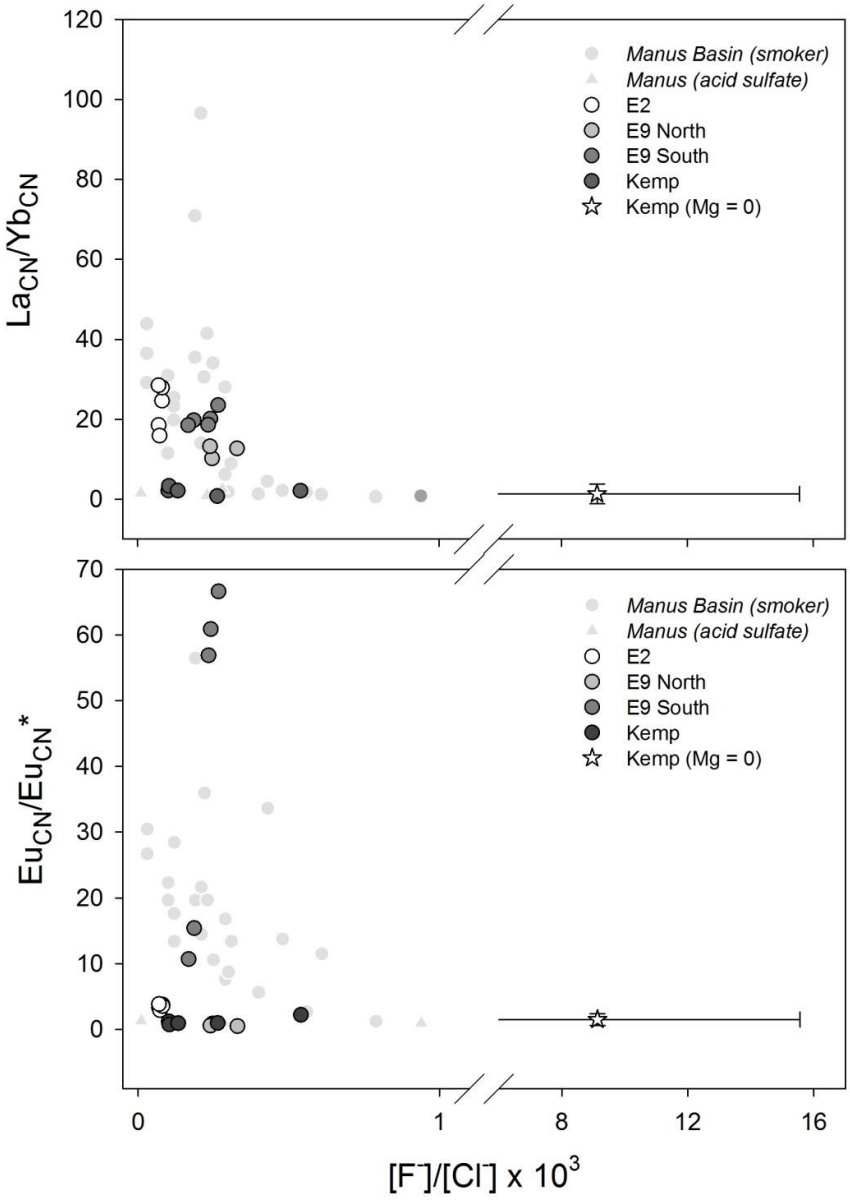

Figure 3.5 Relationship between (a) La_{CN}/Yb_{CN} and (b) Eu_{CN}/Eu_{CN}^* and fluoride/chloride ratio in sampled hydrothermal fluids from the East Scotia subduction zone system. For ESR fluids, only low Mg (< 8 mM) values are included, whilst both sampled (Mg > 43 mM) and estimated endmember (Mg = 0) fluids are shown for Kemp Caldera. Data for vent fluids from the Manus Basin (smoker- and acid sulphate-type) are also shown for comparison (Craddock *et al.*, 2010).

3.4.4 Influence of anhydrite

Anhydrite will precipitate in hydrothermal environments at temperatures > 150 °C, due to conductive heating of seawater or as high-temperature fluids mix with seawater. Anhydrite precipitation represents a major sink for rare earth elements in hydrothermal environments (Mills and Elderfield, 1995), and deposits of this mineral

within vent chimneys on the ESR and Kemp Caldera are enriched in the REEs by a factor of several thousand relative to hydrothermal fluids.

The rare earth element chemistry of hydrothermal fluids can therefore be strongly affected by anhydrite precipitation and dissolution (Craddock *et al.*, 2010). The large ionic radius of divalent Eu inhibits its partitioning into anhydrite, and the magnitude of the Eu anomaly in the remaining fluid is thought to be a proxy for the degree of fluid evolution in mid-ocean ridge systems (Humphris, 1998; Schmidt *et al.*, 2010). Figure 3.6 indicates that there is an inverse relationship between the size of the Eu anomaly and the total REE concentration in endmember fluids from the ESR. Fluids from Black & White (E9 North) have high ∑REE and a negative Eu anomaly, which may be indicative of an early evolutionary stage, prior to significant anhydrite deposition (Schmidt *et al.*, 2010). Similar fluid REE_{CN} distribution patterns have been described at the 'Two Boats' hydrothermal site at 5 °S on the Mid-Atlantic Ridge (Schmidt *et al.*, 2010). Very low vent fluid Cl concentrations, such as those measured in Black & White, are also thought to be indicative of very recent volcanic activity (Butterfield *et al.*, 1990; Haymon *et al.*, 1993; Von Damm *et al.*, 1995; Butterfield *et al.*, 1997). By contrast, fluids from E9 South have low ∑REE but large positive Eu anomalies which point to extensive subsurface anhydrite deposition, potentially augmented by longer reaction times, and strong Eu-Cl complexation.

Although the E9 North fluids appear to be unaffected by sub-surface anhydrite deposition, there is evidence for input of REEs from dissolution of anhydrite. The Black & White vent fluids have very high ∑REE, despite their low chlorinity (Douville *et al.*, 2002), a negative Eu anomaly and, unlike the other vent sites, they exhibit a positive correlation between ∑REE and [Ca] (R^2 = 0.72 compared with < 0.14 for all other sites; Figure 3.7). In addition, the sulphate concentration of the endmember fluids is ~4 mM, rather than zero as it is in most vent fluids (Von Damm, 1990). All of this suggests that the vent fluids are affected by dissolution of anhydrite, which makes up the inner wall of the Black & White chimneys (James *et al.*, in review). Addition of ~4 mM of SO_4 is equivalent to dissolution of 544 mg anhydrite per kg of vent fluid. Calculations indicate that < 1 g of anhydrite from the Black & White chimneys, added to 1 kg of a vent fluid unaffected by anhydrite dissolution (i.e.

the low Cl fluids from E9 South) readily generates a vent fluid with high ∑REE and a negative Eu anomaly, that is enriched in the middle REEs.

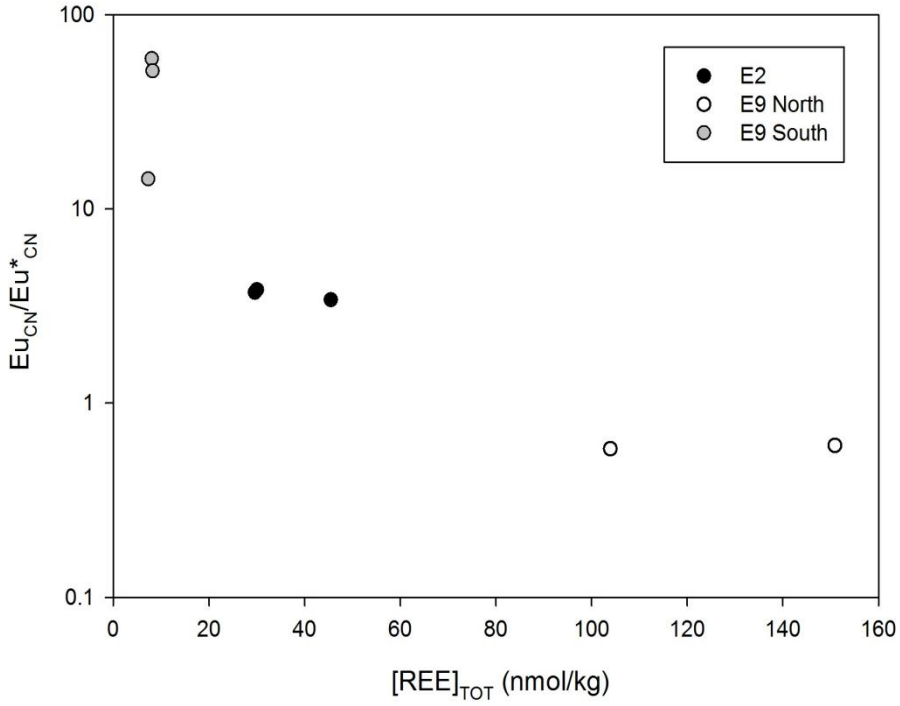

Figure 3.6 Chondrite-normalised Eu anomaly (Eu/Eu*) versus total REE concentration in endmember fluids from the ESR.

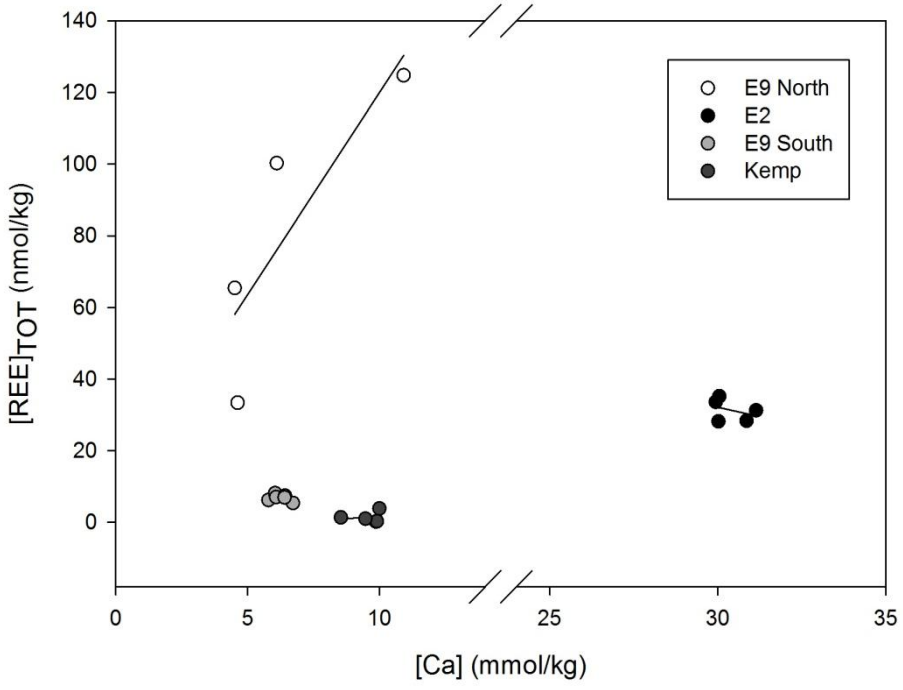

Figure 3.7 Total REE concentration versus Ca concentration in sampled fluids from E2, E9 North, E9 South and Kemp Caldera.

3.4.5 Anhydrite as a recorder of past vent fluid compositions

The distribution pattern of the REEs in anhydrites recovered from white smoker chimneys at Winter Palace in the Kemp Caldera is very different from that of the vent fluids being expelled today. The anhydrites are remarkably enriched in the HREEs (La_{CN}/Yb_{CN} = 0.03 – 0.09; Table 3.4), whereas the vent fluids have relatively flat REE_{CN} patterns, with La_{CN}/Yb_{CN} = 0.8 – 2.2. Thus, either the REEs are strongly fractionated during anhydrite deposition, or the anhydrite precipitated from a fluid that had a different composition from the fluids venting at this site today.

Rare earth elements are incorporated into the $CaSO_4$ lattice by substitution of Ca^{2+}, so crystallographic constraints dictate that ion exchange will favour those REEs with an ionic radius similar to calcium (Morgan and Wandless, 1980). Experimentally determined partition coefficients (K_D) for the REEs in solution and anhydrite are highest for Ce^{3+}, Nd^{3+}, and Sm^{3+}, so the MREEs should be preferentially incorporated into anhydrite (Kagi *et al.*, 1993; Schmidt *et al.*, 2010). However, REE distribution patterns in anhydrite recovered from the TAG hydrothermal site on the Mid-Atlantic Ridge, normalised to the vent fluids, are variable (Humphris, 1998), and K_D values for La, Ce and Nd are anomalously low (Mills and Elderfield, 1995). It has therefore been suggested that uptake of the REEs into anhydrite is principally controlled by fluid composition, because of the effects of complexation on the availability of free ions in fluids (Humphris and Bach, 2005). In support of this, variable REE distribution patterns in anhydrites from PACMANUS (including enrichments in the middle- and heavy-REEs) are considered to reflect variations in the concentration of magmatic volatiles in the vent fluids from which they precipitated (Craddock and Bach, 2010).

As the anhydrites sampled from Kemp Caldera are strongly enriched in the HREEs (Figures 3.2 and 3.3), REE uptake cannot be primarily controlled by crystallographic constraints. By contrast, if the REE composition of the anhydrite reflects that of the fluid, then composition of the vent fluids must have been different at the time the anhydrite was deposited. According to Craddock *et al*. (2010), HREE enrichments are favoured in hydrothermal fluids with high fluoride concentrations, and high F^-/Cl^- ratios, whereas enrichment of all REEs (and relatively flat REE_{CN} patterns, as observed in Kemp Caldera fluids today) is dependent upon very low pH.

As discussed in Chapter 2 (2.3.3) and Connelly *et al.* (in prep.), the floor of Kemp Caldera is covered in ash and sulphur deposits, which suggests that there has been a magmatic blow out event at this site in the recent past. Such a surge in magmatic activity would enhance the supply of REE-binding ligands, including F^-, and high temperatures would enhance phase separation which would increase the F^-/Cl^- ratio of the vent fluids, enhancing the mobilisation of the HREEs in particular (Wood, 1990b). As the path length for fluid flow is likely to have been reduced during a burst of magmatic activity, the extent of SO_2 disproportionation (Equation 2.1) in the subsurface may have been limited, so pH would be higher than it is today (1 ± 1; Section 2.3.3). Consequently, a strong efflux of magmatic HF would have provided free F^- for complexation, enhancing the concentration of HREE in fluids for incorporation into anhydrite. By contrast, the low pH of the fluids venting today results in non-selective REE mobilisation and limits the availability of fluoride as a complexing ligand, producing flat REE distribution patterns.

3.5 Summary and Conclusions

Rare earth element data are reported for a suite of high-temperature and diffuse hydrothermal fluids, and conjugate chimney anhydrite, for newly-discovered vent sites in the East Scotia Sea subduction zone system. High temperature fluids from E2 and E9 South are enriched in the light REEs and have positive Eu anomalies, like most vent fluids from basalt-hosted mid-ocean ridge spreading centres. This REE_{CN} pattern is best described in terms of differential leaching of the REEs from plagioclase, and stabilisation of the REEs as chloride complexes. The fluids appear to be unaffected by inputs of material from the nearby subduction zone. By contrast, fluids from E9 North are enriched in the middle REEs and have negative Eu anomalies, whereas fluids from Kemp Caldera have flat chondrite-normalised REE patterns. Fluids from E9 North appear to be affected by dissolution of anhydrite, which has high $\sum$REE and a negative Eu anomaly. Alternatively, E9 North may be a nascent vent system, with a relatively un-evolved REE pattern. At Kemp Caldera, REE solubility appears to be critically dependent on very low pH and strong complexation with magmatic ligands such as fluoride, similar to fluids from the Manus Basin back-arc system.

The REE_{CN} patterns of chimney anhydrites from E2 and E9 are similar to their conjugate high temperature fluids, but anhydrite recovered from the Winter Palace site at Kemp Caldera is strongly enriched in the heavy REEs relative to the vent fluids. These anhydrites may have precipitated from fluids that were strongly enriched in HF, introduced during a relatively recent magmatic blow-out event.

This study indicates that the REE composition of hydrothermal fluids can provide critical information about sub-seafloor geochemical processes associated with hydrothermal activity in subduction zone settings. These include reactions between host rock and circulating fluids, phase separation and fluid evolution, magmatic acid volatile degassing, and mineral precipitation. This study also shows that analysis of the REE composition of associated anhydrite deposits can provide insight as to the nature of hydrothermal activity in the past, where access to hydrothermal fluids is precluded.

Chapter 4

4 Metal Bioaccumulation in *Kiwa tyleri* sp. nov., a new vent-endemic species of anomuran decapod from the East Scotia Ridge, Southern Ocean

Dense aggregations of a new species of yeti crab (*Kiwa tyleri* nov. sp.) were discovered along hydrothermally active segments of the East Scotia Ridge, in the Atlantic Sector of the Southern Ocean, in 2010. Tissue metal accumulation was investigated in crabs from the 'Crab City' site on ridge segment E2, in relation to the metal composition of seawater. Both essential (Mn, Fe, Cu, Zn) and non-essential (Cd, As, Pb) metals were highly enriched in gill compared to other tissues, reflecting passive uptake during respiration. Significantly lower metal concentrations in hepatopancreas, and sometimes in muscle, suggest metal uptake may be regulated in these tissues. *K. tyleri* are primary consumers, feeding mainly on their episymbiotic bacteria, and may not be subjected to the trophic biomagnification of metals observed in the tissues of predatory vent-endemic crabs at other hydrothermal sites. This study also demonstrates a sex difference in the relationship between size and tissue metal concentrations. In females, the concentration of Mn, Fe, Zn, As and Cd in gill is positively correlated with carapace length, most likely because larger individuals live closer to the vent source, so metal concentrations are likely to be higher. In contrast, concentrations of toxic metals (Cd, As, Pb) and Fe in muscle tissue correlate negatively with carapace length in males, suggesting that metal regulation may be more important in males, and may vary between essential and non-essential metals. This is the first study to explore metal-organism relationships within a chemosynthetic ecosystem where crabs are the dominant macrofauna, residing in hot water close to a hydrothermal vent chimney. Understanding metal regulation in *K. tyleri*, living in large numbers south of the polar front, is particularly important as the decapoda are typically impoverished in the Antarctic.

4.1 Introduction

Early in 2010, the discovery of active hydrothermal vents along the East Scotia Ridge (ESR), first detected in the water column in 1998 (German *et al.*, 2000), revealed a unique chemosynthetically-driven ecosystem representing a new and distinct biogeographical province (Rogers *et al.*, 2012). High temperature (up to 383 °C) 'black smoker' and diffuse venting was observed along ridge segments E2 and E9 (James *et al.*, in review), supporting a high biomass dominated by a new species of anomuran crab, *Kiwa tyleri* nov. sp. (Thatje *et al.*, in prep). Vent-endemic crabs at other hydrothermal sites, including closely related species from the genus *Kiwa*, typically occupy the periphery of a vent field in relatively small numbers (MacPherson *et al.*, 2005). In contrast, *K. tyleri* on the ESR form dense aggregations (up to ~600 m^{-2}) close to chimneys venting high-temperature fluids (Marsh *et al.*, 2012). This niche is more typically associated with alvinocaridid shrimp along the Mid-Atlantic Ridge (Van Dover *et al.*, 1988), or alvinellid polychaetes in the Pacific (Chevaldonné and Jollivet, 1993).

One of the many stressors associated with living in a hydrothermal field, is elevated exposure to heavy metals (Sarradin *et al.*, 1999). Mixing between hot, metal-rich fluids and cold seawater defines steep chemical gradients and the metal load of seawater can change significantly over short distances. *K. tyleri* are primary consumers, feeding directly on filamentous thiotrophic bacteria cultured on their ventral setae (Marsh *et al.*, 2012; Reid *et al.*, 2013), so they tend to cluster close to the hydrothermal fluid source, where supply of reduced sulphide is high (Rogers *et al.*, 2012). Whilst several authors have reported on the trophic transfer and biomagnification of metals within chemosynthetic ecosystems (Cosson and Vivier, 1997; Colaço *et al.*, 2002), very few studies have investigated metal uptake in vent-living crabs (Peng *et al.*, 2011). Bioaccumulation and tissue compartmentalisation of metals in *K. tyleri* on the ESR are of particular interest due to their high biomass and low trophic position compared with many previously studied vent-endemic crab species (Colaço *et al.*, 2002; 2006; Kádár *et al.*, 2007), and their enhanced exposure to metals due to their occupation of sites very close to vent orifices.

Understanding strategies for detoxification in *K. tyleri* from hydrothermal vent sites in the Southern Ocean is important for knowledge of Antarctic biodiversity.

Reptant decapods are exceptionally sparse in deep water south of the polar front, perhaps owing to their inability to regulate haemolymph [Mg] at temperatures below 0.5 °C (Frederich *et al.*, 2000; Thatje and Arntz, 2004; Thatje *et al.*, 2005; Hall and Thatje, 2010). The dense populations of *K. tyleri* observed along the ESR indicate that warm waters associated with hydrothermal vents may have provided 'islands' of refuge during the extinction event associated with the cooling of the Southern Ocean during the Tertiary period (Clarke, 1990).

This study reports on the metal burden of a new species of Kiwaidae from deep-sea hydrothermal vent sites on the E2 segment of the ESR. *K. tyleri* were sampled in 2012 from a diffusely venting area known as Crab City, along with the warm fluids that surround the crab population. The vent systems of the ESR provide a new opportunity to investigate chemosynthetic relationships and community dynamics, within a high-latitude, deep Southern Ocean hydrothermal site.

4.2 Methods

4.2.1 Sample collection and preparation

Diffusely venting fluids from Crab City were collected by the remotely operated vehicle (ROV) *ISIS* during the RRS *James Cook* cruise JC80 in December 2012. Crab City is located at 56° 05.357' S, 30° 19.079 W, at a water depth of 2641 m (Figure 4.1). A specially-constructed diffuse sampler, consisting of a hollow titanium cone, open at both ends and with a heat-resistant 'skirt' fitted around the larger opening, was placed over the target area (Figure 1D). Fluids were collected by insertion of a Ti syringe sampler (750 ml), fitted with an inductively coupled link (ICL) temperature sensor at the nozzle tip, into the top of the cone. Entrainment of ambient seawater during sampling was minimised by delaying syringe activation until the temperature reading had stabilised. Two fluid samples were collected within a few minutes of each other (ISIS 189 Y2-01 and ISIS 189-Y2-04); the temperature of these fluids was 13.6 °C. Onboard the ship, fluids were analysed for pH and alkalinity by potentiometric Gran Titration with 0.05M HCl, using IAPSO seawater as a standard. The remainder of the fluid (~720ml) was transferred to acid-cleaned 1L HDPE bottles and acidified to pH < 2 using concentrated thermally distilled (TD) HNO_3 for metal analysis onshore.

Eighteen *K. tyleri* specimens (11 female and 7 male; 33 – 49 mm carapace length) were sampled from the same area immediately after fluid collection, using a suction sampler manipulated by ROV *ISIS*. Onboard, animals were dissected on ice for gill, hepatopancreas and cheliped muscle using a ceramic scalpel. Tissues were flash-frozen in liquid nitrogen and stored at -80 °C.

4.2.2 Analytical methods

4.2.2.1 Chemical composition of diffuse fluids

Metal concentrations (Mg, Fe, Mn, Cu, Cd, Zn, As, Pb) in the diffuse fluid samples were measured by inductively coupled plasma mass spectrometry (ICP-MS) (Thermo-Scientific X-Series) at the National Oceanography Centre, Southampton, following a 30-fold dilution with 3% TD HNO_3 containing Be (20 ppb), In (5 ppb) and Re (5ppb) as internal standards. Metal concentrations were calibrated against synthetic matrix-matched multi-element external standards, prepared using 1000 mg L^{-1} standard stock solutions in 3% TD HNO_3. The reproducibility of these analyses was better than 5% for all metals, based on replicate (n = 4) analysis of a mid-range standard.

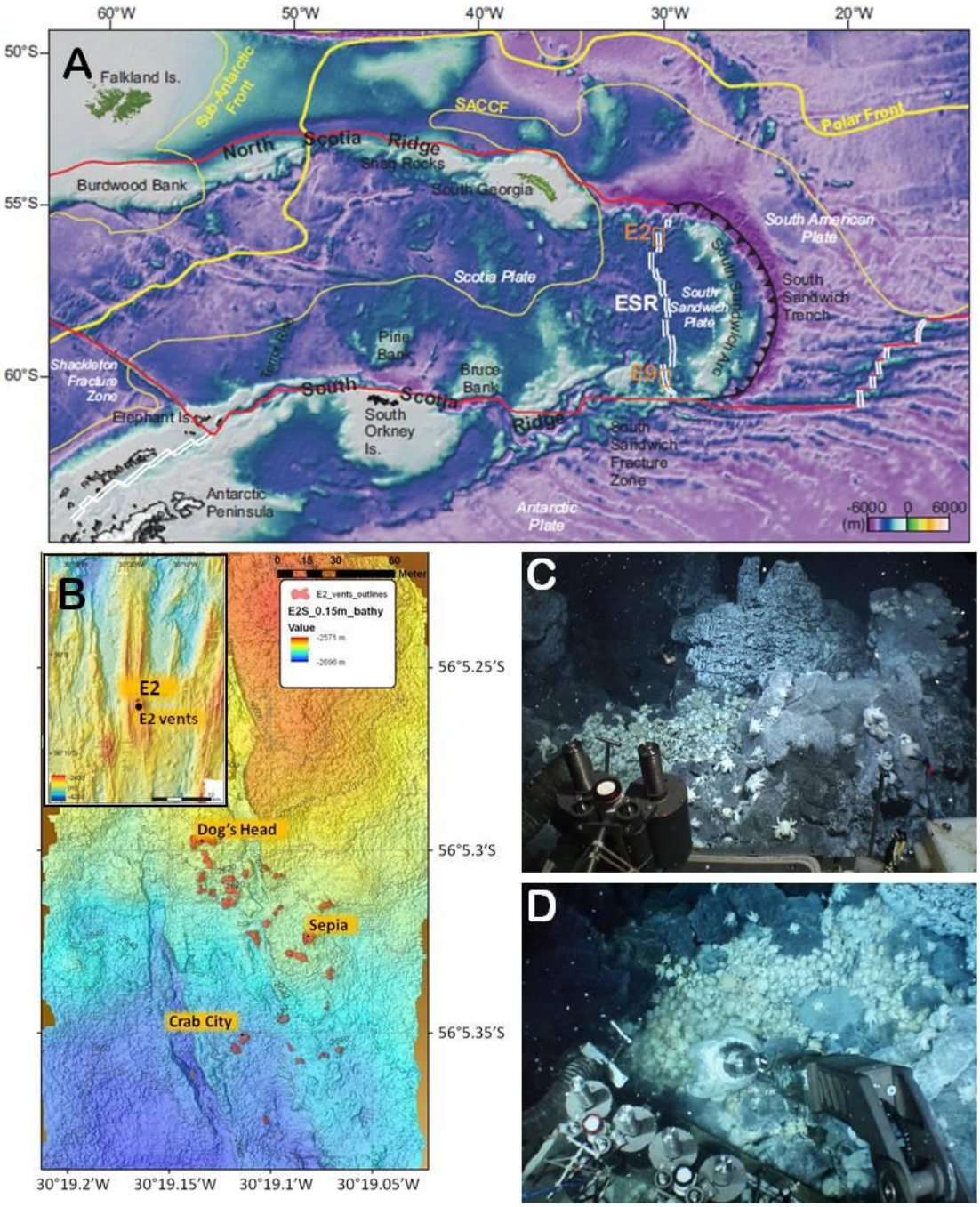

Figure 4.1 Location of the ESR and hydrothermal sites sampled for this study. (A) Map of the ESR within the Scotia Sea, indicating major plate boundaries and oceanographic features. Hydrothermally active ridge segments, E2 and E9 are indicated in orange. (B) Bathymetric map of E2 (insert), showing the location of the E2 vents; Dog's Head, Sepia and Crab City. (C) Photograph of shimmering water (< 40 °C) and the *K. tyleri* population at Crab City. (D) Diffuse sampler collecting fluids over the *K. tyleri* population.

4.2.2.2 Tissue metal concentrations

All tissue samples were freeze-dried and dry weight was recorded. An aliquot of ~ 50 mg was dissolved in concentrated thermally distilled (TD) HNO_3 by heating in a closed Savillex vial (15 ml) on a hotplate at 130 °C for ~24 hours. The digested samples were then dried-down at 130 °C and re-dissolved in 3% TD HNO_3 spiked with Be (20 ppb), In (5 ppb) and Re (5 ppb) as internal standards. Metal concentrations (Fe, Mn, Cu, Cd, Zn, As, Pb) were determined by ICP-MS (Thermo Scientific X-Series) at the National Oceanography Centre, Southampton. External standards were prepared using 1000 ppm standard stock solutions (Inorganic Ventures) in 3% TD HNO_3. Analytical precision was assessed through digestion and analysis of the certified reference material, lobster hepatopancreas TORT-2 (National Research Council of Canada), alongside the samples. Measured values deviated from certified values by < 5% (Mn, Fe, Cu, As) and < 7% (Zn, Cd, Pb) (Table 4.1), and the reproducibility of these analyses was better than 5% for all metals except Pb (< 8%). The concentrations of metals in the digest blank (TD HNO_3) and 3% HNO_3 were also determined and subtracted from the measured concentrations. The blank contribution was always < 6 % of the sample concentration. Metal concentrations are reported in $\mu g\ g^{-1}$ of the tissue dry weight.

Table 4.1 Comparison between measured and certified values of Mn, Fe, Cu, Zn, As, Cd and Pb ($\mu g\ g^{-1}$ dry weight) in the certified reference material, TORT-2. Measured values are the mean ± standard deviation (1σ) of 10 replicate analyses.

	Mn	**Fe**	**Cu**	**Zn**	**As**	**Cd**	**Pb**
Measured	14.2 ± 0.4	109 ± 5	102 ± 3	192 ± 3	21.8 ± 0.5	28.3 ± 0.7	0.37 ± 0.03
Certified	13.6 ± 1.2	105 ± 13	106 ± 10	180 ± 6	21.6 ± 18	26.7 ± 0.6	0.35 ± 0.13

4.2.3 Statistics

Tissue metal concentrations were non-normally distributed for both male and female *K. tyleri*. Consequently, non-parametric analyses of variance in the medians were performed by Kruskal-Wallis Mulitple Comparisons tests (K-W) to assess the differences between tissues and between each sex. In all cases, significant differences are reported at the 95% confidence level where $p < 0.05$. The strength and

significance of association between animal size (carapace length) and tissue metal content was measured using the Spearman Rank Order Correlation as data were non-normally distributed. Moderate (r_s = 0.6 to 0.8 or -0.6 to -0.8) and strong (r_s = 0.8 to 1.0 or -0.8 to -1.0) correlations are reported where $p < 0.05$.

4.3 Results

4.3.1 Chemical composition of diffuse fluids

The chemical composition of diffuse fluids from Crab City is given in Table 4.2, together with the composition of high-temperature fluids from the nearest chimney (Sepia), and background seawater (James *et al.*, in review). Magnesium concentrations in the diffuse fluids are > 52 mM, indicating that these fluids comprise ~98% seawater, whereas Mn (3.8 ± 0.1 mg L^{-1}), Fe (0.191 ± 0.001 mg L^{-1}), Cu (2.32 ± 0.02 μg L^{-1}), Zn (42.9 ± 0.6 μg L^{-1}), Cd (0.48 ± 0.02 μg L^{-1}) and Pb (0.73 ± 0.05 μg L^{-1}) are considerably enriched relative to seawater. Concentrations of As were below the limit of detection. The composition of fluids from other vents where metal studies have been conducted with decapod crab species are also reported in Table 4.2. These include shallow vents offshore Kueishan Island, Taiwan, where *Xenograpsus testudinatus* dominates the macrofaunal assemblage, and where the metal content of the surrounding fluids is relatively low (Chen *et al.*, 2005; Peng *et al.*, 2011). Also included are deep vents on the Mid-Atlantic Ridge (MAR) and 13 °N on the East Pacific Rise (EPR), where *Segonzacia mesatlantica* and *Bythograea thermydron*, respectively, occupy the periphery of the vent field (Bowers *et al.*, 1988; Cosson and Vivier, 1997; Desbruyères *et al.*, 2001; Colaço *et al.*, 2006). At these MAR and EPR sites, metal concentrations have not been reported for low temperature fluids within the crab habitats, but the metal composition of the high-temperature fluids can be used to make a first order comparison with the habitat of *K. tyleri* at E2. On the MAR, high-temperature fluids at Lucky Strike and Rainbow have approximately similar metal concentrations to Sepia, whilst endmember fluids at Menez Gwen typically have metal concentrations that are 1-2 orders of magnitude lower. The metal concentrations of high-temperature fluids from 13 °N on the EPR is similar, or slightly higher, to metal concentrations in Sepia fluids.

4.3.2 Tissue metal concentrations

Metal concentrations in gill, hepatopancreas, and muscle, of male and female *K. tyleri* (Figure 4.2), are reported in Table 4.3 together with data for other species of anomuran and brachyuran decapods from various deep-sea hydrothermal vent and polluted, shallow-water habitats. Between male and female *K. tyleri*, tissue metal content was not significantly different, with the exception of Mn, which was found to be significantly enriched in male gill compared to female gill ($p < 0.05$; K-W). In females, concentrations of Cd and Pb were highest in gill ($p < 0.05$; K-W), whilst Fe and Zn were significantly enriched in both gill ($p < 0.01$; K-W) and muscle tissues ($p < 0.05$; K-W) compared with hepatopancreas, and Pb was enriched in muscle compared with hepatopancreas ($p < 0.05$; K-W). The concentration of Mn was greater in hepatopancreas than gill ($p < 0.01$) and muscle ($p < 0.05$). There is no significant difference in As concentration between the different female tissues ($p > 0.05$; K-W). In males, concentrations of Fe, Cu, Zn, Cd and Pb were significantly enriched in gill compared with both hepatopancreas ($p < 0.01$; K-W) and muscle ($p < 0.05$; K-W), and gill was significantly enriched in As compared with muscle ($p < 0.01$; K-W). No differences were observed in Mn between tissues, nor in any metal between hepatopancreas and muscle in males ($p > 0.05$; K-W). Overall, metal concentrations were highest in gill in males, whilst in females Cd and Pb were highest in gill, whereas gill and muscle were equally enriched in Fe and Zn, and digestive gland was highest in Mn.

In female *K. tyleri*, positive correlations were observed in gill between carapace length and [Mn] ($r_s = 0.69$; $p < 0.05$), [Fe] ($r_s = 0.76$; $p < 0.01$), [Zn] ($r_s = 0.85$; $p < 0.001$), [As] ($r_s = 0.66$; $p < 0.05$), and [Cd] ($r_s = 0.83$; $p < 0.001$) (Figure 4.3). Correlations with size were strongest for Zn and Cd ($r_s > 0.8$). Hepatopancreas and muscle tissues showed no significant correlation between size and metal bioaccumulation in females. In male *K. tyleri*, no correlations were observed between size and metal concentration in gill, but concentrations of Fe, As, Cd and Pb were negatively correlated with carapace length in muscle ($r_s = -0.75$; $p < 0.05$ for Fe; $r_s = -0.71$; $p = 0.05$ for As; $r_s = -0.96$; $p < 0.001$ for Cd; $r_s = -0.93$; $p < 0.001$ for Pb), and Cu was negatively correlated with carapace length in hepatopancreas ($r_s = -0.79$; $p < 0.05$) (Figure 4.3). At the 90% confidence level ($p < 0.1$), Mn was also negatively correlated with carapace length in male hepatopancreas ($r_s = -0.64$).

Table 4.2 Chemical composition of diffusely venting fluids surrounding the *K. tyleri* population at Crab City on segment E2, ESR. Also shown is the composition of high-temperature fluids from the nearest vent (Sepia) at E2, and compositions of diffuse and high-temperature fluids from other vent sites where decapod crabs have been studied with respect to their tissue metal burden (see text for details).

Sample ID	**Location**	**Temp** (°C)	**Mg** (mM)	**pH**	**Alkalinity** (mEq/L)	**Mn** (mg/L)	**Fe** (mg/L)	**Cu** (µg/L)	**Zn** (µg/L)	**Cd** (µg/L)	**Pb** (µg/L)
1) E2 vent sites											
ISIS 189-Y2-01	Crab City (*Kiwa* n. sp.)	13.6	52.4	7.58	2.35	3.89	0.190	2.33	43.3	0.46	0.76
ISIS 189-Y2-04	Crab City (*Kiwa* n. sp.)	13.6	52.3	7.64	2.34	3.73	0.192	2.30	42.5	0.49	0.69
E2 Endmember	Sepia[†]	353	0	3.05	-0.80	113	56	1,210	10,500	n.m	n.m
2) Other vent sites hosting crab populations											
Shallow vents	Kueishan Is., Taiwan[‡]	78-116	43.9-54.4	1.52-6.32	n.m	<1.27	<9.88	0.01-233	0.07-91	0.001-0.53	0.04-57
	Kueishan Is., Taiwan[‡]	30-65	45.8-54.5	1.84-6.96	n.m	<0.12	<1.61	0.01-1.74	0.07-176	0.001-0.29	0.08-15.6
Deep vents	13 °N, EPR[θ]	380	0	3.3	-0.4	112	601	n.m	n.m	7.31	2.90
	Menez Gwen, MAR[β]	265-284	0	4.2-4.8	n.m	3.2-3.7	1.3-1.6	40-180	160-330	1.01-1.34	4.4-11.6
	Lucky Strike, MAR[β]	152-333	0	3.5-4.9	n.m	4.2-24.7	1.7-48	60-1650	330-3790	2.02-8.85	7.2-26.9
	Rainbow, MAR[β]	360-365	0	2.8-3.1	n.m	123	1339	8900	10,500	14.6	30.6
3) Seawater	ESR[†]	-1 to 0	53.5	7.68	2.4	0.003	0.0029	0.28	4.8	b.d	b.d

n.m = not measured; b.d = below detection

†(James *et al.*, in review), [‡](Chen *et al.*, 2005), [θ](Bowers *et al.*, 1988), [β](Colaço *et al.*, 2006)

Table 4.3 Mean concentration (μg g^{-1} dry weight ± SD) of Mn, Fe, Cu, Zn, As, Cd and Pb in gill, hepatopancreas and muscle in *K. tyleri* from the ESR (n = 18; 7 male and 11 female), compared with other vent-endemic anomuran and brachyuran decapods, and some examples of non-vent decapods from shallow, polluted sites.

Species Name	Location	Habitat	Sex	Mn	Fe	Cu	Zn	As	Cd	Pb
1. *GILL*										
***Kiwa* n. sp.**[a]	**E2, ESR**	**Deep vent**	**M**	**79 ± 76**	**2800 ± 3300**	**300 ± 120**	**2490 ± 290**	**20 ± 14**	**6.0 ± 4.2**	**197 ± 106**
			F	**31 ± 22**	**1100 ± 1200**	**310 ± 79**	**1000 ± 800**	**11.8 ± 6.8**	**3.5 ± 1.8**	**59 ± 28**
Bythograea thermydron[b]	13 °N, EPR	Deep vent		n.m	n.m	493 ± 18	1356 ± 69	14.6 ± 1.5	7.6 ± 0.2	n.m
Xenograpsus testudinatus[c]	Kueishan Island, Taiwan	Shallow vent		3.31 ± 1.31	159 ± 71.0	290 ± 91.4	610 ± 171	n.m	1.29 ± 0.97	2.28 ± 1.40
Scylla serrata[d]	Mahanadi Estuary, India	Estuarine (Poll.)	M	18.5 ± 1.7	190 ± 16.2	32.9 ± 2.9	42.2 ± 2.9	n.m	n.m	0.18 ± 0.01
			F	17.2 ± 0.9	183 ± 18.1	31.6 ± 2.4	52.8 ± 5.9	n.m	n.m	0.13 ± 0.01
Charybdia longicollis[e]	Iskenderun Bay, Turkey	Coastal (Poll.)		n.m	491 ± 161	827 ± 92.6	698 ± 118	n.m	75.5 ± 8.77	n.m
2. *HEPATOPANCREAS*										
***Kiwa* n. sp.**[a]	**E2, ESR**	**Deep vent**	**M**	**50 ± 25**	**305 ± 189**	**100 ± 164**	**200 ± 210**	**11.9 ± 4.9**	**0.7 ± 0.2**	**3.0 ± 2.4**
			F	**60 ± 35**	**210 ± 250**	**400 ± 300**	**320 ± 830**	**10.5 ± 4.8**	**1.1 ± 2.1**	**1.6 ± 1.9**
Segonzacia mesatlantica[f]	Rainbow, MAR	Deep vent		n.m	n.m	2850 ± 3329	108 ± 36	n.m	n.m	n.m
	Menez Gwen, MAR	Deep vent		n.m	n.m	150	439	n.m	n.m	n.m
	Lucky Strike, MAR	Deep vent		n.m	n.m	2840 ± 1238	133 ± 68	n.m	n.m	n.m
Bythograea thermydron[b]	13 °N, EPR	Deep vent		n.m	n.m	683 ± 16	442 ± 19	33 ± 1.3	3.8 ± 0.4	n.m
Xenograpsus testudinatus[c]	Kueishan Island, Taiwan	Shallow vent		3.95 ± 2.35	175 ± 99	53.4 ± 37.6	119 ± 66.8	n.m	n.m	2.64 ± 2.11
Charybdia longicollis[e]	Iskenderun Bay, Turkey	Coastal (Poll.)		n.m	685 ± 153	935 ± 50.5	805 ± 103	n.m	111 ± 22.3	n.m
Paralithodes camtschaticus[g]	Norton Sound, Bering Sea	Coastal (Poll.)		n.m	n.m	128	126	19.4	11.2	0.39
3. *MUSCLE*										
***Kiwa* n. sp.**[a]	**E2, ESR**	**Deep vent**	**M**	**38 ± 15**	**600 ± 450**	**129 ± 61**	**710 ± 270**	**6.0 ± 4.8**	**0.92 ± 1.17**	**42 ± 86**
			F	**32 ± 18**	**400 ± 140**	**102 ± 122**	**564 ± 83**	**11.1 ± 3.7**	**0.46 ± 0.18**	**4.9 ± 2.0**
Segonzacia mesatlantica[f]	Rainbow, MAR	Deep vent		n.m	n.m	125 ± 27	271 ± 15	n.m	n.m	n.m
	Menez Gwen, MAR	Deep vent		n.m	n.m	47 ± 7	111 ± 42	n.m	n.m	n.m
	Lucky Strike, MAR	Deep vent		n.m	n.m	125 ± 67	268 ± 37	n.m	n.m	n.m
Xenograpsus testudinatus[c]	Kueishan Island, Taiwan	Shallow vent		0.69 ± 0.5	37.0 ± 21.7	74.6 ± 27.1	230 ± 41.8	n.m	n.m	1.83 ± 0.71
Scylla serrata[d]	Mahanadi Estuary, India	Estuarine (Poll.)	M	12.8 ± 1.3	160 ± 13.2	114 ± 10.4	279 ± 19.6	n.m	n.m	0.19 ± 0.01
			F	11.2 ± 1.3	171 ± 12.9	132 ± 13.0	313 ± 28.6	n.m	n.m	0.23 ± 0.01
Charybdia longicollis[e]	Iskenderun Bay, Turkey	Coastal (Poll.)		n.m	n.m	72.0	172	16.5	0.24	0.54
Paralithodes camtschaticus[g]	Norton Sound, Bering Sea	Coastal (Poll.)		n.m	32.8 ± 7.31	77.6 ± 12.0	32.5 ± 7.03	n.m	25.4 ± 7.84	n.m

n.m = not measured; (Poll.) = polluted site; Refs: [a]This Study; [b](Cosson and Vivier, 1997); [c](Peng *et al.*, 2011); [d](Mohapatra *et al.*, 2009); [e](Firat *et al.*, 2008); [f](Colaço *et al.*, 2006); [g](Jewett and Naidu, 2000).

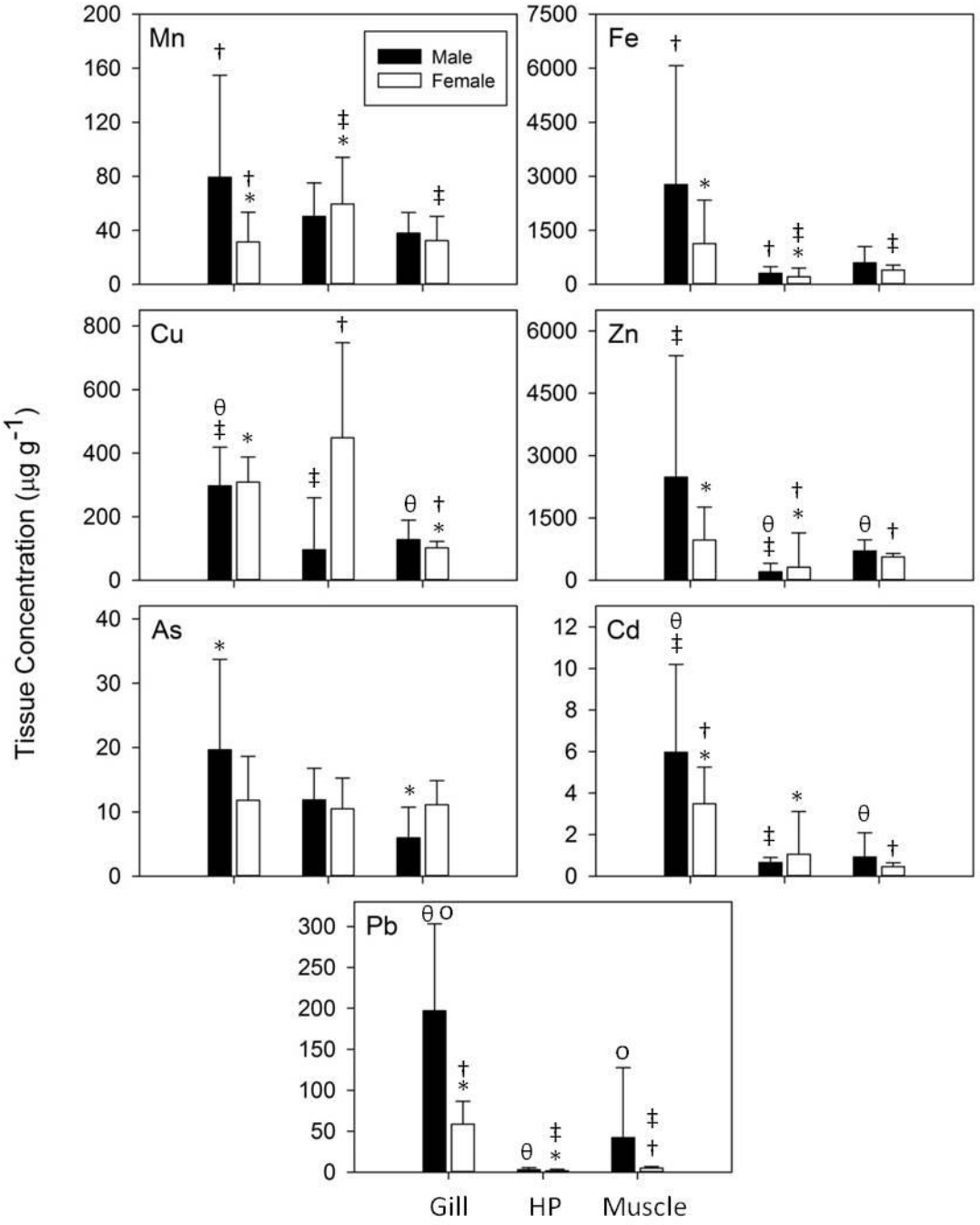

Figure 4.2 Average concentrations (µg g^{-1} dry weight) of Mn, Fe, Cu, Zn, As, Cd and Pb in gill, hepatopancreas (HP) and muscle tissues of male and female *K. tyleri* collected from Crab City. Significant differences between tissues or between sex ($p < 0.05$; K-W) are indicated by symbol pairs (*, †, ‡, θ, o).

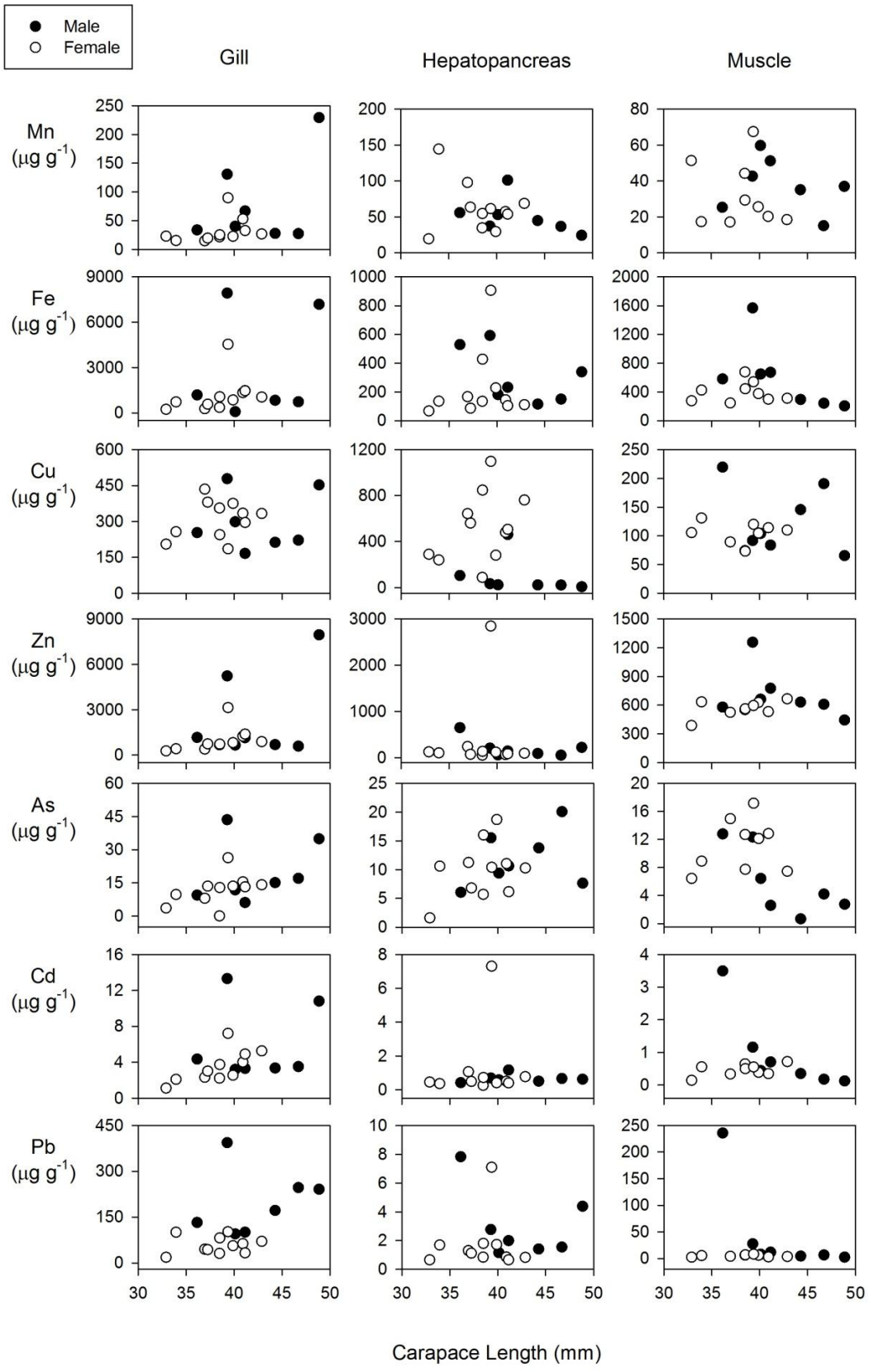

Figure 4.3 Metal concentrations (µg g^{-1} dry weight) in gill, hepatopancreas and muscle tissues against carapace length in male (filled circles) and female (open circles) *K. tyleri*.

4.4 Discussion

Bioaccumulation of metals in fauna occupying hydrothermal vent habitats is dependent on both abiotic and biotic factors. Exposure levels vary with geological setting, venting regime, phase separation, hydrography and proximity to the venting orifice; whilst feeding habit, trophic position and mechanisms of active uptake to satisfy specific cellular demands all influence the assimilation of metallic elements into tissues (Colaço *et al.*, 2006). Additionally, assimilation pathways may differ between essential and non-essential metals (Rainbow, 2002). Here, the tissue composition of essential metals (Fe, Mn, Cu, Zn) and non-essential metals (Cd, As, Pb) are reported in gill, hepatopancreas and muscle of an anomuran crab, *Kiwa tyleri*, from a newly-discovered, biogeographically-distinct province of hydrothermal activity along the ESR in the Southern Ocean.

Metal concentrations are highest in gill compared with hepatopancreas and muscle tissues, consistent with other vent-living crustaceans (Geret *et al.*, 2002a; Peng *et al.*, 2011). Gills are in direct contact with seawater and, when environmental exposures are high, they can accumulate high metal loads through passive uptake by tissues involved in gas exchange. Consequently, metal assimilation in gill tends to reflect the surrounding seawater composition (Kádár *et al.*, 2007). Steep chemical gradients in the mixing zone between hydrothermal fluids and seawater prescribe a strong variation in metal exposure with distance from the vent source (Sarradin *et al.*, 1999). At E2, *K. tyleri* live in very close proximity to high-temperature fluids (Rogers *et al.*, 2012). *K. tyleri* are primary consumers, feeding directly on filamentous thiotrophic bacteria cultured on their dense ventral setae (Marsh *et al.*, 2012; Reid *et al.*, 2013), similarly to *Kiwa puravida* (Thurber *et al.*, 2011), *Kiwa hirsuta* (MacPherson *et al.*, 2005; Goffredi *et al.*, 2008) and *Shinkaia crosnieri* (Miyake *et al.*, 2007; Tsuchida *et al.*, 2011). Rogers *et al.* (2012) observed a decline in the abundance of filamentous bacteria on setae in *K. tyleri* with distance from the vent source, indicating a reliance on reduced sulphur for optimal bacterial growth. The high metal concentrations measured in *K. tyleri* gill tissue compared to those of predatory vent-endemic crabs from other regions (Table 4.3), even where endmember fluid concentrations are higher (Table 4.2), likely reflects their bacterial demand for reduced substrates and therefore their vent-proximal habitat. Whilst animals may be

able to regulate their tissue metal burden up to a certain threshold, once this is exceeded assimilation can reflect external concentrations (White and Rainbow, 1982).

Numerous authors have investigated metal bioaccumulation in shallow-water crab species, where increasing pollutant levels threaten economic populations (Reed *et al.*, 2010; Bordon *et al.*, 2012; Zhang *et al.*, 2012; Ben-Khedher *et al.*, 2013; Luo *et al.*, 2013; Simonetti *et al.*, 2013), however very few studies have quantified metal uptake by crabs in hydrothermal vent environments, where elevated concentrations of heavy metals persist over much longer timescales. Crabs are typically sparse in abundance, occupying the peripheral vent area, and predating on small invertebrates and scavenging (Colaço *et al.*, 2002), while the dense aggregations observed in *K. tyleri* on the ESR are unique (Rogers *et al.*, 2012). Bioaccumulation in vent-endemic crabs has been investigated in *Segonzacia mesatlantica* from the Mid-Atlantic Ridge (Colaço *et al.*, 2006; Kádár *et al.*, 2007), in *Bythograea thermydron* from 13 °N on the East Pacific Rise (Cosson and Vivier, 1997), and also in *Xenograpsus testudinatus* from shallow hydrothermal sites offshore Kueishan Island in Taiwan (Peng *et al.*, 2011). Unfortunately no metal data are available for fluids in the immediate environment of the crab populations at these sites, but the composition of high-temperature fluids (Table 4.2) can be used to make a first order comparison with conditions at Crab City. At Kueishan Island, vent fluid temperatures range from 30 – 116 °C, and metal concentrations are consequently highly variable (Table 4.2). However, as the temperature of the fluids immediately surrounding the crab populations (~23 °C) is close to the lower end of this concentration range (Peng *et al.*, 2011), this indicates a far lower metal burden relative to fluids surrounding the *K. tyleri* population at Crab City. Correspondingly, gill, hepatopancreas and muscle tissues of *X. Testudinatus* have significantly lower metal concentrations compared with *K. tyleri* at E2 (Table 4.3).

High-temperature vent fluids from the vicinity of Crab City are highly enriched in metals compared with Menez Gwen on the MAR, whilst concentrations of Fe and Cu are similar to those of Lucky Strike, and Mn and Zn are comparable to the Rainbow hydrothermal site (Table 4.2) (Colaço *et al.*, 2006; James *et al.*, in review). Tissue metal data for *S. mesatlantica* from these MAR sites is limited to Cu and Zn in hepatopancreas and muscle, but important features can be distinguished none-the-less.

Concentrations of Cu and Zn in crab hepatopancreas are similar between E2 and Menez Gwen (Table 4.3), despite the relative enrichment of these metals in endmember fluids by 1-2 orders of magnitude at E2. In contrast, [Cu] is strongly elevated in hepatopancreas of crabs from Lucky Strike and Rainbow (Table 4.3). Metal concentrations within this digestive tissue appear to be lower in *K. tyleri* at E2 relative to the high temperature fluids, when compared with vent-endemic crabs from the MAR. In muscle tissues however, *K. tyleri* from E2 have relatively high Cu, more comparable with *S. mesatlantica* from Lucky Strike and Rainbow, and sustain higher [Zn] compared with all three MAR vent sites. At 13 °N on the EPR, high-temperature fluids are enriched in Fe by an order of magnitude compared with E2, whilst concentrations of Mn are approximately equal (Table 4.2) (Bowers *et al.*, 1988). Metal concentrations in gill are comparable between *B. thermydron* sampled from this EPR vent field and *K. tyleri* from E2, but *B. thermydron* sustain higher concentrations in hepatopancreas (Table 4.3) (Cosson and Vivier, 1997). In general, *K. tyleri* at E2 have low metal concentrations in their hepatopancreas relative to other vent-endemic crabs, whilst concentrations in muscle tend to be higher. These variations in metal content between tissues and between species likely reflect differences in environmental exposure, feeding regime, trophic level and mechanisms of uptake and regulation, as discussed below.

Metal concentrations within the digestive tissues are partly influenced by nutritional pathway and tend to be low in primary consumers (Kádár *et al.*, 2007). Whilst the metal content of the ventral episymbionts of *K. tyleri* was not analysed in this study, bioconcentration factors in vent-living bacteria have been found to be up to three orders of magnitude lower than organisms in higher trophic levels (Kádár *et al.*, 2007). It is likely that the low metal content of *K. tyleri* hepatopancreas reflects limited trophic biomagnification, which is more evident in predatory vent crabs (Table 4.3). External exposure is also an important control on hepatopancreatic metal accumulation, as indicated by the large variation in [Cu] in *S. mesatlantica* between chemically-distinct vent sites on the MAR (Kádár *et al.*, 2007). As *K. tyleri* are exposed to a strongly metal-enriched environment, low metal concentrations in this tissue may be indicative of regulatory mechanisms within this organ. *B. thermydron* accumulate high concentrations of copper in their digestive gland, which may be indicative of a mechanism for regulating Cu levels in muscle tissue whilst maintaining

a supply of Cu for synthesis of the respiratory pigment, haemocyanin, in a chemically heterogeneous environment (White and Rainbow, 1982; Cosson and Vivier, 1997; Colaço *et al.*, 2006). This mechanism of Cu storage may be more important in peripheral vent decapods, where supply of vent-sourced chemicals is highly variable. *K. tyleri*. sampled from the ESR showed a discrepancy in the Cu content of their digestive gland between males and females. In females, copper concentrations were highest in digestive gland, whilst in males Cu was significantly lower in digestive gland and muscle compared to gill. Males were generally found to be closer to the vent orifices, whilst females resided in slightly cooler waters adjacent to the vent (Rogers *et al.*, 2012), therefore detoxification and excretion of Cu (and other metals) may be more important than storage in male *K. tyleri*.

Metal accumulation in gill and digestive gland has been suggested as a mechanism of regulating enrichment in muscle tissue (Colaço *et al.*, 2006). However, female *K. tyleri* exhibited significant enrichment of Fe and Zn in muscle tissue, compared with hepatopancreas, and may be more comparable to gill. Additionally, Zn concentrations in both male and female *K. tyleri* muscle appear to be higher than those of other vent crab species (Table 4.3). Uptake of essential metals in specific organs is typically indicative of certain physiological roles, such as utilisation in metalloenzymes (Childress *et al.*, 1993; Flores *et al.*, 2005; Peng *et al.*, 2011). Alternatively, enrichment in muscle may reflect diffusion through the delicate exoskeleton facilitated by the large surface area of the chelipeds where muscle was extracted, or it could indicate that a threshold external concentration has been surpassed preventing efficient regulation (White and Rainbow, 1982). Preliminary investigations into the life history of *K. tyleri* indicate that this species may be exceptionally long-lived (Marsh *et al.*, in prep), and high concentrations of certain metals in muscle tissue may simply reflect accumulation over a long (potentially decadal) time-period.

A further interesting discrepancy between male and female *K. tyleri* was observed in their relationship between tissue metal burden and size. In females, most metals analysed (except Cu and Pb) showed an increase in concentration in gill with increasing carapace length, whilst no such relationship was observed in males (Figure 4.3). Larger females may assimilate higher metal concentrations by inhabiting a more

vent-proximal location compared to smaller individuals. Alternatively, as tissue metal content generally declines during periods of faster growth and increases as growth rate slows (Pourang *et al.*, 2004), enhanced metal concentrations in larger females may reflect decelerated growth after obtaining a certain size. In contrast, males exhibit a strong negative relationship between size and concentration of non-essential metals (Cd, As, Pb) and Fe in muscle tissue. This suggests that mechanisms for regulating muscle accumulation, particularly in non-essential metals, are more efficient in larger males. There are a number of pathways via which metals can be detoxified and/or excreted, including complexation with metal-binding proteins such as metallothioneins, sequestration onto insoluble granules, and, in crustaceans, the moulting process (Ahearn *et al.*, 2004). Immediately prior to moulting, essential metals can be reabsorbed from the exoskeleton into the soft tissues, whilst non-essential (toxic) metals are excreted (Bergey and Weis, 2007). For Fe, Cd and Pb in particular, the negative trend with carapace length in muscle appears to be controlled by a high metal concentration in the smallest individual, and much lower metal concentrations in larger animals (Figure 4.3). Large *K. tyleri* may exhibit lower concentrations of Fe, As, Cd and Pb in their muscle tissue as a result of moulting, and this may be more evident in males as they reside closer to the vent source where metal exposure is greatest. Further investigation is required to confirm the role of moulting, and the physiological and biochemical differences between the sexes, on the detoxification of metals in this new species of Kiwaidae.

4.5 Conclusions

Metal bioaccumulation varies significantly between tissues in *K. tyleri* sampled from segment E2 of the East Scotia Ridge. *K. tyleri* live in close proximity to high-temperature fluids, which provide a rich supply of H_2S that enables optimal episymbiont growth. However, this nutritional strategy comes at the cost of high environmental toxicity. Consequently, gill is highly enriched in both essential and non-essential metals, reflecting direct exposure of this organ to vent effluents and passive uptake during respiration. Significantly lower concentrations in hepatopancreas reflect the low trophic position of *K. tyleri* at E2 and limited biomagnification of metals compared with the digestive system of predatory vent-

endemic crabs elsewhere. Muscle tissue tends to sustain a high metal burden in *K. tyleri* relative to vent-living crabs from MAR and EPR hydrothermal fields, and concentrations of Fe and Zn in females are comparable to those measured in gill. This may reflect accumulation of Fe and Zn over a long time period, or it may indicate active uptake of these metals to satisfy metabolic pathways. Further investigations are required to elucidate the physiological role of these metals, if any, in muscle tissue of *K. tyleri*.

This study also indicates that there are sex differences in metal regulation with size between tissues. With increasing carapace length, concentrations of Mn, Fe, Zn, As and Cd increase in gill in females, whilst Fe, As, Cd and Pb decrease in muscle in males. In females, the relationship between size and metal burden in gill may reflect enhanced metal exposure with proximity to the active vent source. Females were located in slightly cooler fluids compared with males, which may explain the absence of a significant relationship between metal content and size in other tissues. In contrast, regulation of toxic metals and Fe in muscle tissue may be more important in males, which reside in warmer fluids where metal concentrations are higher. This research presents a novel insight into the metal organisation of a dominant vent-endemic decapod, whose abundance at ESR vent sites is unprecedented within this Order in the Antarctic.

Chapter 5

5 Adapting to a heavy metal lifestyle: Bioaccumulation and proteomic responses to copper and cadmium exposure in the common blue mussel, *Mytilus edulis* (L.)

Deep-sea hydrothermal vent environments are highly enriched in reduced sulphur species and heavy metals relative to 'normal' seawater, and may be extremely toxic to many organisms. Metals catalyse the formation of reactive oxygen species (ROS), leading to oxidative stress if cellular defences are exceeded. Oxidative stress can cause irreversible damage to every component of the cell, and vent-living fauna may have evolved specialised mechanisms of detoxification. The common blue mussel, *Mytilus edulis* (L.), is the closest shallow-water taxonomic relative of the deep-sea hydrothermal vent mussel subfamily, the Bathymodiolinae. To understand how the Bathymodiolinae may have adapted to tolerate a high-metal environment, this study used a redox proteomics approach to investigate the effects of Cu and Cd exposure on the stress response of *M. edulis*, through changes in protein concentration and thiol oxidation.

In a series of laboratory experiments, *M. edulis* were exposed to Cu and Cd in concentrations representative of the hydrothermal vent mussel habitat (~40 μg/L Cu; ~200 μg/L Cd), over both a 24 hour and a 7 day period. The concentration of Cu in gill tissue increased significantly after 7 days of exposure (3.7 - 4.1-fold) relative to control, whilst Cd was enriched in gill after 24 hours (9.5-fold) and in both gill and digestive gland after 7 days (105 - 150-fold and 64 – 69-fold, respectively). Following 2D PAGE, a significant change in intensity in just one protein spot was measured relative to control after 24 hours, and in 20 protein spots after 7 days, out of 69 matched spots. Seven of these proteins have important roles in cell structure, metabolism, energy regulation, and antioxidant defence. In the thiol subproteome, a greater response was measured following 24 hours of exposure to Cu and Cd compared with 7 days, indicating recovery over a prolonged period. These findings indicate that *M. edulis* is actively able to regulate uptake of Cu and Cd, which supports the idea that Bathymodiolinae may be pre-adapted to a metal-rich environment.

5.1 Introduction

The discovery of deep-sea hydrothermal vents and their distinct faunal assemblages in 1977 sparked an era of exploration that has progressively revealed chemosynthetic ecosystems to be widespread throughout every ocean (Corliss *et al.*, 1979; Van Dover, 1990; 2002). Venting of high temperature fluids, enriched in reduced gases, provides a significant source of energy to the largely oligotrophic deep sea, locally supporting exceptionally high biomass (Van Dover and Fry, 1989; Von Damm, 1990; Stewart *et al.*, 2005). Mechanisms of vent colonisation are long-debated and remain poorly understood, largely due to discrepancies between fossil, phylogenetic and physiological evidence. Whilst the fossil record suggests an ancient vent-endemic lineage dating back to the Paleozoic Era (Newman, 1985), advances in molecular phylogeny have shown that modern vent fauna diverged more recently from shallow taxonomic ancestors, with multiple reversals following extinction events associated with deep-water anoxia/dysoxia during the late Cretaceous and early Tertiary periods (Jacobs and Lindberg, 1998; Distel, 2000; Little and Vrijenhoek, 2003; Jones *et al.*, 2006). Re-population of the deep vents may have occurred progressively via reductive stepping stones such as decomposing wood and bone (Distel, 2000; Samadi *et al.*, 2007; Lorion *et al.*, 2010; Bienhold *et al.*, 2013). Alternatively, direct colonisation may have been possible for some species, as indicated by physiological studies of pressure and temperature tolerance (Mestre *et al.*, 2009; Oliphant *et al.*, 2011; Cottin *et al.*, 2012).

Whilst temperature and pressure define major boundaries for species' distribution, successful colonisation of a hydrothermal vent environment additionally requires the ability to tolerate highly elevated concentrations of many metals. Subsurface hydrothermal circulation enriches fluids in Fe, Mn, Cu, Cd, Zn, Co, Pb, As, Ag, Hg, and other metals (Von Damm *et al.*, 1985; Von Damm, 1990). Whilst concentrations of these metals are highly variable, Sarradin *et al.* (1999) estimate exposure in vent habitats to be on the order of a thousand times greater than in oceanic waters, posing a serious toxicity threat to the vent-living communities. Vent fauna may have evolved specialised mechanisms of detoxification (Hardivillier *et al.*, 2004; 2006), and it is therefore useful to investigate evidence for pre-adaptation to metal stress in related non-vent organisms. This study focuses on the toxic and oxidative

impacts of copper and cadmium on the common blue mussel, *Mytilus edulis*, a close shallow-water taxonomic relative of the deep-sea hydrothermal vent-living mussel subfamily, the Bathymodiolinae (Distel, 2000).

In unpolluted seawater, concentrations of copper and cadmium are typically around 0.21 and 0.08 μg L^{-1}, respectively (Sarradin *et al.*, 1999; Douville *et al.*, 2002), whilst in coastal waters up to 5 μg L^{-1} (Cu) and 0.6 μg L^{-1} (Cd) have been reported (Balls, 1985; Soegianto *et al.*, 1999). However, in the mixing zone between hydrothermal fluids and seawater, concentrations of copper surrounding *Bathymodiolus* spp. groups have been measured between 1.27 and 327 μg L^{-1} (Sarradin *et al.*, 1999; Kádár *et al.*, 2005; Sarradin *et al.*, 2009), whilst cadmium ranges between 0.01 and 15 μg L^{-1} (Desbruyères *et al.*, 1998; Douville *et al.*, 2002; Di Meo-Savoie *et al.*, 2004; Kádár *et al.*, 2005; Sarradin *et al.*, 2008).

Copper is a cofactor in many enzymes and is essential for normal organism function, but can become toxic when concentrations in the environment are high (Al-Subiai *et al.*, 2011). In particular, Cu takes part in Haber-Weiss and Fenton-type reactions, catalysing the formation of hydroxyl radicals (Buettner, 1993; Gaetke and Chow, 2003). Copper can also inactivate key antioxidant enzymes, such as glutathione, by binding to their cysteinyl thiol groups, thereby exacerbating the impact of oxidative stress (Freedman *et al.*, 1989). At Cu concentrations greater than 100 μg L^{-1}, complete mortality has been observed over a 5 day period in *M. edulis* (Al-Subiai *et al.*, 2011), whilst exposure to sub-lethal concentrations (e.g. > 40 μg L^{-1}) has been shown to induce oxidative damage to lipids, proteins and DNA (Viarengo *et al.*, 1981; Lloyd and Phillips, 1999; Zorita *et al.*, 2006), to impair reproductive success (Fitzpatrick *et al.*, 2008; Nadella *et al.*, 2009) and to interfere with critical organ function (Nicholson, 2003b). Unlike copper, cadmium is a non-essential element and is one of the most toxic metals to marine biota, even at low levels. Cadmium is a common anthropogenic pollutant in the marine environment and is known to impair respiration (Poulsen *et al.*, 1982), induce damaging oxidant species (Stohs *et al.*, 2001; Watanabe *et al.*, 2003), inhibit antioxidant enzyme activity (Geret *et al.*, 2002b; Pruski and Dixon, 2002; Company *et al.*, 2006), and enhance carbonylation and glutathionylation of the proteome (McDonagh *et al.*, 2005; Chora *et al.*, 2008; 2009). Exposure to cadmium has also been found to enhance the toxicity of normally

'essential' metals such as iron and copper by competing for protein binding sites and consequently releasing Fe^{2+} and Cu^{2+} ions (Pruski and Dixon, 2002).

The toxicity of both copper and cadmium largely arises through their catalytic activity in the generation of reactive oxygen species (ROS), particularly HO•, which is the most damaging radical known to biological systems (Fridovich, 1998; Tapley *et al.*, 1999). If ROS exceed the cellular antioxidant defences, oxidative stress can result (McDonagh *et al.*, 2005). Carbonylation (introduction of aldehyde and ketone groups) and thiol oxidation are important examples of oxidative modifications within amino acid residues, which can detrimentally affect protein structure and function, and can be used as biomarkers of oxidative stress (Dalle-Donne *et al.*, 2003; Chora *et al.*, 2008; Sheehan *et al.*, 2010). Whilst carbonylation is a primary response to ROS and is a relatively stable, damaging modification (McDonagh *et al.*, 2005; Sheehan, 2006), under moderately oxidising conditions thiol oxidation can be reversible, providing temporary protection to key functional groups, and is critically involved in redox homeostasis, antioxidant defence and cell signalling (Schafer and Buettner, 2001; Eaton, 2006; Hansen *et al.*, 2009). In cases of severe oxidative stress, the irreversible formation of sulphinic ($R\text{-}SO_2H$) and sulphonic ($R\text{-}SO_3H$) acids cause permanent protein damage (Hansen *et al.*, 2009). Quantifying redox transformations such as these in aquatic organisms, in response to various common marine pollutants, is of increasing interest as an environmental monitoring tool (McDonagh *et al.*, 2005; McDonagh and Sheehan, 2006, 2007; 2008; Chora *et al.*, 2009; Sheehan *et al.*, 2010; Tedesco *et al.*, 2010; 2012).

In this study, the proteomic pathways of detoxification have been investigated in *M. edulis* following exposure to copper and cadmium for (i) 24 hours and (ii) 7 days. A redox proteomics approach was used to assess the impact of metal uptake on the organism through changes in both expression and oxidation of proteins, and to assess the potential for a shallow water Mytilid mussel to tolerate the high-metal environment of a hydrothermal vent field. An advanced capacity for metal regulation in *M. edulis* may signify physiological capability of an ancestral species to endure metal stress. Understanding metal tolerance and mechanisms of detoxification also has important implications relating to anthropogenic pollution and habitat deterioration in coastal ecosystems (Braconi *et al.*, 2011).

5.2 Materials and methods

5.2.1 Animal collection and experimental exposure

Mytilus edulis (5 - 8 cm in length) were purchased from Viviers (UK) Ltd in Portsmouth and acclimated for ten days in 10 L tanks filled with filtered and aerated seawater within the aquarium facility of the National Oceanography Centre, Southampton. Tanks were placed in a bath of circulating seawater to limit temperature fluctuations, and animals were fed at 48-hour intervals with a *Tetraselmis suecica* culture (~10^4 cells/ml) prepared on site. Within each tank, water temperature (15 ± 2 °C), salinity (33 ± 0.6 ppt), and dissolved oxygen (≥ 80% saturated) were monitored 3-4 times daily.

Following the acclimation period, the mussels were divided between eight tanks (10 L), each containing 30 animals. Tanks were treated in duplicate with copper (Cu), cadmium (Cd), or copper and cadmium together (CuCd), with two controls (Con). Three additional abiotic control tanks for each metal treatment were set up to monitor the aqueous metal concentration in the absence of mussels. Ecologically-relevant concentrations of copper and cadmium were chosen based on those measured around hydrothermal vent mussel habitats (Sarradin *et al.*, 1999; Hardivillier *et al.*, 2006; Martins *et al.*, 2011a) and in previous metal exposure studies with *Bathymodiolus azoricus* and *Bathymodiolus thermophilus* (Hardivillier *et al.*, 2006; Company *et al.*, 2011; Martins *et al.*, 2011b), moderated by the maximum tolerated concentrations reported for *M. edulis* (Al-Subiai *et al.*, 2011). Exposure tanks were spiked with Cu from an 80 mg/L stock solution of $CuCl_2.2H_2O$ in MQ water, and Cd from a 100 mg/L stock solution of $CdCl_2.2.5H_2O$ to final seawater concentrations of ~40 µg/L Cu and ~200 µg/L Cd. Exposure was maintained over both a 24 hour and a 7 day period, each followed by a 24 hour period of depuration in untreated seawater. The 24-hour 'recovery' period has been shown to enhance clearance of the 'un-reacted' contaminants and prevent further protein oxidation in cell extracts (McDonagh *et al.*, 2006). Tank seawater was changed every day and metal concentrations re-established. Water samples were collected from each tank three-four times daily to monitor variations in Cu and Cd concentration throughout the exposure period.

Gill and digestive gland were dissected on ice and pooled in groups of five animals. Pooled tissues were flash-frozen in liquid nitrogen and stored at -80 °C for proteomic analysis at University College Cork, Ireland. Samples were homogenised in 10 mM Tris-HCl (pH 7.2), 0.5 M sucrose, 0.15 M KCl, 1 mM ethylenediaminetetraacetic acid (EDTA), 1 mM phenylmethylsulfonyl fluoride (PMSF), and centrifuged at 15,000 x *g* (60 min, 4 °C) to separate the soluble fraction from the insoluble pellet. Protein concentration in the supernatant phase was quantified using the method of Bradford (1976), using bovine serum albumin (BSA) as a calibration standard.

5.2.2 Analysis of metals in exposure tanks

Water samples were collected in 20 ml HNO_3-cleaned LDPE bottles from each tank three-four times every 24 hours. Samples were acidified to pH 2 by addition of concentrated thermally distilled (TD) HNO_3. Metal concentrations (Cu, Cd, Fe, Zn, Pb) were determined by inductively coupled plasma mass spectrometry (ICP-MS) (Thermo-Scientific ELEMENT) at the National Oceanography Centre, University of Southampton, with addition of Be (20 ppb), In (5 ppb) and Re (5 ppb) as internal standards. Samples were calibrated against synthetic multi-element external standards, prepared using 1000 μg ml^{-1} standard stock solutions in 3% TD HNO_3. Based on duplicate analyses of each standard, the external precision (2σ) was better than 5% for all metals.

5.2.3 Analysis of metals in mussel tissues

Tissue accumulation of Cu and Cd, in addition to Fe, Pb and Zn, was quantified in gill and digestive gland from the soluble and insoluble fractions obtained by centrifugation as described in Section 5.2.1. Solid pellets were freeze-dried, and corresponding supernatant fluids were heated to dryness at 130 °C. The dry-weight of each sample was measured, and ~100 mg was dissolved in concentrated TD HNO_3 at 60 °C for ~24 hours. The digested samples were then dried-down at 130 °C and re-dissolved in 3% TD HNO_3 spiked with Be (20 ppb), In (5 ppb) and Re (5 ppb) as internal standards. Metal content was determined by ICP-MS (Thermo Scientific X-Series) at the National Oceanography Centre, Southampton. External standards were prepared using 1000 μg ml^{-1} standard stock solutions (Inorganic Ventures) in 3% TD HNO_3. The precision of the analytical procedure was measured through digestion and

analysis of the certified reference material (CRM), lobster hepatopancreas TORT-2 (National Research Council of Canada), alongside the samples (Table 5.1). The reproducibility of these analyses was better than 5% for all metals, and measured values for the CRM were within error of the certified values for all metals, except Fe (< 16%). The concentrations of metals in the Tris-HCl buffer and HNO_3 were also determined (< 1% of sample concentrations for Cu, Cd, Fe and Zn; < 4% for Pb) and subtracted from the measured sample concentrations. Metal concentrations are reported as the sum of the soluble and insoluble fractions, in μg g^{-1} of the tissue dry weight.

Table 5.1 Mean values (n = 5 ± SD) of Cu, Cd, Fe, Zn and Pb in μg g^{-1} dry weight measured in certified reference material, TORT-2 (NRCC), together with certified values.

	Cu	**Cd**	**Fe**	**Zn**	**Pb**
Certified	106 ± 10	26.7 ± 0.6	105 ± 13	180 ± 6	0.35 ± 0.13
Measured	101 ± 1	27.8 ± 0.4	126 ± 6	191 ± 3	0.36 ± 0.01

5.2.4 Fluorescein labelling

Fluorescent labelling of targeted functional groups of amino acid side chains provides a quantitative means of assessing oxidative damage to proteins. Fluorescein-5-thiosemicarbide (5-FTSC) reacts with carbonyl groups to form relatively stable hydrazones, whilst iodoacetamidofluorescein (IAF) reacts with free sulphydryl groups (but not the oxidised products) to form stable thio ethers. These fluorescein-protein conjugates can be visualised as fluorescent bands/spots after electrophoresis (Ahn *et al.*, 1987; Baty *et al.*, 2002; Chaudhuri *et al.*, 2006). This technique has recently been shown to be a powerful indicator of oxidative stress in *Mytilus edulis* exposed to a pro-oxidant environment (McDonagh and Sheehan, 2007; 2008).

Protein thiols were labelled with 0.2 mM IAF from a 20 mM stock solution in dimethyl sulfoxide (DMSO). Protein carbonyl groups were labelled with 1 mM FTSC from a 100 mM stock solution in DMSO. Sample aliquots containing 25 μg protein (1D PAGE) and 150 μg protein (2D PAGE) were incubated with IAF or FTSC for two hours on ice in the dark. Proteins were precipitated by incubating extracts in 10% (v/v) trichloroacetic acid (TCA) for 5 minutes on ice, followed by centrifugation at

11,000 x *g* for 3 minutes. The resulting pellet was washed in an excess of ice-cold acetone (for IAF-labelled samples) or 1:1 ethylacetate:ethanol (for FTSC-labelled samples) to remove TCA and any interfering salts and non-protein contaminants. Protein extracts were re-suspended in 15 µl of sample buffer for 1D PAGE (62.5 mM Tris-HCl (pH 6.8) containing 25% (v/v) glycerol, 2% (w/v) SDS, 5% (v/v) β-mercaptoethanol and a trace amount of bromophenol blue) or 125 µl of rehydration buffer for 2D PAGE (7 M urea, 2 M thiourea, 2% (w/v) CHAPS, 4% (v/v) ampholyte (Pharmalyte 3-10), 1.2% (v/v) DeStreak reagent and a trace amount of bromophenol blue).

5.2.5 Polyacrylamide Gel Electrophoresis (PAGE)

5.2.5.1 1D PAGE

Gill and digestive gland samples (25 µg protein in 15 µl sample buffer) were heat-denatured and loaded alongside a protein molecular mass marker (ThermoScientific, Dublin, Ireland) into wells embedded within a stacking gel of 4.5% (v/v) polyacrylamide in 0.5 M Tris-HCl, pH 6.8, set above a resolving gel of 14% (v/v) polyacrylamide in 1.5 M Tris-HCl, pH 8.8. Gel electrophoresis was carried out at 4 °C using an Atto AE-6450 mini PAGE system (BioRad; Hercules, CA, USA) at a constant voltage of 90 V until samples entered the resolving gel, then 120 V until the dye front reached the bottom of the gel. Fluorescently labelled bands were visualised using a Typhoon Trio+ Variable-Mode Imager (GE Healthcare, Little Chalfont, Bucks, UK) measuring excitation of Fluorescein at 532 nm and emission at 526 nm. Protein bands were visualised by colloidal Coomassie-staining using the method of Dyballa and Metzger (2009).

5.2.5.2 2D PAGE

Gill samples (150 µg protein in 125 µl rehydration buffer) were loaded onto 7 cm non-linear immobilised pH gradient (IPG) strips (pH 3 – 10) and rehydrated for 18 hours in the dark at room temperature (Leung *et al.*, 2011). Rehydrated IPG strips were focused on a Protean isoelectric focusing (IEF) cell (Bio-Rad) with linear voltage increases in the following sequence: 250 V for 15 min; 4000 V for 2 hours; then up to 20,000 Vh. Prior to 2D PAGE, focused strips were incubated in equilibration buffer (6M urea, 0.375M tris-HCl, pH 8.8, 2% (w/v) SDS, 20% (v/v)

glycerol), first with 2% (w/v) dithiothreitol (DTT) to ensure complete reduction of disulfide bridges and secondly with 2.5% (w/v) iodoacetamide (IAM) to reduce streaking. Equilibrated strips were loaded onto 14% SDS-polyacrylamide gels alongside a wick containing an unstained protein molecular mass marker, and sealed with agarose (0.5%) containing a trace amount of bromophenol blue. Gel electrophoresis was carried out as for 1D PAGE.

5.2.6 Image analysis

Coomassie-stained gels were scanned with a calibrated imaging densitometer (GS-800; Bio-Rad). Background subtraction and optical density quantification of protein bands in 1D PAGE gels was performed using Quantity One image analysis software (Bio-Rad). For each gel lane, intensity of fluorescence (counts) was normalised against protein content (optical density) to account for differences in sample loading and enable the extent of thiol oxidation or carbonylation to be compared between samples.

Progenesis SameSpots image analysis software (Version 4.5; Nonlinear Dynamics, Durham, NC, USA) was used to align gels, match spots, and quantify spot volumes in 2D PAGE gel images of Coomassie-stained and thiol-labelled protein separations. Spots with a significant change in intensity (determined by a fold change of > 1.5; $p < 0.05$; ANOVA or Kruskal-Wallis) between control and treated samples were selected for protein identification.

5.2.7 Protein digestion and identification

Proteins were manually picked from 2D PAGE separations, lightly stained with colloidal Coomassie. Following in-gel tryptic digestion, extracted peptides were loaded onto a R2 micro-column (RP-C18 equivalent) where they were desalted, concentrated and eluted directly onto a MALDI plate using α-cyano-4-hydroxycinamic acid (CHCA) as the matrix solution in 50 % (v/v) acetonitrile and 5% (v/v) formic acid. Mass spectra of the peptides were acquired in positive reflectron MS and MS/MS modes using a MALDI-TOF/TOF MS instrument (4800*plus* MALDI TOF/TOF analyzer) with exclusion list of the trypsin autolysis peaks (842.51, 1045.56, 2211.11 and 2225.12). The collected MS and MS/MS spectra were analysed in combined mode by Mascot search engine (version 2.2; Matrix Science, Boston,

MA) and the NCBI database restricted to 50 ppm peptide mass tolerance for the parent ions, an error of 0.3 Da for the fragments, one missed cleavage in peptide masses, and carbamidomethylation of Cys and oxidation of Met as fixed and variable amino acid modifications, respectively. No taxonomic restrictions were applied. The identified proteins were only considered if a MASCOT score above 95% confidence was obtained ($p < 0.05$) and at least one peptide was identified with a score above 95% confidence ($p < 0.05$). This analysis was conducted by the Analytical Services Unit, Instituto de Tecnologia Química e Biológica (ITQB), New University of Lisbon, Lisbon, Portugal.

5.2.8 GST assay

Glutathione S-transferase (GST) activity was quantified in *M. edulis* gill from control and treated groups. Four biological replicates (5 pooled animals in each; n = 20) were analysed in sample aliquots containing 15 μg of protein diluted to a 50 μl volume. Samples were loaded into a 96-well microplate with 100 μl of 2 mM 1-chloro-2,4-dinitrobenzene (CDNB) (from a 40 mM stock in ethanol) in 0.15 M potassium phosphate buffer (pH 6.5). GST activity was measured spectrophotometrically by adding 50 μl of 20 mM reduced glutathione (GSH) and measuring absorbance at 340 nm immediately and every 15 seconds for 5 minutes. GST activity was calculated from equation 5.1 (Habig *et al.*, 1974):

$$\text{GST activity } (\mu\text{mol/min/mg}) = (\Delta A_{340}\ V) / (\varepsilon\ l\ M) \qquad (5.1)$$

Where, ΔA_{340} represents the blank-subtracted initial rate of reaction between CDNB and GSH (min^{-1}); V is the volume of reaction (0.2 ml); ε_{is} the extinction coefficient of the reaction product at 340 nm ($9.6 \times 10^3\ \mu M^{-1}\ cm^{-1}$); l is the path length (0.524 cm); and M is the mass of protein (15 μg).

5.2.9 Statistical analysis

Metal exposures were conducted for both 24 hours and 7 days, each with a control group; so these are treated as two independent experiments for statistical analysis. Where data exhibited equal variance but were non-normally distributed, both parametric and non-parametric tests were performed. In these cases, no difference was observed in the level of significance between the two tests, and the parametric (t-test/ANOVA) '*p*' values are quoted only. Within the 24-hour exposure

experiment, metal concentrations in tissues were normally distributed, with equal variance, and the student's 2-sample t-test was performed to evaluate the differences in accumulation of each metal in gill between control and CuCd-treated groups. Within the 7-day exposure experiment, metal concentrations in gill were found to be non-normally distributed for Cu, Cd, Fe and Zn, but normally distributed for Pb; whilst equal variance was only observed for Cu, Zn and Pb. In digestive gland, all metal concentrations were normally distributed with equal variance, except for Cd. Consequently, non-parametric analyses of variance in the median concentration between treatment groups were performed by Kruskal-Wallis Multiple Comparisons tests (K-W) for Cu, Cd, Fe and Zn in gill and Cd in digestive gland. For Pb (and also for Cu and Zn) in gill, and for Fe, Cu, Zn and Pb in digestive gland, ANOVA, followed by Tukey's *post-hoc* tests, were performed to analyse the significance of differences in the means between treatment groups. K-W tests were performed to assess the significance of differences in metal concentrations between gill and digestive gland tissues. In all cases, significant relationships are reported at the 95% confidence level where $p < 0.05$.

Metal concentrations in water samples collected during the 24-hour exposure experiment were normally distributed with equal variance for Pb and Zn, but deviated from normality and equal variance in the case of Cu, Cd and Fe. Differences in the mean concentration between control and CuCd-treated tanks were assessed using the student's two sample t-test for Pb and Zn, whilst variations in the median were evaluated using the Mann-Whitney U test (M-W) for Cu, Cd and Fe. Metal concentrations in water samples from a 24-hour period from the 7-day exposure were not normally distributed. Kruskal-Wallis Multiple Comparisons tests were applied to examine the significance of differences in concentrations of each metal between the four groups. In all cases, significant relationships are reported at the 95% confidence level where $p < 0.05$.

After 1D PAGE, fluorescent count values were normalised to optical density from Coomassie staining and further normalised to the control from within the same analytical set. Normalised fluorescence data were not normally distributed for gill within the 7-day exposure, and Kruskal-Wallis Multiple Comparisons tests were performed to analyse significance in differences between groups with both IAF and

FTSC. Normalised fluorescence data were normally distributed in digestive gland, and both IAF and FTSC datasets were subject to ANOVA tests, followed by Tukey's *post-hoc* analysis. Following 2D PAGE, all spots matched within Coomassie-stained and IAF-labelled gel images were tested for normality. Spot intensity data from the 7 day exposure were analysed for significant intergroup differences by ANOVA and Tukey's post-hoc tests, or by non-parametric Kruskal-Wallis Multiple Comparisons tests. Spot intensity data from the 24 hour exposure were normally distributed and were analysed using the student's t-test. Significant variations in spot intensity are reported at the 95% confidence interval, where $p < 0.05$.

GST activity data were normally distributed, with equal variance, for both the 24-hour and 7-day exposed groups. The student's t-test was applied to test for significant differences in the means between control and CuCd-treated groups after 24 hours, whilst ANOVA followed by Tukey's *post-hoc* analysis was conducted to assess differences in the means between all groups after 7 days of exposure.

5.3 Results

5.3.1 Tank metal concentrations

Average concentrations of total dissolvable metals (Cu, Cd, Pb, Fe, Zn) in control and treatment tanks for each exposure period are reported in Table 5.2. During the 24-hour exposure, tanks treated with both copper and cadmium (CuCd) were enriched in Cu by a factor of 4.9 and in Cd by a factor of 230 compared to control ($p < 0.01$; M-W). During the 7-day exposure, tanks spiked with copper (Cu and CuCd) were enriched in Cu by a factor of 5.4 – 5.8 compared to control, whilst cadmium-treated tanks (Cd and CuCd) were enriched in Cd by a factor of 217 – 223 ($p < 0.001$; K-W). Significant differences were also measured in Fe, Pb and Zn between tanks in the 7-day exposure, however these were comparatively very small (< 1.7-fold difference; $p < 0.01$; K-W), and are likely to reflect minor contamination. Tanks were kept within a shelter outside, and air-borne particles may be responsible for the small variations measured in these metals between tanks.

Table 5.2 Average concentration of Cu, Cd, Pb, Fe and Zn (μg L^{-1} ± SD) in control and metal-treated tanks during 24-hour and 7-day exposure periods.

	Control	**CuCd**	**Control**	**Cu**	**Cd**	**CuCd**
Exposure	*24 hr*	*24 hr*	*7 day*	*7 day*	*7 day*	*7 day*
n	*7*	*6*	*13*	*12*	*12*	*25*
Cu	5.96 ± 0.10	29.2 ± 1.72	6.03 ± 0.96	35.1 ± 3.29	6.21 ± 0.97	32.5 ± 6.66
Cd	0.88 ± 0.04	202 ± 0.28	0.94 ± 0.08	0.93 ± 0.02	210 ± 11.8	205 ± 17.2
Pb	0.46 ± 0.04	0.47 ± 0.06	0.45 ± 0.04	0.43 ± 0.01	0.41 ± 0.02	0.40 ± 0.04
Fe	7.64 ± 2.83	11.1 ± 3.94	7.11 ± 3.22	12.4 ± 3.03	12.0 ± 2.44	7.80 ± 5.53
Zn	49.6 ± 3.65	42.4 ± 4.84	49.0 ± 4.02	49.3 ± 3.85	50.6 ± 6.22	46.3 ± 4.37

Number of water samples analysed in each treatment indicated by n.

Changes in the concentration of copper and cadmium in tank seawater were monitored throughout a representative 24-hour period during each exposure experiment, both in the presence and absence of mussels. In tanks treated with both metals for 24 hours, the aqueous concentration of copper and cadmium in the presence of mussels compared to without, was reduced by 22% and 4%, respectively, at the start of the exposure, and by 29% and 6%, respectively, after 21.5 hours (Figure 5.1). During a 24 hour period within the 7-day exposure (Figure 5.2), Cu-treated tanks showed a reduction in [Cu] by 13% in mussel-containing tanks compared with no-mussel tanks at the start of the experiment, and by 21% after 22.5 hours. In Cd-treated tanks, [Cd] was elevated in mussel-containing tanks by 13% at the start of the experiment, but was lower by 6.7% after 23 hours. In CuCd tanks, [Cu] was elevated by 9.2% at the start, but reduced by 28% after 23 hours, and [Cd] was reduced by 3.6% at the start and by 30% after 23 hours. During the course of a 24 hour treatment period, Cu and Cd appear to be progressively depleted in the tank water relative to the abiotic control, suggesting uptake by the mussels, however it should be noted that changes of < 5% are within the error of the analyses.

In summary, these data demonstrate that tanks treated with Cu and/or Cd were significantly enriched in these metals relative to control, whilst concentrations of Fe, Zn and Pb were similar between all tanks (Table 5.2).

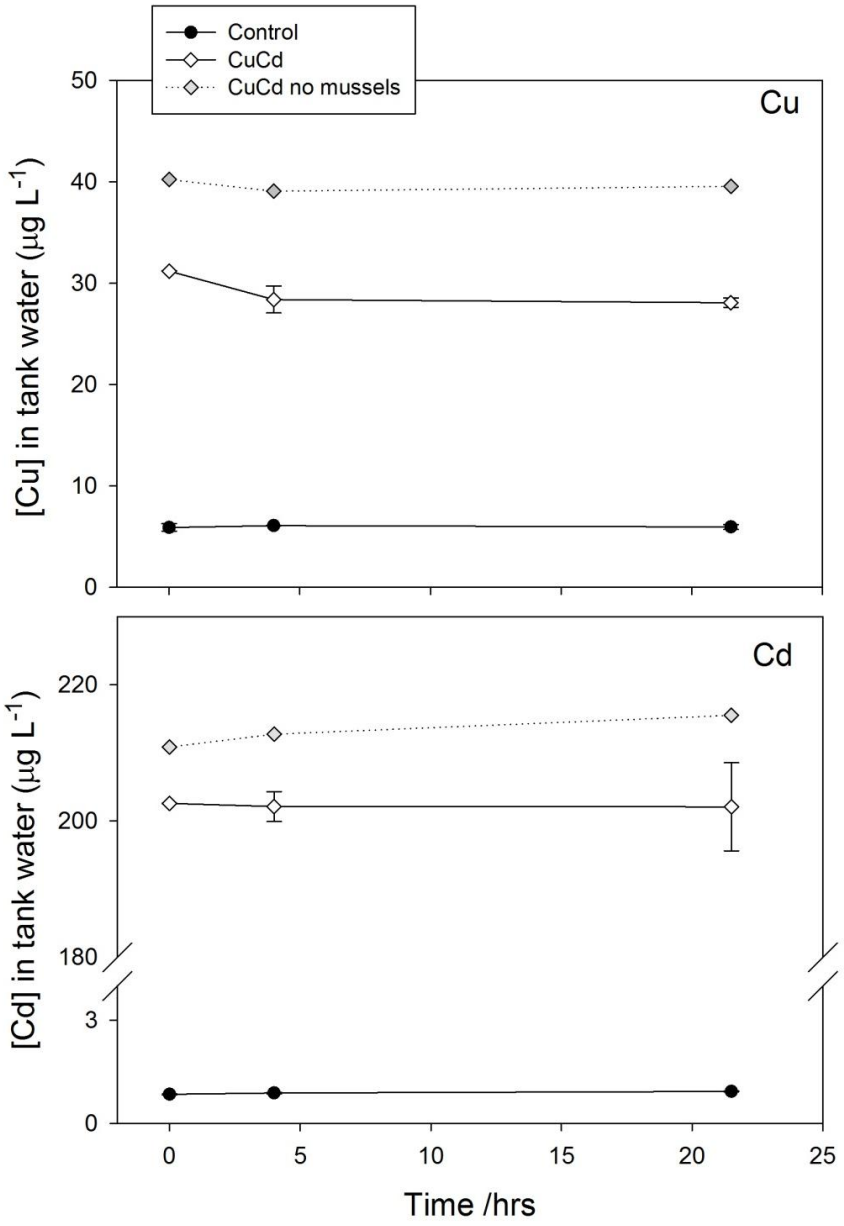

Figure 5.1 Aqueous concentrations of copper (top) and cadmium (bottom) in control and CuCd-treated tanks, both with and without mussels, throughout the 24-hour exposure period. Error bars indicate the standard deviation on the mean between duplicate tanks.

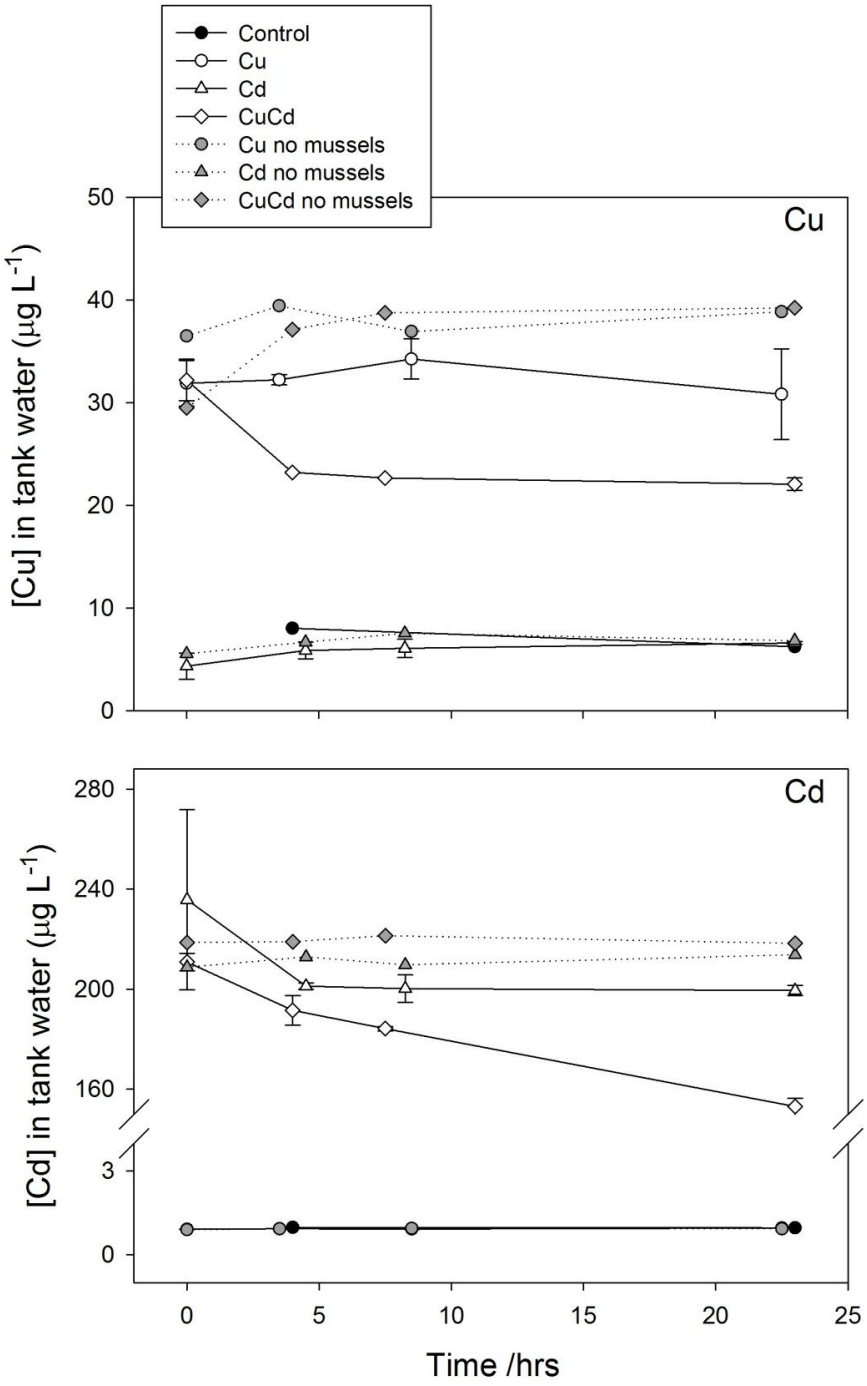

Figure 5.2 Aqueous concentrations of copper (top) and cadmium (bottom) in all experimental tanks, across a 24-hour period during the 7-day exposure. Control and treated (Cu, Cd, CuCd) tank environments, both with and without mussels, are shown. Error bars indicate the standard deviation on the mean between duplicate tanks.

5.3.2 Tissue metal concentrations

Tissue concentrations are reported in Table 5.3 for essential (Fe, Cu, Zn) and toxic metals (Cd, Hg, Pb) in *M. edulis* experimentally exposed to copper (40 μg L^{-1}), cadmium (200 μg L^{-1}) and both metals together (40 μg L^{-1} Cu; 200 μg L^{-1} Cd) over 24-hour and 7-day exposure periods. After 24 hours of exposure to Cu and Cd, concentrations of Cd were significantly enriched in gill compared with control (9.5-fold; $p < 0.05$), but no significant differences were observed with Cu or with Fe, Pb or Zn. After 7 days, mussels exposed to copper, both alone and with Cd, showed a highly significant increase in concentration of Cu in their gill (3.7 - 4.1 fold) compared with control animals (K-W; $p < 0.001$). No significant change in Cu concentration was measured in digestive gland between treatment groups. Mussels exposed to cadmium showed a large and significant Cd enrichment in gill compared to control (105-fold; $p < 0.01$; K-W), whilst those exposed to cadmium in the presence of copper showed a greater accumulation of Cd in comparison to control groups, which was highly significant (150-fold; $p < 0.001$; K-W). Cadmium accumulation in digestive gland was also significantly greater in exposed mussels compared with control (64-fold increase in Cd-treated mussels, $p < 0.05$; 69-fold increase in CuCd-treated mussels, $p < 0.05$; K-W). Iron was found to be enriched in digestive gland compared with gill by a factor of 1.6 ± 0.09 (K-W; $p < 0.05$) in all treated mussel groups, but not in control animals. No significant differences were found in concentrations of Fe, Pb and Zn between groups, and no significant differences were found in Pb and Zn between tissues. Tissue accumulation of Cu and Cd after each exposure period is presented in Figure 5.3.

Table 5.3 Total concentration of Fe, Cu, Zn, Cd and Pb (μg g^{-1} dry weight) in gill and digestive gland of *M. edulis* after 24 hour and 7 day experimental treatments. Significant differences relative to control within each experiment are indicated by an asterisk (*)

	Tissue	Fe	Cu	Zn	Cd	Pb
Gill, 24-hour experiment *(n = 20 ± SD)*						
Control	Gill	116 ± 7.2	5.17 ± 0.88	74.1 ± 11.2	0.43 ± 0.06	1.10 ± 0.16
CuCd	Gill	120 ± 15.0	**6.52 ± 1.41**	84.3 ± 24.7	**4.12 ± 1.64***	1.34 ± 0.28
Gill, 7-day experiment *(n = 30 ± SD)*						
Control	Gill	90.3 ± 12.2	4.13 ± 0.42	91.8 ± 41.6	0.39 ± 0.07	0.82 ± 0.24
Cu	Gill	71.2 ± 5.22	**17.0 ± 2.71***	76.1 ± 25.5	0.55 ± 0.18	0.85 ± 0.30
Cd	Gill	72.4 ± 3.66	3.51 ± 0.95	63.1 ± 12.8	**41.0 ± 7.68***	0.60 ± 0.12
CuCd	Gill	73.8 ± 8.44	**15.4 ± 2.66***	83.2 ± 27.5	**58.4 ± 11.7***	0.67 ± 0.18
Digestive Gland, 7-day experiment *(n = 20 ± SD)*						
Control	DG	164 ± 31	8.06 ± 1.02	114 ± 27	1.07 ± 0.28	0.89 ± 0.17
Cu	DG	104 ± 18	**8.59 ± 0.70**	69 ± 19	0.91 ± 0.10	0.46 ± 0.12
Cd	DG	117 ± 29	6.50 ± 0.66	83 ± 26	**68.6 ± 12.7***	0.63 ± 0.21
CuCd	DG	119 ± 24	**8.01 ± 0.55**	91 ± 41	**73.9 ± 16.1***	0.53 ± 0.10

Where mussels were exposed to Cu and/or Cd, the resulting tissue concentrations are highlighted in bold font.

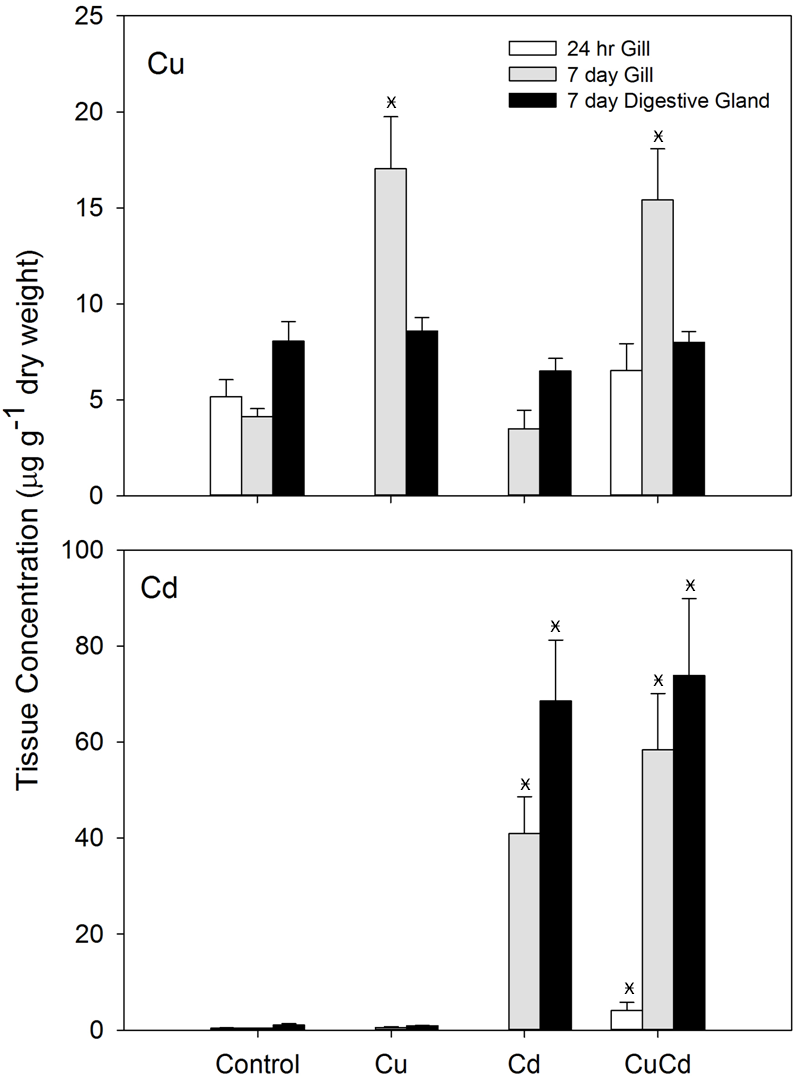

Figure 5.3 Copper (top) and cadmium (bottom) concentrations in gill and digestive gland tissues of *M. edulis* following 24 hours and 7 days of exposure in control and metal-treated (Cu, Cd, CuCd) tanks. Error bars indicate the standard deviation on the mean, where n = 20 (24 hr gill; 7 day digestive gland) and n = 30 (7 day gill). Significant differences in metal concentration between treatment and control groups are indicated by x.

5.3.3 Global thiol oxidation and carbonylation

Figure 5.4 illustrates a typical coomassie gel and IAF-labelled scan pair, where two biological replicates of each control and metal treatment have been electrophoresed. Following 1D PAGE, the global (total) extent of thiol oxidation and carbonylation relative to control is quantified from fluorescence intensity in IAF- and FTSC-labelled protein separations, respectively, normalised to protein content to correct for minor differences in sample loading (Baty *et al.*, 2002; Chaudhuri *et al.*,

2006). Significant day-to-day variations in scanner calibration for optical density were detected in this study, necessitating further normalisation of fluorescence in treated samples to control within each analytical set. Normalised fluorescence (IAF and FTSC), for gill and digestive gland tissues of control and treated *Mytilus edulis* groups after 7 days of exposure are presented in Table 5.4 and Figure 5.5. High fluorescence values with IAF indicates a greater abundance of free thiol (-SH) groups, whilst high fluorecence count values with FTSC indicates greater carbonylation (Baty *et al.*, 2002; Chaudhuri *et al.*, 2006).

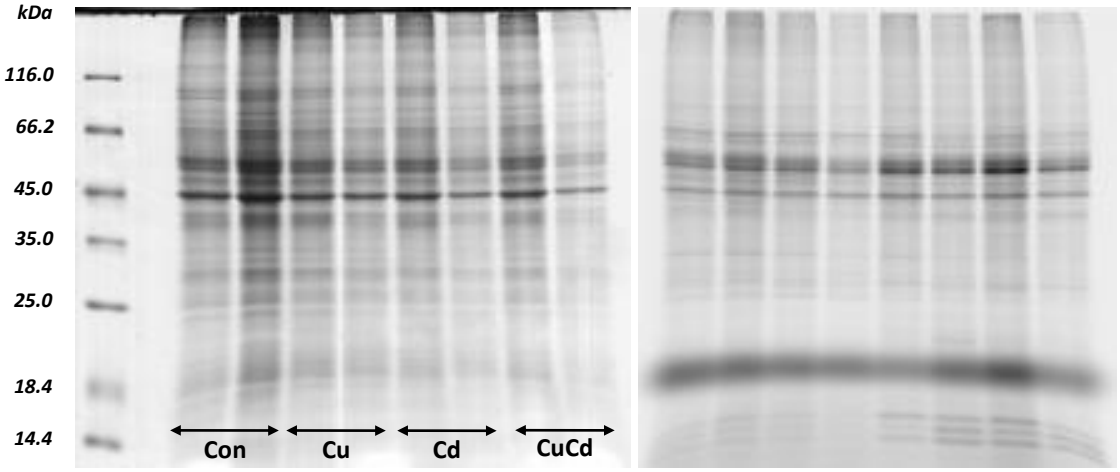

Figure 5.4 Representative images of electrophoretically-separated protein bands in a Coomassie-stained gel (left) and an IAF-labelled fluorescent scan (right). Two biological replicates of each control and metal treatment in gill samples are shown following 7 days of exposure. A protein molecular mass marker ranging from 14.4 kDa (bottom) to > 116.0 kDa (top) was run for size reference, and is shown on the left.

Table 5.4 Fluorescence intensity measured in IAF- and FTSC-labelled gill and digestive gland tissues of *M. edulis* in control and metal-treated tanks, normalised to protein content. Values are expressed as a % of the control, averaged over *n* biological replicates and 4 technical replicates.

Average (%) ± SEM	**Control**	**Cu**	**Cd**	**CuCd**
IAF				
Gill (n = 30)	100 ± 23	190 ± 44	330 ± 146	400 ± 190
Digestive Gland (n = 20)	100 ± 9	160 ± 16	200 ± 36	200 ± 41
FTSC				
Gill (n = 30)	100 ± 6	91 ± 6	77 ± 11	91 ± 5
Digestive Gland (n = 20)	100 ± 11	97 ± 21	97 ± 21	95 ± 11

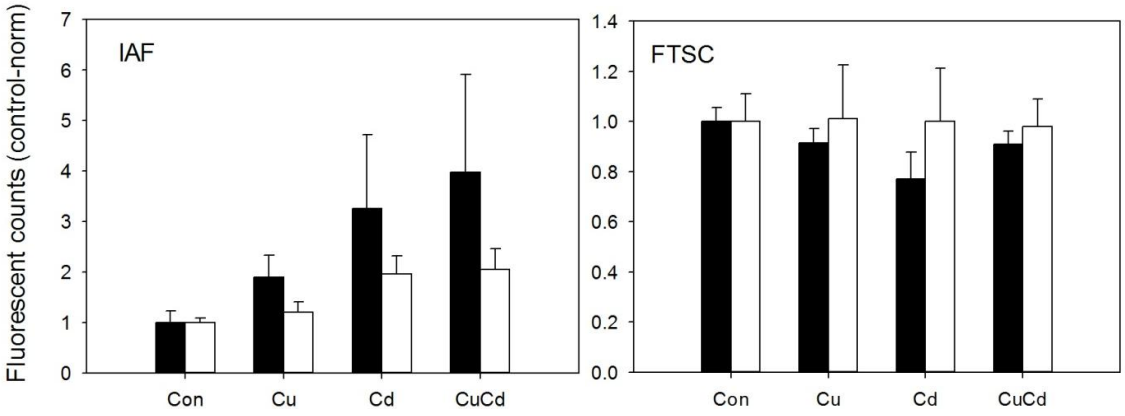

Figure 5.5 Intensity of fluorescence measured in IAF-labelled (left) and FTSC-labelled (right) gill (black bars) and digestive gland (white bars) tissues of *Mytilus edulis* in control and metal-treated tanks. Count values are normalised to protein content, as measured by optical density in Coomassie-stained gels, and also to the control to calibrate against observed daily technical fluctuations. Error bars represent the standard error on the mean.

No statistically signficant difference was found between treatment groups in gill or digestive gland with either IAF or FTSC fluorescence intesity ($p > 0.05$) (Figure 5.5).

5.3.4 Protein expression profiles: 2D PAGE

Proteomic responses to conditions of oxidative stress can be analysed on the scale of individual proteins using the higher-resolution separation technique of 2D PAGE. As metal treatment appeared to initiate a greater response in thiol groups compared with carbonyl groups, and this response was greater in gill compared with digestive gland, 2D PAGE analysis was focused on IAF-labelled protein separations in gill. Figure 5.6 shows representative gel images of coomassie-stained 2D separations of gill proteins in control and CuCd-treated mussels after a 24-hour exposure period, and in control, Cu-, Cd- and CuCd-treated mussel groups after 7 days of exposure.

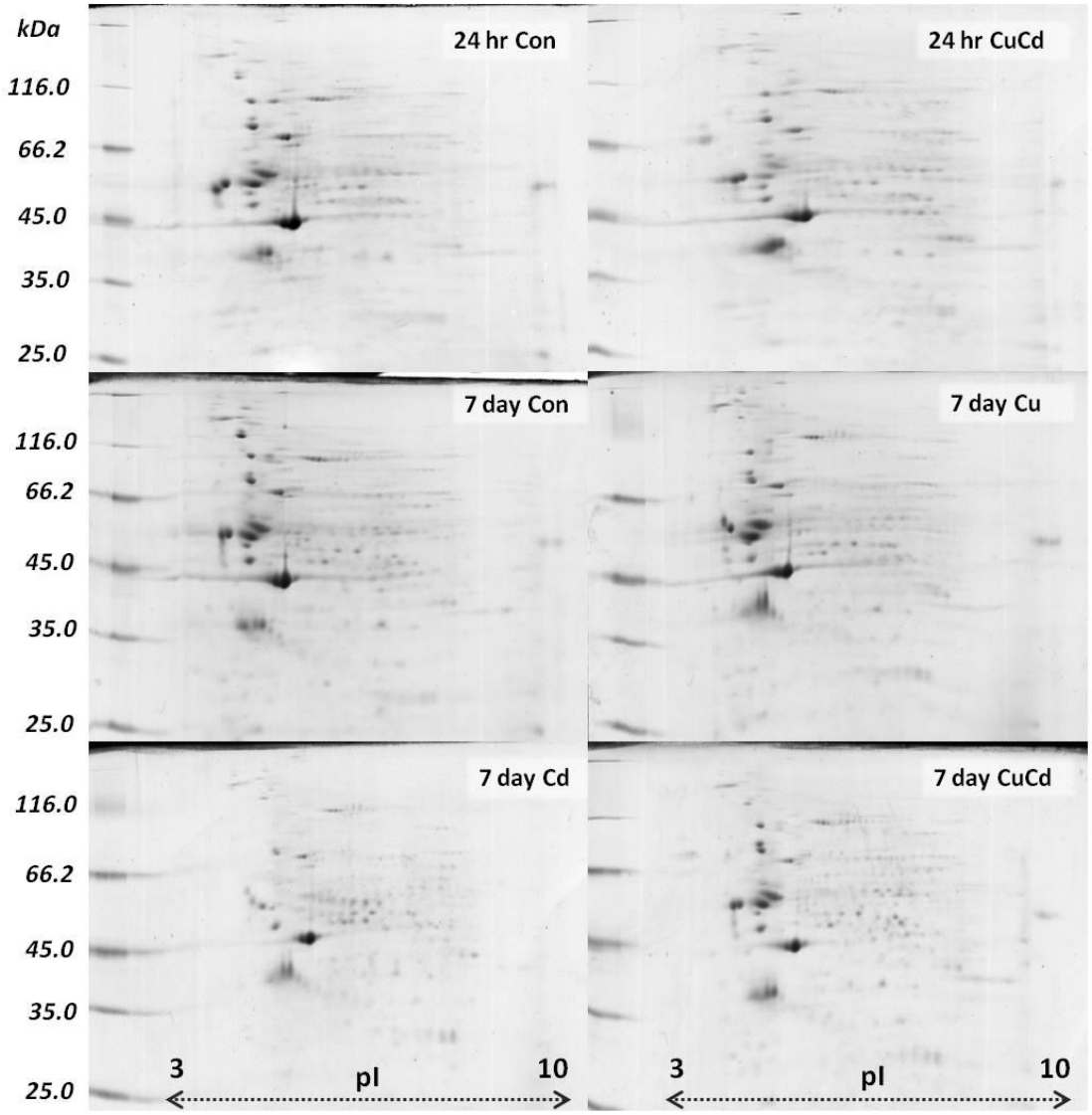

Figure 5.6 Representative images of electrophoretically-separated (2D PAGE), Coomassie-stained protein spots for *Mytilus edulis* gill tissues in control and CuCd-treated groups following 24 hours of exposure, and in control and Cu- Cd- and CuCd-treated groups following a 7 day exposure. A protein molecular mass marker ranging from 25.0 kDa (bottom) to > 116.0 kDa (top) is shown for size reference on the left. Isoelectric point (pI) is indicated along the pH range (3-10).

All protein spots were inspected to ensure that smears and gel defects were not included in the analysis, and only well-defined Gaussian spots were subject to comparison between treatments. A total of 69 protein spots were matched between gels of control and treated animals. Of these, a significant change in intensity between control and treated groups was observed in just one spot (Creatine kinase b-type) after a metal exposure period of 24 hours (Figure 5.7), and in 20 protein spots where animals were exposed to metal treatment for 7 days (Figure 5.8). After 24 hours, a

significant change in intensity was observed in 9 IAF-labelled spots compared to control ($p < 0.05$). Of these, 7 were significantly increased in treated groups and 2 were decreased (Figure 5.7).

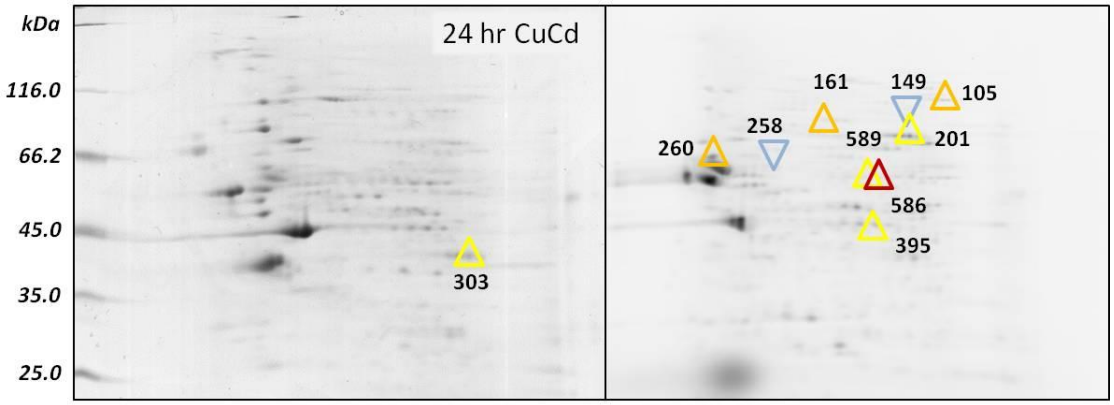

Figure 5.7 Coomassie stain (left) and IAF-labelled fluorescent scan (right) of proteins separated by 2D PAGE from gill tissue of *M. edulis* (n = 20) exposed to both Cu and Cd. Spots that varied significantly in intensity compared to control ($p < 0.05$) are indicated. Triangles in yellow, orange and red indicate spots which were more intense in the CuCd-treated group by a factor of > 1, > 1.5, and > 2, respectively. Inverted triangles in blue indicate spots which were reduced in the CuCd-treated group by a factor of 1 – 1.5.

After 7 days of exposure, mussels treated with copper showed a significant increase in intensity in 4 protein spots and a decrease in 2 spots compared to control ($p < 0.05$) (Figure 5.8). After exposure to cadmium, mussels showed a significant increase in intensity in 10 spots and a decrease in 5 compared to control ($p < 0.05$). Exposure to both cadmium and copper for 7 days resulted in a significant increase in intensity of 2 spots and a decrease in 2 compared to control ($p < 0.05$). Where identification of these proteins was possible, these are presented in Table 5.5. Groups treated with Cu-only showed a significant reduction in IAF intensity in 6 spots and an increase in intensity in 5 spots compared to control ($p < 0.05$); whilst Cd-treated groups showed an increase in 11 spots and a decrease in 12 spots with IAF ($p < 0.05$) (Figure 5.8). Exposure to Cu and Cd together for 7 days resulted in a significant increase in intensity in 2 IAF-labelled spots and a decrease in 3 compared to control ($p < 0.05$) (Figure 5.8).

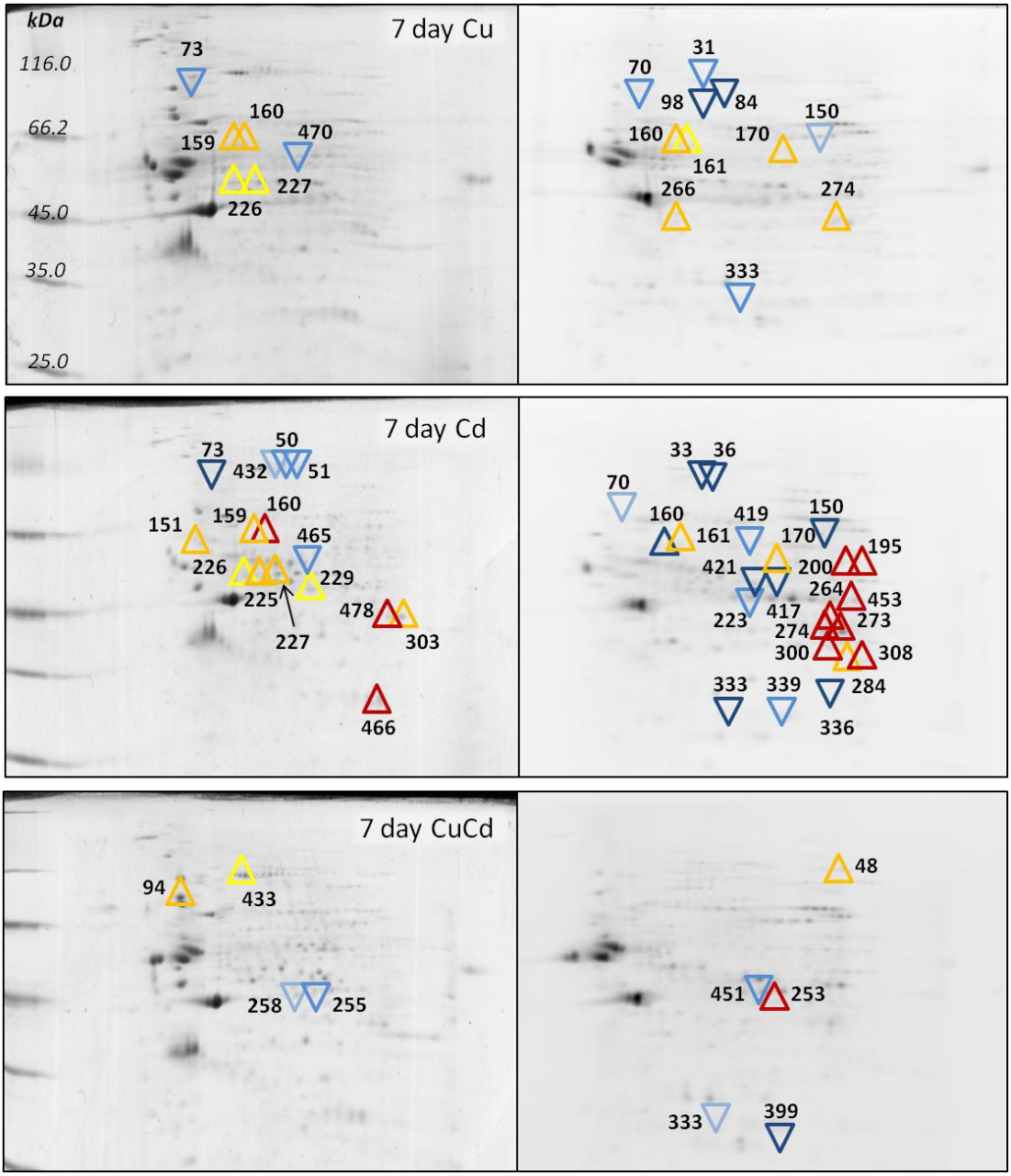

Figure 5.8 Coomassie stain (left) and IAF-labelled fluorescent scan (right) of proteins separated by 2D PAGE from gill tissue of *M. edulis* (n = 20) exposed to Cu, Cd and CuCd for 7 days. Spots that showed a significant difference in intensity compared to control ($p < 0.05$) are indicated. Triangles in yellow, orange and red indicate spots which were more intense in treated groups by a factor of > 1, > 1.5, and > 2, respectively. Inverted triangles in light, mid and dark blue indicate spots which were reduced in treated groups by a factor of > 1, > 1.5, and > 2, respectively.

Table 5.5 Identities of proteins which vary significantly in concentration in gill tissue between control and metal-treated *M. edulis* groups

Spot No.	Identified Protein	Mw (Da)	Fold change ± SD	*p*	Treatment group	GI number	Mascot Score	Matched peptides	Sequence Coverage (%)	Function
478	**Arginine kinase**	39379	+2.1 ± 0.08	*< 0.05*	Cd (7d)	301341836	113	1	9	Enzyme involved in energy buffering and regulation of ATP
465	**Alpha tubulin, partial**	44447	-1.8 ± 0.05	*< 0.05*	Cd (7d)	131573174	561	4	52	Cell structure: forms microtubules with β-tubulin
303	**Creatine kinase b-type**	42703	+1.7 ± 0.05 +1.4 ± 0.02	*< 0.001* *< 0.001*	Cd (7d) CuCd (24h)	317768001	176	2	25	Enzyme involved in energy buffering and regulation of ATP
225/227	**Alpha enolase**	39924	+1.4 ± 0.01 +1.6 ± 0.01	*< 0.05* *< 0.05*	Cu (7d) Cd (7d)	120972524	247	2	14	Enzyme involved in glycolysis; growth control; hypoxia tolerance.
94	**HSP 90**	83073	+1.5 ± 0.03	*< 0.001*	CuCd (7d)	205362524	1210	10	42	Heat shock protein, core cellular stress response. Selective chaperone assisting in protein folding and degradation
226	**Tubulin alpha-3 chain**	86229	+1.5 ± 0.01 +1.5 ± 0.01	*< 0.01* *< 0.01*	Cu (7d) Cd (7d)	432094860	414	2	32	Cell structure: forms microtubules with β-tubulin
433	**Major vault protein**	31693	+1.3 ± 0.01	*< 0.05*	CuCd (7d)	118151639	322	1	44	Nucleo-cytoplasmic transport

Fold change (+/-) indicates the average variation (± the standard deviation, SD) in spot intensity in treated mussel groups relative to control, with the significance of this variation shown by the p value (ANOVA). N = 20 (4 gels, each representing gill tissue from 5 pooled animals). The metal treatments responsible for variations in protein concentration are indicated by 'Treatment group', where 7d = 7 days and 24h = 24 hour exposure.

5.3.5 Antioxidant enzymes: GST activity

Following 24-hour and 7-day exposures, GST activity in gill did not vary significantly between treatment groups ($p > 0.05$; ANOVA) (Figure 5.9).

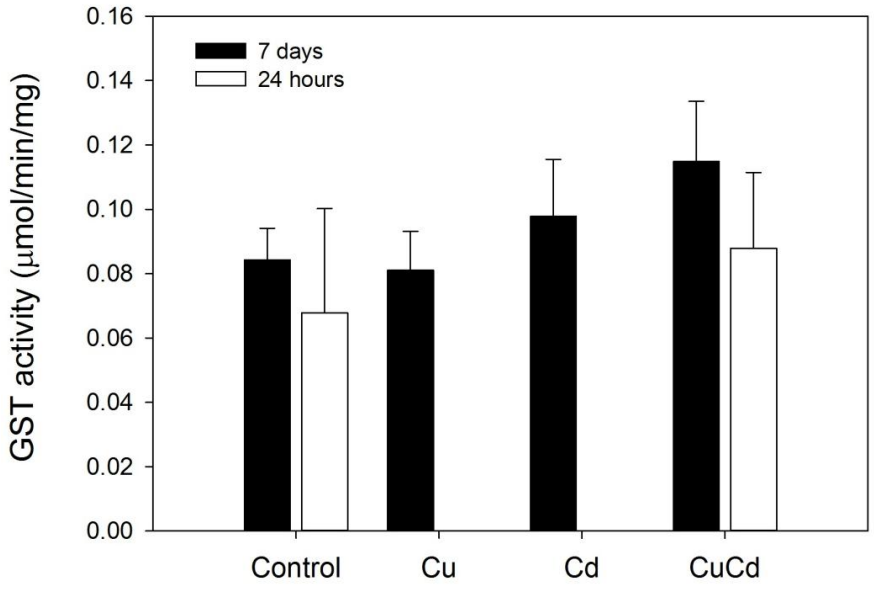

Figure 5.9 Glutathione S-Transferase activity in gill tissues of *M. edulis* in control and metal-treated samples after exposure periods of 24 hours or 7 days. Error bars indicate the standard deviation on the mean across 4 biological replicates (each consisting of 5 pooled samples, n = 20).

5.4 Discussion

This study investigated the proteomic response of *Mytilus edulis* to elevated copper and cadmium, and their mechanisms of detoxification are discussed in the context of prolonged exposure to extreme metal-induced oxidative stress and pre-adaptation in an ancestral species. Following exposure to Cu and Cd, *M. edulis* accumulated high concentrations of these metals in their gill, triggering significant changes in their protein expression profile and thiol subproteome that may indicate active regulation of Cu and Cd.

5.4.1 Tissue metal burden

Considerable depletion of both Cu (up to 22%) and Cd (up to 4%) was observed in seawater in mussel tanks within the < 30 minute period between initiation

of metal exposure and collection of the first water sample, compared to the abiotic control (Figures 5.1 and 5.2). Concentrations of Cu and Cd continued to decline throughout each 24-hour period; however the rate of metal depletion was much reduced after ~4 hours. This indicates either that filtration rate slowed in response to algal depletion of the tank water, or that metal uptake reached a maximum threshold. Based on a range of filtration rates measured by Riisgård *et al.* (2011), the entire 10 L water volume is estimated to pass through the 30 mussels in 16 to 24 minutes. The rate of metal depletion in tanks is similar to that described by Langston *et al*. (1998), who observed rapid initial uptake of metals into mussel tissues, followed by a levelling off in tissue metal levels as external absorption sites become saturated. Alternatively, this time point may represent activation of the detoxification system, enabling greater metal excretion, through the induction of metal-binding proteins such as metallothioneins (MTs) (Viarengo *et al.*, 1980; Bebianno and Langston, 1991; Amiard *et al.*, 2006).

Correspondingly, the concentration of Cu and Cd in mussel tissues increased with increasing duration of exposure (Table 5.3; Figure 5.3). Copper was not significantly enriched above control in gill after 24 hours of exposure, but was enriched by ~4-fold after 7 days. Cadmium was enriched in gill after 24 hours of exposure (9.5-fold) but this enrichment was considerably greater after 7 days (up to 150-fold). Accumulation of metals in tissues is determined by their relative rates of influx and efflux (Wang and Rainbow, 2010). Complexes of essential metals with metallothionein have a faster turnover rate compared to non-essential metals, and therefore have a much shorter half life in mussel tissues (Cu and Cd; 10 and 300 days, respectively) (Bebianno and Langston, 1993). Since Cd also has a greater potential to induce metallothionein than Cu (Langston *et al.*, 1998), more Cd can be complexed, thereby maintaining its ionic gradient and enhancing the influx of dissolved cadmium across the cell membrane (Blackmore and Wang, 2002; Shi and Wang, 2004b). Greater accumulation of Cd in gill and digestive gland tissues compared with Cu, whilst influenced by their different concentrations in tank water, also likely reflects the greater uptake of Cd in response to strong MT induction, and the efficiency of the cell in excreting excess Cu^{2+} ions as a normal process in homeostasis.

Interestingly, the reduction in aqueous Cu and Cd levels in tank seawater was more pronounced when mussels were exposed to both metals together. Further, Cd concentrations continued to decline throughout the 24 hour period in tanks treated with both Cu and Cd for 7 days, but this was not observed with Cu and was not observed during the 24 hour exposure for either metal. Correspondingly, Cd concentrations in gill were significantly greater after 7 days of exposure to Cd in the presence of Cu, compared with Cd alone (105- and 150-fold increase compared to control, respectively), whilst copper concentrations in gill were not significantly different between Cu- and CuCd-exposed groups after 7 days. Whilst the presence of cadmium does not appear to influence copper uptake in tissues, consistent with previous studies (Lecoeur *et al.*, 2004), copper appears to have a synergistic effect on cadmium bioaccumulation and this effect is more pronounced after prolonged exposure, presumably reflecting an initial lag phase prior to MT induction. This is a critical finding in the context of multi-contaminant exposure, characteristic of both hydrothermal vent habitats and areas influenced by anthropogenic pollution, where interference between different metals can either exacerbate or reduce their accumulation and toxicity in tissues (Calabrese *et al.*, 1984; Da Ros *et al.*, 1995; Shi and Wang, 2004a; Ng and Wang, 2007; Serafim and Bebianno, 2010; Raftopoulou and Dimitriadis, 2011; Trevisan *et al.*, 2011; Liu *et al.*, 2012).

Accumulation of Cu and Cd varied considerably between digestive gland and gill, indicating tissue-specific mechanisms of sequestration, detoxification and elimination for these metals. After 7 days of exposure to copper, no significant enrichment in Cu in digestive gland was observed either in Cu-only or CuCd-treated groups compared to control, whilst cadmium was significantly and equally enriched in digestive gland following exposure to Cd-only and CuCd in comparison to control (64 – 69-fold enrichment), and concentrations were higher than those in gill (Table 5.3). As filter feeders, mussels expose their gill to direct contact with the aqueous chemical environment, passively accumulating dissolved metals during respiration/nutrition (Marigómez *et al.*, 2002). Whilst dissolved metals can also be assimilated directly into the digestive gland, either following incorporation into mucus layers on the gills or through water intake into the gut (Langston *et al.*, 1998), this storage organ tends to accumulate metals reflective of longer-term exposure compared to gill (Bebianno and Serafim, 2003). Metallothionein concentrations are higher in digestive gland than in

gill, enabling greater Cd accumulation in this organ over longer time periods (Bebianno and Langston, 1991, 1993), consistent with the findings of this study. The lack of Cu-enrichment in the digestive gland of exposed mussels may be indicative of the efficiency of copper excretion and consequently its short biological half-life (Viarengo *et al.*, 1981).

Concentrations of Cu and Cd in gill and digestive gland tissues of *M. edulis* following exposure are comparable to those measured in the hydrothermal vent mussel, *Bathymodiolus* sp., sampled from hydrothermal vent habitats on the Southwest Indian Ridge (Cole *et al.*, 2013). In *Bathymodiolus* sp. gill, copper and cadmium concentrations ranged between 33 - 124, and 24 – 75 μg g^{-1}, respectively, whilst concentrations in *M. edulis* exposed in this study reached 17 and 58 μg g^{-1} for Cu and Cd, respectively. In digestive gland, Cu and Cd concentrations in the vent mussels were 11 – 40 and 5 - 22 μg g^{-1}, respectively, compared to < 8.6 and < 74 μg g^{-1} in *M. edulis* after exposure. This suggests that the *M. edulis* tissues in our laboratory experiments assimilated a metal burden that was ecologically-relevant to a hydrothermal vent environment, and the proteome changes consequently induced are therefore likely to be representative of acclimatisation potential to a metal-rich vent habitat.

5.4.2 Redox proteomics (thiol oxidation and carbonylation)

Mytilid mussels accumulate high concentrations of metals, and other xenobiotics, and their mechanisms of detoxification have been the subject of extensive investigation owing to their widespread use as biological indicators of marine pollution (Nicholson, 2003b;a). The focus of many of these studies is the induction of metallothioneins (MT) and their role in maintaining adequate cellular concentrations of essential metals, and in sequestering and facilitating the excretion of non-essential metals (Viarengo *et al.*, 1980; Bebianno and Langston, 1991, 1993; Amiard *et al.*, 2006; Wang and Rainbow, 2010). This group of metal-binding proteins is essential in defence against pro-oxidants in many organisms, and whilst many isoforms of MT exist, they are highly conserved in the animal Kingdom. Indeed, Hardivillier *et al.* (2004) demonstrate strong similarities in cDNA sequences for MT between *Bathymodiolus* spp. and *M. edulis*. Other peptides are also important, such as reduced glutathione (GSH), which rapidly sequesters toxic metals via the cysteine group prior

to induction of MT (Regoli and Principato, 1995; Langston *et al.*, 1998; Masella *et al.*, 2005), and is crucially involved in cellular redox homeostasis (Schafer and Buettner, 2001; Hansen *et al.*, 2009).

Extreme exposure to metals enhances the production of reactive oxygen species (ROS), which can impair the activity of these metal-binding proteins and weaken their ability to control the level of free metal ions in the cell (Viarengo *et al.*, 1996; Langston *et al.*, 1998). The impact of ROS on the proteome is an expanding field in ecotoxicology (Sheehan, 2006), and several studies have reported on the redox modifications to proteins in a number of shallow-water bivalves (McDonagh *et al.*, 2005; Dowling *et al.*, 2006; McDonagh and Sheehan, 2006, 2007; Chora *et al.*, 2008; McDonagh and Sheehan, 2008; Tedesco *et al.*, 2010; 2012). However, these studies have focused on the oxidative response either to a short-term toxic shock, often a 24-hour treatment period, or to exposure to one contaminant in isolation.

Following 1D PAGE, no significant differences were observed in fluorescence counts with IAF or FTSC in treated mussel groups compared to their respective control, in either gill or digestive gland (Figure 5.5). Whilst oxidative stress is typically associated with a decrease in free thiol groups (Åslund and Beckwith, 1999; Baty *et al.*, 2002), cysteine-containing proteins can be induced in response to an increase in the activity of free metal ions in the cell (Hansen *et al.*, 2009). Efficient formation of metal-MT complexes may prevent measurable oxidative damage from the assimilated metals across the complete proteome. It is therefore arguable that exposure to copper and/or cadmium at concentrations representative of a hydrothermal vent habitat does not trigger a significant oxidative stress response in *M. edulis*.

However, following 2D PAGE of IAF-labelled protein extracts, gel analysis revealed a considerable difference in the redox response of gill tissue to copper and cadmium, both between treatments and between different durations of exposure (Figures 5.7 and 5.8). After 24 hours of exposure to both Cu and Cd, 9 spots showed a change in the number of free thiol groups compared with control (Figure 5.7), increasing in 7 spots and decreasing in 2, whilst after 7 days only 5 spots varied in intensity compared to control, increasing in 2 and decreasing in 3. Whilst this does not suggest an extreme level of oxidative stress in either case, it does indicate that there may be a lag period prior to the induction of antioxidant enzymes during which

individual proteins are more vulnerable to oxidative damage. Following 24 hours of exposure, a greater number of spots showed an increase in free thiols compared to a 7 day exposure, suggesting enhanced expression of cysteine-rich proteins during the initial toxic shock period. Within the 7 day exposure experiment, Cd was found to induce the greatest change in the thiol subproteome, with a significant change in intensity from control measured in 23 spots (compared to 11 with Cu, and 5 with Cu and Cd together). Copper is an essential element and cellular mechanisms for regulating its concentration are better established compared to Cd. When mussels were exposed to both metals for 7 days, there appeared to be an antagonistic effect on the proteome, despite the significant enrichment in tissue metal concentrations. The influx of metal ions, particularly Cu and Cd, is well-known to trigger strong induction of MTs and other metal-binding proteins, which efficiently sequester metals through complexation, thereby protecting components of the cell from oxidative damage. Whilst these proteins are not resolved in the molecular mass range achieved by our electrophoretic technique, owing to their very small size (< 6.8 kDa), it is likely that they are increasingly up-regulated with cellular metal concentration and are most abundant in the CuCd treated mussel groups. This finding highlights the need for multi-contaminant studies in the investigation of proteomic responses to pro-oxidant environments, particularly in the selection of suitable biomarkers for stress in polluted areas.

5.4.3 Variations in protein expression

Despite the substantial bioaccumulation of Cu and Cd measured in gill in this study, relatively few proteins varied significantly in expression (Figures 5.7 and 5.8). Among 69 matched spots; only one varied in intensity after 24 hours of exposure to Cu and Cd, whilst 6, 15 and 4 spots were variably expressed after 7 days of exposure to Cu, Cd and CuCd, respectively. Interestingly, exposure to both copper and cadmium together induced a change in a very small number of proteins, following both 24-hour and 7-day exposures, whilst mussels exposed to Cd-only showed the greatest proteomic change. In the Chinese mitten crab, *Eriocheir sinensis*, Silvestre *et al*., (2006) demonstrated that a greater number of proteins may be differently expressed following chronic exposure (i.e. 50 μg L^{-1} Cd; 30 days) compared with acute exposure (500 μg L^{-1} Cd; 10 days). Prolonged exposure to a moderate level of

toxicity may enable acclimation via changes in the proteome, and consequently increased resistance to the contaminant(s) in question. Indeed, many studies have reported on the enhanced tolerance to metal stress where organisms are pre-exposed to certain contaminants (Calabrese *et al.*, 1984; Amiard-Triquet and Amiard, 1998; Blackmore and Wang, 2002; Shi and Wang, 2004a; Trevisan *et al.*, 2011) suggesting an ability to adapt to resist oxidative damage. Cadmium is one of the most toxic metals known to aquatic life, and accumulation of this metal can be extremely damaging if un-regulated. Whilst the presence of Cu may help to induce metal-binding proteins that can also sequester Cd, the cellular response to excess Cd on its own may be less efficient. [Cd] in gill tissue from the Cd-only mussel group may have increased at a faster rate than MT induction, therefore triggering a greater proteomic response as means of resisting oxidative damage.

As demonstrated in this study and others (Sheehan *et al.*, 2010), the proteome is remarkably robust and xenobiotic stress typically triggers expression changes in only a small number of proteins. By identifying these proteins, their relative abundances can be assessed as reliable and pollutant-specific biomarkers. In this study, significant changes in 21 protein spots were measured between treated and control mussel groups, and 7 of these were successfully identified. The proteins have important roles in metabolism, cell structure, energy storage and antioxidant defence (Table 5.5). Arginine kinase (AK), creatine kinase (CK), alpha enolase (α-E) and tubulin alpha-3 chain (T-α3) were all up-regulated following 7 days of exposure to Cd, whilst α-E and T-α3 were also up-regulated by Cu. Following 7 days of exposure to Cu and Cd together, the expression of CK, heat shock protein 90 (HSP 90) and a major vault protein (MVP) increased significantly relative to control, whilst only CK was significantly up-regulated after 24 hours. Alpha tubulin (αT) was suppressed following 7 days of Cd treatment.

Both AK and CK are critically involved in regulating ATP by catalysing the reversible transfer of a phosphate group (from an enzyme-specific phosphagen, i.e. arginine phosphate or creatine phosphate) to ADP (Ellington, 2001). Previous proteomic analyses of *M. edulis* sampled from a polluted harbour, and the Chinese mitten crab, *Eriocheir sinensis*, following chronic Cd exposure, have shown strong down-regulation in these phosphagen kinases relative to control groups (Silvestre *et*

al., 2006; Tedesco *et al.*, 2012). However, these enzymes are considered to play an important role in facilitating tolerance to variable environmental stressors in invertebrates (Ellington, 2001), and *M. edulis* may up-regulate AK and CK following Cd exposure as a mechanism for maintaining ATP supply during this (shorter; 7 days) period of stress. Alpha enolase is an important enzyme involved in carbohydrate catabolism by glycolysis (Pancholi, 2001), but also plays a protective role against oxidative and thermal stress as a hypoxic stress protein (Aaronson *et al.*, 1995) and a heat shock protein (Iida and Yahara, 1985). Alpha tubulin forms the major constituent of cytoskeletal microtubules, structural features which are involved in maintaining the shape of the cell and the intracellular transport of organelles. Cd exposure has previously been shown to induce microtubular disorganisation (Silvestre *et al.*, 2005) in line with down-regulation of αT (Silvestre *et al.*, 2006). This study indicates that αT is suppressed in *M. edulis* following Cd exposure, whereas T-α3 increases in expression in response to Cu and Cd (individually). HSP 90 is a molecular chaperone with a key role in proteostasis, promoting the correct folding and assembly of proteins, and can be induced rapidly in response to oxidative stress (Benarroch, 2011). HSP 90 is one of a large subset of heat shock proteins, which are critical components of the antioxidant defence system owing to their ability to prevent inappropriate protein aggregations under heightened stress conditions (Benarroch, 2011). MVP is a multi-subunit ribonucleoprotein that forms hollow, barrel-like structures thought to function in nucleo-cytoplasmic transport and/or sequestration of cellular molecules (Yu *et al.*, 2002). Whilst very little is known about these ubiquitous cellular organelles, their elevated expression in cells chronically exposed to xenobiotics (Scheffer *et al.*, 1995) and their ability to bind calcium (van Zon *et al.*, 2002), may indicate an important antioxidant function. GST catalyses the conjugation of GSH to a range of pro-oxidant substrates to promote their excretion and is key to phase II detoxification (Strange *et al.*, 2001), yet a significant change in abundance of this enzyme was not observed with metal-treatment in this study. Whilst a greater sample number may yet resolve a significant change in GST, the concentration and/or length of exposure to Cu and Cd here may be insufficient to induce a significant response.

5.5 Conclusions

Following exposure of *M. edulis* to Cu and Cd, this study shows that metal uptake increases significantly with duration of metal treatment; metals are more concentrated in gill compared with digestive gland; and uptake of Cd is enhanced in the presence of Cu. Metals are assimilated into tissues along concentration gradients, and metal-binding proteins help to maintain these gradients and facilitate uptake. Mechanisms for sequestering excess Cu, as an essential element, are better established and may also facilitate accumulation of Cd, whilst induction of metal-binding proteins may be slower in response to Cd alone. However, whilst metal enrichment in tissues was greatest in mussels exposed to Cu and Cd together, the greatest proteomic change was observed in mussels exposed to Cd alone. Cadmium is one of the most toxic metals known to marine biota, and exposure stimulated significant up-regulation of numerous proteins involved in antioxidant defence, energy regulation, cell structure, and metabolism, in addition to an overall increase in cysteine groups. In an environment characterised by multiple contaminants, such as a hydrothermal vent habitat, interactions between metals may alter their relative toxicity. Where Cu and Cd are assimilated together, their intracellular form may be less toxic compared to the single metals, potentially via complexation with MTs. Understanding mechanisms of metal regulation in the context of tolerating the many stressors of a vent field clearly requires further research into metal-organism relationships, particularly where animals are exposed to metal mixtures.

Chapter 6

6 Proteomic Responses to Metal-Induced Oxidative Stress in Hydrothermal vent-Living Mussels, *Bathymodiolus* sp., on the Southwest Indian Ridge[1]

Bathymodiolin mussels are amongst the dominant fauna occupying hydrothermal vent ecosystems throughout the World's oceans. This subfamily inhabits a highly ephemeral and variable environment, where exceptionally high concentrations of reduced sulphur species and heavy metals necessitate adaptation of specialised detoxification mechanisms. Whilst cellular responses to common anthropogenic pollutants are well-studied in shallow-water species they remain limited in deep-sea vent fauna. *Bathymodiolus* sp. were sampled from two newly-discovered vent sites on the Southwest Indian Ridge (Tiamat and Knuckers Gaff) by the remotely operated vehicle Kiel 6000 during the *RRS James Cook* cruise, JC 067 in November 2011. Here, the effects of tissue metal accumulation on protein expression and thiol oxidation in gill were investigated using a redox proteomics approach.

Following 2D PAGE, a significant difference in intensity in 30 protein spots were observed in gill between the two vent sites out of 205 matched spots. Significant variations were also measured in thiol oxidation in 15 spots, out of 143 matched. At Tiamat, 23 protein spots were up-regulated compared to Knuckers Gaff and 5 of these were identified with important roles in metabolism, cell structure, stress response, and redox homeostasis. This study demonstrates that increased metal exposure may trigger changes in the proteome, regulating tissue uptake. This is evident both between vent sites and across a chemical gradient within the Knuckers Gaff vent site. These findings highlight the importance of proteomic plasticity in successful adaptation to the spatially and temporally fluctuating chemical environments that are characteristic of hydrothermal vent habitats.

[1]This chapter is in press as Cole, C., Coelho, A., James, R. H., Connelly, D., Sheehan, D., Proteomic responses to metal-induced oxidative stress in hydrothermal vent-living mussels, *Bathymodiolus* sp., on the Southwest Indian Ridge, Marine Environmental Research (2013), doi: 10.1016/j.marenvres.2013.09.003.

6.1 Introduction

The circulation of conductively-heated seawater in tectonically active regions of the Earth's crust generates high-temperature hydrothermal fluids, which are highly enriched in volatile gases, sulphide and metals, and are discharged through focused and diffuse springs at the seabed (Von Damm, 1988). In the mixing zone between hydrothermal fluids and seawater, chemoautotrophic bacteria synthesise organic carbon using reduced compounds (sulphide and methane), supporting a highly productive ecosystem (Stewart *et al.*, 2005; Fisher and Girguis, 2007). Bathymodiolin mussels are amongst the dominant vent fauna inhabiting the hydrothermal environment at the global scale (Miyazaki *et al.*, 2010). These mussels host bacterial endosymbionts in their gills (Cavanaugh *et al.*, 1987; McKiness and Cavanaugh, 2005; Stewart *et al.*, 2005), but they can also feed heterotrophically on particulate organic matter (Page *et al.*, 1991). This mixotrophic diet is an important adaptation to the spatially and temporally fluctuating supply of reducing agents. Adapting to survive in the chemically variable hydrothermal environment also requires an ability to cope with highly toxic concentrations of many metals. In these hydrothermal sites animals are exposed to metal concentrations of the order of a thousand times higher than in oceanic waters (Sarradin *et al.*, 1999) and may have evolved specialised mechanisms of detoxification.

Elevated metal exposure can result in oxidative stress in an organism, as some metals lead to production of reactive oxygen species (ROS) which can exceed cellular antioxidant defences (McDonagh *et al.*, 2005). In hydrothermal environments, metals catalyse the oxidation of sulphide to form a number of oxygen- and sulphur-based radicals. This initiates a chain reaction ultimately producing HO•, the most oxidising radical in biological systems (Fridovich, 1998; Tapley *et al.*, 1999). The bulk of ROS are absorbed by proteins and prolonged exposure to metals can therefore cause damaging changes to proteins involved in detoxification. Thiol oxidation is a well-known deleterious proteomic change resulting from the action of ROS produced in response to xenobiotics (Chora *et al.*, 2008; Sheehan *et al.*, 2010; Tedesco *et al.*, 2010; Company *et al.*, 2012; 2012). Proteins containing thiol groups (-SH) are critical components of the antioxidant defence system, and are important in enzyme catalysis and in control of the cellular redox environment (Eaton, 2006; Hansen *et al.*, 2009).

These groups are particularly susceptible to oxidation, leading to reversible or irreversible formation of a variety of sulphoxidation products. Many of the reversible reactions are integral to protein structure and cell signalling, and they may also provide temporary protection to key functional groups under conditions of oxidative stress (Schafer and Buettner, 2001). The irreversible formation of sulphinic ($R\text{-}SO_2H$) and sulphonic ($R\text{-}SO_3H$) acids are indicative of more severe oxidation (Hansen *et al.*, 2009), and these changes can be detrimental to protein structure and function.

Fluorescent labelling of targeted functional groups of amino acid side chains provides a quantitative means of assessing oxidative damage to proteins. Iodoacetamidofluorescein (IAF) reacts with free –SH groups (but not with the oxidised variants) to form stable thioethers. These fluorescein-protein conjugates can be visualised as fluorescent bands/spots in electrophoretic separations (Ahn *et al.*, 1987; Baty *et al.*, 2002). This technique has proved to be a powerful indicator of oxidative stress in *Mytilus edulis* exposed to pro-oxidants (McDonagh and Sheehan, 2007; 2008), but studies in vent organisms are few (Fisher and Girguis, 2007; Mary *et al.*, 2010; Company *et al.*, 2011; 2012).

Bathymodiolin mussels inhabit hydrothermal vents in every ocean, and are therefore an ideal genus for enhancing understanding of proteomic responses to the highly variable environmental stressors characteristic of vent habitats. This study uses redox proteomics to investigate the effect of tissue metal accumulation on protein expression and oxidation in a species of hydrothermal vent-living mussel, *Bathymodiolus* sp., sampled from newly-discovered sites on the Southwest Indian Ridge (SWIR). Hydrothermal ecosystems hosted on the SWIR are of great importance to understanding of vent-faunal biogeography, owing to the along-axis connections with the Atlantic and Pacific Oceans (German *et al.*, 1998; Gamo *et al.*, 2001; Gallant and Von Damm, 2006). Protein-based mechanisms of detoxification are relatively poorly understood in vent fauna, and may form an important piece in the puzzle of vent colonisation, and contribute to understanding the emergence of distinct faunal assemblages throughout the global mid-ocean ridge.

6.2 Materials and methods

6.2.1 Vent mussel sample collection and preparation

Hydrothermal vent mussels, *Bathymodiolus* sp. (6 – 9 cm) (Figure 6.1), were sampled from two newly-discovered vent sites on the SWIR; Tiamat (37° 47.029' S, 49° 38.965' E, 2770m depth) and Knuckers Gaff (37° 47.030 S, 49° 38.967' E, 2785m depth) by ROV Kiel 6000 (GEOMAR) during the *RRS James Cook* cruise JC 067, in November 2011.

Figure 6.1 Photograph of the *Bathymodiolus* sp. population located on the Knuckers Gaff hydrothermal vent, SWIR, in November 2011.

Whole animals were flash-frozen in liquid nitrogen and stored at -80 °C. Onshore, animals were defrosted on ice and dissected for gill and digestive gland at University College Cork, where all proteomic work was conducted. Bacteria were not removed from dissected tissues. Due to the relatively limited number of animals available (n = 10), samples were not pooled but were homogenised individually in 10 mM Tris-HCl (pH 7.2), 0.5 M sucrose, 0.15 M KCl, 1 mM ethylenediaminetetraacetic acid (EDTA), and 1 mM phenylmethylsulfonyl fluoride (PMSF) using a motor-driven Teflon Potter-Elvehjem homogeniser, and centrifuged at 15,000 x *g* (60 min, 4 °C) to separate the soluble fraction from the pellet. Protein concentration in the supernatant phase was quantified in gill samples using the Bradford method (1976), using bovine serum albumin (BSA) as a calibration standard.

6.2.2 Analysis of metals in mussel tissues

A number of both essential (Fe, Mn, Cu, Zn) and toxic (Cd, Pb, Hg, As, Al) metals, known to be enriched in hydrothermal fluids relative to seawater, were analysed in gill and digestive gland tissues of *Bathymodiolus* sp. from the soluble and insoluble fractions generated through centrifugation as described in section 6.2.1. Solid pellets were freeze-dried, and corresponding supernatant fluids were heated to dryness at 130 °C. The dry-weight of the sample was then determined and an aliquot of ~100 mg was dissolved in concentrated thermally distilled (TD) HNO_3 by heating in a closed Savillex vial (15ml) on a hotplate at 60 °C for ~24 hours. The digested samples were then dried-down at 130 °C and re-dissolved in 3% TD HNO_3 spiked with Be (20 ppb), In (5 ppb) and Re (5 ppb) as internal standards. Metal concentrations were determined by inductively coupled plasma mass spectrometry (ICP-MS) (Thermo Scientific X-Series) at the National Oceanography Centre, Southampton. External standards were prepared using 1000 μg ml^{-1} standard stock solutions (Inorganic Ventures) in 3% TD HNO_3. The precision of the analytical procedure was confirmed through digestion and analysis of certified reference material (CRM); lobster hepatopancreas TORT-1 (National Research Council of Canada), alongside the samples. The reproducibility of these analyses was better than 8% for all metals, and measured values for the CRM were within error of the certified values for all metals. The concentrations of metals in the Tris-HCl buffer and HNO_3 were also determined and subtracted from the measured concentrations. Metal concentrations are reported as the sum of the soluble and insoluble fractions, in μg g^{-1} of the tissue dry tissue weight.

6.2.3 Fluorescein labelling

Protein thiols were labelled with 0.2 mM iodoacetamidofluorescein (IAF) from a 20 mM stock solution in dimethyl sulphoxide. Gill sample aliquots containing 25 μg protein (1D PAGE) and 150 μg protein (2D PAGE) were incubated with IAF for two hours on ice in the dark. Proteins were precipitated by incubating extracts in 10% (v/v) trichloroacetic acid (TCA) for 5 min on ice, followed by centrifugation at 11,000 x *g* for 3 min. The resulting pellet was washed in an excess of ice-cold acetone to remove TCA and any interfering salts or non-protein contaminants. Protein extracts were re-suspended in 15 μl sample buffer for 1D PAGE (62.5 mM Tris-HCl (pH 6.8)

containing 25% (v/v) glycerol, 2% (w/v) SDS, 5% (v/v) β-mercaptoethanol and a trace amount of bromophenol blue) or 125 µl rehydration buffer for 2D PAGE (7 M urea, 2 M thiourea, 2% (w/v) CHAPS, 4% (v/v) ampholyte (Pharmalyte 3-10), 1.2% (v/v) DeStreak reagent and a trace amount of bromophenol blue).

6.2.4 Polyacrylamide Gel Electrophoresis (PAGE)

6.2.4.1 1D PAGE

Gill samples (25 µg protein in 15 µl sample buffer) were heat-denatured and loaded alongside protein molecular mass markers (ThermoScientific, Dublin, Ireland) into wells embedded within a stacking gel of 4.5% (v/v) polyacrylamide in 0.5 M Tris-HCl, pH 6.8, set above a resolving gel of 14% (v/v) polyacrylamide in 1.5 M Tris-HCl, pH 8.8. Gel electrophoresis was carried out at 4 °C using an Atto AE-6450 mini PAGE system (BioRad; Hercules, CA, USA) at a constant voltage of 90 V until samples entered the resolving gel, then 120 V until the dye front reached the bottom of the gel. Fluorescently labelled bands were visualised using a Typhoon Trio+ Variable-Mode Imager (GE Healthcare, Little Chalfont, Bucks, UK) measuring excitation of Fluorescein at 532 nm and emission at 526 nm. Protein bands were visualised by colloidal coomassie-staining using the protocol of Dyballa and Metzger (2009).

6.2.4.2 2D PAGE

Gill samples (150 µg protein in 125 µl rehydration buffer) were loaded onto 7 cm non-linear immobilised pH gradient (IPG) strips (pH 3 – 10) and rehydrated for 18 hours in the dark at room temperature (Leung *et al*., 2011). Rehydrated IPG strips were focused on a Protean isoelectric focusing (IEF) cell (Bio-Rad) with linear voltage increases in the following sequence: 250 V for 15 min; 4,000 V for 2 hours; then up to 20,000 Vh. Prior to 2D PAGE, focused strips were incubated in equilibration buffer (6M urea, 0.375M tris-HCl, pH 8.8, 2% (w/v) SDS, 20% (v/v) glycerol), first with 2% (w/v) dithiothreitol (DTT) to ensure complete reduction of disulphide bridges and secondly with 2.5% (w/v) iodoacetamide (IAM) to reduce streaking. Equilibrated strips were loaded onto 14% SDS-polyacrylamide gels alongside a wick containing an unstained protein molecular mass marker, and sealed

with agarose (0.5%) containing a trace amount of bromophenol blue. Gel electrophoresis was carried out as for 1D PAGE.

6.2.5 Image analysis

Coomassie-stained gels were scanned with a calibrated imaging densitometer (GS-800; Bio-Rad). Background subtraction and optical density quantification of protein bands in 1D PAGE gels was performed using Quantity One image analysis software (Bio-Rad). For each gel lane, intensity of fluorescence (counts) was normalised against protein content (optical density) to correct for differences in sample loading and enable the extent of thiol oxidation to be compared between samples. Progenesis SameSpots image analysis software (Version 4.5; Nonlinear Dynamics, Durham, NC, USA) was used to align gels, match spots, and quantify spot volumes in 2D PAGE gel images of coomassie-stained, and thiol-labelled protein separations. Spots with a significant change in expression intensity (determined by a fold change of > 1.5; $p < 0.05$; student's t-test) between mussels from Tiamat and Knuckers Gaff were selected for protein identification.

6.2.6 Protein digestion and identification

Proteins were manually picked from 2D PAGE separations, lightly stained with colloidal coomassie. Following in-gel tryptic digestion, extracted peptides were loaded onto a R2 micro-column (RP-C18 equivalent) where they were desalted, concentrated and eluted directly onto a MALDI plate using α-cyano-4-hydroxycinnamic acid (CHCA) as the matrix solution in 50 % (v/v) acetonitrile and 5% (v/v) formic acid. Mass spectra of the peptides were acquired in positive reflectron MS and MS/MS modes using a MALDI-TOF/TOF MS instrument (4800*plus* MALDI TOF/TOF analyzer) with exclusion list of the trypsin autolysis peaks (842.51, 1045.56, 2211.11 and 2225.12). The collected MS and MS/MS spectra were analysed in combined mode by Mascot search engine (version 2.2; Matrix Science, Boston, MA) and the NCBI database restricted to 50 ppm peptide mass tolerance for the parent ions, an error of 0.3 Da for the fragments, one missed cleavage in peptide masses, and carbamidomethylation of Cys and oxidation of Met as fixed and variable amino acid modifications, respectively. No taxonomy restrictions were applied as the genome has not been fully sequenced for species within the

Bathymodiolus genus. The identified proteins were only considered if a MASCOT score above 95% confidence was obtained ($p < 0.05$) and at least one peptide was identified with a score above 95% confidence ($p < 0.05$). This analysis was conducted by the Analytical Services Unit, Instituto de Tecnologia Química e Biológica (ITQB), New University of Lisbon, Lisbon, Portugal.

6.2.7 GST assay

Glutathione transferase (GST) activity was quantified in gill tissues (n = 8) from sample aliquots containing 15 μg of protein diluted to a volume of 50 μl. Samples were loaded into a 96-well microtitre plate with 100 μl of 2 mM 1-chloro-2,4-dinitrobenzene (CDNB) (from a 40 mM stock in ethanol) in 0.15 M potassium phosphate buffer (pH 6.5). GST activity was measured spectrophotometrically by adding 50 μl of 20 mM reduced glutathione (GSH) and measuring absorbance at 340 nm immediately and every 15 seconds for 5 minutes.

GST activity was calculated from the Equation 6.1 (Habig *et al.*, 1974):

$$\text{GST activity } (\mu\text{mol/min/mg}) = (\Delta A_{340}\ V) / (\varepsilon\ l\ M) \qquad (6.1)$$

Where, ΔA_{340} represents the blank-subtracted initial rate of reaction between CDNB and GSH (min^{-1}); V is the volume of reaction (0.2 ml); ε is the extinction coefficient of the reaction product at 340 nm (9.6×10^{-3} μM^{-1} cm^{-1}); *l* is the path length (0.524 cm); and M is the mass of protein (15 μg).

6.2.8 Statistical analyses

The distribution of the tissue metal concentrations was significantly different from a normal distribution, so a non-parametric statistical test was required to analyse the variation between groups. Kruskal-Wallis multiple comparison tests (K-W) were applied together with Dunn's post-hoc analysis to quantify the significance of the variation in metal content between gill and digestive gland tissues, both within each vent site and between the two sites. Correlation analyses were conducted to evaluate any relationship between metal concentration and IAF fluorescence counts at each of the two sites. Significant differences in the means of global fluorescence intensity (1D), GST activity, and of coomassie-stained and IAF-labelled spot volumes (2D), in

mussel gills between the two vent sites were analysed using the student's t-test after testing for normality in the data. In all cases, significant relationships are reported at the 95% confidence level where $p < 0.05$.

6.3 Results

6.3.1 Tissue metal concentrations

Tissue concentrations for essential (Mn, Fe, Cu, Zn) and toxic metals (Al, As, Cd, Hg, Pb) in gill and digestive gland of the hydrothermal vent-living mussel, *Bathymodiolus* sp., for both vent sites are shown in Figure 6.2. Where significant differences between tissues were observed, gill was found to have higher concentrations of each metal than digestive gland, with the exception of Fe. At the Tiamat vent site, Mn, Zn, Cd, Hg and Pb were all significantly enriched in gill compared with digestive gland at the 95% confidence interval (K-W, $p < 0.05$), whilst Cu was also enriched in gill and Fe enriched in digestive gland at the 90% confidence interval (K-W, $p < 0.1$). At the Knuckers Gaff vent site, gill tissues were significantly enriched in Cu, Zn, Cd, Hg and Pb compared with digestive gland (K-W, $p < 0.05$). Between the two vent sites, metal concentrations in tissues were consistently higher in mussels sampled from the Knuckers Gaff site compared with those from Tiamat. Whilst large biological variation and small group size, inherent in deep-sea vent sampling, hinders statistical confirmation of these differences, Fe concentrations were found to be significantly higher in gill tissues of mussels from Knuckers Gaff compared with Tiamat (K-W, $p < 0.05$). Aluminium and arsenic showed no statistical variation between tissues or between sites (K-W, $p > 0.05$).

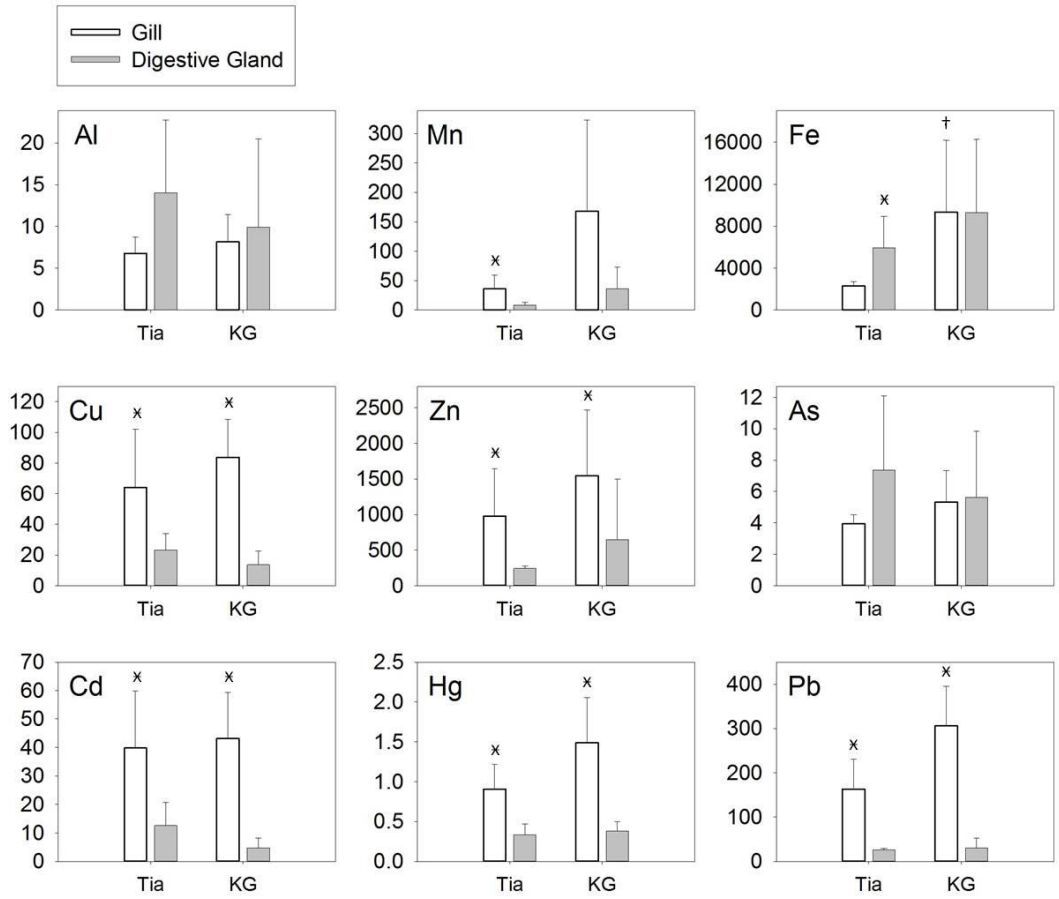

Figure 6.2 Mean concentration (μg g^{-1} dry weight; n = 5) of essential (Mn, Fe, Cu, Zn) and toxic (Al, As, Cd, Hg, Pb) metals in gill (white bars) and digestive gland (grey bars) tissues of *Bathymodiolus* sp. from SW Indian Ridge hydrothermal vent sites; Tiamat (Tia) and Knuckers Gaff (KG). Error bars indicate the standard deviation on the mean. Significant differences between gill and digestive gland are indicated by *, and between sites by †.

6.3.2 Global thiol oxidation

Fluorescence intensity (IAF) measured over 1D PAGE separations, normalised to protein content to correct for any minor differences in sample loading, provides an indication of the global extent of thiol oxidation (Baty *et al.*, 2002) in gill tissues of *Bathymodiolus* sp. (Figure 6.3). Greater fluorescence intensity was observed in IAF-labelled gill samples at Knuckers Gaff (163,000 ± 60%) compared with Tiamat (86,400 ± 9%), however this difference was not statistically significant (t-test, p = 0.16).

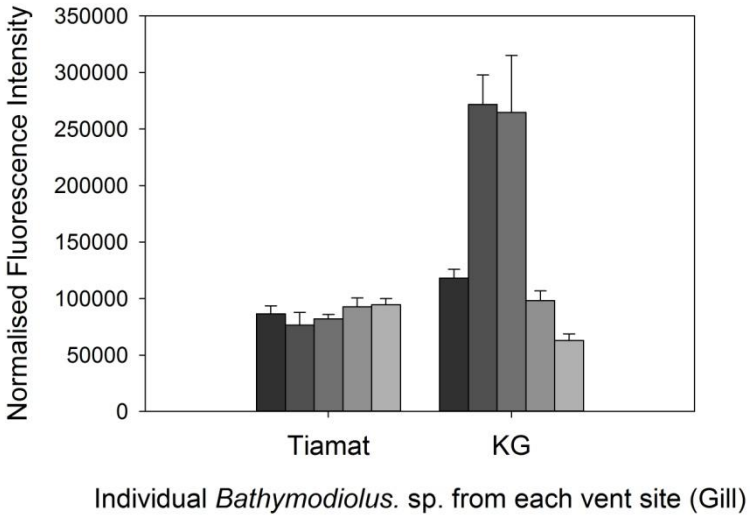

Figure 6.3 Intensity of fluorescence measured in IAF-labelled gill tissues of *Bathymodiolus* sp. individuals collected from Tiamat (n = 5) and Knuckers Gaff (n = 5) vent sites. Count values are normalised to protein content, as measured by optical density in coomassie-stained gels. Error bars indicate the standard deviation from the mean measured over four technical replicates.

Global comparison of the redox modifications to the proteome between the two sites studied is impaired by the extent of biological variation in mussels from Knuckers Gaff. Video footage of the sample collection indicates that individual specimens were collected over a wider area at the Knuckers Gaff vent site compared with Tiamat. Hydrothermal vent habitats are characterised by steep chemical gradients as high-temperature fluids mix with cold seawater, and mussels will be exposed to a spatially variable chemical composition. Greater biological variation in thiol oxidation at Knuckers Gaff may therefore reflect greater chemical diversity within this group compared with Tiamat where individuals were sampled from a more tightly constrained area. In Figure 6.4, the relationship between global thiol oxidation and tissue metal content in gills of individual animals is analysed for each site. Correlation analyses between metal concentration and coomassie-normalised fluorescence counts (1D PAGE) reveal a number of significant relationships. IAF counts decrease significantly with increasing As at Tiamat ($R = -0.895$; $p < 0.05$) and Fe at Knuckers Gaff ($R = -0.895$; $p < 0.05$), but increase significantly with increasing Pb at Tiamat ($R = 0.957$; $p < 0.05$).

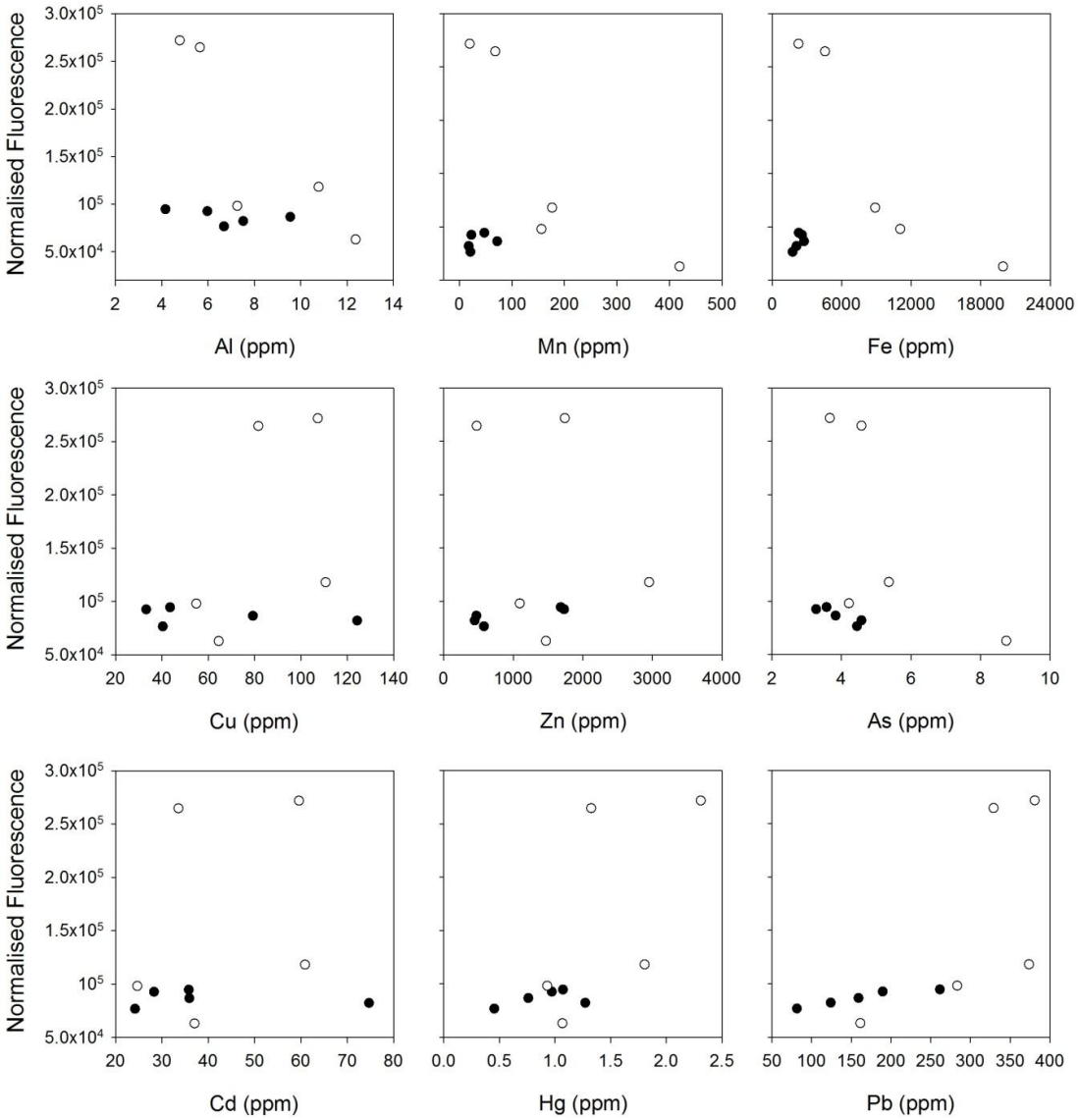

Figure 6.4 Coomassie-normalised fluorescence intensity for IAF-labelled proteins in relation to metal content in gill tissues of *Bathymodiolus* sp. individuals sampled from Tiamat (black circles) and Knuckers Gaff (white circles) hydrothermal vent sites.

6.3.3 Protein expression profiles: 2D PAGE

Whilst the 1D PAGE approach discussed in Section 6.3.2 provides a global indication of thiol oxidation status in tissues, it does not readily distinguish effects at the level of individual proteins. The response of individual proteins to oxidative stress can be better assessed using 2D PAGE. As metal concentration in this study was found to be higher in gill than digestive gland, 2D PAGE analysis was chosen to focus on IAF-labelled proteins in gill tissues (Figure 6.5).

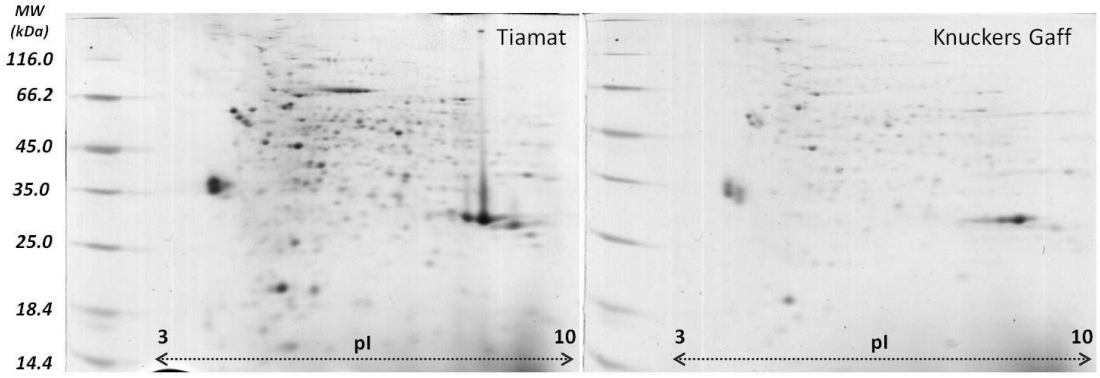

Figure 6.5 Representative images of electrophoretically separated, coomassie-stained protein spots for *Bathymodiolus* sp. gill tissues sampled from Tiamat and KG vent sites. A protein molecular mass marker ranging from 14.4 kDa (bottom) to > 116.0 kDa (top) is shown for size reference. Isoelectric point (pI) is indicated along the pH range (3-10).

Excluding smears and gel defects, a total of 205 well-resolved spots were matched in coomassie-stained protein separations between the two groups. A significant difference in signal level between the two sites was measured in 30 protein spots ($p < 0.05$), of which 10 were highly significant ($p < 0.01$). Of these, 23 spots were elevated at Tiamat and 7 were elevated at Knuckers Gaff (Figure 6.6). Successful protein identifications are presented in Table 6.1. In fluorescent scans of the same gels, a total of 143 IAF-labelled spots were matched in gill, and 15 of these showed a significant difference in spot volume between the two vent sites ($p < 0.05$). At Tiamat, 10 spots showed a reduction in fluorescence with IAF in comparison with Knuckers Gaff, whilst 5 spots showed an increase (Figure 6.6). These changes in fluorescence intensity occurred independently of any significant change in protein expression, suggesting redox modification to proteins present in all 15 spots.

6.3.4 GST activity

GST activity was found to be higher in gills from *Bathymodiolus* sp. at Tiamat (0.085 ± 0.03) compared to Knuckers Gaff (0.043 ± 0.03), though statistical comparison of the means of each group revealed that this difference was only significant at the 90% confidence level (t-test; $p = 0.094$).

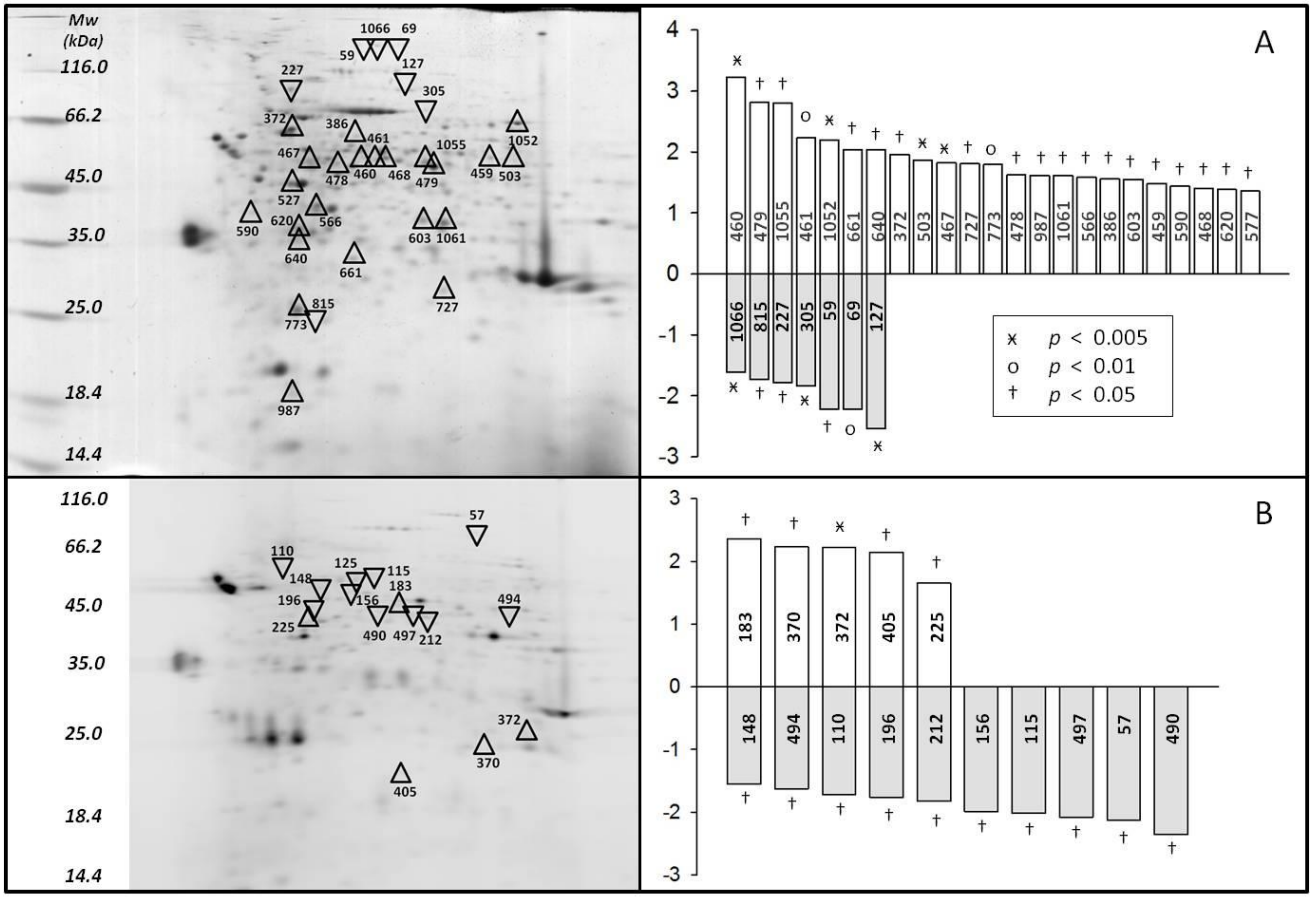

Figure 6.6 (**A**: Left) Coomassie-stained and (**B**: Left) IAF-labelled protein separations of a *Bathymodiolus* sp. gill tissue sample from the Tiamat site. Significant changes in spot intensity, compared with the Knuckers Gaff site, are indicated by upright triangles (greater at Tiamat) and inverted triangles (greater at Knuckers Gaff). A protein molecular mass marker ranging from 14.4 kDa (bottom) to > 116.0 kDa (top) is shown for size reference. (**A** and **B**: Right) Fold-differences in spot intensity at Tiamat, in comparison with Knuckers Gaff. Corresponding spot numbers are shown on each vertical bar, and the level of significance (t-test; *p* value) associated with each fold change is indicated by the symbols *, o, and †.

Table 6.1 Identifications of proteins significantly up-regulated in gill of *Bathymodiolus* sp. from Tiamat compared with Knuckers Gaff

Spot #	Identified Protein	Mw (Da)	Fold change	ANOVA *p*	GI Number	Mascot Score	Matched peptides	Sequence Coverage (%)	Function
479	**S-adenosylhomocysteine hydrolase**	47498	+2.8 ± 0.06	*0.016*	253769244	392	3	22	Cytosolic enzyme involved in cysteine synthesis and consequently glutathione-based redox homeostasis
461	**Alpha enolase**	40415	+2.2 ± 0.04	*0.007*	4416381	122	1	21	Enzyme involved in glycolysis, growth control, hypoxia tolerance, heat shock allergic responses
372	**Glutamine synthetase type I**	51968	+2.0 ± 0.02	*0.03*	345876672	205	2	24	Enzyme specific to prokaryotes, likely from bacterial endosymbionts in mussel gill
773	**Actin**	28947	+1.8 ± 0.03	*0.01*	8895877	566	3	53	Cytoskeleton maintenance; muscle contraction; cell motility; cell signalling; ROS target
478	**Fumarylacetoacetate hydrolase**	45979	+1.6 ± 0.06	*0.045*	157131060	158	2	18	Hydrolase enzyme involved in metabolism of aromatic amino acids

Fold change indicates the average variation (± the standard deviation, SD) in spot intensity in the Tiamat group relative to Knuckers Gaff, with the significance of this variation shown by the p value (t-test). N = 10 animals per group.

6.4 Discussion

Bathymodiolin mussels are amongst the dominant fauna occupying hydrothermal vent ecosystems throughout the world's oceans (Fisher *et al.*, 1988; Desbruyères *et al.*, 2000; Cuvelier *et al.*, 2009; Miyazaki *et al.*, 2010). In these deep-sea vent environments, environmental stressors are manifold and extreme exposure to heavy metals may have necessitated the adaptation of specialised mechanisms of detoxification. In particular, metals trigger the production of ROS, which can disturb the cellular redox balance and lead to oxidative stress (Sheehan, 2006; Hansen *et al.*, 2009). A ubiquitous cellular strategy for detoxification involves the binding of metals to specific low molecular mass, thiol-containing proteins known as metallothioneins (MT) (Viarengo and Nott, 1993), and MT expression has been well-studied in *Bathymodiolus* spp. (Geret *et al.*, 1998; Company *et al.*, 2006; Hardivillier *et al.*, 2006; 2010; Martins *et al.*, 2011b). Oxidative stress also stimulates redox modifications to proteins involved in detoxification, and can detrimentally influence protein structure and function (Berlett and Stadtman, 1997). Whilst redox proteomics has frequently been employed in ecotoxicological studies with shallow-water animals (Manduzio *et al.*, 2005; McDonagh *et al.*, 2006; McDonagh and Sheehan, 2007; Chora *et al.*, 2008; 2008; Tedesco *et al.*, 2010), studies in vent fauna are comparatively rare (Company *et al.*, 2011; 2012).

Mussels from Knuckers Gaff appear to have a higher metal load in their tissues, but a larger sample group would be needed to test whether this is significant, representing a considerable challenge for deep-sea, remote sampling. Statistical tests performed here indicate that tissue metal concentrations are generally similar between the two groups, with the exception of iron in gill. Higher concentrations of Fe in gill at Knuckers Gaff could indicate greater bioavailability of this element, potentially through a higher hydrothermal flux, or may reflect a slower rate of removal. Two-dimensional PAGE separations of gill proteins revealed significant changes in intensity of 30 spots between the two vent sites, of which 23 were more intense at Tiamat and 7 were more intense at Knuckers Gaff. Whilst it is difficult to elucidate whether these changes indicate suppression of protein expression in response to greater xenobiotic stress at one site, or up-regulation of proteins involved in antioxidant defence at the other, it is clear that the proteome of *Bathymodiolus* sp. is

highly sensitive to changes in chemical environment, as previously observed with *B. azoricus* on the Mid-Atlantic Ridge (Company *et al.*, 2011). Significant differences in the thiol subproteome were also observed between the two groups, with 10 spots showing reduced intensity at Tiamat, and 5 showing greater intensity. Reduced IAF-associated fluorescence may reflect greater thiol oxidation, but may also indicate lower abundance of thiol-containing proteins. In this study, changes in spot intensity with IAF occurred independently of differences in intensity with coomassie, therefore it may be that the thiol subproteome of Tiamat mussels is more sensitive to oxidant attack than at Knuckers Gaff.

Exposure to metal-induced ROS has previously been shown to trigger up-regulation of numerous antioxidant enzymes in hydrothermal vent fauna (Company *et al.*, 2004; 2006; Marie *et al.*, 2006; Gonzalez-Rey *et al.*, 2007; 2010). However, few studies have applied a redox proteomic approach to screen for changes in expression and oxidative transformations of individual proteins involved in key biological structures and processes (Boutet *et al.*, 2009; Mary *et al.*, 2010; Company *et al.*, 2011; 2012). Identifying individual proteins in deep-sea vent fauna is challenging owing to the relative paucity in their genome information. Nevertheless, this study reports enhanced expression of S-adenosylhomocysteine hydrolase (SAHH), alpha enolase, glutamine synthetase type I, actin, and fumarylacetoacetate hydrolase (FAH) in gill tissues of *Bathymodiolus* sp. sampled at Tiamat compared to those sampled at Knuckers Gaff. These proteins occupy diverse roles in metabolism, cell structure, stress response and redox homeostasis and may be variably regulated in response to conditions of oxidative stress.

SAHH is a cytosolic enzyme with an important antioxidant role owing to its involvement in regulating the synthesis of GSH via metabolism and regeneration of cysteine and methionine (Kloor *et al.*, 2000; Martinov *et al.*, 2010; Liao *et al.*, 2012), and in regulating biological transmethylation (Turner *et al.*, 2000). Enhanced expression of this enzyme has previously been linked to oxidative stress caused by metal exposure (Bagnyukova *et al.*, 2007), and has been identified as a stress response in hydrothermal vent mussels, *B. azoricus* from the Mid-Atlantic Ridge (Company *et al.*, 2011), and *B. thermophilus* from the East Pacific Rise (Boutet *et al.*, 2009). Alpha enolase, a cytosolic enzyme, is both abundant and highly conserved in eukaryotic and

prokaryotic organisms owing to its critical role in carbohydrate catabolism via the glycolytic pathway (Pancholi, 2001). Alpha enolase has also been found to protect cells from oxidative and thermal stress, functioning as a hypoxic stress protein (Aaronson *et al.*, 1995) and a heat shock protein (Iida and Yahara, 1985), and can be considered as a marker of pathological stress with multiple stress response roles (Díaz-Ramos *et al.*, 2012). Glutamine synthetase type I is exclusive to prokaryotes and must therefore derive from the bacterial symbionts hosted in gill tissue. Elevated expression of this bacterial protein may indicate a greater population of gill endosymbionts at Tiamat in response to a greater exposure to reduced substrates. Actin is an abundant cytoskeletal protein in eukaryotic cells, polymerising to form a network of microfilaments with numerous functions including cell motility, cell division, cell signalling and protein synthesis (Pollard and Cooper, 1986). Actin is highly sensitive to oxidant attack (Dalle-Donne *et al.*, 2001) and has been shown in many studies to be a target of oxidative stress in bivalves inhabiting both shallow-water (Rodríguez-Ortega *et al.*, 2003; Manduzio *et al.*, 2005; McDonagh *et al.*, 2005; McDonagh and Sheehan, 2007; 2008; Chora *et al.*, 2009) and hydrothermal vent environments (Company *et al.*, 2011). Under moderate conditions of oxidative stress, the formation of disulphide bonds between cysteine sulphydryl groups in actin and those of GSH, prevents excessive intra-molecular polymerisation and enables microfilament preservation (Dalle-Donne *et al.*, 2001). Thus, actin not only responds to ROS-induced stress but may be actively involved in buffering potential damage to cells. FAH is one of just ten enzymes known to have the capacity to hydrolyse carbon-carbon bonds in aromatic amino acids (Timm *et al.*, 1999). It is involved in the catabolism of tyrosine and phenylalanine, catalysing the cleavage of fumerylacetoacetate in the final step of this essential metabolic pathway (Bateman, 2001). This enzyme is more abundant in mussels sampled from Tiamat compared with Knuckers Gaff, perhaps reflecting greater need for efficient break down of tyrosine metabolites which can further contribute to oxidative stress in cells (Fisher *et al.*, 2008).

GST activity is also enhanced in gills of mussels from Tiamat compared with Knuckers Gaff, though this difference is only significant at the 90% confidence interval ($p < 0.1$). GST is a key enzyme involved in phase II detoxification, which catalyses conjugation of GSH to electrophilic centres on a range of xenobiotic

substrates, facilitating their dissolution and subsequent excretion from the organism (Strange *et al.*, 2001). Elevated expression of GST, and of proteins involved in diverse cellular processes (discussed above), suggests that mussels at Tiamat may have a greater battery of defences against xenobiotic substrates.

A recent study has shown that hydrothermal vent mussels from the Mid-Atlantic Ridge, *B. azoricus*, differ in their systems of antioxidant defence depending on the specific environmental conditions to which they are exposed (Company *et al.*, 2012). *Bathymodiolus* sp. sampled from the SWIR in this study demonstrate significant proteomic variability between two vent sites. Enhanced expression of a number of proteins involved in redox homeostasis was measured in mussels at Tiamat, suggesting that chemical stress may in fact be greater at this site than at Knuckers Gaff. Additionally, an increase in oxidative modifications to the thiol subproteome was observed in mussels from Tiamat compared with Knuckers Gaff, further indicating a higher metal environment. Elevated exposure to metals is known to trigger the up-regulation of metal-binding proteins, facilitating excretion (Langston *et al.*, 1998). It is possible that mussels from Tiamat experience greater exposure to metals, but maintain redox homeostasis through enhanced induction of GST and other antioxidant enzymes. Consequently, metal concentrations in tissues are regulated at a similar level to those in mussels at the Knuckers Gaff site.

Gill tissues of mussels from both Tiamat and Knuckers Gaff were found to contain higher concentrations of many of the metals analysed compared with digestive gland. This suggests greater exposure of gill to bioavailable metals in seawater and supports a primary feeding mechanism of chemoautotrophy via endosymbiotic bacteria (Fiala-Médioni *et al.*, 2002; Duperron *et al.*, 2006; Riou *et al.*, 2008). Mussels in this study were sampled from active chimney structures where methane and sulphide are likely to have been in plentiful supply. Whilst Bathymodiolin mussels have a mixotrophic diet in which their energy requirements can be maintained both by symbionts in their gills and by suspension feeding on particulate organic matter (Le Pennec *et al.*, 1990), filter feeding may be negligible as mussels increase in size and proximity to the vent (Martins *et al.*, 2008; De Busserolles *et al.*, 2009). Gill tissue represents the direct interface between environmental metals and cellular physiology, and studies with *B. azoricus* collected from Mid-Atlantic Ridge vent sites

have also shown a greater metal burden in gill compared with digestive gland (Geret *et al.*, 1998; Kádár *et al.*, 2005; Cosson *et al.*, 2008). Whilst accumulation in digestive gland is considerably greater in vent mussels compared with non-vent fauna, reflecting long-term metal exposure (Cosson *et al.*, 2008; Chora *et al.*, 2009; Martins *et al.*, 2011b), higher MT concentrations in this organ compared with gill enable greater metal regulation (Langston *et al.*, 1998).

6.5 Conclusions

This is the first study to incorporate a redox proteomics approach to investigate stress tolerance in hydrothermal vent mussels (*Bathymodiolus* sp.) collected from the Southwest Indian Ridge. Although, as yet, no environmental or fluid chemistry data are available for these sites, there is significant variability in the proteome between Tiamat and Knuckers Gaff, including the expression of proteins involved in a range of metabolic and detoxification processes, which is likely to reflect variability in response to environmental stressors. Gills were found to be significantly enriched relative to digestive gland in Mn, Zn, Cd, Hg and Pb at Tiamat, and Cu, Zn, Cd, Hg and Pb at Knuckers Gaff, indicating enhanced exposure of this tissue to bioavailable metals, and may indicate a greater reliance on the gill for nutrition via chemoautotrophic endosymbionts at both sites. At Knuckers Gaff, biological variation was very high in all analyses of metal content, protein expression and redox changes to the proteome. Mussels sampled at this site cover a wider geographic area, and consequently they are likely to have experienced more variation in their exposure to toxic compounds. This study highlights the variable proteomic response of *Bathymodiolus* sp. to a rapidly fluctuating and highly ephemeral chemical environment, and demonstrates the sensitivity of the redox proteomic approach to evaluating stress response between vent habitats within the same hydrothermal system. Five proteins are identified as potential markers of oxidative stress in *Bathymodiolus* sp., and demonstrate the importance of proteomic plasticity in adaptation to the hydrothermal vent habitat.

Chapter 7

7 Conclusions and Future Perspectives

In nearly four decades of hydrothermal vent exploration and research, understanding of these systems has developed considerably. Once considered exclusive to fast-spreading mid-ocean ridges, these seafloor expressions of convective lithospheric cooling have been progressively revealed throughout the global ocean ridge, in every ocean basin, across a diverse range of geological settings. Hydrothermal vents are now recognised as important contributors to ocean chemistry with a key role in the biogeochemical cycling of many elements, in supporting highly productive ecosystems in the deep-sea, and as economic sources of metal sulphide deposits. The Antarctic, isolated by high-latitude and impenetrable ice-cover for large parts of the year, was the last region to be explored for hydrothermal activity. Plume signals were first detected in the water column above the East Scotia Ridge (ESR) in 1998 (German *et al.*, 2000), but active venting was not observed until 2010 (Rogers *et al.*, 2012). At 56 – 60 °S, the East Scotia Sea vents are the most southerly discovered to date; they exhibit remarkably diverse fluid chemistries; and they host a unique faunal assemblage, forming a new and distinct biogeographic province.

The aim of this thesis was to further understanding of the geochemical controls on the composition of hydrothermal fluids, focusing on the unusual back-arc and island-arc setting of vent systems in the East Scotia Sea, and to understand the chemical constraints on faunal colonisation by investigating the relationships between the composition of vent fluids and metal uptake/regulation in faunal tissues. In particular, the rare earth elements (REEs) were employed as geochemical tracers of hydrothermal processes and to assess whether the variable REE distribution patterns observed in the Manus Basin in Papua New Guinea (Craddock and Bach, 2010; Craddock *et al.*, 2010) are characteristic of back-arc environments. Metal accumulation in tissues of *Kiwa tyleri* sp. nov., the dominant macrofaunal species of ESR vent habitats, was also investigated in relation to the composition of the fluids

they inhabit, and the abiotic and biotic controls on metal uptake in this species was evaluated. Hydrothermal fauna are well-adapted to their environment, but mechanisms for tolerating extreme metal stress are poorly understood. Although the number of specimens from the ESR is limited, due to the challenges of remote deep-sea sampling, pathways for metal regulation have been evaluated using proteomic techniques. These were applied to the vent-living mussel, *Bathymodiolus* sp., as well as a closely-related shallow water mussel, *Mytilus edulis*, which were exposed to elevated metal concentrations in a series of laboratory experiments. The results of this work are discussed in terms of the mechanisms of adaptation to a hydrothermal vent habitat, and evidence for pre-adaptation in related non-vent species. The main achievements and findings of this research are summarised below.

7.1 Conclusions

- Fluids venting from 'black-smoker' chimneys along two segments of the back-arc spreading ESR (E2 and E9), and 'white-smoker' chimneys and diffuse vents within the Kemp submarine volcano, encompass a wide range of chemical compositions. Whilst these systems are all basalt-hosted, fluids are variably influenced by phase separation and magmatic activity, temperature, and pH, and concentrations of Cl^-, F^-, H_2S, and SO_4, in vent fluids differ remarkably between the three sites. Consequently, fluids exhibit heterogeneous REE distribution patterns and provide an ideal opportunity to investigate the geochemical controls on REE behaviour. End-member (zero-Mg) fluids from the ESR have total REE concentrations ranging from 7 – 127 nmol/kg, and chondrite-normalised distribution patterns are either LREE-enriched with a positive Eu anomaly (E2 and E9 South), or MREE-enriched with a negative Eu anomaly (E9 North), whilst fluids from the Kemp Caldera have almost flat REE_{CN} patterns. At E2 and E9 South, fluids are similar in their chemical composition to typical mid-ocean ridge fluids, and REE_{CN} distribution patterns primarily reflect plagioclase dissolution and complexation by chloride. Fluids from E9 North may be influenced by anhydrite dissolution, or they may indicate a very young hydrothermal system (in support of this, temperature is high (> 383 °C) and chlorinity is low (98 mmol/kg)), where sulphate precipitation has been minimal and fluids consequently retain a REE-enriched, un-evolved REE_{CN} pattern. At Kemp Caldera, highly elevated concentrations of H_2S and F^- in vent fluids indicate a strong magmatic influence, and

enhanced solubility of all the REEs suggests pH and ligand complexation are the dominant controls on REE composition in fluids at this site.

- Anhydrite assimilates high concentrations of REEs in hydrothermal environments, and the distribution of these elements within the mineral lattice often reflects conditions of venting at the time of deposition. Anhydrite grains sampled from 'black-smoker' chimneys at E2 and E9 have relatively flat REE distributions when normalised to the REE composition of contemporary fluids, indicating minimal fractionation during mineral deposition. Where anhydrite is depleted in Eu relative to fluids, this indicates deposition from a reducing, vent fluid-dominated solution, where substitution of Ca^{2+} for Eu^{2+} is inhibited owing to the mismatch in ionic radius. Anhydrites lacking a Eu anomaly relative to fluids were likely precipitated from a more oxidising fluid dominated by conductively heated seawater. 'White-smoker' chimneys at Kemp Caldera exhibit very different REE_{CN} distribution patterns to those of contemporary fluids. Strong enrichment in the HREEs in anhydrite suggests deposition from a different fluid to that venting today. Anhydrites recovered from Kemp likely record a much stronger magmatic influence in the recent past.

- Hydrothermal vents along the ESR support dense aggregations of a new species of anomuran decapod, *Kiwa tyleri* sp. nov., living in close proximity to active high-temperature vent chimneys. High environmental metal concentrations are reflected in gill tissue, which is directly exposed to diffuse fluids and passively assimilates a high metal load during gas exchange. In both male and female animals, hepatopancreas tends to be depleted relative to gill in most essential (Fe, Mn, Cu, Zn) and non-essential (As, Cd, Pb) metals. *K. tyleri* are primary consumers, feeding at a low trophic level on their ventral episymbionts, and may consequently avoid the biomagnification of metals more evident in predatory vent-endemic crabs from other hydrothermal sites. Muscle tissue is also generally depleted relative to gill in both sexes, indicating that metal uptake is regulated in muscle. However, the difference in metal content between gill and muscle in *K. tyleri* is not significant for Mn, Fe and Zn in males and females, nor for As in females, and muscle tissues appear to be enriched in metals relative to vent-living crabs from other hydrothermal sites that have similar concentrations of metal in their high-temperature fluids. Preliminary investigation into the life history of *K. tyleri* indicates that this species is exceptionally long-lived

and metal accumulation in muscle tissue may simply reflect prolonged exposure over a decadal timescale. This study is the first to investigate metal-organism interactions in *K. tyleri*, a species whose abundance along the ESR is remarkable owing to the scarcity of reptant decapods in Antarctica.

- *Mytilus edulis*, the common shallow-water blue mussel, was exposed to high levels of Cu (40 μg/L) and/or Cd (200 μg/L) in a series of laboratory experiments to assess tissue uptake and the response of the proteome, and to evaluate mechanisms of metal detoxification that could imply pre-adaptation to a metal-enriched vent habitat. Metal accumulation increased with duration of exposure (e.g. mussels exposed to both metals showed a 9.5-fold and a 150-fold increase in [Cd] in gill after 24 hours and 7 days, respectively, relative to control), and after 7 days of exposure the concentration of Cd in gill (105-fold increase relative to control) was significantly greater than Cu (3.7-fold increase relative to control). Further, uptake of Cd was significantly enhanced in the presence of Cu over a 7 day period. It is likely that pathways of uptake differ between 'essential' and 'non-essential' metals, and that their impact on the proteome is dependent on the availability of free metal ions. Whilst [Cd] was most enriched in gill in mussels exposed to Cu and Cd together, the greatest proteomic response was observed in mussels exposed to Cd alone. The presence of Cu may enable more rapid metallothionein induction, and the cellular concentration of free metal ions may be reduced through complexation with these metal-binding proteins. Metals are well-known to cause oxidative stress in biological systems, but they may have either antagonistic or synergistic effects on organisms in a multi-contaminant environment. In response to Cu and/or Cd treatment, *M. edulis* were able to up-regulate a number of proteins involved in antioxidant defence, energy regulation, metabolism and cell structure, indicating an active battery of defence mechanisms against metal uptake.

- *Bathymodiolus* sp., sampled from two active hydrothermal vents on the Southwest Indian Ridge, Tiamat and Knuckers Gaff, exhibited significant proteomic variability, likely in response to differences in environmental stressors. Following 2D PAGE analysis of gill proteins, a significant difference in intensity was measured in 30 spots between the two vent sites, out of 205 matched spots. At Tiamat, 23 protein spots were up-regulated compared with Knuckers Gaff, including five proteins with

important roles in metabolism, cell structure, stress response, and redox homeostasis. One of these proteins, alpha enolase, was also up-regulated in *M. edulis* following exposure to Cu or Cd for 7 days, demonstrating an important anti-oxidant function in both related species. Oxidation of protein thiols was also measured in a greater number of proteins in *Bathymodiolus* sp. from Tiamat compared to Knuckers Gaff, indicating that exposure to metals and other pro-oxidants may be higher at Tiamat. Increased metal exposure may trigger changes in the proteome, regulating tissue uptake, and this plasticity is likely to be important in enabling successful adaptation to the spatially and temporally fluctuating chemical environments that are characteristic of hydrothermal vent habitats.

7.2 Future perspectives

This research reveals a number of questions relating to hydrothermal fluid chemistry in back-arc and island-arc environments, and to metal regulation in vent-living fauna, that merit future investigation. The discovery of hydrothermal venting along the ESR (Rogers *et al.*, 2012; James *et al.*, in review) and within the Kemp Caldera (Connelly *et al.*, in prep) has provided an excellent opportunity for investigating controls on fluid chemistry in back-arc and island-arc settings, which are hugely under-studied compared to mid-ocean ridge vent systems. Island-arcs are particularly interesting owing to their shallow depth and potential to influence seawater chemistry in the upper ocean. Fluids collected from 'white-smoker' chimneys within the Kemp Caldera during the *RRS James Cook* cruise, JC42, in 2010, entrained a significant volume of seawater (> 80%) due to the fragility of the chimney structures, which hindered accurate determination of endmember composition. As the REEs do not behave conservatively during seawater mixing, estimates of endmember concentrations for these elements are uncertain. Fluids were greatly depleted in all metals relative to those from the ESR, despite the high concentrations of acid-volatile gases and the relatively low pH values. It is likely that fluids sampled at this site had mixed with seawater in the subsurface, resulting in extensive deposition of metal-rich sulphates/sulphides. Further sampling of high-temperature fluids, with reduced seawater entrainment, is needed to fully understand the unusual magmatic-hydrothermal vent system at Kemp Caldera, and to quantify the effect on the REEs.

Chimney anhydrites recovered from Kemp Caldera were strongly enriched in the HREEs relative to the LREEs; remarkably different to the REE_{CN} composition of contemporary vent fluids. This has been interpreted to reflect deposition from a HREE-enriched fluid following a magmatic event in the recent past. The REE composition of anhydrite is controlled both by crystal lattice constraints on ionic substitution and by the composition and speciation of fluids from which it precipitated (Mills and Elderfield, 1995; Humphris, 1998; Humphris and Bach, 2005). The presence of particular ligands, such as fluoride, can strongly influence the solubility of the REEs in fluids, and therefore their assimilation into anhydrite. However, there is some debate in the literature as to the specific REE-binding capacity of fluoride in high-temperature hydrothermal fluids (Migdisov *et al.*, 2009; Craddock and Bach, 2010; Craddock *et al.*, 2010; Williams-Jones *et al.*, 2012). It would be interesting to assess partitioning of the REEs into anhydrite from a saturated solution containing variable concentrations of F^-, and other important ligands such as Cl^- and SO_4, in a series of laboratory experiments. These experiments would confirm whether the unusual REE_{CN} distribution patterns measured in anhydrites at Kemp Caldera could be explained by precipitation from a fluoride-rich solution, in which high concentrations of the HREE were maintained by strong complexation. In a wider context, this information would be key to our understanding of REE transport and deposition by hydrothermal fluids, which is vital for exploration of new REE mineral resources.

In this thesis, a significant variation in the concentration of metals was demonstrated between tissues of *K. tyleri* sampled from a diffusely venting area at E2 on the ESR. *K. tyleri* live in very close proximity to sources of active venting, where metal exposure is high, and the success of this species may be partly due to their ability to regulate their internal metal concentrations. Using a range of proteomic techniques, mechanisms of metal detoxification have been studied in dominant vent-living fauna elsewhere, particularly within the Bathymodiolinae (Cosson *et al.*, 2008; Company *et al.*, 2011; 2012), but to date no such analysis has been carried out for vent-endemic crabs. Marsh *et al*. (2012) identified a distinct spatial distribution of *K. tyleri* across the ESR vent fields according to their size and sex; the largest males compete for a position in the warmest fluids, whilst smaller males and females reside in slightly cooler waters, and brooding females move off-vent where a more stable environment can be provided for their young. Individuals occupying the warmest

fluids must be able to tolerate highly elevated concentrations of many metals. To understand the remarkable ability of *K. tyleri* to survive in such a metal-rich environment, it will be necessary to investigate their proteomic mechanisms of defence against metal toxicity, and to assess the spatial variation and plasticity in this response across the population, and also between distinct populations. Metals may have played an important role in shaping vent communities, and understanding mechanisms of metal regulation in vent-living fauna may be important in our global understanding of vent colonisation and community structure.

8 Bibliography

Aaronson R. M., Graven K. K., Tucci M., McDonald R. J. and Farber H. W. (1995) Non-neuronal enolase is an endothelial hypoxic stress protein. *Journal of Biological Chemistry* **46,** 27752-27757.

Ahearn G. A., Mandal P. K. and Mandal A. (2004) Mechanisms of heavy-metal sequestration and detoxification in crustaceans: a review. *Journal of Comparative Physiology B* **174,** 439-452.

Ahn B., Rhee S. G. and Stadtman E. R. (1987) Use of Fluorescein hydrazide and fluorescein thiosemicarbazide reagents for the fluorometric determination of protein carbonyl groups and for the detection of oxidised protein on polyacrylamide gels. *Analytical Biochemistry* **161,** 245-257.

Aiuppa A., Baker D. R. and Webster J. D. (2009) Halogens in volcanic systems. *Chem. Geol.* **263,** 1-18.

Al-Subiai S. N., Moody A. J., Mustafa S. A. and Jha A. N. (2011) A multiple biomarker approach to investigate the effects of copper on the marine bivalve mollusc, *Mytilus edulis*. *Ecotoxicology and Environmental Safety* **74,** 1913-1920.

Allen D. E. and Seyfried Jr W. E. (2005) REE controls in ultramafic hosted MOR hydrothermal systems: An experimental study at elevated temperature and pressure. *Geochim. Cosmochim. Acta* **69,** 675-683.

Alt J. C. (2013). Subseafloor Processes in Mid-Ocean Ridge Hydrothermal Systems. *In:* Humphris S., Zierenberg R. A., Mullineaux L. S. and Thomson R. E. (eds.) *Seafloor Hydrothermal Systems: Physical, Chemical, Biological, and Geological Interactions.* Washington, D. C.: American Geophysical Union, pp.

Amiard-Triquet C. and Amiard J.-C. (1998). Influence of ecological factors on accumulation of metal mixtures. *In:* Langston W. J. and Bebianno M. J. (eds.) *Metal Metabolism in Aquatic Environments.* London: Chapman & Hall, pp. 351-386

Amiard J.-C., Amiard-Triquet C., Barka S., Pellerin J. and Rainbow P. (2006) Metallothioneins in aquatic invertebrates: Their role in metal detoxification and their use as biomarkers. *Aquatic Toxicology* **76,** 160-202.

Anderson R. N., Langseth M. G. and Sclater J. G. (1977) The mechanisms of heat transfer through the floor of the Indian Ocean. *J. Geophys. Res.* **82,** 3391-3409.

Åslund F. and Beckwith J. (1999) Bridge over Troubled Waters: Sensing Stress by Disulphide Bond Formation. *Cell* **96,** 751-753.

Auzende J.-M., Ballu V., Batiza R., Bideau D., Charlou J. L., Cormier M. H., Fouquet Y., Geistdoerfer P., Lagabrielle Y., Sinton J. and Spadea P. (1996) Recent tectonic, magmatic, and hydrothermal activity on the East Pacific Rise between 17°S and 19°S: Submersible observations. *J. Geophys. Res.* **101,** 17995-18010.

Bach W., Banerjee N. R., Dick H. J. B. and Baker E. T. (2002). Discovery of ancient and active hydrothermal systems along the ultra-slow spreading Southwest Indian Ridge 10°-16°E. *Geochem. Geophys. Geosys.*, **3**, 10.1029/2001GC000279

Bach W., Roberts S., Vanko D. A., Binns R. A., Yeats C. J., Craddock P. R. and Humphris S. E. (2003) Controls of fluid chemistry and complexation on rare-earth element contents of anhydrite from the Pacmanus subseafloor hydrothermal system, Manus Basin, Papua New Guinea. *Miner. Deposita* **38,** 916-935.

Bach W., Roberts S. and Binns R. A. (2005). Data Report: Chemical and Isotopic (S, Sr) Composition of Anhydrite from ODP Leg 193, PACMANUS Hydrothermal System, Manus Basin, Papua New Guinea. *In:* Barriga F. J. A. S., Binns R. A., Miller D. J. and Herzig P. (eds.) *Proceedings of the Ocean Drilling Program, Scientific Results.* pp. 1-23

Bachraty C., Legendre P. and Desbruyères D. (2009) Biogeographic relationships among deep-sea hydrothermal vent faunas at global scale. *Deep Sea Research Part I: Oceanographic Research Papers* **56,** 1371-1378.

Bagnyukova T. V., Luzhna L. I., Pogribny I. P. and Lushchak V. I. (2007) Oxidative stress and antioxidant defenses in goldfish liver in response to short-term exposure to arsenite. *Environmental and Molecular Mutagenesis* **48,** 658-665.

Bai T. B. and Koster van Groos A. F. (1999) The distribution of Na, K, Rb, Sr, Al, Ge, Cu, W, Mo, L, and Ce between granitic melts and coexisting aqueous fluids. *Geochim. Cosmochim. Acta* **63,** 1117-1131.

Baker E. T. and German C. (2004). On the global distribution of hydrothermal vent fields. *In:* German C., Lin J. and Parson L. M. (eds.) *Mid-Ocean Ridges: Hydrothermal Interactions between the Lithosphere and Oceans.* American Geophysical Union, pp. 245-266

Baker E. T. (2009). Relationships between hydrothermal activity and axial magma chamber distribution, depth, and melt content. *Geochem. Geophys. Geosyst.*, **10**, 10.1029/2009gc002424

Baker M. C., Ramirez-Llodra E. and Perry D. (2010). *ChEssBase: an online information system on species distribution from deep-sea chemosynthetic ecosystems*; http://www.noc.soton.ac.uk/chess/science/sci_resources.php.

Balls P. W. (1985) Copper, lead and cadmium in coastal waters of the western North Sea. *Marine Chemistry* **15,** 363-378.

Barker P. F. (1970) Plate tectonics of the Scotia Sea Region. *Nature* **228,** 1293-1296.

Bateman R. L. (2001) Mechanistic inferences from the crystal structure of Fumarylacetoacetate Hydrolase with a bound phosphorus-based inhibitor. *Journal of Biological Chemistry* **276,** 15284-15291.

Baty J. W., Hampton M. B. and Winterbourn C. C. (2002) Detection of oxidant sensitive thiol proteins by fluorescence labeling and two-dimensional electrophoresis. *Proteomics* **2,** 1261-1266.

Bau M. (1991) Rare-earth element mobility during hydrothermal and metamorphic fluid-rock interaction and the significance of the oxidation state of europium. *Chem. Geol.* **93,** 219-230.

Bau M. and Dulski P. (1999) Comparing yttrium and rare earths in hydrothermal fluids from the Mid-Atlantic Ridge: implications for Y and REE behaviour during near-vent mixing and for the Y/Ho ratio of Proterozoic seawater. *Chem. Geol.* **155,** 77-90.

Bebianno M. J. and Langston W. J. (1991) Metallothionein induction in *Mytilus edulis* exposed to cadmium. *Marine Biology* **108,** 91-96.

Bebianno M. J. and Langston W. J. (1993) Turnover rate of metallothionein and cadmium in *Mytilus edulis*. *BioMetals* **6,** 239-244.

Bebianno M. J. and Serafim A. (2003) Variation of metal and metallothionein concentrations in a natural population of *Ruditapes decussatus*. *Archives of Environmental Contamination and Toxicology* **44,** 53-66.

Ben-Khedher S., Jebali J., Kamel N., Banni M., Rameh M., Jrad A. and Boussetta H. (2013) Biochemical effects in crabs (*Carcinus maenas*) and contamination levels in the Bizerta Lagoon: an integrated approach in biomonitoring of marine complex pollution. *Environmental Science and Pollution Research* **20,** 2616-2631.

Benarroch E. E. (2011) Heat shock proteins. *Neurology* **76,** 660-667.

Bergey L. L. and Weis J. S. (2007) Molting as a mechanism of depuration of metals in the fiddler crab, *Uca pugnax*. *Marine Environmental Research* **64,** 556-562.

Berlett B. S. and Stadtman E. R. (1997) Protein Oxidation in Aging, Disease, and Oxidative Stress. *The Journal of Biological Chemistry* **272,** 20313-20316.

Bevis M., Taylor F. W., Schutz B. E., recy J., Isacks B. L., Helu S., Singh R., Kendrick E., Stowell J., Taylor B. and Calmant S. (1995) Geodectic observations of very rapid convergence and back-arc extension at the Tonga arc. *Nature* **374,** 249-251.

Bibee L. D., Shor Jr. G. G. and Lu R. S. (1990) Inter-arc Spreading in the Mariana Trough. *Mar. Geol.* **35,** 183-197.

Bienhold C., Ristova P. P., Wenzhöfer F., Dittmar T. and Boetius A. (2013). How Deep-Sea Wood Falls Sustain Chemosynthetic Life. *PLoS ONE*, **8**, 10.1371/journal.pone.0053590

Bird P. (2003). An updated digital model of plate boundaries. *Geochem. Geophys. Geosyst.*, **4**, 10.1029/2001gc000252

Bischoff J. L. and Dickson F. W. (1975) Seawater-basalt interaction at 200°C and 500 bars: Implications for origin of sea-floor heavy-metal deposits and regulation of seawater chemistry. *Earth Planet. Sci. Lett.* **25,** 385-397.

Bischoff J. L. and Seyfried W. E. (1978) Hydrothermal Chemistry of Seawater from 25° to 350°C. *American Journal of Science* **278,** 838-860.

Bischoff J. L. and Rosenbauer R. J. (1984) The critical point and two-phase boundary of seawater, 200 - 500 ˚C. *Earth Planet. Sci. Lett.* **68,** 172-180.

Bischoff J. L. and Rosenbauer R. J. (1988) Liquid-vapor relations in the critical region of the system NaCl-H_2O from 380 to 415°C: A refined determination of the critical point and two-phase boundary of seawater. *Geochim. Cosmochim. Acta* **52,** 2121-2126.

Blackmore G. and Wang W.-X. (2002) Uptake and Efflux of Cd and Zn by the Green Mussel *Perna viridis* after Metal Preexposure. *Environmental Science and Technology* **36,** 989-995.

Bordon I. C. A. C., Sarkis J. E. S., Tomas A. R. G., Scalco A., Lima M., Hortellani M. A. and Andrade N. P. (2012) Assessment of Metal Concentrations in Muscles of the Blue Crab, *Callinectes danae* S., from the Santos Estuarine System. *Bulletin of Environmental Contamination and Toxicology* **89,** 484-488.

Both R., Crook K., Taylor B., Brogan S., Chappell B., Frankel E., Liu L., Sinton J. and Tiffin D. (1986) Hydrothermal Chimneys and Associated Fauna in the Manus Back-Arc Basin, Papua New Guinea. *EOS (Transactions, American Geophysical Union)* **67,** 489-490.

Boutet I., Jollivet D., Shillito B., Moraga D. and Tanguy A. (2009) Molecular identification of differentially regulated genes in the hydrothermal-vent species

Bathymodiolus thermophilus and *Paralvinella pandorae* in response to temperature. *BMC Genomics* **10,** 222.

Bowers T. S., Campbell A. C., Measures C. I., Spivack A. J., Khadem M. and Edmond J. M. (1988) Chemical Controls on the Composition of Vent Fluids at 13°-11°N and 21°N, East Pacific Rise. *J. Geophys. Res.* **93,** 4522-4536.

Braconi D., Bernardini G. and Santucci A. (2011) Linking protein oxidation to environmental pollutants: Redox proteomic approaches. *Journal of Proteomics* **74,** 2324-2337.

Bradford M. (1976) A rapid and sensitive method for the quantification of microgram quantities of protein utilizing the principle of protein-dye binding. *Analytical Biochemistry* **72,** 248-254.

Brett C. P. (1977) Seismicity of the South Sandwich Islands region. *Geophys. J. Roy. Astr. S.* **51,** 453-464.

Bruguier N. J. and Livermore R. A. (2001) Enhanced magma supply at the southern East Scotia Ridge: evidence for mantle flow around the subducting slab? *Earth Planet. Sci. Lett.* **191,** 129-144.

Buettner G. (1993) The packing order of free radical and antioxidants: lipid peroxidation, alpha-tocopherol and ascorbate. *Archives of Biochemistry and Biophysics* **300,** 535-543.

Butterfield D., Massoth G. J., McDuff R. E., Lupton J. and Lilley M. D. (1990) Geochemistry of hydrothermal fluids from Axial Seamount Hydrothermal Emissions Study Vent Field, Juan de Fuca Ridge: Subseafloor boiling and subsequent fluid-rock interaction. *J. Geophys. Res.* **95,** 12895-12921.

Butterfield D. A. and Massoth G. J. (1994) Geochemistry of north Cleft segment vent fluids: Temporal changes in chlorinity and their possible relation to recent volcanism *J. Geophys. Res.* **99,** 4951-4968.

Butterfield D. A., Jonasson I. R., Massoth G. J., Feely R. A., Roe K. K., Embley R. E., Holden J. F., McDuff R. E., Lilley M. D. and Delaney J. R. (1997) Seafloor eruptions and evolution of hydrothermal fluid chemistry. *Phil. Trans. R. Soc. A* **355,** 369-386.

Calabrese A., MacInnes J. R., Nelson D. A., Greig R. A. and Yevich P. P. (1984) Effects of long-term exposure to silver or copper on growth, bioaccumulation and histopathology in the Blue Mussel *Mytilus edulis*. *Marine Environmental Research* **11,** 253-274.

Campbell A. C., Bowers T. S., Measures C. I., Falkner K. K., Khadem M. and Edmond J. M. (1988a) A time series of vent fluid compositions from 21°N, East Pacific Rise (1979, 1981, 1985), and the Guaymas Basin, Gulf of California (1982, 1985). *J. Geophys. Res.* **93,** 4537-4549.

Campbell A. C., Palmer M. R., Klinkhammer G. P., Bowers T. S., Edmond J. M., Lawrence J. R., Casey J. F., Thompson G., Humphris S., Rona P. and Karson J. A. (1988b) Chemistry of hot springs on the Mid-Atlantic Ridge. *Nature* **335,** 514-519.

Cavanaugh C. M., Gardiner S. L., Jones M. L., Jannasch H. W. and Waterbury J. B. (1981) Prokaryotic cells in the hydrothermal vent tube worm *Riftia pachyptila* Jones: Possible chemoautotrophic symbionts. *Science* **213,** 340-342.

Cavanaugh C. M., Levering P. R., Maki J. S., Mitchell R. and Lidstrom M. E. (1987) Symbiosis of methylotrophic bacteria and deep-sea mussels. *Nature* **325,** 346-348.

Cavanaugh C. M. (1994) Microbial symbiosis: Patterns of diversity in the marine environment. *American Zoologist* **34,** 79-89.

Charlou J. L., Fouquet Y., Donval J. P. and Auzende J.-M. (1996) Mineral and gas chemistry of hydrothermal fluids on an ultrafast spreading ridge: East Pacific Rise, 17° to 19°S (Naudur cruise, 1993). Phase separation processes controlled by volcanic and tectonic activity. *J. Geophys. Res.* **101,** 15899-15919.

Charlou J. L., Fouquet Y., Bougault H., Donval A., Etoubleau J., Jean-Baptiste P., Dapoigny A., Appriou P. and Rona P. (1998) Intense CH_4 plumes generated by serpentinization of ultramafic rocks at the intersection of the 15°20'N fracture zone and the Mid-Atlantic Ridge. *Geochim. Cosmochim. Acta* **62,** 2323-2333.

Charlou J. L., Donval J. P., Douville E., Jean-Baptiste P., Radford-Knoery J., Fouquet Y., Dapoigny A. and Stievenard M. (2000) Compared geochemical signatures and the evolution of Menez Gwen (37°50'N) and Lucky Strike (37°17'N) hydrothermal fluids, south of the Azores Triple Junction on the Mid-Atlantic Ridge. *Chem. Geol.* **171,** 49-75.

Charlou J. L., Donval J. P., Fouquet Y., Jean-Baptiste P. and Holm N. (2002) Geochemistry of high H_2 and CH_4 vent fluids issuing from ultramafic rocks at the Rainbow hydrothermal field (36° 14'N, MAR). *Chem. Geol.* **191,** 345-359.

Chaudhuri A. R., de Waal E. M., Pierce A., Van Remmen H., Ward W. F. and Richardson A. (2006) Detection of protein carbonyls in aging liver tissue: A fluorescence-based proteomic approach. *Mechanisms of Ageing and Development* **127,** 849-861.

Chemineé J.-L., Stoffers P., McMurty G. M., Richnow H., Puteanus D. and Sedwick P. N. (1991) Gas-rich submarine exhalations during the 1989 eruption of MacDonald Seamount. *Earth Planet. Sci. Lett.* **107,** 318-327.

Chen C.-T. A., Zeng Z., Kuo F.-W., Yang T. F., Wang B.-J. and Tu Y.-Y. (2005) Tide-influenced acidic hydrothermal system offshore NE Taiwan. *Chemical Geology* **224,** 69-81.

Chevaldonné P. and Jollivet D. (1993) Videoscopic study of deep-sea hydrothermal vent alvinellid polychaete populations: biomass estimation and behaviour. *Marine Ecology Progress Series* **95,** 251-262.

Childress J. J., Fisher C. R., Favuzzi J. A., Arp A. J. and Oros D. R. (1993) The role of a zinc-based, serum-borne sulphide-binding component in the uptake and transport of dissolved sulphide by the chemoautotrophic symbiont-containing clam *Calyptogena elongata*. *Journal of Experimental Biology* **179,** 131-158.

Chora S., McDonagh B., Sheehan D., Starita-Geribaldi M., Roméo M. and Bebianno M. J. (2008) Ubiquitination and carbonylation as markers of oxidative-stress in *Ruditapes decussatus*. *Marine Environmental Research* **66,** 95-97.

Chora S., Starita-Geribaldi M., Guigonis J.-M., Samson M., Roméo M. and Bebianno M. J. (2009) Effect of cadmium in the clam *Ruditapes decussatus* assessed by proteomic analysis. *Aquatic Toxicology* **94,** 300-308.

Clarke A. (1990). Temperature and evolution: Southern Ocean cooling and the Antarctic marine fauna. *In:* Kerry K. R. and Hempel G. (eds.) *Ecological Change and Conservation.* Berline, Heidelberg: Springer-Verlag, pp. 9-22

Clarke A. and Johnston N. M. (2003) Antarctic marine benthic biodiversity. *Oceanography and Marine Biology: An Annual Review* **41,** 47-114.

Colaço A., Dehairs F. and Desbruyères D. (2002) Nutritional relations of deep-sea hydrothermal fields at the Mid-Atlantic Ridge: a stable isotope approach. *Deep-Sea Research I* **49,** 395-412.

Colaço A., Bustamante P., Fouquet Y., Sarradin P. M. and Serrão-Santos R. (2006) Bioaccumulation of Hg, Cu, and Zn in the Azores triple junction hydrothermal vent fields food web. *Chemosphere* **65,** 2260-2267.

Cole C., Coelho A. V., James R. H., Connelly D. P. and Sheehan D. (2013). Proteomic responses to metal-induced oxidative stress in hydrothermal vent-living mussels, *Bathymodiolus* sp., on the Southwest Indian Ridge. *Marine Environmental Research*, 10.1016/j.marenvres.2013.09.003.

Company R., Serafim A., Bebianno M. J., Cosson R., Shillito B. and Fiala-Médioni A. (2004) Effect of cadmium, copper and mercury on antioxidant enzyme activities and lipid peroxidation in the gills of the hydrothermal vent mussel *Bathymodiolus azoricus*. *Marine Environmental Research* **58,** 377-381.

Company R., Serafim A., Cosson R., Camus L., Shillito B., Fiala-Médioni A. and Bebianno M. J. (2006) The effect of cadmium on antioxidant responses and the susceptibility to oxidative stress in the hydrothermal vent mussel *Bathymodiolus azoricus*. *Marine Biology* **148,** 817-825.

Company R., Serafim A., Cosson R. P., Fiala-Médioni A., Camus L., Serrão-Santos R. and João Bebianno M. (2010) Sub-lethal effects of cadmium on the antioxidant defence system of the hydrothermal vent mussel *Bathymodiolus azoricus*. *Ecotoxicology and Environmental Safety* **73,** 788-795.

Company R., Antúnez O., Bebianno M. J., Cajaraville M. P. and Torreblanca A. (2011) 2-D difference gel electrophoresis approach to assess protein expression profiles in *Bathymodiolus azoricus* from Mid-Atlantic Ridge hydrothermal vents. *Journal of Proteomics* **74,** 2909-2919.

Company R., Torreblanca A., Cajaraville M., Bebianno M. J. and Sheehan D. (2012) Comparison of thiol subproteome of the vent mussel *Bathymodiolus azoricus* from different Mid-Atlantic Ridge vent sites. *Science of The Total Environment* **437,** 413-421.

Connelly D. P., German C. R., Asada M., Okino K., Egorov A., Naganuma T., Pimenov N., Cherkashev G. and Tamaki K. (2007). Hydrothermal activity on the ultra-slow spreading southern Knipovich Ridge. *Geochem. Geophys. Geosyst.*, **8**, 10.1029/2007gc001652

Connelly D. P., Copley J. T., Murton B. J., Stansfield K., Tyler P. A., German C. R., Van Dover C. L., Amon D., Furlong M., Grindlay N., Hayman N., Hühnerbach V., Judge M., Le Bas T., McPhail S., Meier A., Nakamura K.-i., Nye V., Pebody M., Pedersen R. B., Plouviez S., Sands C., Searle R. C., Stevenson P., Taws S. and Wilcox S. (2012) Hydrothermal vent fields and chemosynthetic biota on the world's deepest seafloor spreading centre. *Nature Communications* **3,** 620.

Corliss J. B., Dymond J., Gordon L. I., Edmond J. M., von Herzen R. P., Ballard R. D., Green K., Williams D., Bainbridge A., Crane K. and van Andel T. H. (1979) Submarine thermal springs on the Galápagos Rift. *Science* **203,** 1073-1083.

Cosson R. and Vivier J.-P. (1997) Interactions of metallic elements and organisms within hydrothermal vents. *Cahiers de Biologie Marine* **38,** 43-50.

Cosson R. P., Thiébaut É., Company R., Castrec-Rouelle M., Colaço A., Martins I., Sarradin P.-M. and Bebianno M. J. (2008) Spatial variation of metal

bioaccumulation in the hydrothermal vent mussel *Bathymodiolus azoricus*. *Marine Environmental Research* **65,** 405-415.

Cottin D., Brown A., Oliphant A., Mestre N. C., Ravaux J., Shillito B. and Thatje S. (2012) Sustained hydrostatic pressure tolerance of the shallow water shrimp *Palaemonetes varians* at different temperatures: Insights into the colonisation of the deep sea. *Comparative Biochemistry and Physiology Part A* **162,** 357-363.

Coumou D., Driesner T., Weis P. and Heinrich C. A. (2009). Phase separation, brine formation, and salinity variation at Black Smoker hydrothermal systems. *J. Geophys. Res.*, **114**, 10.1029/2008jb005764

Craddock P. R. and Bach W. (2010) Insights to magmatic–hydrothermal processes in the Manus back-arc basin as recorded by anhydrite. *Geochim. Cosmochim. Acta* **74,** 5514-5536.

Craddock P. R., Bach W., Seewald J. S., Rouxel O. J., Reeves E. and Tivey M. K. (2010) Rare earth element abundances in hydrothermal fluids from the Manus Basin, Papua New Guinea: Indicators of sub-seafloor hydrothermal processes in back-arc basins. *Geochim. Cosmochim. Acta* **74,** 5494-5513.

Crooks W. (1887) Genesis of the elements. *Chem. News, Lond.* **55,** 83-99.

Cuvelier D., Sarrazin J., Colaço A., Copley J., Desbruyères D., Glover A. G., Tyler P. and Serrão Santos R. (2009) Distribution and spatial variation of hydrothermal faunal assemblages at Lucky Strike (Mid-Atlantic Ridge) revealed by high-resolution video image analysis. *Deep Sea Research Part I: Oceanographic Research Papers* **56,** 2026-2040.

Da Ros L., Nasci C., Campesan G., Sartorello P., Stocco G. and Menetto A. (1995) Effects of Linear Alkylbenzene Sulphonate (LAS) and cadmium in the digestive gland of mussel, *Mytilus* sp. *Marine Environmental Research* **39,** 321-324.

Dalle-Donne I., Rossi R., Milzani A., Simplicio P. D. and Colombo R. (2001) The actin cytoskeleton response to oxidants: from small heat shock protein phosphorylation to changes in the redox state of actin itself. *Free Radical Biology and Medicine* **31,** 1624-1632.

Dalle-Donne I., Rossi R., Giustarini D., Milzani A. and Colombo R. (2003) Protein carbonyl groups as biomarkers of oxidative stress. *Clinica Chimica Acta* **329,** 23-38.

Davies M. J. (2005) The oxidative environment and protein damage. *Biochimica et Biophysica Acta (BBA) - Proteins and Proteomics* **1703,** 93-109.

De Busserolles F., Sarrazin J., Gauthier O., Gélinas Y., Fabri M. C., Sarradin P. M. and Desbruyères D. (2009) Are spatial variations in the diets of hydrothermal fauna linked to local environmental conditions? *Deep Sea Research Part II: Topical Studies in Oceanography* **56,** 1649-1664.

Desbruyères D., Alayse-Danet A.-M. and Ohta S. (1994) Deep-sea hydrothermal communities in Southwestern Pacific back-arc basins (the North Fiji and Lau Basins): Composition, microdistribution and food web. *Mar. Geol.* **116,** 227-242.

Desbruyères D., Chevaldonné P., Alayse A.-M., Jollivet D., Lallier F. H., Jouin-Toulmond C., Zal F., Sarradin P.-M., Cosson R., Caprais J.-C., Arndt C., O'Brien J., Guezennec J., Hourdez S., Riso R., Gaill F., Laubier L. and Toulmond A. (1998) Biology and ecology of the "Pompeii worm" (*Alvinella pompejana* Desbruyères and Laubier), a normal dweller of an extreme deep-sea environment: A synthesis of current knowledge and recent developments. *Deep-Sea Research II* **45,** 383-422.

Desbruyères D., Almeida A., Biscoito M., Comtet T., Khripounoff A., Le Bris N., Sarradin P. M. and Segonzac M. (2000) A review of the distribution of hydrothermal vent communities along the northern Mid-Atlantic Ridge: dispersal vs. environmental controls. *Hydrobiologia* **440,** 201-216.

Desbruyères D., Biscoito M., Caprais J.-C., Colaço A., Comtet T., Crassous P., Fouquet Y., Khripounoff A., Le Bris N., Olu K., Riso R., Sarradin P. M., Segonzac M. and Vangriesheim A. (2001) Variations in deep-sea hydrothermal vent communities on the Mid-Atlantic Ridge near the Azores plateau. *Deep Sea Research Part I: Oceanographic Research Papers* **48,** 1325-1346.

Di Meo-Savoie C. A., Luther G. W. and Cary S. C. (2004) Physicochemical characterization of the microhabitat of the epibionts associated with *Alvinella pompejana*, a hydrothermal vent annelid. *Geochimica et Cosmochimica Acta* **68,** 2055-2066.

Díaz-Ramos À., Roig-Borrellas A., García-Melero A. and López-Alemany R. (2012) α-Enolase, a multifunctional protein: Its role on pathophysiological situations. *Journal of Biomedicine and Biotechnology* **2012,** 1-12.

Distel D. (2000) Phylogenetic relationships among Mytilidae (Bivalvia): 18S rRNA data suggest convergence in Mytilid body plans. *Molecular Phylogenetics and Evolution* **15,** 25-33.

Douville E., Bienvenu P., Charlou J. L., Donval J. P., Fouquet Y., Appriou P. and Gamo T. (1999) Yttrium and rare earth elements in fluids from various deep-sea hydrothermal systems. *Geochim. Cosmochim. Acta* **63,** 527-643.

Douville E., Charlou J. L., Oelkers E. H., Bienvenu P., Jove Colon C. F., Donval J. P., Fouquet Y., Prieur D. and Appriou P. (2002) The Rainbow vent fluids (36° 14’N,

MAR): the influence of ultramafic rocks and phase separation on trace metal content in Mid-Atlantic Ridge hydrothermal fluids. *Chem. Geol.* **184,** 37-48.

Dowling V., Hoarau P. C., Romeo M., O'Halloran J., van Pelt F., O'Brien N. and Sheehan D. (2006) Protein carbonylation and heat shock response in *Ruditapes decussatus* following p,p′-dichlorodiphenyldichloroethylene (DDE) exposure: A proteomic approach reveals that DDE causes oxidative stress. *Aquatic Toxicology* **77,** 11-18.

Duperron S., Bergin C., Zielinski F., Blazejak A., Pernthaler A., McKiness Z. P., DeChaine E., Cavanaugh C. M. and Dubilier N. (2006) A dual symbiosis shared by two mussel species, *Bathymodiolus azoricus* and *Bathymodiolus puteoserpentis* (Bivalvia: Mytilidae), from hydrothermal vents along the northern Mid-Atlantic Ridge. *Environmental Microbiology* **8,** 1441-1447.

Dyballa N. and Metzger S. (2009) Fast and Sensitive Colloidal Coomassie G-250 Staining for Proteins in Polyacrylamide Gels. *Journal of Visualized Experiments*.

Eaton P. (2006) Protein thiol oxidation in health and disease: Techniques for measuring disulfides and related modifications in complex protein mixtures. *Free Radical Biology and Medicine* **40,** 1889-1899.

Edmond J. M., Measures C. I., McDuff R. E., Chan L. H., Collier R., Grant B., Gordon L. I. and Corliss J. B. (1979) Ridge crest hydrothermal activity and the balances of the major and minor elements in the Ocean: The Galapagos data. *Earth Planet. Sci. Lett.* **46,** 1-18.

Edmond J. M. (1980) Ridge crest hot springs: The story so far. *EOS (Transactions, American Geophysical Union)* **61,** 129-131.

Edmond J. M. and Von Damm K. L. (1982) Chemistry of hydrothermal solutions in the Guaymas Basin, Gulf of California. *EOS (Transactions, American Geophysical Union)* **63,** 1015.

Edmonds H. N., Michael P. J., Baker E. T., Connelly D., Snow J. E., Langmuir C. H., Dick H. J. B., Muhe R., German C. and Graham D. W. (2003) Discovery of abundant hydrothermal venting on the ultraslow-spreading Gakkel ridge in the Arctic Ocean. *Nature* **421,** 252-256.

Einsele G., Gieskes J. M., Curray J., Moore D. M., Aguayo E., Aubry M.-P., Fornari D. J., Guerrero J., Kastner M., Kelts K., Lyle M., Matoba Y., Molina-Cruz A., Niemitz J., Rueda J., Saunders A., Schrader H., Simoneit B. and Vacquier V. (1980) Intrusion of basaltic sills into highly porous sediments, and resulting hydrothermal activity. *Nature* **283,** 441-445.

Elderfield H. (1988) The oceanic chemistry of the rare earth elements. *Phil. Trans. R. Soc. A* **325,** 105-126.

Elderfield H. and Schultz A. (1996) Mid-Ocean Ridge Hydrothermal Fluxes and the Chemical Composition of the Ocean. *Annu. Rev. Earth Planet. Sci.* **24,** 191-224.

Ellington W. R. (2001) Evolution and physiological roles of phosphagen systems. *Annual Review of Physiology* **63,** 289-325.

Embley R. W., Chadwick W. W., Baker E. T., Butterfield D. A., Resing J. A., de Ronde C. E. J., Tunnicliffe V., Lupton J. E., Juniper S. K., Rubin K. H., Stern R. J., Lebon G. T., Nakamura K.-i., Merle S. G., Hein J. R., Wiens D. A. and Tamura Y. (2006) Long-term eruptive activity at a submarine arc volcano. *Nature* **441,** 494-497.

Embley R. W., Baker E. T., Butterfield D. A., Chadwick W. W., Lupton J. E., Resing J. A., de Ronde C. E. J., Nakamura K.-i., Tunnicliffe V., Dower J. F. and Merle S. G. (2007) Exploring the submarine ring of fire. Mariana Arc to Western Pacific. *Oceanography* **20,** 68-79.

Fiala-Médioni A., McKiness Z. P., Dando P., Boulegue J., Mariotti A., Alayse-Danet A. M., Robinson J. J. and Cavanaugh C. M. (2002) Ultrastructural, biochemical, and immunological characterization of two populations of the mytilid mussel *Bathymodiolus azoricus* from the Mid-Atlantic Ridge: evidence for a dual symbiosis. *Marine Biology* **141,** 1035-1043.

Firat Ö., Gök G., Çoğun H. Y., Yüzereroğlu T. A. and Kargin F. (2008) Concentrations of Cr, Cd, Cu, Zn and Fe in crab *Charybdis longicollis* and shrimp *Penaeus semisulcatus* from the Iskenderun Bay, Turkey. *Environmental Monitoring and Assessment* **147,** 117-123.

Fisher A. L., Page K. E., Lithgow G. J. and Nash L. (2008) The *Caenorhabditis elegans* K10C2.4 gene encodes a member of the Fumarylacetoacetate Hydrolase Family: A *Caenorhabditis elegans* model of Type I Tyrosinemia *Journal of Biological Chemistry* **283,** 9127-9135.

Fisher C. R., Childress J. J., Arp A. J., Brooks J. M., Distel D., Favuzzi J. A., Felbeck H., Hessler R., Johnson K. S., Kennicutt M. C., Macko S. A., Newton A., Powell M. A., Somero H. N. and Soto T. (1988) Microhabitat variation in the hydrothermal vent mussel, *Bathymodiolus thermophilus*, at the Rose Garden vent on the Galapagos Rift. *Deep-Sea Research* **35,** 1769-1791.

Fisher C. R. and Girguis P. (2007) A proteomic snapshot of life at a vent. *Science* **315,** 198-199.

Fitzpatrick J. L., Nadella S., Bucking C., Balshine S. and Wood C. M. (2008) The relative sensitivity of sperm, eggs and embryos to copper in the blue mussel (*Mytilus trossulus*). *Comparative Biochemistry and Physiology Part C* **147,** 441-449.

Flores J. F., Fisher C. R., Carney S. L., Green B. N., Freytag J. K., Schaeffer S. W. and Royer W. E. (2005) Sulfide binding is mediated by zinc ions discovered in the crystal structure of a hydrothermal vent tubeworm hemoglobin. *Proceedings of the National Academy of Sciences* **102,** 2713-2718.

Fouquet Y., von Stackelberg U., Charlou J. L., Donval J. P., Foucher J. P., Erzinger J., Herzig P., Mühe R., Wiedicke M., Soakai S. and Whitechurch H. (1991) Hydrothermal activity in the Lau back-arc basin: Sulfides and water chemistry. *Geology* **19,** 303.

Frederich M., Sartoris F. J., Arntz W. E. and Pörtner H.-O. (2000) Haemolymph Mg^{2+} regulation in decapod crustaceans: physiological correlates and ecological consequences in polar areas. *The Journal of Experimental Biology* **203,** 1383-1393.

Freedman J. H., Ciriolo M. R. and Peisach J. (1989) The role of Glutathione in copper metabolism and toxicity. *The Journal of Biological Chemistry* **264,** 5598-5605.

Fretzdorff S., Livermore R. A., Devey C. W., Leat P. T. and Stoffers P. (2002) Petrogenesis of the Back-arc East Scotia Ridge, South Atlantic Ocean. *J. Petrol.* **43,** 1435-1467.

Fridovich I. (1998) Oxygen Toxicity: A Radical Explanation. *The Journal of Experimental Biology* **201,** 1203-1209.

Früh-Green G. L., Kelley D. S., Bernasconi S. M., Karson J. A., Ludwig K., Butterfield D. A., Boschi C. and Proskurowski G. (2003) 30,000 years of hydrothermal activity at the Lost City vent field. *Science* **301,** 495-498.

Frustec A., Desbruyères D. and Juniper S. K. (1987) Deep-sea hydrothermal vent communities at 13°N on the East Pacific Rise: microdistribution and temporal variation. *Biological Oceanography* **4,** 121-164.

Gaetke L. and Chow C. K. (2003) Copper toxicity, oxidative stress, and antioxidant nutrients. *Toxicology* **189,** 147-163.

Gallant R. M. and Von Damm K. L. (2006). Geochemical controls on hydrothermal fluids from the Kairei and Edmond Vent Fields, 23°-25°S, Central Indian Ridge. *Geochem. Geophys. Geosyst.*, **7**, 10.1029/2005gc001067

Gammons C. H., Wood S. A. and Williams-Jones A. E. (1996) The aqueous geochemistry of the rare earth elements and yttrium: VI. Stability of neodymium chloride complexes from 25 to 300°C. *Geochim. Cosmochim. Acta* **60,** 4615-4630.

Gamo T., Ishibashi J., Sakai H. and Tilbrook B. (1987) Methane anomalies in seawater above the Loihi submarine summit area, Hawaii. *Geochim. Cosmochim. Acta* **51,** 2857-2864.

Gamo T., Chiba H., Masuda H., Edmonds H. N., Fujioka K., Kodama Y., Nanba H. and Sano Y. (1996) Chemical characteristics of hydrothermal fluids from the TAG mound of the mid-Atlantic Ridge in August 1994: implications for spatial and temporal variability of hydrothermal activity. *Geophys. Res. Lett.* **23,** 3483-3486.

Gamo T., Okamura K., Charlou J.-L., Urabe T., Auzende J.-M., Ishibashi J., Shitashima K., Chiba H. and Shipboard Scientific Party of the ManusFlux C. (1997) Acidic and sulfate-rich hydrothermal fluids from the Manus back-arc basin, Papua New Guinea. *Geology* **25,** 139-142.

Gamo T., Chiba H., Yamanaka T., Okuyama Y., Hashimoto J., Tsuchida S., Ishibashi J.-I., Kataoka S., Tsunogai U., Okamura K., Sano Y. and Shinjo R. (2001) Chemical characteristics of newly discovered black smoker fluids and associated hydrothermal plumes at the Rodriguez Triple Junction, Central Indian Ridge. *Earth and Planetary Science Letters* **193,** 371-379.

Geret F., Rousse N., Riso R., Sarradin P. M. and Cosson R. (1998) Metal compartmentalization and metallothionein isoforms in mussels from the Mid-Atlantic Ridge; preliminary approach to the fluid-organism relationship. *Cahiers de Biologie Marine* **39,** 291-293.

Geret F., Riso R., Sarradin P. M., Caprais J.-C. and Cosson R. (2002a) Metal bioaccumulation and storage forms in the shrimp, *Rimicaris exoculata*, from the Rainbow hydrothermal field (Mid-Atlantic Ridge); preliminary approach to the fluid-organism relationship. *Cahiers de Biologie Marine* **43,** 43-52.

Geret F., Serafim A., Barreira L. and Bebianno M. J. (2002b) Effect of cadmium on antioxidant enzyme activities and lipid peroxidation in the gills of the clam *Ruditapes decussatus*. *Biomarkers* **7,** 242-256.

German C. R., Klinkhammer G. P., Edmond J. M., Mitra A. and Elderfield H. (1990) Hydrothermal scavenging of rare-earth elements in the ocean. *Nature* **345,** 516-518.

German C. R., Baker E. T., Mevel C., Tamaki K. and Team F. S. (1998) Hydrothermal activity along the southwest Indian Ridge. *Nature* **395,** 490-493.

German C. R., Livermore R. A., Baker E. T., Bruguier N. I., Connelly D. P., Cunningham A. P., Morris P., Rouse I. P., Statham P. J. and Tyler P. A. (2000) Hydrothermal plumes above the East Scotia Ridge: an isolated high-latitude back-arc spreading centre. *Earth Planet. Sci. Lett.* **184,** 241-250.

German C. R., Bennett S. A., Connelly D. P., Evans A. J., Murton B. J., Parson L. M., Prien R. D., Ramirez-Llodra E., Jakuba M., Shank T. M., Yoerger D. R., Baker E. T., Walker S. L. and Nakamura K. (2008) Hydrothermal activity on the southern Mid-Atlantic Ridge: Tectonically- and volcanically-controlled venting at 4–5°S. *Earth Planet. Sci. Lett.* **273,** 332-344.

German C. R., Bowen A., Coleman M. L., Honig D. L., Huber J. A., Jakuba M. V., Kinsey J. C., Kurz M. D., Leroy S., McDermott J. M., Mercier de Lepinay B., Nakamura K., Seewald J. S., Smith J. L., Sylva S. P., Van Dover C. L., Whitcomb L. L. and Yoerger D. R. (2010) Diverse styles of submarine venting on the ultraslow spreading Mid-Cayman Rise. *Proceedings of the National Academy of Sciences* **107,** 14020-14025.

German C. R., Ramirez-Llodra E., Baker M. C., Tyler P. A. and Committee C. S. S. (2011). Deep-Water Chemosynthetic Ecosystem Research during the Census of Marine Life Decade and Beyond: A Proposed Deep-Ocean Road Map. *PLoS ONE*, **6**, 10.1371/journal.pone.0023259

Gieskes J. M., Simoneit B., Shanks W. C., Goodfellow W. D., James R. H., Baker P. A. and Ishibashi J.-i. (2002) Geochemistry of fluid phases and sediments: relevance to hydrothermal circulation in Middle Valley, ODP Legs 139 and 169. *Applied Geochemistry* **17,** 1381-1399.

Giggenbach W. F. (1987) Redox processes governing the chemistry of fumarolic gas discharges from White Isand, New Zealand. *Applied Geochemistry* **2,** 143-161.

Gillis K. M., Smith A. D. and Ludden J. N. (1990). Trace element and Sr-isotopic contents of hydrothermal clays and sulfides from the Snake Pit hydrothermal field: ODP Site 649. *In:* Detrick R., Honnorez J., Bryan W. B. and Juteau T. (eds.) *Proceedings of the Ocean Drilling Program, Scientific Results.* pp. 315-319

Goffredi S. K., Jones W. J., Erhlich H., Springer A. and Vrijenhoek R. C. (2008) Epibiotic bacteria associated with the recently discovered Yeti crab, *Kiwa hirsuta*. *Environmental Microbiology* **10,** 2623-2634.

Gonzalez-Rey M., Serafim A., Company R. and Bebianno M. J. (2007) Adaptation to metal toxicity: a comparison of hydrothermal vent and coastal shrimps. *Marine Ecology* **28,** 100-107.

Gonzalez-Rey M., Serafim A., Company R., Gomes T. and Bebianno M. J. (2008) Detoxification mechanisms in shrimp: Comparative approach between hydrothermal vent fields and estuarine environments. *Marine Environmental Research* **66,** 35-37.

Gràcia E., Charlou J. L., Radford-Knoery J. and Parson L. M. (2000) Non-transform offsets along the Mid-Atlantic Ridge south of the Azores (38°N-34°N):

ultramafic exposures and hosting of hydrothermal vents. *Earth Planet. Sci. Lett.* **177,** 89-103.

Guichard F., Church T. M., Treuil M. and Jaffrezic H. (1979) Rare earths in barites: distribution and effects on aqueous partitioning. *Geochim. Cosmochim. Acta* **43,** 983-997.

Haas J. R., Shock E. L. and Sassani D. C. (1995) Rare earth elements in hydrothermal systems: Estimates of standard partial molal thermodynamic properties of aqueous complexes of the rare earth elements at high pressures and temperatures. *Geochim. Cosmochim. Acta* **59,** 4329-4350.

Haase K. M., Petersen S., Koschinsky A., Seifert R., Devey C. W., Keir R., Lackschewitz K. S., Melchert B., Perner M., Schmale O., Süling J., Dubilier N., Zielinski F., Fretzdorff S., Garbe-Schönberg D., Westernströer U., German C. R., Shank T. M., Yoerger D., Giere O., Kuever J., Marbler H., Mawick J., Mertens C., Stöber U., Walter M., Ostertag-Henning C., Paulick H., Peters M., Strauss H., Sander S., Stecher J., Warmuth M. and Weber S. (2007). Young volcanism and related hydrothermal activity at 5°S on the slow-spreading southern Mid-Atlantic Ridge. *Geochem. Geophys. Geosyst.*, **8**, 10.1029/2006gc001509

Habig W. H., Pabst M. J. and Jakoby W. B. (1974) Glutathione S-Transferases: The first enzymatic step in mercapturic acid formation. *Journal of Biological Chemistry* **249,** 7130-7139.

Hall S. and Thatje S. (2010) Temperature-driven biogeography of the deep-sea family Lithodidae (Crustacea: Decapoda: Anomura) in the Southern Ocean. *Polar Biology* **34,** 363-370.

Hansen R. E., Roth D. and Winther J. R. (2009) Quantifying the global cellular thiol-disulfide status. *Proceedings of the National Academy of Sciences* **106,** 422-427.

Hardivillier Y., Leignel V., Denis F., Uguen G., Cosson R. and Laulier M. (2004) Do organisms living around hydrothermal vent sites contain specific metallothioneins? The case of the genus Bathymodiolus (Bivalvia, Mytilidae). *Comparative Biochemistry and Physiology Part C* **139,** 111-118.

Hardivillier Y., Denis F., Demattei M.-V., Bustamante P., Laulier M. and Cosson R. (2006) Metal influence on metallothionein synthesis in the hydrothermal vent mussel *Bathymodiolus thermophilus*. *Comparative Biochemistry and Physiology Part C* **143,** 321-332.

Hathorne E. C., Haley B., Stichel T., Grasse P., Zieringer M. and Frank M. (2012). Online preconcentration ICP-MS analysis of rare earth elements in seawater. *Geochem. Geophys. Geosys.*, **13**, 10.1029/2011GC003907

Haymon R. M. (1983) Growth history of hydrothermal black smoker chimneys. *Nature* **301,** 695-698.

Haymon R. M., Fornari D. J., Edwards M. H., Carbotte S., Wright D. and Macdonald K. C. (1991) Hydrothermal vent distribution along the East Pacific Rise crest (9°09' - 54'N) and its relationship to magmatic and tectonic processes on fast-spreading mid-ocean ridges. *Earth Planet. Sci. Lett.* **104,** 513-534.

Haymon R. M., Fornari D. J., Von Damm K. L., Lilley M. D., Perfitt M., Edmond J. M., Shanks W. C., Lutz R., Grebmeier J., Carbotte S., Wright D., McLaughlin E., Smith M., Beedle N. and Olson E. J. (1993) Volcanic eruption of the mid-ocean ridge along the East Pacific Rise crest at 9°45-52'N: Direct submersible observations of seafloor phenomena associated with an eruption event in April, 1991. *Earth Planet. Sci. Lett.* **119,** 85-101.

Hekinian R., Fevrier M., Avedik F., Cambon P., Charlou J. L., Needham H. D., Raillard J., Boulegne J., Merlivat L., Moinet A., Manganini S. and Lange J. (1983) East Pacific Rise near 13°N: geology of new hydrothermal fields. *Science* **219,** 1321-1324.

Hessler R. and Lonsdale P. F. (1991) Biogeography of Mariana Trough hydrothermal vent communities. *Deep-Sea Research* **38,** 185-199.

Humphris S. (1998). Rare earth element composition of anhydrite: Implications for deposition and mobility within the active TAG hydrothermal mound. *In:* Herzig P., Humphris S., Miller D. J. and Zierenberg R. A. (eds.) *Proceedings of the Ocean Drilling Program, Scientific Results.* pp. 143-159

Humphris S. and Bach W. (2005) On the Sr isotope and REE compositions of anhydrites from the TAG seafloor hydrothermal system. *Geochim. Cosmochim. Acta* **69,** 1511-1525.

Iida H. and Yahara I. (1985) Yeast heat-shock protein of M_r 48,000 is an isoprotein of enolase. *Nature* **315,** 688-690.

Ishibashi J.-i., Sato M., Sano Y., Wakita H., Gamo T. and Shanks W. C. (2002) Helium and carbon gas geochemistry of pore fluids from the sediment-rich hydrothermal system in Escanaba Trough. *Applied Geochemistry* **17,** 1457-1466.

Iwasaki I. and Ozawa T. (1960) Genesis of sulfate in acid hot spring. *B. Chem. Soc. Jpn.* **33,** 1018-1019.

Jacobs D. K. and Lindberg D. R. (1998) Oxygen and evolutionary patterns in the sea: Onshore/offshore trends and recent recruitment of deep-sea faunas. *Proceedings of the National Academy of Sciences USA* **95,** 9396-9401.

James R. H., Elderfield H. and Palmer M. (1995) The chemistry of hydrothermal fluids from the Broken Spur site, 29°N Mid-Atlantic Ridge. *Geochim. Cosmochim. Acta* **59,** 651-659.

James R. H. and Elderfield H. (1996) Chemistry of ore-forming fluids and mineral formation rates in an active hydrothermal sulfide deposit on the Mid-Atlantic Ridge. *Geology* **24,** 1147-1150.

James R. H., Green D. R. H., Stock M. J., Alker B. J., Banerjee N. R., Cole C., German C. R., Huvenne V. A. I., Powell A. M. and Connelly D. P. (in review) Geochemistry of hydrothermal fluids and associated mineralisation on the East Scotia Ridge.

Jewett S. C. and Naidu A. S. (2000) Assessment of heavy metals in Red King Crabs following offshore placer gold mining. *Marine Pollution Bulletin* **40,** 478-490.

Jones W. J., Won Y. J., Maas P. A. Y., Smith P. J., Lutz R. A. and Vrijenhoek R. C. (2006) Evolution of habitat use by deep-sea mussels. *Marine Biology* **148,** 841-851.

Kádár E., Costa V., Martins I., Santos R. S. and Powell J. J. (2005) Enrichment in trace metals (Al, Mn, Co, Cu, Mo, Cd, Fe, Zn, Pb and Hg) of macro-invertebrate habitats at hydrothermal vents along the Mid-Atlantic Ridge. *Hydrobiologia* **548,** 191-205.

Kádár E., Costa V. and Segonzac M. (2007) Trophic influences of metal accumulation in natural pollution laboratories at deep-sea hydrothermal vents of the Mid-Atlantic Ridge. *Science of The Total Environment* **373,** 464-472.

Kagi H., Dohmoto Y., Takano S. and Masuda A. (1993) Tetrad effect in lanthanide partitioning between calcium sulfate crystal and its saturated solution. *Chem. Geol.* **107,** 71-82.

Karl D. M., McMurty G. M., Malahoff A. and Garcia M. O. (1988) Loihi Seamount, Hawaii: a mid-plate volcano with a distinctive hydrothermal system. *Nature* **335,** 532-535.

Kelley D. S., Karson J. A., Blackman D. K., Früh-Green G. L., Butterfield D. A., Lilley M. D., Olson E. J., Schrenk M. O., Roe K. K., Lebon G. T., Rivizzigno P. and Party A.-S. (2001) An off-axis hydrothermal vent field near the Mid-Atlantic Ridge. *Nature* **412,** 145-149.

Kelley D. S., Baross J. A. and Delaney J. R. (2002) Volcanoes, fluids, and life at mid-ocean ridge spreading centers. *Annu. Rev. Earth Planet. Sci.* **30,** 385-491.

Kelley D. S., Karson J. A., Früh-Green G. L., Yoerger D., Shank T. M., Butterfield D. A., Hayes J. M., Schrenk M. O., Olson E. J., Proskurowski G., Jakuba M., Bradley A., Larson B., Ludwig K., Glickson D., Buckman K., Bradley A. S., Brazelton W. J., Roe K. K., Elend M. J., Delacour A., Bernasconi S. M., Lilley M. D., Baross J. A., Summons R. E. and Sylva S. P. (2005) A serpentinite-hosted ecosystem: The Lost City hydrothermal field. *Science* **307,** 1428-1434.

Klinkhammer G. P., Elderfield H., Edmond J. M. and Mitra A. (1994) Geochemical implications of rare earth element patterns in hydrothermal fluids from mid-ocean ridges. *Geochim. Cosmochim. Acta* **58,** 5105-5113.

Kloor D., Yao K., Delabar U. and Osswald H. (2000) Simple and sensitive binding assay for measurement of adenosine using reduced S-adenosylhomocysteine hydrolase. *Clinical Chemistry* **46,** 537-542.

Kurz M. D., Le Roex A. P. and Dick H. J. B. (1998) Isotope geochemistry of the oceanic mantle near the Bouvet triple junction. *Geochim. Cosmochim. Acta* **62,** 841-852.

Langmuir C. H., Humphris S., Fornari D. J., Van Dover C. L., Von Damm K. L., Tivey M. K., Colodner D., Charlou J. L., Desonie D., Wilson C., Fouquet Y., Klinkhammer G. P. and Bougault H. (1997) Hydrothermal vents near a mantle hot spot: the Lucky Strike vent field at 37°N on the Mid-Altlantic Ridge. *Earth Planet. Sci. Lett.* **148,** 69-91.

Langston W. J., Bebianno M. J. and Burt G. R. (1998). Metal handling strategies in molluscs. *In:* Langston W. J. and Bebianno M. J. (eds.) *Metal Metabolism in Aquatic Environments.* London: Chapman & Hall, pp.

Larter R., Vanneste L., Morris P. and Smythe D. K. (2003). Structure and tectonic evolution of the South Sandwich arc. *In:* Larter R. and Leat P. T. (eds.) *Intra-Oceanic Subduction Systems: Tectonic and Magmatic Processes.* London: The Geological Society of London, pp. 255-284

Le Pennec M., Donval A. and Herry A. (1990) Nutritional strategies of the hydrothermal ecosystem bivalves *Progress in Oceanography* **24,** 71-80.

Leat P. T., Livermore R. A., Millar I. L. and Pearce J. A. (2000) Magma supply in back-arc spreading centre segment E2, East Scotia Ridge. *J. Petrol.* **41,** 845-866.

Leat P. T., Pearce J. A., Barker P. F., Millar I. L., Barry T. L. and Larter R. D. (2004) Magma genesis and mantle flow at a subducting slab edge: the South Sandwich arc-basin system. *Earth Planet. Sci. Lett.* **227,** 17-35.

Lecoeur S., Videmann B. and Berny P. (2004) Evaluation of metallothionein as a biomarker of single and combined Cd/Cu exposure in *Dreissena polymorpha*. *Environmental Research* **94,** 184-191.

Leung P. T. Y., Wang Y., Mak S. S. T., Ng W. C. and Leung K. M. Y. (2011) Differential proteomic responses in hepatopancreas and adductor muscles of the green-lipped mussel *Perna viridis* to stresses induced by cadmium and hydrogen peroxide. *Aquatic Toxicology* **105,** 49-61.

Liao S., Li R., Shi L., Wang J., Shang J., Zhu P. and Chen B. (2012) Functional analysis of an S-adenosylhomocysteine hydrolase homolog of chestnut blight fungus. *FEMS Microbiology Letters* **336,** 64-72.

Little C. T. S. and Vrijenhoek R. C. (2003) Are hydrothermal vent animals living fossils? *Trends in Ecology & Evolution* **18,** 582-588.

Liu F., Wang D.-Z. and Wang W.-X. (2012) Cadmium-induced changes in trace element bioaccumulation and proteomics perspective in four marine bivalves. *Environmental Toxicology and Chemistry* **31,** 1292-1300.

Livermore R. A., McAdoo D. and Marks K. (1994) Scotia Sea tectonics from high-resolution satellite gravity. *Earth Planet. Sci. Lett.* **123,** 255-268.

Livermore R. A., Cunningham A., Vanneste L. and Larter R. (1997) Subduction influence on magma supply at the East Scotia Ridge. *Earth Planet. Sci. Lett.* **150,** 261-275.

Lloyd D. R. and Phillips D. H. (1999) Oxidative DNA damage mediated by copper(II), iron(II)and nickel(II) Fenton reactions: evidence for site-specific mechanisms in the formation of double-strand breaks, 8-hydroxydeoxyguanosine and putative intrastrand cross-links. *Mutation Research* **424,** 23-36.

Lonsdale P. F. and Becker K. (1985) Hydrothermal plumes, hot springs, and conductive heat flow in the Southern Trough of Guaymas Basin. *Earth Planet. Sci. Lett.* **73,** 211-225.

Lorion J., Buge B., Cruaud C. and Samadi S. (2010) New insights into diversity and evolution of deep-sea Mytilidae (Mollusca: Bivalvia). *Molecular Phylogenetics and Evolution* **57,** 71-83.

Luo W., Lu Y., Wang T., Kong P., Jiao W., Hu W., Jia J., Naile J. E., Khim J. S. and Giesy J. P. (2013) Environmental concentrations and bioaccumulations of cadmium and zinc in coastal watersheds along the Chinese Northern Bohai and Yellow Seas. *Environmental Toxicology and Chemistry* **32,** 831-840.

Luoma S. N. and Rainbow P. S. (2008) *Metal Contamination in Aquatic Environments: Science and Lateral Management,* New York, Cambridge University Press.

Lupton J., Butterfield D., Lilley M., Evans L., Nakamura K.-i., Chadwick W., Resing J., Embley R., Olson E., Proskurowski G., Baker E., de Ronde C., Roe K., Greene R., Lebon G. and Young C. (2006). Submarine venting of liquid carbon dioxide on a Mariana Arc volcano. *Geochem. Geophys. Geosyst.*, **7**, 10.1029/2005gc001152

Lupton J., Lilley M., Butterfield D., Evans L., Embley R., Massoth G., Christenson B., Nakamura K.-i. and Schmidt M. (2008). Venting of a separate CO_2-rich gas phase from submarine arc volcanoes: Examples from the Mariana and Tonga-Kermadec arcs. *J. Geophys. Res.*, **113**, 10.1029/2007jb005467

Macdonald K. C. (1982) Mid-Ocean Ridges: Fine Scale Tectonic, Volcanic and Hydrothermal Processes Within the Plate Boundary Zone. *Annu. Rev. Earth Planet. Sci.* **10,** 155-190.

MacPherson E., Jones W. and Segonzac M. (2005) A new squat lobster family of Galatheoidea (Crustacea, Decapoda, Anomura) from the hydrothermal vents of the Pacific-Antarctic Ridge. *Zoosystema* **27,** 709-723.

Manduzio H., Cosette P., Gricourt L., Jouenne T., Lenz C., Andersen O.-K., Leboulenger F. and Rocher B. (2005) Proteome modifications of blue mussel (*Mytilus edulis* L.) gills as an effect of water pollution. *Proteomics* **5,** 4958-4963.

Marie B., Genard B., Rees J.-F. and Zal F. (2006) Effect of ambient oxygen concentration on activities of enzymatic antioxidant defences and aerobic metabolism in the hydrothermal vent worm, *Paralvinella grasslei*. *Marine Biology* **150,** 273-284.

Marigómez I., Soto M., Cajaraville M. P., Angulo E. and Giamberini L. (2002) Cellular and subcellular distribution of metals in molluscs. *Microscopy Research and Technique* **56,** 358-392.

Marsh L., Copley J. T., Huvenne V. A. I., Linse K. T., Reid W. D. K., Rogers A. D., Sweeting C. J. and Tyler P. A. (2012). Microdistribution of Faunal Assemblages at Deep-Sea Hydrothermal Vents in the Southern Ocean. *PLoS ONE*, **7**, 10.1371/journal.pone.0048348

Martinov M. V., Vitvitsky V. M., Banerjee R. and Ataullakhanov F. I. (2010) The logic of the hepatic methionine metabolic cycle. *Biochimica et Biophysica Acta (BBA) - Proteins and Proteomics* **1804,** 89-96.

Martins I., Colaço A., Dando P. R., Martins I., Desbruyères D., Sarradin P.-M., Marques J. C. and Serrão-Santos R. (2008) Size-dependent variations on the nutritional pathway of *Bathymodiolus azoricus* demonstrated by a C-flux model. *Ecological Modelling* **217,** 59-71.

Martins I., Bettencourt R., Colaço A., Sarradin P.-M., Santos R. S. and Cosson R. (2011a) The influence of nutritional conditions on metal uptake by the mixotrophic dual symbiosis harboring vent mussel *Bathymodiolus azoricus*. *Comparative Biochemistry and Physiology Part C* **153,** 40-52.

Martins I., Cosson R. P., Riou V., Sarradin P.-M., Sarrazin J., Santos R. S. and Colaço A. (2011b) Relationship between metal levels in the vent mussel *Bathymodiolus azoricus* and local microhabitat chemical characteristics of Eiffel Tower (Lucky Strike). *Deep Sea Research Part I: Oceanographic Research Papers* **58,** 306-315.

Mary J., Rogniaux H., Rees J.-F. and Zal F. (2010) Response of *Alvinella pompejana* to variable oxygen stress: A proteomic approach. *Proteomics* **10,** 2250-2258.

Masella R., Di Benedetto R., Varì R., Filesi C. and Giovannini C. (2005) Novel mechanisms of natural antioxidant compounds in biological systems: involvement of glutathione and glutathione-related enzymes. *The Journal of Nutritional Biochemistry* **16,** 577-586.

Massoth G. J., Butterfield D., Lupton J., McDuff R. E., Lilley M. D. and Jonasson I. R. (1989) Submarine venting of phase-separated hydrothermal fluids at Axial Volcano, Juan de Fuca Ridge. *Nature* **340,** 702-705.

McDonagh B., Tyther R. and Sheehan D. (2005) Carbonylation and glutathionylation of proteins in the blue mussel *Mytilus edulis* detected by proteomic analysis and Western blotting: Actin as a target for oxidative stress. *Aquatic Toxicology* **73,** 315-326.

McDonagh B. and Sheehan D. (2006) Redox proteomics in the blue mussel *Mytilus edulis*: Carbonylation is not a pre-requisite for ubiquitination in acute free radical-mediated oxidative stress. *Aquatic Toxicology* **79,** 325-333.

McDonagh B., Tyther R. and Sheehan D. (2006) Redox proteomics in the mussel, *Mytilus edulis*. *Marine Environmental Research* **62,** S101-S104.

McDonagh B. and Sheehan D. (2007) Effect of oxidative stress on protein thiols in the blue mussel *Mytilus edulis*: Proteomic identification of target proteins. *Proteomics* **7,** 3395-3403.

McDonagh B. and Sheehan D. (2008) Effects of oxidative stress on protein thiols and disulphides in *Mytilus edulis* revealed by proteomics: Actin and protein disulphide isomerase are redox targets. *Marine Environmental Research* **66,** 193-195.

McKiness Z. P. and Cavanaugh C. M. (2005) The ubiquitous mussel: *Bathymodiolus* aff. *brevior* symbiosis at the Central Indian Ridge hydrothermal vents. *Marine Ecology Progress Series* **295,** 183-190.

McMurty G. M., Sedwick P. N., Fryer P., VonderHaar D. L. and Yeh H.-W. (1993) Unusual geochemistry of hydrothermal vents on submarine arc volcanoes: Kasuga Seamounts, Northern Mariana Arc. *Earth Planet. Sci. Lett.* **114,** 517-528.

Mestre N. C., Thatje S. and Tyler P. A. (2009) The ocean is not deep enough: pressure tolerances during early ontogeny of the blue mussel *Mytilus edulis*. *Proceedings of the Royal Society B: Biological Sciences* **276,** 717-726.

Michard A., Albarède F., Michard G., Minster J. F. and Charlou J. L. (1983) Rare-earth elements and uranium in high temperature solutions from the East Pacific Rise hydrothermal vent field (13°N). *Nature* **303,** 795-897.

Michard A. and Albarède F. (1986) The REE content of some hydrothermal fluids. *Chem. Geol.* **55,** 51-60.

Migdisov A. A., Williams-Jones A. E. and Wagner T. (2009) An experimental study of the solubility and speciation of the Rare Earth Elements (III) in fluoride- and chloride-bearing aqueous solutions at temperatures up to 300°C. *Geochim. Cosmochim. Acta* **73,** 7087-7109.

Mills R. and Elderfield H. (1995) Rare earth element geochemistry of hydrothermal deposits from the active TAG mound, 26°N Mid-Atlantic Ridge. *Geochim. Cosmochim. Acta* **59,** 3511-3524.

Mitra A., Elderfield H. and Greaves M. J. (1994) Rare earth elements in submarine hydrothermal fluids and plumes from the Mid-Atlantic Ridge. *Mar. Chem.* **46,** 217-235.

Miyake H., Kitada M., Tsuchida S., Okuyama Y. and Nakamura K.-i. (2007) Ecological aspects of hydrothermal vent animals in captivity at atmospheric pressure. *Marine Ecology* **28,** 86-92.

Miyazaki J. I., de Oliveria Martins L., Fujita Y., Matsumoto H. and Fujiwara Y. (2010). Evolutionary Process of Deep-Sea *Bathymodiolus* Mussels. *PLoS ONE*, **5**, 10.1371/journal.pone.0010363

Mohapatra A., Rautray T. R., Patra A. K., Vijayan V. and Mohanty R. K. (2009) Elemental composition in mud crab *Scylla serrata* from Mahanadi estuary, India: In situ irradiation analysis by external PIXE. *Food and Chemical Toxicology* **47,** 119-123.

Morgan J. W. and Wandless G. A. (1980) Rare earth element distribution in some hydrothermal minerals: Evidence for crystallographic control. *Geochim. Cosmochim. Acta* **44,** 973-980.

Morton J. L., Holmes M. L. and Koski R. A. (1987) Volcanism and massive sulfide formation at a sedimented spreading centre, Escanaba Trough, Gorda Ridge, Northeast Pacific Ocean. *Geophys. Res. Lett.* **14,** 769-772.

Mottl M. J., Seewald J. S., Wheat C. G., Tivey M. K., Michael P. J., Proskurowski G., McCollom T. M., Reeves E., Sharkey J., You C. F., Chan L. H. and Pichler T. (2011) Chemistry of hot springs along the Eastern Lau Spreading Center. *Geochim. Cosmochim. Acta* **75,** 1013-1038.

Murton B. J., Van Dover C. L. and Southward E. (1995) Geological setting and ecology of the Broken Spur hydrothermal vent field: 29°10'N on the Mid-Atlantic Ridge. *Geological Society of London, Special Publication* 33-41.

Nadella S. R., Fitzpatrick J. L., Franklin N., Bucking C., Smith S. and Wood C. M. (2009) Toxicity of dissolved Cu, Zn, Ni and Cd to developing embryos of the blue mussel (*Mytilus trossolus*) and the protective effect of dissolved organic carbon. *Comparative Biochemistry and Physiology Part C* **149,** 340-348.

Naveira-Garabato A. C., Heywood K. J. and Stevens D. P. (2002) Modification and pathways of the Southern Ocean Deep Waters in the Scotia Sea. *Deep-Sea Research I* **49,** 681-705.

Newman W. A. (1985) The abyssal hydrothermal vent invertebrate fauna. A glimpse of antiquity? *Bulletin of the Biological Society of Washington* **6,** 159-166.

Ng T. Y.-T. and Wang W.-X. (2007) Interactions of silver, cadmium, and copper accumulation in green mussels (*Perna viridis*). *Environmental Toxicology and Chemistry* **26,** 1764-1769.

Nicholson S. (2003a) Lysosomal membrane stability, phagocytosis and tolerance to emersion in the mussel *Perna viridis* (Bivalvia: Mytilidae) following exposure to acute, sublethal, copper. *Chemosphere* **52,** 1147-1151.

Nicholson S. (2003b) Cardiac and branchial physiology associated with copper accumulation and detoxication in the mytilid mussel *Perna viridis* (L.). *Journal of Experimental Marine Biology and Ecology* **295,** 157-171.

Ohara Y., Stern R. J., Ishii T., Yurimoto H. and Yamazaki T. (2002) Peridotites from the Mariana Trough: first look at the mantle beneath an active back-arc basin. *Contributions to Mineralogy and Petrology* **143,** 1-18.

Oliphant A., Thatje S., Brown A., Morini M., Ravaux J. and Shillito B. (2011) Pressure tolerance of the shallow-water caridean shrimp *Palaemonetes varians* across its thermal tolerance window. *The Journal of Experimental Biology* **214,** 1109-1117.

Onuma N., Higuchi H., Wakita H. and Nagasawa H. (1968) Trace element partion between two pyroxenes and the host lava. *Earth Planet. Sci. Lett.* **5,** 47-51.

Orsi A. H., Whitworth III T. and Nowlin Jr W. D. (1995) On the meridional extent and fronts of the Antarctic Circumpolar Current. *Deep-Sea Research I* **42,** 641-673.

Page H. M., Fiala-Médioni A., Fisher C. R. and Childress J. J. (1991) Experimental evidence for filter-feeding by the hydrothermal vent mussel, *Bathymodiolus thermophilus*. *Deep-Sea Research* **38,** 1455-1461.

Palmer M. (1992) Controls over the chloride concentration of submarine hydrothermal vent fluids - evidence from Sr/Ca and Sr-87/Sr-86 ratios. *Earth Planet. Sci. Lett.* **109,** 37-46.

Pancholi V. (2001) Multifunctional α-enolase: its role in diseases. *Cellular and Molecular Life Sciences* **58,** 902-920.

Pedersen R. B., Rapp H. T., Thorseth I. H., Lilley M. D., Barriga F. J. A. S., Baumberger T., Flesland K., Fonseca R., Früh-Green G. L. and Jorgensen S. L. (2010) Discovery of a black smoker vent field and vent fauna at the Arctic Mid-Ocean Ridge. *Nature Communications* **1,** 126.

Pelayo A. M. and Wiens D. A. (1989) Seismotectonics and relative plate motions in the Scotia Sea region. *J. Geophys. Res.* **94,** 7293-7320.

Peng S.-H., Hung J.-J. and Hwang J.-S. (2011) Bioaccumulation of trace metals in the submarine hydrothermal vent crab *Xenograpsus testudinatus* off Kueishan Island, Taiwan. *Marine Pollution Bulletin* **63,** 396-401.

Phinney W. C. and Morrison D. A. (1990) Partition coefficients for calcic plagioclase: Implications for Archean anorthosites. *Geochim. Cosmochim. Acta* **54,** 1639-1654.

Piepgras D. J. (1984). *The isotopic composition of neodymium in the marine environment: Investigations of the sources and transport of rare earth elements in the oceans.* Ph.D Thesis, California Institute of Technology.

Pollard T. D. and Cooper J. A. (1986) Actin and actin-binding proteins. A critical evaluation of mechanisms and functions. *Annual Review of Biochemistry* **55,** 978-1035.

Poulsen E., Riisgård H. U. and Møhlenberg F. (1982) Accumulation of cadmium and bioenergetics in the mussel *Mytilus edulis*. *Marine Biology* **68,** 25-29.

Pourang N., Dennis J. H. and Ghourchian H. (2004) Tissue distribution and redistribution of trace elements in shrimp species with the emphasis on the roles of metallothionein. *Ecotoxicology* **13,** 519-533.

Pruski A. M. and Dixon D. R. (2002) Effects of cadmium on nuclear integrity and DNA repair efficiency in the gill cells of *Mytilus edulis*. *Aquatic Toxicology* **57,** 127-137.

Purdy G. M., Kong L. S. L., Christeson G. L. and Solomon S. C. (1992) Relationship between spreading rate and the seismic structure of mid-ocean ridges. *Nature* **355,** 815-817.

Quinnell S., Hulsman K. and Davie P. J. F. (2004) Protein model for pollutant uptake and elimination by living organisms and its implication for ecotoxicology. *Marine Ecology Progress Series* **274,** 1-16.

Raftopoulou E. K. and Dimitriadis V. K. (2011) Comparative study of the accumulation and detoxification of Cu (essential metal) and Hg (nonessential metal) in the digestive gland and gills of mussels *Mytilus galloprovincialis*, using analytical and histochemical techniques. *Chemosphere* **83,** 1155-1165.

Rainbow P. (2002) Trace metal concentrations in aquatic invertebrates: why and so what? *Environmental Pollution* **120,** 497-507.

Ramirez-Llodra E., Shank T. M. and German C. (2007) Biodiversity and biogeography of hydrothermal vent species. Thirty years of discovery and investigations. *Oceanography* **20,** 30-41.

Ramirez-Llodra E., Brandt A., Danovaro R., De Mol B., Escobar E., German C. R., Levin L. A., Martinez Arbizu P., Menot L., Buhl-Mortensen P., Narayanaswamy B. E., Smith C. R., Tittensor D. P., Tyler P. A., Vanreusel A. and Vecchione M. (2010) Deep, diverse and definitely different: unique attributes of the world's largest ecosystem. *Biogeosciences* **7,** 2851-2899.

Reed L. A., Pennington P. L. and Wirth E. (2010) A survey of trace element distribution in tissues of stone crabs (*Menippe mercenaria*) from South Carolina Coastal Waters. *Marine Pollution Bulletin* **60,** 2297-2302.

Reeves E. P., Seewald J. S., Saccocia P., Bach W., Craddock P. R., Shanks W. C., Sylva S. P., Walsh E., Pichler T. and Rosner M. (2011) Geochemistry of hydrothermal fluids from the PACMANUS, Northeast Pual and Vienna Woods hydrothermal fields, Manus Basin, Papua New Guinea. *Geochim. Cosmochim. Acta* **75,** 1088-1123.

Regoli F. and Principato G. (1995) Glutathione, glutathione-depenent and antioxidant enzymes in mussel, *Mytilus galloprovincialis*, exposed to metals under field and

laboratory conditions: implications for the use of biochemical biomarkers. *Aquatic Toxicology* **31,** 143-164.

Reid W. D. K., Sweeting C. J., Wigham B. D., Zwirglmaier K., Hawkes J. A., McGill R. A. R., Linse K. and Polunin N. V. C. (2013). Spatial differences in East Scotia Ridge hydrothermal vent food webs: Influences of chemistry, microbiology and predation on trophodynamics. *PLoS ONE*, **8**, 10.1371/journal.pone.0065553

Riisgård H. U., Egede P. P. and Barreiro Saavedra I. (2011) Feeding behaviour of the mussel, *Mytilus edulis*: New observations, with a minireview of current knowledge. *Journal of Marine Biology* **2011,** 1-13.

Riou V., Halary S., Duperron S., Bouillon S., Elskens M., Bettencourt R., Santos R. S., Dehairs F. and Colaço A. (2008) Influence of CH_4 and H_2S availability on symbiont distribution, carbon assimilation and transfer in the dual symbiotic vent mussel *Bathymodiolus azoricus*. *Biogeosciences* **5,** 1681-1691.

Roberts S., Bach W., Binns R. A., Vanko D. A., Yeats C. J., Teagle D. A. H., Blacklock K., Blusztajn J. S., Boyce A. J., Cooper M. J., Holland N. and McDonald B. (2003) Contrasting evolution of hydrothermal fluids in the PACMANUS system, Manus Basin: The Sr and S isotope evidence. *Geology* **31,** 805.

Rodríguez-Ortega M. J., Grøsvik B. E., Rodríguez-Ariza A., Goksøyr A. and López-Barea J. (2003) Changes in protein expression profiles in bivalve molluscs (*Chamaelea gallina*) exposed to four model environmental pollutants. *Proteomics* **3,** 1535-1543.

Roesijadi G. (1994) Metallothionein induction as a measure of response to metal exposure in aquatic animals. *Environmental Health Perspectives* **102,** 91-95.

Rogers A. D., Tyler P. A., Connelly D. P., Copley J. T., James R., Larter R. D., Linse K., Mills R. A., Garabato A. N., Pancost R. D., Pearce D. A., Polunin N. V. C., German C. R., Shank T., Boersch-Supan P. H., Alker B. J., Aquilina A., Bennett S. A., Clarke A., Dinley R. J. J., Graham A. G. C., Green D. R. H., Hawkes J. A., Hepburn L., Hilario A., Huvenne V. A. I., Marsh L., Ramirez-Llodra E., Reid W. D. K., Roterman C. N., Sweeting C. J., Thatje S. and Zwirglmaier K. (2012). The discovery of new deep-sea hydrothermal vent communities in the Southern Ocean and implications for biogeography. *PLoS Biol.*, **10**, 10.1371/journal.pbio.1001234

Rona P., Klinkhammer G. P., Nelsen T. A., Trefry J. H. and Elderfield H. (1986) Black smokers, massive sulphides and vent biota at the Mid-Atlantic Ridge. *Nature* **321,** 33-37.

Samadi S., Quéméré E., Lorion J., Tillier A., von Cosel R., Lopez P., Cruaud C., Couloux A. and Boisselier-Dubayle M.-C. (2007) Molecular phylogeny in

mytilids supports the wooden steps to deep-sea vents hypothesis. *Comptes Rendus Biologies* **330,** 446-456.

Sarradin P.-M., Caprais J.-C., Riso R., Kerouel R. and Aminot A. (1999) Chemical environment of the hydrothermal mussel communities in the Lucky Strike and Menez Gwen vent fields, Mid Atlantic Ridge. *Cahiers de Biologie Marine* **40,** 93-104.

Sarradin P.-M., Lannuzel D., Waeles M., Crassous P., Le Bris N., Caprais J. C., Fouquet Y., Fabri M. C. and Riso R. (2008) Dissolved and particulate metals (Fe, Zn, Cu, Cd, Pb) in two habitats from an active hydrothermal field on the EPR at 13°N. *Science of The Total Environment* **392,** 119-129.

Sarradin P.-M., Waeles M., Bernagout S., Le Gall C., Sarrazin J. and Riso R. (2009) Speciation of dissolved copper within an active hydrothermal edifice on the Lucky Strike vent field (MAR, 37°N). *Science of The Total Environment* **407,** 869-878.

Schafer F. Q. and Buettner G. (2001) Redox environment of the cell as viewed through the redox state of the glutathione disulfide/glutathione couple. *Free Radical Biology and Medicine* **30,** 1191-1212.

Scheffer G. L., Wijngaard P. L. J., Flens M. J., Izquierdo M. A., Slovak M. L., Pindeo H. M., Meijer C. J. L. M., Clevers H. C. and Scheper R. J. (1995) The drug resistance-related protein LRP is the human major vault protein. *Nature Medicine* **1,** 578-582.

Schmidt K., Garbe-Schönberg D., Bau M. and Koschinsky A. (2010) Rare earth element distribution in >400°C hot hydrothermal fluids from 5°S, MAR: The role of anhydrite in controlling highly variable distribution patterns. *Geochim. Cosmochim. Acta* **74,** 4058-4077.

Schultz A. and Elderfield H. (1997) Controls on the physics and chemistry of seafloor hydrothermal circulation. *Phil. Trans. R. Soc. A* **355,** 387-425.

Sedwick P. N., McMurty G. M. and MacDougall J. D. (1992) Chemistry of hydrothermal solutions from Pele's Vents, Loihi Seamount, Hawaii. *Geochim. Cosmochim. Acta* **56,** 3643-3667.

Serafim A. and Bebianno M. J. (2010) Effect of a polymetallic mixture on metal accumulation and metallothionein response in the clam *Ruditapes decussatus*. *Aquatic Toxicology* **99,** 370-378.

Seyfried Jr W. E. and Ding K. (1995) The hydrothermal chemisty of fluoride in seawater. *Geochim. Cosmochim. Acta* **59,** 1063-1071.

Shannon R. D. (1976) Revised effective ionic radii and systematic studies of interatomic distances in halides and chalcogenides. *Acta Crystallogr.* **32,** 751-767.

Sheehan D. (2006) Detection of redox-based modification in two-dimensional electrophoresis proteomic separations. *Biochemical and Biophysical Research Communications* **349,** 455-462.

Sheehan D., McDonagh B. and Barcena A. (2010) Redox Proteomics. *Expert Reviews in Proteomics* **7,** 1-4.

Sherrell R. M., Field M. P. and Ravizza G. (1999) Uptake and fractionation of rare earth elements on hydrothermal plume particles at 9° 45'N, East Pacific Rise. *Geochim. Cosmochim. Acta* **63,** 1709-1722.

Shi D. and Wang W.-X. (2004a) Modification of trace metal accumulation in the green mussel *Perna viridis* by exposure to Ag, Cu, and Zn. *Environmental Pollution* **132,** 265-277.

Shi D. and Wang W.-X. (2004b) Understanding the differences in Cd and Zn bioaccumulation and subcellular storage among different populations of marine clams. *Environmental Science and Technology* **38,** 449-456.

Silvestre F., Trausch G. and Devos P. (2005) Hyper-osmoregulatory capacity of the Chinese mitten crab (Eriocheir sinensis) exposed to cadmium; acclimation during chronic exposure. *Comparative Biochemistry and Physiology Part C: Toxicology & Pharmacology* **140,** 29-37.

Silvestre F., Dierick J.-F., Dumont V., Dieu M., Raes M. and Devos P. (2006) Differential protein expression profiles in anterior gills of *Eriocheir sinensis* during acclimation to cadmium. *Aquatic Toxicology* **76,** 46-58.

Simkiss K. (1998). Mechanisms of Metal Uptake. *In:* Langston W. J. and Bebianno M. J. (eds.) *Metal Metabolism in Aquatic Environments.* London: Chapman and Hall, pp. 1-17

Simoneit B. R. T. and Lonsdale P. F. (1982) Hydrothermal petroleum in mineralized mounds at the seabed of Guaymas Basin. *Nature* **295,** 198-202.

Simonetti P., Elizabeth Botte S., Marcela Fiori S. and Eduardo Marcovecchio J. (2013) Burrowing crab (*Neohelice granulata*) as a potential bioindicator of heavy metals in the Bahia Blanca Estuary, Argentina. *Archives of Environmental Contamination and Toxicology* **64,** 110-118.

Singer A. J. and Nicolson G. L. (1972) The fluid mosaic model of the structure of cell membranes. *Science* **175,** 720-731.

Sleep B. R. and Rosendahl B. R. (1979) Topography and Tectonics of Mid-Oceanic Ridge Axes. *J. Geophys. Res.* **84,** 6831-6839.

Soegianto A., Charmantier-Daures M., Trilles J. P. and Charmantier G. (1999) Impact of copper on the structure of gills and epipodites of the shrimp *Penaeus japonicus* (Decopoda). *Journal of Crustacean Biology* **19,** 209-223.

Speiss F. N., Macdonald K. C., Atwater T., Ballard R. D., Carranza A., Cordoba D., Cox C., Diaz Garcia V. M., Francheteau J., Guerrero J., Hawkins J., Hayman N., Hessler R., Juteau T., Kastner M., Larson R., Luyendyke B., MacDougall J. D., Miller S., Normark W., Orcutt J. and Rangin C. (1980) East Pacific Rise; hot springs and geophysical experiments. *Science* **207,** 1421-1433.

Stein C. A. and Stein S. (1994) Constraints on hydrothermal heat flux through the oceanic lithosphere from global heat flow. *J. Geophys. Res.* **99,** 3081-3095.

Stern R. J. (2002). Subduction zones. *Reviews of Geophysics*, **40**, 10.1029/2001rg000108

Stewart F. J., Newton I. L. G. and Cavanaugh C. M. (2005) Chemosynthetic endosymbioses: adaptations to oxic–anoxic interfaces. *Trends in Microbiology* **13,** 439-448.

Stichel T., Frank M., Rickli J. and Haley B. A. (2012) The hafnium and neodymium isotope composition of seawater in the Atlantic sector of the Southern Ocean. *Earth Planet. Sci. Lett.* **317-318,** 282-294.

Stohs S. J., Bagchi D., Hassoun E. and Bagchi M. (2001) Oxidative mechanisms in the toxicity of chromium and cadmium ions. *Journal of Environmental Pathology, Toxicology and Oncology* **20,** 77-88.

Strange R. C., Spiteri M. A., Ramachandran S. and Fryer A. A. (2001) Glutathione-S-transferase family of enzymes. *Mutation Research* **482,** 21-26.

Sverjensky D. A. (1984) Europium redox equilibria in aqueous solution. *Earth Planet. Sci. Lett.* **67,** 70-78.

Tapley D. W., Buettner G. and Shick J. M. (1999) Free radicals and chemiluminescence as products of the spontaneous oxidation of sulfide in seawater, and their biological implications. *Biology Bulletin* **196,** 52-56.

Taylor S. R. and McClennan S. M. (1985) *The Continental Crust: Its Composition and Evolution,* Oxford, UK, Blackwell Scientific Publications.

Tedesco S., Doyle H., Blasco J., Redmond G. and Sheehan D. (2010) Oxidative stress and toxicity of gold nanoparticles in *Mytilus edulis*. *Aquatic Toxicology* **100,** 178-186.

Tedesco S., Jaafar S. N. T., Coelho A. V. and Sheehan D. (2012) Protein thiols as novel biomarkers in ecotoxicology: A case study of oxidative stress in *Mytilus edulis* sampled near a former industrial site in Cork Harbour, Ireland. *Journal of Integrated OMICS* **2,** 39-47.

Thatje S. and Arntz W. E. (2004) Antarctic reptant decapods: more than a myth? *Polar Biology* **27,** 195-201.

Thatje S., Anger K., Calcagno J. A., Lovrich G. A., Pörtner H.-O. and Arntz W. E. (2005) Challenging the cold: Crabs reconquer the Antarctic. *Ecology* **86,** 619-625.

Thomas C., Livermore R. A. and Pollitz F. (2003) Motion of the Scotia Sea plates. *Geophys. J. Int.* **155,** 789-804.

Thurber A. R., Jones W. J. and Schnabel K. (2011). Dancing for food in the deep-sea: Bacterial farming by a new species of yeti crab. *PloS One*, **6**, 10.1371/journal.pone.0026243

Timm D. E., Mueller H. A., Bhanumoorthy P., Harp J. M. and Bunick G. J. (1999) Crystal structure and mechanism of a carbon-carbon bond hydrolase. *Structure* **7,** 1023-1033.

Tivey M. K. (1995). Modeling Chimney Growth and Associated Fluid Flow at Seafloor Hydrothermal Vent Sites. *Seafloor Hydrothermal Systems: Physical, Chemical, Biological, and Geological Interactions, Geophysical Monograph 91*. American Geophysical Union, pp. 158-177

Trevisan R., Ferraz Mello D., Fisher A. S., Schuwerack P.-M., Dafre A. L. and Moody A. J. (2011) Selenium in water enhances antioxidant defenses and protects against copper-induced DNA damage in the blue mussel *Mytilus edulis*. *Aquatic Toxicology* **101,** 64-71.

Tsuchida S., Suzuki Y., Fujiwara Y., Kawato M., Uematsu K., Yamanaka T., Mizota C. and Yamamoto H. (2011) Epibiotic association between filamentous bacteria and the vent-associated galatheid crab, *Shinkaia crosnieri* (Decapoda: Anomura). *Journal of the Marine Biological Association of the United Kingdom* **91,** 23-32.

Tunnicliffe V., Botros M., De Burgh M. E., Dinet A., Johnson H. P., Juniper S. K. and McDuff R. E. (1986) Hydrothermal vents of Explorer Ridge, northeast Pacific *Deep-Sea Research* **33,** 401-412.

Tunnicliffe V. and Fowler C. M. R. (1996) Influence of sea-floor spreading on the global hydrothermal vent fauna. *Nature* **379,** 531-533.

Turner I. M., Peirce C. and Sinha M. C. (1999) Seismic imaging of the axial region of the Valu Fa Ridge, Lau Basin - the accretionary processes of an intermediate back-arc spreading ridge. *Geophys. J. Int.* **138,** 495-519.

Turner M., Yang X., Yin D., Kuczera K., Borchardt R. and Howell P. (2000) Structure and function of S-adenosylhomocysteine hydrolase. *Cell Biochemistry and Biophysics* **33,** 101-125.

Tyler P. A., German C., Ramirez-Llodra E. and Van Dover C. L. (2003) Understanding the biogeography of chemosynthetic ecosystems. *Oceanologica Acta* **25,** 227-241.

van de Flierdt T., Pahnke K., Amakawa H., Andersson P., Basak C., Coles B., Colin C., Crocket K., Frank M. and Frank N. (2012) GEOTRACES intercalibration of neodymium isotopes and rare earth element concentrations in seawater and suspended particles. Part 1: reproducibility of results for the international intercomparison. *Limnol. Oceanogr. Methods* **10,** 234-251.

Van Dover C. L., Fry B., Grassle J. F., Humphris S. and Rona P. A. (1988) Feeding biology of the shrimp *Rimicaris exoculata* at hydrothermal vents on the Mid-Atlantic Ridge. *Marine Biology* **98,** 209-216.

Van Dover C. L. and Fry B. (1989) Stable isotopic compositions of hydrothermal vent organisms. *Marine Biology* **102,** 257-263.

Van Dover C. L. (1990) Biogeography of hydrothermal vent communities along seafloor spreading centres. *Trends in Ecology & Evolution* **5,** 242-246.

Van Dover C. L. (2000) *The Ecology of Deep Sea Hydrothermal Vents*, Princeton University Press.

Van Dover C. L. (2001) Biogeography and Ecological Setting of Indian Ocean Hydrothermal Vents. *Science* **294,** 818-823.

Van Dover C. L., German C. R., Speer K. G., Parson L. M. and Vrijenhoek R. C. (2002) Evolution and biogeography of deep-sea vent and seep invertebrates. *Science* **295,** 1253-1257.

van Zon A., Mossink M. H., Schoester M., Scheffer G. L., Scheper R. J., Sonneveld P. and Wiemer E. A. C. (2002) Structural domains of vault proteins: A role for the coiled coil domain in vault assembly. *Biochemical and Biophysical Research Communications* **291,** 535-541.

Vanneste L. and Larter R. (2002). Sediment subduction, subduction erosion, and strain regime in the northern South Sandwich forearc. *J. Geophys. Res.*, **107**, 10.1029/2001JB000396

Viarengo A., Pertica M., Mancinelli G. and Orunesu M. (1980) Rapid induction of copper-binding proteins in the gills of metal exposed mussels. *Comparative Biochemistry and Physiology Part C* **67,** 215-218.

Viarengo A., Zanicchi G., Moore M. N. and Orunesu M. (1981) Accumulation and detoxication of copper by the mussel *Mytilus galloprovincialis* LAM.: A study of the subcellular distribution in the digestive gland cells. *Aquatic Toxicology* **1,** 147-157.

Viarengo A. and Nott J. A. (1993) Mechanisms of heavy metal cation homeostasis in marine invertebrates. *Comparative Biochemistry and Physiology Part C* **104,** 355-371.

Viarengo A., Pertica M., Mancinelli G., Burlando B., Canesi L. and Orunesu M. (1996) *In vivo* effects of copper on the calcium homeostasis mechanisms of mussel gill cell plasma membranes. *Comparative Biochemistry and Physiology Part C* **113,** 421-425.

Von Damm K. L., Edmond J. M., Grant B., Measures C. I., Walden B. and Weiss R. F. (1985) Chemistry of submarine hydrothermal solutions at 21°N, East Pacific Rise. *Geochim. Cosmochim. Acta* **49,** 2197-2220.

Von Damm K. L. and Bischoff J. L. (1987) Chemistry of hydrothermal solutions from the southern Juan de Fuca Ridge. *J. Geophys. Res.* **92,** 11334-11346.

Von Damm K. L. (1988) Systematics of and postulated controls on submarine hydrothermal solution chemistry. *J. Geophys. Res.* **93,** 4551-4561.

Von Damm K. L. (1990) Seafloor hydrothermal activity: black smoker chemistry and chimneys. *Annu. Rev. Earth Planet. Sci.* **18,** 173-204.

Von Damm K. L., Oostling S. E., Kozlowski R., Buttermore L. G., Colodner D., Edmonds H. N., Edmond J. M. and Grebmeier J. (1995) Evolution of East Pacific Rise hydrothermal vent fluids following a volcanic eruption. *Nature* **375,** 47-50.

Von Damm K. L., Lilley M. D., Shanks W. C., Brockington M., Bray A. M., O'Grady K. M., Olson E. J., Graham A., Proskurowski G. and Party S. S. (2003) Extraordinary phase separation and segregation in vent fluids from the southern East Pacific Rise. *Earth Planet. Sci. Lett.* **206,** 365-378.

Wang W.-X. and Rainbow P. S. (2010) Significance of metallothioneins in metal accumulation kinetics in marine animals. *Comparative Biochemistry and Physiology Part C: Toxicology & Pharmacology* **152,** 1-8.

Watanabe M. K., Ogawa H. K. and Suzuki T. (2003) Cadmium dependent generation of reactive oxygen species and mitochondrial DNA breaks in photosynthetic and nonphotosynthetic strains of *Euglena gracilis*. *Comparative Biochemistry and Physiology Part C: Molecular & Integrative Physiology* **134,** 227-234.

Welhan J. A. (1988) Origins of methane in hydrothermal systems. *Chem. Geol.* **71,** 183-198.

White S. L. and Rainbow P. (1982) Regulation and accumulation of copper, zinc and cadmium by the shrimp *Palaemon elegans*. *Marine Ecology Progress Series* **8,** 95-101.

Williams-Jones A. E., Migdisov A. A. and Samson I. M. (2012) Hydrothermal mobilisation of the rare earth elements - a tale of "ceria" and "yttria". *Elements* **8,** 355-360.

Wirsen C. O., Jannasch H. W. and Molyneaux S. J. (1993) Chemosynthetic microbial activity at Mid-Atlantic Ridge hydrothermal vent sites. *J. Geophys. Res.* **98,** 9693.

Wood S. A. (1990a) The aqueous geochemistry of the rare-earth elements and yttrium. 1. Review of available low-temperature data for inorganic complexes and the inorganic REE speciation of natural waters. *Chem. Geol.* **82,** 159-186.

Wood S. A. (1990b) The aqueous geochemistry of the rare-earth elements and yttrium. 2. Theoretical predictions of speciation in hydrothermal solutions to 350°C at saturation water vapour pressure. *Chem. Geol.* **88,** 99-125.

Yang K. and Scott S. D. (1996) Possible contribution of a metal-rich magmatic fluid to a seafloor hydrothermal system. *Nature* **383,** 420-423.

Yao H.-Q., Zhou H.-Y., Peng X.-T., Bao S.-X., Wu Z.-J., Li J.-T., Sun Z.-L., Chen Z.-Q., Li J.-W. and Chen G.-Q. (2009) Metal sources of black smoker chimneys, Endeavour Segment, Juan de Fuca Ridge: Pb isotope constraints. *Applied Geochemistry* **24,** 1971-1977.

Yu Z., Fotouhi-Ardakani N., Wu L., Maoui M., Wang S., Banville D. and Shen S.-H. (2002) PTEN Associates with the Vault Particles in HeLa Cells. *Journal of Biological Chemistry* **277,** 40247-40252.

Zhang G., Liu D., Wu H., Chen L. and Han Q. (2012) Heavy metal contamination in the marine organisms in Yantai coast, northern Yellow Sea of China. *Ecotoxicology* **21,** 1726-1733.

Zorita I., Ortiz-Zarragoitia M., Soto M. and Cajaraville M. P. (2006) Biomarkers in mussels from a copper site gradient (Visnes, Norway): An integrated biochemical, histochemical and histological study. *Aquatic Toxicology* **78,** S109-S116.